DIGITAL SUBTRACTION MAMMOGRAPHY VIA GEOMETRIC UNWARPING

FOR DETECTION OF EARLY BREAST CANCER

BY

XIAOHUA ZHOU

A THESIS

SUBMITTED TO THE FACULTY OF GRADUATE STUDIES

IN PARTIAL FULFILLMENT OF THE REQUIREMENTS

FOR THE DEGREE OF

DOCTOR OF PHILOSOPHY

DEPARTMENT OF ELECTRICAL AND COMPUTER ENGINEERING

UNIVERSITY OF MANITOBA

WINNIPEG, MANITOBA

DIGITAL SUBTRACTION MAMMOGRAPHY VIA GEOMETRIC UNWARPING

FOR DETECTION OF EARLY BREAST CANCER

BY

XIAOHUA ZHOU

A thesis submitted to the Faculty of Graduate Studies of
the University of Manitoba in partial fulfillment of the requirements
of the degree of

DOCTOR OF PHILOSOPHY

© 1991

ACKNOWLEDGMENTS

CONTENTS

LIST OF FIGURES

LIST OF TABLES

ABSTRACT

Breast cancer is the most common malignant neoplasm and a leading cause of cancer deaths in women. The means to prevent breast cancer has not yet been found. Although there exist alternative breast imaging techniques, mammography is at present the only reliable means of detecting nonpalpable cancers, and can detect many small breast cancers in early stages, when they may be curable.

The smallest tumors usually detected by mammography are 0.5 to 1 cm in diameter, though the resolution of mammograms is about 0.1 mm. The discrepancy may be due to the mammogram's intricate detail showing superimposed, fine structures above and below any tumor on the same two dimensional image. X-ray computed tomography (CT) solves the superposition problem. Digital subtraction from longitudinal mammograms may detect the small, growing tumors.

Registration of longitudinal breast images will be difficult because of the global deformation, or "warping", caused by our inability to position a breast exactly the same way twice in any instrument, and from changes during the menstrual cycle, aging, etc. It will be necessary to find the transformation or "geometric warping" T that relates an earlier (*reference*) image to a current (*warped*) one. We call its inverse transformation T^{-1} a "geometric unwarping". In order to estimate the transformation T and its inverse transformation T^{-1}, we must start with pairs of corresponding "control points", i.e., mammographic features whose coordinates can be unambiguously determined in both the warped and reference images.

The following essential steps towards digital subtraction mammography have been solved in this thesis. With the local unwarping approach, we can represent a complex transformation T as a simple piecewise approximation. That is, a set of contiguous triangles

across the reference image are defined by connecting neighboring control points, and a different polynomial transformation is allowed within each triangle. With the global unwarping approach, on the other hand, we can also use a single transformation function to register the whole image. We have proposed and implemented a template matching procedure by using correlation of Zernike moments as the measure of similarity. In this way a set of corresponding control points can be extracted from local mammographic structures regardless of their position and orientation. Two algorithms have also been developed to extract information of orientation and symmetry from the local structures, which may be incorporated in the feature matching.

We have evaluated the geometric unwarping algorithms for accuracy in recovering a known test transformation and unwarping a breast tissue image taken after mechanical distortion. Test results indicate that the local unwarping methods are far better than the global ones. Test results on the feature matching by Zernike moments, orientation recognition, and symmetry detection are presented as well. A number of prospective research topics on improvements of the geometric unwarping methods, and their generalization to three dimensions, are also given in this thesis.

To my parents

CHAPTER 1

INTRODUCTION

Breast cancer is approaching an epidemic rate, affecting 1 out of every 10 women, and no means of preventing its occurrence has yet been found. Detection and treatment of breast cancer at early stages is the only method with proven potential for lowering the death rate from this disease. Practices of monthly breast self-examination, regular clinical breast examinations, as well as regular mammography screening are highly recommended by many health organizations.

Because of its demonstrated ability to detect cancer at nonpalpable stages, and because of its high resolution, mammography has been in the forefront of methods of breast imaging [1.2]. The widespread use of mammography has been tempered by the possible risk from low doses of ionizing radiation and by the fact that it may still find only 80-90% of breast cancers. When all factors are considered, it has been convincingly demonstrated that the potential benefits of mammography far outweigh the minimal, clinically undetected radiation risk incurred by the examination [1.3]. New technologies such as computed tomography, magnetic resonance imaging, transillumination scanning, ultrasound, monoclonal antibody tagging, and positron emission tomography offer a variety of alternative breast imaging modalities. It has been shown that these alternatives are capable of providing clinically useful information that complements that currently available from X-ray mammography, and that there are indeed some specifically defined situations in which these alternatives prove helpful [1.7]. None of these procedures has, however, yet been applied in a manner which offers improvement over two-dimensional (2D) projection mammography for detection of early breast cancer.

Because benign and malignant nonpalpable abnormalities at early stages may have similar radiographic appearance, we must search not only for the classic mammographic features of malignancy, such as microcalcifications, but also for more subtle and "indirect" signs in predicting the presence of developing breast cancer in order to make a better diagnosis [1.5]. Ordinary projection mammography is, unfortunately, generally incapable of detecting tumors smaller than 1 cm in diameter [1.1]. Tumors of this large size may have already metastasized and do so in most cases [1.4]. Thus, if we are to improve the survival rate for breast cancer, we must successfully locate and treat smaller tumors.

Mammography is now our chief tool in detecting early breast cancer, yet it is far from perfect because of its 2D character. We propose that two three-dimensional (3D) images of a breast, taken some time apart, may be digitally subtracted to bring out breast carcinomas at early stages [1.6],[1.8]. The problem of 3D digital subtraction mammography may break down to the following steps:

1) Take a set of X-ray projection images at high spatial and density resolution. The resolution must be comparable to that of film mammography, so that details, such as microcalcifications, are not lost. The dose must be limited to about that of standard screening mammography, because if we are looking for small tumors, most women will be disease free.

2) Digitize the data and run it through an appropriate computed tomography algorithm. Because of the dose limitation, an algorithm must be chosen or developed that makes maximal use of the available photons.

3) Repeat steps 1 and 2 for the same breast at a later date.

4) Identify a set of corresponding control points in these two 3D images, A and B, obtained in the above mentioned steps. Note that control points may, in a general sense, represent some specific structures although they are chosen as simple geometric elements in this study.

5) Estimate the geometric warping or transformation T between images A and B.

6) Apply the geometric unwarping or inverse transformation T^{-1} to image B, and resample the pixel densities in the unwarped image of B, namely $T^{-1}(B)$.

7) Calculate the difference picture $D = A - T^{-1}(B)$.

8) Filter the difference picture D to try to distinguish noise from the signal provided by a small, growing tumor.

Production of the 3D images itself requires new approaches to computed tomography. The problems of image reconstruction from limited-view and few projections also need to be addressed thoroughly. Filtration of the difference images requires further studies on some fundamental problems, such as mammographic features indicating malignancy (especially at early stages). This study will address the problems of identifying a set of corresponding control points and estimating the geometric unwarping transformation between two mammographic images.

The organization of this thesis is as follows. The problem of detection of early breast cancer is reviewed in Chapter 2, which includes a brief overview of such issues as the current understanding of breast cancer, the mortality and survival of patients with breast cancer, and screening programs. Chapter 2 also discusses developments in mammography and other breast imaging modalities over the last decade, and gives an overview of future prospects for research in mammography. In Chapter 3 and Chapter 4 the geometric unwarping methods, and gray level resampling using interpolation and approximation techniques are presented, respectively. In Chapter 5 I discuss in detail geometric normalization, definition of Zernike moments, and mammographic feature matching by using Zernike moments. Algorithms for recognition of orientation and detection of axes of symmetry in planar images, which make use of the phase information derived from Zernike moments, are given in Chapter 6. In Chapter 7 we propose some topics for future studies and research on 3D geometric unwarping for detection of early breast cancer. These include the problems of characterization of mammographic features, identification of

mammographic features by template matching, 3D mammographic feature matching, and

3D geometric unwarping.

References

[1.1]   L. W. Bassett and R. H. Gold, Eds., *Breast Cancer Detection: Mammography and Other Methods in Breast Imaging,* 2nd ed., Orlando, FL: Grune and Stratton, 1987.

[1.2]   H. Cuckle, "Breast cancer screening by mammography: An overview," *Clin. Radiol.,* vol. 43, pp. 77-80, 1991.

[1.3]   S. Feig and S. M. Ehrlich, "Estimation of radiation risk from screening mammography: Recent trends and comparison with expected benefits," *Radiology,* vol. 174, pp. 638-647, 1990.

[1.4]   K. H. Kopald, J. R. Hiatt, C. Irving and A. E. Giuliano, "The pathology of nonpalpable breast cancer," *Amer. Surgeon,* vol. 56, pp. 782-787, 1990.

[1.5]   E. A. Sickles, "Mammographic features of 300 consecutive nonpalpable breast cancers," *Am. J. Roentgenol.,* vol. 146, pp. 661-663, 1986.

[1.6]   X. Zhou and R. Gordon, "Geometric unwarping for digital subtraction mammography," In *Proc. Vision Interface '88,* Edmonton, Canada, June 6-10, 1988, pp. 25-30.

[1.7]   X. Zhou and R. Gordon, "Detection of early breast cancer: An overview and future prospects," *CRC Critic. Rev. Biomed. Eng.,* vol. 17, pp. 203-255, 1989.

[1.8]   X. Zhou and R. Gordon, "3D digital subtraction mammography," In *Proc. 16th Canadian Med. and Biol. Eng. Soc. Conf.,* Winnipeg, Canada, June 9-12, 1990, pp. 29-30.

CHAPTER 2
DETECTION OF EARLY BREAST CANCER †

2.1. Introduction

The medical profession and the general public are justly concerned with the epidemic of breast cancer [2.62]. Statistics shows that approximately 1 in 10 women in North America will develop breast cancer in the course of their lifetimes [2.22],[2.42]. Although curable, particularly when detected at early stages, breast cancer is a major cause of cancer deaths among women [2.6],[2.55]-[2.57]. Because it tends to occur earlier in life than other cancers, and earlier than other major causes of death such as cardiovascular disease, breast cancer has been shown to be the greatest cause of years of life lost by women. It is our purpose here to review the magnitude of the problem, the efficacy of current methods of detection, and the potential for detection of earlier carcinomas.

2.2. Epidemiology of Breast Cancer

2.2.1. On the Understanding of Breast Cancer

At present there is no way of detecting *in vivo* the precise time that one or a few epithelial cells of the mammary parenchyma become neoplastic [2.31]. Estimation of the growth rate has been derived from a determination of the "doubling time," i.e., the time

---

† Chapter 2 is a condensation of a comprehensive review paper in *CRC Critical Reviews in Biomedical Engineering* [2.67], see Appendix 1 for references. Only references not given in Appendix 1 are given here.

required for a tumor to double its diameter (an eight-fold increase in mass if no necrosis occurs) during a known period of time. Data obtained by this method indicate that doubling times of breast carcinomas vary extensively from one tumor to another, e.g., from 1.2 to 900 days, depending on the locations of measured lesions.

It has been suggested that when breast carcinoma is first detected by any means now available, metastatic spread has already occurred [2.20],[2.36]; therefore, clinically detectable breast cancer is often not a localized disease. For instance, studies using both physical examination and mammography indicate that if mammography were not performed and patients were screened by physical examination alone, most tumors would metastasize before they reach a palpable size. A major task is thus to characterize the preclinicial phase of breast cancer, in particular to predict which lesion, morphologically definable only as hyperplastic, already has the potential for unrestrained growth and metastasis [2.38]. The present knowledge of the mechanism of metastasis suggests that a primary breast carcinoma can metastasize when it consists of a relatively small number of cells that is far below our present capacity of detection. Two conclusions can be drawn from the the mechanisms of breast carcinoma metastasis: the primary carcinoma may be a continuous source of neoplastic cells which spread through hematic and lymphatic vessels; and manipulation of breast carcinomas may produce extensive transfer of neoplastic cells into the circulation. Early detection and removal of the primary tumor is thus essential, and may be effective, since generally only a few of the cells that depart a primary tumor succeed in forming a secondary tumor. Hopefully, perhaps, the smallest primary tumors will have low metastasis rates. Our general inability to detect these small tumors now is a motivating factor for finding improved imaging and image processing/analysis methods.

There are documented large variations in incidence of breast cancer in different ethnic and culturally and geographically diverse groups. Diet is a common factor in these studies, and is assuming an increasingly dominant role. Further studies of this question are

undoubtedly required, however, before specific recommendations on dietary modifications can be made.

The question whether certain groups of persons are at higher risk for the development of breast cancer has already been the subject of discussion from the point of view of the epidemiologist, looking at large segments of the population. Such factors as age and sex are so obvious as to be intuitive, i.e., women are at higher risk than men, and older women are at higher risk than younger women. However, it might be essential to differentiate what might be considered as risks that are significant enough to influence the practice of medicine, from those factors that, although perhaps statistically important when dealing with large populations, are not enough to cause physicians to alter the advice they give patients about intervals between examinations, the need for mammograms, and so on.

It is well established that a family history of breast cancer is an important determinant of breast cancer risk. The reported associations with reproductive characteristics are of particular interest, as they imply a hormonal etiology for breast cancer. It is also possible that age at menarche and age at menopause represent independent risk factors for breast cancer.

It is generally accepted that relatively high doses of ionizing radiation can cause breast cancer. It is not known whether very low doses of radiation such as those from current mammographic techniques can cause breast cancer. It has been suggested, however, that if any low-dose risk does exist, it is immeasurably small, especially when compared with the overwhelmingly large incidence of naturally occurring breast cancers. With modern low-dose mammography, even when a conservative estimate of possible reduction in mortality due to detection at an early stage is applied to the data, the estimated benefit substantially exceeds any possible hazard of low-dose radiation.

Blood testing has the potential of forming a portion of a routine checkup for breast cancer, similar to the PAP test for uterine cancer. More importantly, it could become an important tool for following high-risk patients, and those already treated for breast cancer

[2.50]. Numerous investigators have reported the existence of human mammary tumor-associated antigens. Studies on breast cancer imaging with monoclonal antibodies have also been reported.

While progress continues to be made in providing leads to various factors associated with the development of breast cancer, its biological complexities are still not fully understood, nor has any one factor or group of variables been identified that explains or predicts more than a minority of the cases of this disease. Most of the risk factors do not readily lead to the implementation of preventive methods. However, current and future research in such areas as diet, physical exercise and hormones may help find preventable causes, or at the least lead to a better understanding of the pathogenesis of breast cancer.

2.2.2. Incidence, Mortality, and Survival of Patients with Breast Cancer

The probabilities of a newly born girl developing invasive cancer of various sites at some point during her life-time have been computed. For breast cancer, the probability was calculated to be about 10%: one out of every 10 women will develop this disease during her life.

Generally, incidence rates tend to be low in most Asian and developing countries, intermediate in Southern European countries, and high in North America, Scandinavian countries, and other Westernized areas. Differences in body mass, and perhaps breast mass in particular, may account for some of these international variations in breast cancer rates. In U.S. and other Western countries, incidence rates increase rapidly with age until the menopausal period (45 to 55), during which they tend to level off, and after which they increase at a slower rate. The difference in the patterns of pre- and post-menopausal incidence rates tends to lend support to the hypothesis that these are two distinct diseases. Women in urban areas are more likely to be affected than are those in rural areas, although

this differential has been decreasing over time. Women with higher income and higher educational level are more likely to be affected with breast cancer than are women in lower categories. There is also concern that recent reproductive trends, specifically the decrease in fertility rates and the postponement of childbearing until after the age of 30, may result in even high rates, since nulliparity and a late age at first birth are known to increase the risk of breast cancer.

Overall mortality rates have remained relatively stable for the past several decades. In general, the reported age-adjusted death rates are high in developed countries (with the notable exception of Japan) and low in the developing countries.

Survival of cancer of the breast has usually been analyzed according to such cancer characteristics as extent of metastases, size of tumor, histologic type, anatomic location and grade of malignancy. The number of positive axillary nodes was found to have an important effect on survival. The clinical size of tumors also correlated well with survival.

The relatively stable overall mortality rates indicate that the increasing survival rates are being offset by an increasing probability of developing breast cancer. Since prevention of breast cancer is not yet well understood, we should thus realize that there is much work ahead of us to further improve the survival rates for patients with breast cancer through early detection, diagnosis and treatment.

2.2.3. Breast Cancer Screening Programs

Screening is predicated on the assumption that with the detection of a disease in an early or asymptomatic state the probability of cure is greater than that if the disease were permitted to progress and present with later symptoms. (A contrary opinion, denying a simple progression of breast cancer, is based on less certain data which suggests that breast cancer is a systemic disease of the pair of breasts, a whole breast, or at least a substantial portion of one. In this case, detection and excision of early tumors may not lead to a cure

[2.20].) Screening is presumed to lead to appropriate treatment that, in turn, will lead to reduced mortality from the disease.

Many organizations recommend that women regularly undergo screening for breast cancer. For asymptomatic women 50 and older, both the American Cancer Society (ACS) and the U.S. National Cancer Institute (NCI) recommend annual or annual routine screening with mammography. For younger women, however, the NCI would restrict mammographic screening to those at high risk. The ACS, on the other hand, recommends a baseline mammogram for all asymptomatic women at 35 to 40 years of age, and screenings every one to two years for asymptomatic women aged 40 to 49. The American College of Radiology (ACR) makes similar recommendations for the various age groups. These organizations also support the recommended practices of monthly breast self-examination (BSE) and regular clinical breast examinations.

In women 50 years of age or older, the reduction in mortality due to screening as compared with control groups has been demonstrated in many studies. It has been suggested that aggressively screening younger women (aged 35 to 50), and finding and treating breast lesions while they are intraductal, *in situ*, and invasive but still smaller than 5 mm in diameter, may reduce mortality. With the improvement of breast imaging technology, the benefit is likely to extend to women under 50 as well.

The suitability of mammography for screening is still controversial regarding its benefits versus risk of long-term carcinogenic effects to the breast due to radiation exposure [2.9],[2.14],[2.52],[2.58]. This controversy, which peaked in the late 1970's, created widespread confusion and fear among women, many of whom were the very ones who would have potentially benefited the greatest from mammography. The carcinogenic risk from mammography screening is hypothetical, with no basis in clinical experience. Technological advances in both screen/film mammography and xeromammography have resulted in a marked reduction in radiation dose and improved image quality since the 1960's. Given the low levels of radiation exposure from state-of-the-art mammographic

equipment, the theoretical risk is quite small, especially compared to the failure to detect cancers when they are early, small and curable [2.19].

Screening procedures should be sensitive, reasonably specific, safe, and inexpensive. The high cost may be the single greatest deterrent to the use of screening mammography today. Studies of lay attitudes toward mammography suggest that the recommendation of physicians is a critical intervening factor that influences the beliefs and behavior of patients. Another may be the awareness that many radiologists do not know how effective or accurate they are with the procedure. All these factors suggest that the cost-effectiveness or affordability of compliance with the ACR/ACS guidelines is at least doubtful, especially for women under 50.

One way to increase screening program effectiveness and reduce total costs is to implement a selective screening program, i.e., to use present knowledge about the risk factors of breast cancer to select a group of women for screening. High volume practice and limiting the role of radiologist to interpretation versus performance of the examination have also been suggested as means of cost reduction for mammography. It might be possible to use nonphysician radiology assistants, possibly aided by computer, to interpret examinations. Artificial intelligence techniques have been shown to help radiologists improve their diagnostic accuracy, as well as to train non-radiologist assistants.

Studies have shown that mammography is being performed mainly for the diagnosis of symptomatic women instead of screening of asymptomatic women and that mammography is being underused [2.34]. There is some evidence that most women are well-disposed toward mammographic screening. One explanation for the underuse of mammography by physicians is probably that the majority of referrals appear to be made for the purpose of the diagnosis of disease, and that physicians erroneously regard mammography as a relatively unimportant prevention strategy, even for women age 50 and older.

Mammographic screening in women under age 50 is less clearly established. This is probably because of the lack of supporting data from controlled randomized studies and

hypothetical projections of radiation risk. The generally more dense images of their breasts may also contribute to a lower detectability of tumors in mammograms of younger women. A significant volume of data suggests that radiation exposure after the age of 35 has far less potential for inducing breast cancer than it does in younger age groups. It has been suggested that aggressive screening of younger women (less than 50 years at entry) at yearly intervals with mammographic and clinical examinations can most likely alter the natural history of the disease as it does in older women. The strongest evidence that mammography significantly reduces breast cancer deaths in women under 50 has been recently revealed by a new analysis of a long-term U.S. study. Mammography is usually not recommended for women under the age of 35 when the woman is asymptomatic.

Mammography is certainly not flawless. A system, such as mammography, with the demonstrated ability to detect occult cancer may be poor at diagnosis. Mammographic criteria to distinguish malignant from benign carcinomas still remain ambiguous and contradictory. Scientifically derived data from better-organized screening programs are clearly needed to help set up these criteria. Furthermore, although more accurate than any other modality, including physical examination, mammography may still find only 80-90% of breast cancers.

Although mammography has proved to be effective in detecting early breast cancers, the history of its usage provides evidence for caution in its application as a screening technique. Prospects for change in the use of mammography will depend on the success or failure of consensus policy-making, marketing strategies, cost reductions, risk reductions, and technological improvements in sensitivity and specificity.

2.2.4. Breast Self-Examination

Since more than 90% of breast cancer is now first detected by the women themselves, indoctrination into BSE is vital as a first step in screening. Recent study has shown that the

accidental discovery of a symptom leads to the detection of tumors that are 2 cm in diameter or more, but a systematic BSE month after month discovers symptoms of tumors that are only 0.5 - 1 cm in diameter. Although many investigators have found a positive association between BSE and detection of breast cancer at early stages, controversies still exist about this procedure.

Like mammography, however, BSE (and clinical examination) have been underused, although to different extents. Few women practice BSE on a monthly basis, as recommended, although it has long been promoted as a useful procedure in screening. Personnel involved in BSE education must deal with three challenges: (1) persuading women to perform BSE for the first time; (2) getting women to perform BSE on a regular basis, and (3) ensuring the correctness of BSE practice.

There are no widely accepted standards for the BSE practice. Self-reporting practice has been found not adequate as an indicator of the quality of BSE performed. Reliable methods for measuring all components of BSE should continue to be developed. BSE must be properly taught, used, and reinforced by health professionals. BSE, the patient's part in the total health care, must also be integrated with routine physical examination and mammography. This is because studies on mortality reduction by screening show that combined screening by both physical examination and mammography could reduce breast cancer mortality by 56%, and that the combination of mammography and physical examination may be today the most effective method of screening for breast cancer.

Because of the high cost, only limited groups of women in the world can be involved in screening mammography. Instead of being a single procedure at a given date, an effective screening program should constitute a continuous, multi-component program, probably containing BSE on a monthly basis year after year and a massive referral system. The program should also be able to apply to large populations in developed and developing countries without requiring a substantial increase in health care resources.

2.3. Mammography: An Overview and Future Prospects

2.3.1. Brief Historical Review

In 1913, Salomon used X-rays to image gross mastectomy specimens. But it was not until 1930 that Warren reported the successful performance of mammography on patients. In 1960, Egan reported on the development of a high-milliamperage/low-kilovoltage method that resulted in dependable diagnostic quality mammographic images on industrial X-ray film.

Another breakthrough in mammography occurred when Gros introduced two innovations: a molybdenum target, in place of tungsten, heightened the contrast between water, fat, and calcific densities, while a built-in compression device diminished scattered radiation, motion artifacts, and separated breast structures. In 1969, a dedicated mammographic unit became available, which included a molybdenum target tube and a filter based on the emission spectrum of molybdenum. In 1972, the DuPont Company, stimulated by the investigation of Ostrum, marketed a high-definition intensifying screen combined with a single-emulsion film, held in intimate contact by a vacuum, and revolutionized mammography by permitting rapid automatic processing, shorter exposures with diminished motion unsharpness, and greatly reduced surface exposure.

The introduction of xeromammography in 1972 provided an alternate breast imaging method. Xeromammograms have two unique characteristics which improve the visualization of breast pathology: wide recording latitude and edge enhancement. While clinical investigations have failed to reveal a significant difference in accuracy between screen-film mammography performed with dedicated equipment and xeromammography, screen-film mammography currently requires considerably less radiation than xeromammography for the same two-view examination.

2.3.2. State of the Art

Special imaging problems arise in mammography since the imaging conditions are unique. The differences in attenuation of the various soft tissue structures in the female breast are small, and it is necessary to use X-rays with low photon energy in order to get a sufficiently high contrast in the mammographic film.

The factors that may affect the quality of any radiographic image include the composition of the target of the X-ray tube, the size and shape of the focal spot on the target, the distance of the focal spot from the object, and the distance of the object from the recording medium. Also of importance is the composition of the object being imaged, the characteristics of the recording system, as well as the darkroom and film developing technique employed. Since contrast between the soft tissues of the breast is inherently low and because relatively minor changes in mammary structure can signify the presence of a malignant breast tumor, the margin for error is more critical in mammography than in most other forms of radiography. There have been a few studies on image quality attainable in mammography and new photographic techniques have been tried to obtain images at low dose.

During the past few years considerable emphasis has been placed on better understanding of the mammographic imaging process and on radiation dose reduction [2.13],[2.30]. More accurate methods of measuring radiation exposure in the energy range of mammography, and more relevant calculations of radiation dose to the breast tissue which is at risk, have been realized. Equally important is the effect of the X-ray technique on image quality. The relationship between absorbed dose and image quality should be further investigated.

Many of the technical changes that occurred in mammography during the last decade are directly related to the development of screen-film systems [2.28],[2.33]. The new dedicated units for screen-film mammography have smaller focal spots, longer (and fixed)

source-to-image distance to reduce geometric unsharpness, more effective compression devices to eliminate motion and to separate mammary structures, moving grids to reduce scattered radiation, automatic exposure control for more consistent quality, configurations that promote easy and rapid positioning by permitting the patient to stand during exposures, and an alternate even smaller focal spot for the production of magnified images.

For screen-film mammography, only the dedicated X-ray units with either a molybdenum target tube and a molybdenum filter or a specially designed tungsten target tube with a beryllium window are recommended. The shape of the focal spot has an impact on its imaging performance, and the focal spot shape is furthermore a function of the filament shape and position. The emission X-ray spectra for mammographic screen-film combinations have been studied by several investigators. It has been found that the energy distribution of the image-forming photons transmitted through the breast also influences subject contrast.

Motion blurring can be minimized by using a short exposure time and by firmly compressing the breast. To minimize geometric blurring, the focal spot size and object-to-image detector distance should be minimized, whereas focal spot-to-object distance should be maximized. While the current dedicated units are better in this regard, some units could be improved to ensure that the image detector (such as film), but not geometric blurring, is the limiting factor in resolution. In screen-film mammography, light diffusion (spreading of the light emitted by the screen before it is recorded by the film) also causes blurring. Factors include thickness and size of the screen phosphor, light-absorbing dyes and pigments in the screen, and screen-film contact. Screen-film combinations for mammography utilize a single high-definition screen in contact with a single-emulsion film, instead of the double-coated film (with one emulsion on either side of the support, and sandwiched between two intensifying screens). Cassettes designed for mammography with front panels which provide low X-ray absorption and intimate screen-film contact also reduce blur.

It has been demonstrated that radiation passing through the breast to the detector contains a significant amount of scattered radiation, and that scattered radiation will reduce image contrast accordingly. Good breast compression is a very important factor in reducing scattered radiation in screen-film mammography. In addition to contributing to a reduction in scattered radiation, compression can provide several other advantages: immobilization of the breast reduces blurring caused by motion; juxtaposition of structures in the breast closer to the image detector reduces geometric blurring; production of a more uniformly thick breast, which, in turn, results in more even penetration by X-ray radiation and less difference in radiographic density in the area between the chest wall and the nipple; reduction of radiation dose; and the spreading of breast tissue enables suspicious lesions to be more easily identified. Compression also provides the opportunity to optimize the X-ray photon energy for a given X-ray optimal thickness, which has not yet been exploited.

The use of specially-designed grids for mammography can further reduce scattered radiation and improve contrast. Note that patient exposure is also increased. Moving grids are now included with most of the new, dedicated mammographic x-ray units. For use with older dedicated systems without a built-in grid, an ultrahigh-strip-density, stationary, focused grid that fits inside a standard mammographic cassette is commercially available.

Slit radiography has been known for many years to be a technique that reduces scatter, but it has not come into general use. However, development work in slit radiography continues both with film and electronic systems. Slit radiography can make low contrast images more readily detectable by film, but film often cannot make these images perceptible to the unaided eye. Moreover, when slit radiography removes the background, the dynamic range of the X-ray image can increase beyond the acceptance range of film; however, electronic systems now have the ability to accept larger dynamic ranges than film, and are thus able to take fuller advantage of slit radiography. A new version of slit radiography to remove such background effects as scatter, off-focal radiation and intensifier glare has been

reported. Initial experimental results of scatter reduction in slit mammography has been reported.

Because magnification mammography requires considerably more radiation, its major role currently is to supplement the occasionally inadequate information provided by conventional mammography. In magnification mammography, the projected radiographic image is enlarged and the scattered radiation reaching the film is reduced. Because of the resultant increase in imaging distance, one must use higher kVp, faster film, longer exposures, or a combination of these factors to produce magnification mammograms. Magnification technique also requires the use of an X-ray tube that has a very small focal spot, to reduce the considerable unsharpness that otherwise would accompany geometric image enlargement. A possible alternative may be digital or optical deconvolution of the focal spot from the image. It is also important for magnification mammography equipment to permit vigorous breast compression, primarily because the relatively long exposure times used for magnification imaging provide an increased opportunity for image blurring due to motion unsharpness, and any motion is also magnified.

While limiting the number of mammographic views or projections per examination lowers the radiation risk, this limited number of views yields an unacceptably low rate of cancer detection. Other investigators favor xeromammography for seeing fine details and imaging microcalcifications with better contrast. However, xeromammography requires a higher radiation dose than film-screen methods and has lower spatial resolution. It has been suggested that the information in mammograms can be enhanced by subtraction film techniques. A combination of film-screen mammographic and xeromammographic examination may optimize the diagnostic abilities of mammographic examination.

Digital image processing techniques have been suggested for the feature enhancement of mammograms. Algorithms based on computerized adaptive neighborhood image processing to enhance the contrast of selected features of a mammogram were reported. New techniques have been developed, based on region growing techniques, to determine

the adaptive neighborhoods. There may be a further generalization in which pictures are segmented into a picture-dependent set of "feature pixels" or "fixels", which are local regions defined by an adaptive neighborhood function. These new image processing techniques may succeed in bringing out the desired, but unseen or barely seen features of a mammogram for better human visibility, without the requirement of additional X-ray dose. They may also permit a reduction in dose.

One major problem encountered in mammographic screening programs would involve the interpretation of the large volume of images produced. Some automated prescreening methods have been suggested to relieve humans of the more tedious aspects of screening programs, utilizing recent advances in image processing and pattern recognition techniques. Computer evaluations would also produce quantitative, objective data (geographical and time-invariant), which are further useful for standardization and quality control. Computerization procedures have been proposed for the management of screening mammography centres [2.53].

2.3.3. Expected Trends

The primary goal of the future development of mammography is further improvement in image quality, leading to increased diagnostic accuracy [2.37]. Dose reduction should continue to be sought, but not at the expense of diagnostic sensitivity and specificity.

Accurate film digitization via laser scanning permits recording and display of the entire 12-bit dynamic range of film while retaining high spatial resolution. High-quality film digitizers have become available for use in clinical testing. A system for digital processing of film radiographs can combine the excellent characteristics of film as a detector (in terms of dynamic range and spatial resolution) with the flexible image processing and display capabilities of a digital system.

One potentially fruitful area for research is electronic digital mammography, bypassing film altogether. Digital mammographic systems may use specially designed photoelectronic imaging devices to eliminate the use of film as the primary recording medium. Aside from the obvious advantages of accuracy and performance, since the images are digital, many digital processing techniques are available without further instrumentation to significantly enhance the diagnostic quality of the final images. Advantages of such digital systems over traditional film-based ones also include the capability for electronic archival and matching with computerized patient records, flexibility of display, and so on. High-efficiency detector systems are being developed that will be more effective than mammography in detecting X-ray photons, permitting a considerable reduction in the dose required. The addition of microfocal spot magnification to grids or scanning slits to reduce scattered radiation could also lead to future digital mammography systems that are both practical and effective. Several important projects for digital processing of mammographic images include very-high-resolution film digitization, computed radiography, slit scanning techniques, and time-resolved optical spectroscopy.

It has been suggested that mammograms, as normally viewed, display only about 3% of the total information detected. Many attempts have been made to improve the characterization and detection of breast tumors with the aid of computers [2.7],[2.10],[2.11],[2.15],[2.46]. It may be possible to enhance mammograms to bring out the diagnostic information. There is a clear need for further research in automation of mammographic screening programs and computerization for management of such programs. The potential for dual-energy image subtraction may produce significant improvements in radiographic detection of breast cancer. A new approach for detection of early breast cancer has also been proposed by using 3D digital subtraction techniques via a geometric unwarping procedure, of which several problems are addressed in this thesis.

2.4. CT, MRI, and Other Modalities for Breast Imaging

2.4.1. Computed Tomographic Mammography

Clinical trials demonstrated slightly increased cancer detection for CT scanning over mammography, whereas the others showed no difference [2.54]. It was also showed that CT scanning is inappropriate as a primary diagnostic test for breast cancer, because of the high cost of the examination, the need for intravenous contrast administration, and the relatively high radiation dose involved. Despite the lack of general clinical utility for breast CT scanning, there are several specific, narrowly defined situations in which the examination can prove helpful.

There is another promising approach that is yet to be explored: understanding the physiological processes that cause malignant tissues to have an increased affinity for iodinated contrast material. This may prove useful for breast MRI (see below) by facilitating production of successful paramagnetic contrast agents for breast cancer detection. The feasibility and substantial potential of positron emission tomography (PET) scanning to detect and localize both primary and metastatic breast cancers have been demonstrated recently [2.64].

2.4.2. Breast Magnetic Resonance Imaging

Even with high-resolution surface coils, the spatial resolution of MRI is, however, far inferior to mammography. Moreover, the tiny clustered calcifications of intraductal carcinoma and the fine spiculations of invasive breast cancer are not imaged. The very high cost of examination, as well as possible toxicity from intravenous paramagnetic agents, which highlight differences in signal intensity between regions of differing tissue perfusion, would prevent their use in screening programs. However, MRI is superior to mammography in differentiating solid from cystic lesions, and equivalent to mammography

in providing information regarding different parenchymal patterns. Fatty and fibroglandular regions of the breast are clearly distinguished, and areas of dense fibroglandular tissue are imaged with a greater range of contrast than either mammography or CT scanning.

Despite these shortcomings for screening, breast MRI offers considerable promise in breast disease diagnosis, as a complement to mammography and physical examination [2.54]. The additional information provided by multispectral analysis of MR images has been found to be valuable for distinguishing different kinds of tissues and structures [2.63]. Multispectral analysis of MR images of the breast has been reported recently [2.23]. It is possible to combine X-ray CT and MRI pixels in a way that extracts more information than available from viewing CT and MRI images side by side [2.24]. The multimodality imaging technique may then become a very powerful tool for breast imaging.

2.4.3. Breast Transillumination Light Scanning

Reports on the efficacy of transillumination light scanning to detect breast cancer have shown discrepant results. Other reports have noted varied findings, and further studies are being conducted. The primary theoretical limitation to transillumination techniques is that only a very small portion of the incident light, if any, is transmitted in a straight path through the breast. Thus, the great majority of photons are scattered extensively, thereby producing low resolution images. The fact that current equipment uses large-area light sources and short imaging distances further degrades the transillumination image. Transillumination's major weaknesses appear to be a relative inability to image deep lesions, and a questionable ability to detect the small cancers (1 cm) now routinely detected by mammography.

There has been no conclusive demonstration that transillumination can serve even as an adjunct to mammography and physical examination in the evaluation of either symptomatic or asymptomatic patients and therefore remains an investigational tool. Scatter reduction

methods, for instance, the use of low-energy lasers, or by raster scanning with a fiber optic point source touching the breast and by carrying out an inverse radiative transfer (3D deconvolution) computation, should be further investigated. The basic physical properties of light absorption in the breast should also be investigated. The application of time-resolved optical spectroscopic measurement to breast imaging is currently being studied.

2.4.4. Breast Sonography

Sonography, while capable of imaging and categorizing most palpable breast masses, often failed to detect small, nonpalpable masses that present only as clustered calcifications on mammograms, often the sole indicators of breast cancer. An important clinical role for breast sonography currently is the differentiation of benign cysts from indeterminate solid masses [2.4].

In spite of its failure as a screening method, sonography has emerged as the single most helpful adjunct to mammography in the evaluation of the clinically or mammographically abnormal breast. Other proposed applications of sonography include imaging dense breasts, the application of Doppler techniques to make benign-malignant differentiations of sonographically detectable masses, the evaluation of tissue surrounding augmentation prostheses, where the effectiveness of X-ray mammography and physical examination is limited, and, perhaps, the initial evaluation of asymptomatic women under 35 years of age. Ultrasound-guided aspiration biopsy of nonpalpable lesions is beginning to be explored. The detection of axillary lymph node metastases in breast cancer by ultrasound has also been reported.

Continuing refinements in transducer design and signal processing techniques can be expected to produce better images. The development of acoustic transmission computed tomography for *in vivo* determination of sonic attenuation and velocity should permit much more successful imaging of fatty tissues, currently a major weakness limiting the utility of

breast sonography. Efforts to establish the ultrasonic characteristics of breast structures and breast carcinomas have also been reported.

2.4.5. Breast Thermography

Because most of the reported investigations on breast thermography have been anecdotal and/or lacked definitive comparisons with other modalities, the value of thermography cannot be accurately assessed. There is little evidence to indicate that thermography lowers the stage at detection, and neither does a positive thermogram in screening seem to have a strong predictive value.

Because it is rapid, noninvasive, and safe, however, thermography may still be an investigational tool, to be used in breast cancer screening only when a specific protocol is available that allows subsequent objective evaluation of results. The role of thermography in determining prognosis and treatment of breast cancer patients should continue to be scientifically investigated. It is especially important that additional research be undertaken to determine the nature of tumor thermogenesis.

2.4.6. Stereotactic Fine-Needle Aspiration Cytology of Nonpalpable Breast Lesions

With the widespread use of mammography, especially for screening of asymptomatic women, an increasing number of nonpalpable breast lesions will be detected. Since 15-35% of nonpalpable mammographically identified lesions prove to be malignant at time of biopsy [2.26], a diagnostic technique for further characterization of such lesions is needed to minimize the number of surgical biopsies and to improve preoperative planning of surgical procedures.

Fine-needle aspiration biopsy has been accepted as a means of diagnosing palpable breast lesions for years [2.1],[2.2],[2.8],[2.21],[2.25],[2.35],[2.39],[2.51],[2.59], [2.65],[2.66]. On the contrary, experience with nonpalpable lesions is more limited. The major problem with the two-dimensional coordinate-grid technique [2.40],[2.43],[2.45], is that it does not give the depth of the lesion. The three-dimensional stereotactic technique, originally described by Nordenström [2.44], overcomes the depth problem in the 2D coordinate-grid approach. "This is an exciting technology that could reduce the number of unnecessary excisional breast biopsies" [2.32]. There have been reports on stereotactic fine-needle aspiration for cytologic diagnosis of nonpalpable lesions [2.3],[2.12],[2.16]-[2.18],[2.27],[2.29],[2.41],[2.60],[2.61]. It has been suggested that stereotactic core biopsy with a biopsy gun and an automated cutting needle may be superior to fine-needle aspiration biopsy [2.5],[2.47]-[2.49].

2.5. Conclusions

Detection and treatment of breast cancer at early stages is the only method with proven potential for lowering the death rate from this disease. Detection of early breast cancer is promoted by many health organizations by encouraging the regular use of three types of screening: breast self-examination, clinical breast examination, and mammography. Mammography is the first-line imaging technique for the detection of breast cancer. It is necessary to detect much smaller tumors than that mammography can do at present in order to improve the survival rate for breast cancer. A variety of alternative breast imaging modalities can provide useful information, in some situations, that complements that available from mammography.

References

[2.1]   J. Abele, T. Miller, W. Goodson, T. Hunt and D. Hohn, "Fine-needle aspiration of palpable breast masses," *Arch. Surg.*, vol. 118, pp. 859-863, 1983.

[2.2]   B. Adye, P. C. Jolly and D. E. Bauermeister, "The role of fine-needle aspiration in the management of solid breast masses," *Arch. Surg.*, vol. 123, pp. 37-39, 1988.

[2.3]   E. Azavedo, G. Svane and G. Auer, "Stereotactic fine-needle biopsy in 2594 mammographically detected non-palpable lesions," *Lancet*, vol. 1, pp. 1033-1036, 1989.

[2.4]   L. W. Bassett and C. Kimme-Smith, "Breast sonography," *AJR*, vol. 156, pp. 449-455, 1991.

[2.5]   M. E. Bernardino, "Automated biopsy devices: Significance and safety (Editorial)," *Radiology*, vol. 176, pp. 615-616, 1990.

[2.6]   C. C. Boring, T. S. Squires and T. Tong, "Cancer statistics, 1991," *Ca*, vol. 41, pp. 19-36, 1991.

[2.7]   C. B. Caldwell, S. J. Stapleton, D. W. Holdsworth, R. A. Jong, W. J. Weiser, G. Cooke and M. J. Yaffe, "Characterisation of mammographic parenchymal pattern by fractal dimension," *Phys. Med. Biol.*, vol. 35, pp. 235-247, 1990.

[2.8]   G. W. Carlson and C. M. Ferguson, "Needle aspiration cytology of breast masses," *Am. Surg.*, vol. 53, pp. 235-237, 1987.

[2.9]   J. Chamberlain, "An insurance policy to reduce the risk of dying from breast cancer," *Clin. Radiol.*, vol. 40, pp. 1-3, 1989.

[2.10] H. P. Chan, C. J. Vyborny, H. MacMahon, C. E. Metz, K. Doi and E. A. Sickles, "ROC studies of the effects of pixel size and unsharp-mask filtering on the detection of subtle microcalcifications," *Invest. Radiol.*, vol. 22, pp. 581-589, 1987.

[2.11] H. P. Chan, K. Doi, C. J. Vyborny, K. M. Lam and R. A. Schmidt, "Computer-aided detection of microcalcifications in mammograms, methodology and preliminary clinical study," *Invest. Radiol.*, vol. 23, pp. 664-671, 1988.

[2.12] S. Ciatto, M. R. Del Turco and P. Bravetti, "Nonpalpable breast lesions: Stereotaxic fine-needle aspiration cytology," *Radiology*, vol. 173, pp. 57-59, 1989.

[2.13] B. J. Conway, J. L. McCrohan, F. G. Rueter and O. H. Suleiman, "Mammography in the eighties," *Radiology*, vol. 177, pp. 335-339, 1990.

[2.14] H. Cuckle, "Breast cancer screening by mammography: An overview," *Clin. Radiol.*, vol. 43, pp. 77-80, 1991.

[2.15] D. H. Davies and D. R. Dance, "Automatic computer detection of clustered calcifications in digital mammograms," *Phys. Med. Biol.*, vol. 35, pp. 1111-1118, 1990.

[2.16] K. Dowlatshahi, H. J. Gent, R. Schmidt, P. M. Jokich, M. Bibbo and E. Sprenger, "Nonpalpable breast tumors: Diagnosis with stereotaxic localization and fine-needle aspiration," *Radiology*, vol. 170, pp. 427-433, 1989.

[2.17] W. P. Evans and S. H. Cade, "Needle localization and fine-needle aspiration biopsy of nonpalpable breast lesions with use of standard ans stereotactic equipment," *Radiology*, vol. 173, pp. 53-56, 1989.

[2.18]   L. L. Fajardo, J. R. Davis, J. Wiens and D. C. Trego, "Mammography-guided stereotactic fine-needle aspiration cytology of nonpalpable breast lesions: Prospective comparison with surgical biopsy results," *AJR*, vol. 155, pp. 977-981, 1990.

[2.19]   S. Feig and S. M. Ehrlich, "Estimation of radiation risk from screening mammography: Recent trends and comparison with expected benefits," *Radiology*, vol. 174, pp. 638-647, 1990.

[2.20]   E. R. Fisher, "The impact of pathology on the biologic, diagnostic, prognostic, and therapeutic considerations in breast cancer," *Surgical Clinics N. Amer.*, vol. 64, pp. 1073-1093, 1984.

[2.21]   W. J. Frable, "Needle aspiration of the breast," *Cancer*, vol. 53, pp. 671-676, 1984.

[2.22]   E. R. Frykberg, K. I. Bland and E. M. Copeland III, "The detection and treatment of early breast cancer," *Adv. Surg.*, vol. 23, pp. 119-194, 1990.

[2.23]   J. K. Gohagan, E. L. Spitznag, W. A. Murphy, M. W. Vannier, W. T. Dixon, D. J. Gersell, S. L. Rossnick, W. G. Totty, J. M. Destouet and D. L. Rickman, "Multispectral analysis of MR images of the breast," *Radiology*, vol. 163, pp. 703-707, 1987.

[2.24]   R. Gordon and J. Coumans, "Combining multiple imaging techniques for in vivo pathology: a quantitative method for coupling new imaging modalities," *Med. Phys.*, vol. 11, pp. 79-80, 1984.

[2.25]   C. S. Grant, J. R. Goellner, J. S. Welch and J. K. Martin, "Fine-needle aspiration of the breast," *Mayo Clin. Proc.*, vol. 61, pp. 377-381, 1986.

[2.26]   F. M. Hall, J. M. Storella, D. Z. Silverstone and G. Wyshak, "Nonpalpable breast lesions: Recommendations for biopsy based on suspicion of carcinoma at mammography," *Radiology*, vol. 167, pp. 353-358, 1988.

[2.27]   L. Hann, B. S. Ducatman, H. H. Want, V. Fein and J. M. McIntire, "Nonpalpable breast lesions: Evaluation by means of fine-needle aspiration cytology," *Radiology*, vol. 171, pp. 373-376, 1989.

[2.28]   A. G. Haus, "Technologic improvements in screen-film mammography," *Radiology*, vol. 174, pp. 628-637, 1990.

[2.29]   M. A. Helvie, D. E. Baker, D. D. Adler, I. Andersson, B. Naylor and K. A. Buckwalter, "Radiographically guided fine-needle aspiration of nonpalpable breast lesions," *Radiology*, vol. 174, pp. 657-661, 1990.

[2.30]   R. E. Hendrick, "Standardization of image quality and radiation dose in mammography," *Radiology*, vol. 174, pp. 648-654, 1990.

[2.31]   L. Holmberg, J. Pontén and H. O. Adami, "The biology and natural history of breast cancer from the screening perspective," *World J. Surg.*, vol. 13, pp. 25-30, 1989.

[2.32]   V. P. Jackson and L. W. Bassett, "Stereotactic fine-needle biopsy for nonpalpable breast lesions," *AJR*, vol. 154, pp. 1196-1197, 1990.

[2.33]   C. Kimme-Smith, L. W. Bassett, R. H. Gold, J. Zheutlin and J. A. Gornbein, "New mammography screen/film combinations: Imaging characteristics and radiation dose," *AJR*, vol. 154, pp. 713-719, 1990.

[2.34]   A. E. Kirkpatrick, "Breast cancer screening: An appraisal (Editorial)," *Clin. Radiol.*, vol. 43, pp. 75-76, 1991.

[2.35]   T. Kline, L. Joshi and H. Neal, "Fine-needle aspiration of the breast - diagnoses and pitfalls: A review of 3545 cases," *Cancer*, vol. 44, pp. 1458-1464, 1979.

[2.36]   K. H. Kopald, J. R. Hiatt, C. Irving and A. E. Giuliano, "The pathology of nonpalpable breast cancer," *Amer. Surgeon*, vol. 56, pp. 782-787, 1990.

[2.37]   D. B. Kopans, "Breast imaging," *Invest. Radiol.*, vol. 25, pp. 105, 1990.

[2.38]   S. Koscielny, M. Tubiana, M. G. Le, A. J. Valleron, H. Mouriesse, G. Contesso and D. Sarrazin, "Breast cancer: relationship between the size of the primary tumour and the probability of metastatic dissemination," *Br. J. Cancer*, vol. 49, pp. 709-715, 1984.

[2.39]   D. R. Lannin, J. F. Silverman, W. J. Pories and C. Walker, "Cost-effectiveness of fine needle biopsy of the breast," *Ann. Surg.*, vol. 203, pp. 474-480, 1986.

[2.40]   M. Löfgren, I. Andersson, L. Bondeson and K. Lindholm, "X-ray guided fine-needle aspiration for the cytologic diagnosis of nonpalpable breast lesions," *Cancer*, vol. 61, pp. 1032-1037, 1988.

[2.41]   M. Löfgren, I. Andersson and K. Lindholm, "Stereotactic fine-needle aspiration for cytologic diagnosis of nonpalpable breast lesions," *AJR*, vol. 154, pp. 1191-1195, 1990.

[2.42]   R. McLelland, "Earlier detection of breast cancer: An overview," *Recent Results Cancer Res.*, vol. 119, pp. 10-17, 1990.

[2.43]   A. Mühlow, "A device for precision needle biopsy of the breast at mammography," *AJR*, vol. 121, pp. 843-845, 1974.

[2.44]   B. Nordenström, "Stereotaxic crew needle biopsy of nonpalpable breast lesions," In *Breast Carcinoma: The Radiologist's Expanded Role*, W. Logan , Ed., New York, NY: John Wiley & Sons, 1977, pp. 313-318.

[2.45]   R. Novak, "A method for control of the target at aspiration biopsy of nonpalpable breast lesions," *Acta Radiol. [Diagn.] (Stockh.)*, vol. 27, pp. 65-70, 1986.

[2.46]   J. W. Oestmann, D. Kopans, D. A. Hall, K. A. McCarthy, J. R. Rubens and R. Greene, "A comparison of digitized storage phosphors and conventional mammography in the detection of malignant microcalcifications," *Invest. Radiol.*, vol. 23, pp. 725-728, 1988.

[2.47]   S. H. Parker, K. D. Hopper, W. F. Yakes, M. D. Gibson, J. L. Ownbey and T. E. Carter, "Image-directed percutaneous biopsies with a biopsy gun," *Radiology*, vol. 171, pp. 663-669, 1989.

[2.48]   S. H. Parker, J. D. Lovin, W. E. Jobe, J. M. Luethke, K. D. Hopper, W. F. Yakes and B. J. Burke, "Stereotactic breast biopsy with a biopsy gun," *Radiology*, vol. 176, pp. 741-747, 1990.

[2.49]   S. H. Parker, J. D. Lovin, W. E. Jobe, B. J. Burke, K. D. Hopper and W. F. Yakes, "Nonpalpable breast lesions: Stereotactic automated large-core biopsies," *Radiology*, vol. 180, pp. 403-407, 1991.

[2.50]   N. J. Robert, "Biological indicators of prognosis in breast cancer," *Hospital Practice*, vol. 25, pp. 93-102, 1990.

[2.51]   D. R. Salter and A. A. Bassett, "Role of needle aspiration in reducing the number of unnecessary breast biopsies," *Can. J. Surg.*, vol. 24, pp. 311-313, 1981.

[2.52]   S. Shapiro, "The status of breast cancer screening: A quarter of a century of research," *World J. Surg.*, vol. 13, pp. 9-18, 1989.

[2.53]   E. A. Sickles, "The usefuleness of computers in managing the operation of a mammography screening practice," *AJR*, vol. 155, pp. 755-761, 1990.

[2.54]   E. A. Sickles, "Imaging techniques other than mammography for the detection and diagnosis of breast cancer," *Recent Results Cancer Res.*, vol. 119, pp. 127-135, 1990.

[2.55]   E. Silverberg, C. C. Boring and T. S. Squires, "Cancer statistics, 1990," *Ca*, vol. 40, pp. 9-26, 1990.

[2.56]   E. Silverberg and J. A. Lubera, "Cancer statistics, 1988," *Ca*, vol. 38, pp. 5-22, 1988.

[2.57]   E. Silverberg and J. A. Lubera, "Cancer statistics, 1989," *Ca*, vol. 39, pp. 3-20, 1989.

[2.58]   P. Skrabanek, "Shadows over screening mammography," *Clin. Radiol.*, vol. 40, pp. 4-5, 1989.

[2.59]   R. G. Somers, G. P. Young, M. J. Kaplan, V. M. Bernhard, M. Rosenberg and D. Somers, "Fine needle aspiration biopsy in the management of solid breast tumors," *Arch. Surg.*, vol. 120, pp. 673-677, 1985.

[2.60]   G. Svane, "Stereotaxic needle biopsy of nonpalpable breast lesions: A clinical and radiologic follow-up," *Acta Radiol. [Diagn.] (Stockh.)*, vol. 24, pp. 385-390, 1983.

[2.61]   G. Svane and C. Silfverswärd, "Stereotaxic needle biopsy of non-palpable breast lesions: Cytologic and histopthologic findings," *Acta Radiol. [Diagn.] (Stockh.)*, vol. 24, pp. 283-288, 1983.

[2.62]   L. Tabár, "Control of breast cancer through screening mammography," *Radiology*, vol. 174, pp. 655-656, 1990.

[2.63]   M. W. Vannier, R. L. Butterfield, D. L. Rickman, D. M. Jordon, W. A. Murphy and P. R. Biondetti, "Multispectral magnetic resonance image analysis," *CRC Critic. Rev. Biomed. Eng.*, vol. 15, pp. 117-144, 1987.

[2.64]   R. L. Wahl, T. L. Cody, G. D. Hutchins and E. E. Mudgett, "Primary and metastatic breast carcinoma: Initial clinical evaluation with PET with the radiolabeled glucose analogue 2-[F-18]-fluoro-2-deoxy-D-glucose," *Radiology*, vol. 179, pp. 765-770, 1991.

[2.65]   H. J. Wanebo, P. S. Feldman, M. C. Wilhelm, J. L. Covell and R. L. Binns, "Fine needle aspiration cytology in lieu of open biopsy in management of primary breast cancer," *Ann. Surg.*, vol. 199, pp. 569-579, 1984.

[2.66]   G. P. Young, R. G. Somers, I. Young, M. Kaplan and D. F. Cowan, "Experience with a modified fine needle aspiration biopsy technique in 533 breast cases," *Diagn. Cytopathol.*, vol. 2, pp. 91-98, 1986.

[2.67]   X. Zhou and R. Gordon, "Detection of early breast cancer: An overview and future prospects," *CRC Critic. Rev. Biomed. Eng.*, vol. 17, pp. 203-255, 1989.

CHAPTER 3
GEOMETRIC UNWARPING FOR DIGITAL SUBTRACTION MAMMOGRAPHY

3.1. Introduction

The problem of serial image evaluation for detecting serial changes over images in biomedical applications has been addressed by several investigators, such as Bookstein [3.15]-[3.18], Cheverud [3.20],[3.21], and Thompson [3.55]. Three-dimensional (3D) mammographic images taken some time apart could be subtracted to bring out changes that might be due to small, slowly growing breast carcinomas [3.27],[3.58],[3.59]. However, registration of multitemporal (longitudinal) breast images is sometimes difficult because of the global deformation, or "warping", that follows from our inability to position a breast exactly the same way twice in any instrument, and from changes during the menstrual cycle, aging, etc. Therefore, it is necessary to find the 3D transformation or "geometric warping" T that relates an earlier (*reference*) image to a current (*warped*) one. We call its inverse transformation T^{-1} a "geometric unwarping".

In order to estimate the transformation T, we start with pairs of corresponding points between the warped and reference images. (However, there may exist alternative methods for estimating the transformation without knowing corresponding points.) We will show, in Chapter 5, how pairs of "control points" (or landmarks, homologous points, fiducial marks), i.e., features which are visible or can be defined unambiguously, and whose coordinates can be determined in both images, could be extracted from two images by local mammographic feature matching. For now, we will take the control points as given or

estimate them by eye. Note that control points may, in a general sense, represent some specific features although they are chosen as simple geometric elements in this study.

If a sufficient number of pairs of control points in the two images could be determined, then the images could be accurately registered over their whole extent. This chapter will address optimal geometric interpolation between and extrapolation from control points. The optimal pixel intensity (grey level) interpolation algorithms, and the selection and number of control points will be covered in Chapter 4 and Chapter 5, respectively.

Production of 3D mammographic images itself needs new approaches, and 2D mammographic images are currently obtainable through CT scanning of the breast. It is rational and appropriate to first work out the methodology of finding the geometric transformation in two dimensions and then generalize these 2D algorithms to three dimensions. All the derivations of geometric unwarping algorithms in this thesis are presented in two dimensions. Generalization of these 2D results to 3D will be discussed in Chapter 7.

We will use (x, y) and (u, v) to designate the coordinates of the reference and warped images, respectively. The *unwarped image* will be designated by coordinates (x^*, y^*). These relationships can be represented by the following notations (Fig. 3.1.1)

$$(u, v) = T(x, y) \quad \text{and} \quad (x^*, y^*) = T^{-1}(u, v). \tag{3.1.1}$$

Since the form and amount of geometric distortion between two images may not be known, it seems acceptable to use polynomials to represent the transformation T [3.35], [3.38],[3.52],[3.57]. Adams *et al.* [3.1] presented hardware for geometric unwarping, in which a global quadratic warping function is used to correct the pixel coordinates, i.e., a single set of transformation functions is used to register the whole image. This approach may become too complicated to manage as the degree of the polynomial increases, and polynomials of higher degree sometimes exhibit excessive spatial undulations. In many images, geometric distortions are mainly due to local factors such as topographic elevation
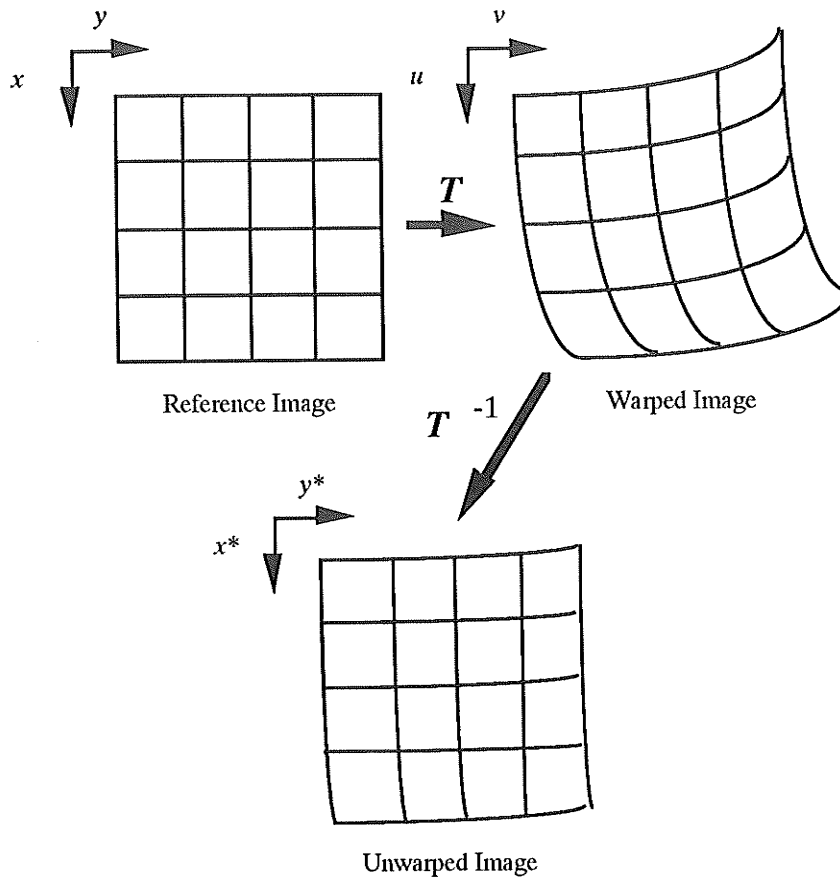
Fig. 3.1.1. The relationship between geometric warping and unwarping. A grid representing a reference image which is warped by the transformation T. A numerical approximation to T^{-1}, produces the unwarped image, which is then similar to, but generally not identical to, the reference image.

[3.46], sensor nonlinearity [3.32], fixation artifacts requiring "microregistration" in electron microscopy [3.53],[3.54], breast compression [3.12], physiological factors mentioned above, etc. Therefore, geometric unwarping methods based on locally defined transformation functions are potentially more accurate in these cases. By defining a set of contiguous quadrilaterals or triangles across the image made by connecting neighboring control points, and allowing a different polynomial transformation within each, we can represent a complex transformation function T as a simple piecewise approximation. This piecewise distortion modeling technique has been applied extensively to severely distorted

planetary spacecraft images [3.19]. Similar piecewise mapping methods [3.28],[3.29] were also reported recently.

In the field of computer aided geometric design (CAGD), surface representation and approximation problems have been studied extensively. For a comprehensive survey, see Barnhill [3.7]. C^0, C^1 and C^2 continuous rectangular and non-rectangular interpolants have been investigated and are currently used. In applications such as geometric unwarping, it is difficult or impracticable to restrict control points to those on rectangular grids. Triangular interpolants or distance-weighted interpolants have to be used instead [3.6]. (In cases such as these multi-stage methods have also been suggested [3.11],[3.25],[3.47]. Part of the motivation for multi-stage interpolation is that some methods that apply directly to ungridded data give undesirable results or are inefficient when the number of data points is large. On the other hand, many methods that are accurate and efficient only apply to data on regular grids.) In the following, we show how the unwarping problem can be solved by surface approximation approaches using one stage triangular interpolants, yielding what we call the *local geometric unwarping method.*

3.2. Geometric Unwarping Methods

3.2.1. The Geometric Unwarping Problem

The 2D geometric unwarping problem can be stated as follows: Given the coordinates for N pairs of control points in two images of the same scene, $\{(x_i, y_i), (u_i, v_i), i = 1, 2,..., N\}$, estimate the geometric unwarping transformation T^{-1} that will produce (x^*, y^*) $\approx (x, y)$ to a good approximation over the common domain of the reference and unwarped images. It is not sufficient to just calculate the geometric correspondence of points in the reference and unwarped images. If we designate their intensities as $f(x, y)$ and $f^*(x^*, y^*)$ then we also require, at corresponding points, that $f(x, y) \approx f^*(x^*, y^*)$. Note that f^* is

generated by intensity interpolation from $g(u, v)$, where g designates the intensity values of the warped image. This process of matching the coordinates and correcting the intensities is called *registration* of the reference and unwarped images [3.43]. When the whole procedure is simulated, an additional interpolation procedure must be applied to the grey levels of the reference image to produce the warped image, which is discussed in Chapter 4.

3.2.2. Geometric Unwarping Algorithms

Consider the determination of the geometric unwarping functions x^* and y^* (3.1.1). Let **D** be a domain in the u-v plane, and suppose x^* and y^* are defined on **D**. Suppose we are given the coordinate values $x_i = x^*(u_i, v_i)$ and $y_i = y^*(u_i, v_i)$ at some set of control points (u_i, v_i) located in **D**, for $i = 1, 2, ..., N$. Our problem is to find functions x^* and y^* defined on **D** which reasonably approximate the reference coordinates (x, y). The determination of the geometric unwarping function x^* (and similarly y^*) consists of the following steps:

(1) Partition the convex hull[1] of the set of control points into triangles by connecting neighboring control points with noncrossing line segments, forming a planar graph[2].

(2) Estimate partial derivatives of x^* with respect to u and v at each of the control points using the data values on either a set of nearby control points within a given neighborhood (a local method) or all of the control points (a global method).

---

[1] A domain D is *convex* if, for any two points p and q in D, the straight line segment pq is entirely contained in D. The *convex hull* of a set of points S is the boundary of such a smallest convex domain containing S [3.44].

[2] A graph G = (V, E) (vertex set V, edge set E) is *planar* if it can be embedded in the plane without crossings [3.44].

(3) For an arbitrary point (u, v) in the convex hull of the set of the control points, determine which triangle contains the point (point-inclusion problem[1]), and calculate an interpolated value $x^*(u, v)$ using an appropriate interpolant over triangles. Capability of extrapolation for a point outside the convex hull should also be provided.

The geometric unwarping procedure ends by resampling of the grey values $g(u, v)$ of the warped image (u, v) by the unwarping functions (x^*, y^*) which are obtained above and their interpolation to give new grey values $f^*(x^*, y^*)$.

3.2.3. Delaunay Triangulation

Given a set of N distinct points, a triangulation which covers the convex hull of the data points can be constructed. In many applications it is desirable to have triangles as "equilateral" as possible. In most cases interpolation over equilateral triangles produces better results than that over thin (or obtuse) ones. The optimal triangulation can be obtained by initially creating an arbitrary triangulation of the data and then optimizing it by reassigning edges using various criteria. Lawson [3.34] has given three optimal criteria: the max-min angle criterion, circle criterion and Thiessen region criterion. In computational geometry, Thiessen regions are also referred to as Delaunay, Dirichlet and Voronoi regions. The corresponding triangulation is usually referred to as a Delaunay triangulation. For a review of properties of Voronoi tessellation [3.56] and Delaunay triangulation [3.22], see Lee and Schachter [3.36]. Triangulation can also be done by the divide-and-conquer approach [3.36],[3.37] and recursive algorithms [3.30],[3.36]. In our study, the Lawson's triangulation algorithm with the max-min angle criterion was used.

---

[1] *Point-inclusion problem* consists of identifying the region, a partition of the geometric space, the point lies in. The difficulty will essentially depend on the nature of the space and of its partition [3.44].

3.2.4. Triangular Interpolants

For C^0 interpolation methods only positional data about the control points is used to calculate the unwarping functions. There is a need to estimate the partial derivatives $(\frac{\partial x^*}{\partial u}, \frac{\partial y^*}{\partial u}, \frac{\partial x^*}{\partial v}, \frac{\partial y^*}{\partial v},$ etc.) to approximate the bivariate functions x^* and y^* when C^1 and C^2 or smoother methods are to be used. A simple method would be to fit a quadratic bivariate polynomial to each cluster of n points consisting of a point $\mathbf{P}_0$ and five of its nearest neighbors (not necessarily sharing an edge with $\mathbf{P}_0$) and then determine the partial derivatives of the resultant polynomial at point $\mathbf{P}_0$. By a weighted least squares technique more accurate estimates can be obtained for $n \geq 6$ points.

Akima [3.2] proposed the following approach. To estimate the partial derivatives at point $\mathbf{P}_0$ using $\mathbf{P}_0$ and its m nearest points $\mathbf{P}_1$, $\mathbf{P}_2$, ..., $\mathbf{P}_m$, form vector products $\mathbf{V}_{ij} = (\mathbf{P}_0 - \mathbf{P}_i) \times (\mathbf{P}_0 - \mathbf{P}_j)$, $i, j = 1, ...\ m$, where $\mathbf{P}_1$, $\mathbf{P}_2$, ..., $\mathbf{P}_m$ are arranged to be counterclockwise about point $\mathbf{P}_0$. The vector sum $\mathbf{V}$ of all $\mathbf{V}_{ij}$'s is calculated. Finally, the partial first derivatives are estimated from the slopes of a plane which is normal to the vector sum. A similar procedure was used by Klucewicz [3.33]. In a later paper Akima [3.3] further suggested an improvement by weighting the contribution of each triangle: a small weight was given to the contribution of a large triangle or a thin triangle when the vector sum was calculated. Barnhill [3.7] proposed three useful methods for the estimation of derivative data. Stead [3.51] made an experimental comparison of different derivative estimation techniques. For an overview of methods for estimation of partial derivatives, see Nielson and Franke [3.39]. The improved Akima method for estimation of partial derivatives was used in this study.

Smooth, finite dimensional interpolants over triangles have been known for more than 20 years. Their practical uses have been as "finite elements." Many triangular interpolants are polynomial [3.2],[3.33],[3.41],[3.42], while the Coons and Bernstein-Bezier

representation [3.8],[3.9],[3.24], as well as triangular splines [3.13],[3.14],[3.26], have also been reported.

The simplest C^0 interpolation over triangles can be stated as follows. Given three 3D points (x_i, y_i, z_i) for $i = 1$, 2 and 3, where z_i is the function value at point (x_i, y_i), determine parameters of the plane which pass through these points. For any point (x, y) which is inside the triangle, the value z can be calculated from this plane.

There are two widely known C^1 triangular interpolants: the 21 parameter quintic and the Clough-Tocher triangle. Akima [3.2] used the former interpolant for bivariate interpolation and surface fitting from irregularly distributed data. The proof of smoothness of the quintic interpolation along the side of the triangle was also given in [3.2]. This interpolation method was tested here for the geometric unwarping problem. Goshtasby [3.29] used the Clough-Tocher triangular interpolant for the mapping procedures. Barnhill [3.5] wrote a complete review on triangular interpolants.

The capability of extrapolating outside the convex hull of data points is desirable, especially since we cannot expect to use control points on the skin of the breast. An exterior point lies in either a semi-infinite rectangle or a semi-infinite triangle defined by the lines which pass through the boundary data points and are perpendicular to the boundary edges. For the quintic approach, a polynomial which is quintic in the variable measured in the direction of the border line segment and quadratic in the distance from the line segment is used for extrapolation into the semi-infinite rectangle. A bivariate quadratic polynomial which smoothly connects to the two polynomials in the neighboring semi-infinite rectangles is used for extrapolation into the semi-infinite triangles. In the linear approximation approach, however, the plane which is just the extension of the border triangular plane, and the plane which passes the boundary data point and connects the neighboring rectangular planes, are used in the semi-infinite rectangle and semi-infinite triangle, respectively (Fig. 3.2.1).

Control Point P_{i-1}

Convex Hull
Boundary

Semi-infinite
Rectangle

Control Point P_i

Control Point P_{i+1}

Semi-infinite
Triangle

Picture Boundary
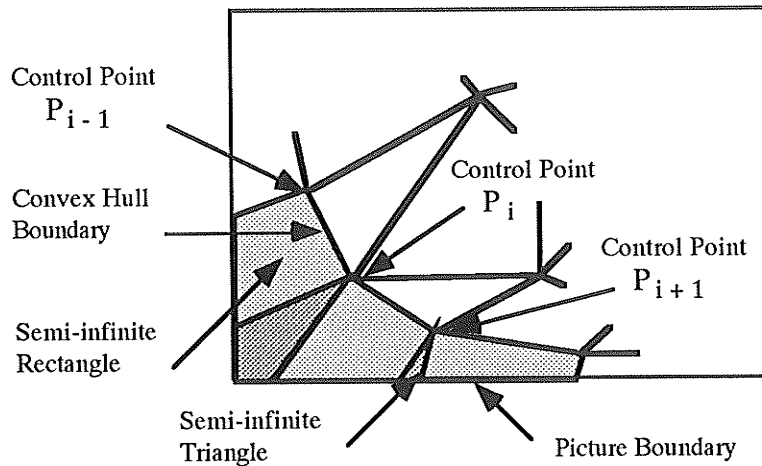
Fig. 3.2.1. Partition of the exterior region into semi-infinite rectangles and triangles.

3.3. Digital Subtraction Mammography

3.3.1. Breast Tissue Images for Testing Unwarping Methods

We tested the unwarping algorithms using CT images of real breast tissue. It was important to use CT images rather than projection radiographs, because the CT images have pixel values which are proportional to local tissue density rather than line integrals of density. If projection radiographs are taken before and after mechanical distortion of a tissue sample, there will generally not be an unwarping function that will map the second image onto the first because of differential motion of tissue structure in different planes perpendicular to the imaging direction. With CT images, there is always a one-to-one relationship between structure in images of distorted and undistorted tissue.

The complication that comes into play with CT is that structure can sometimes move out of a given slice plane following distortion, and ultimately this will require a 3D approach using a set of contiguous CT slices and true 3D unwarping for relating a set of contiguous images taken after distortion to a set taken before. That is the goal toward which our work is directed, and full sets of contiguous images were taken during the laboratory phase of

this project, but for now we settle for 2D analysis of the images which were taken in the following manner.

Using a unique high-resolution "Micro-CT" X-ray scanner[1] [3.48],[3.49], we took a set of contiguous CT images of a sample of fixed human breast tissue before and after mechanical distortion. The distortion was accomplished through compression[2] with a mechanism illustrated schematically in Fig. 3.3.1. The CT images have 50-μm pixels representing tissue density averaged over a 0.4-mm "slice thickness". A 5-cm imaging field is represented by 1024 x 1024 images whose pixel values have 12 bits of resolution, and
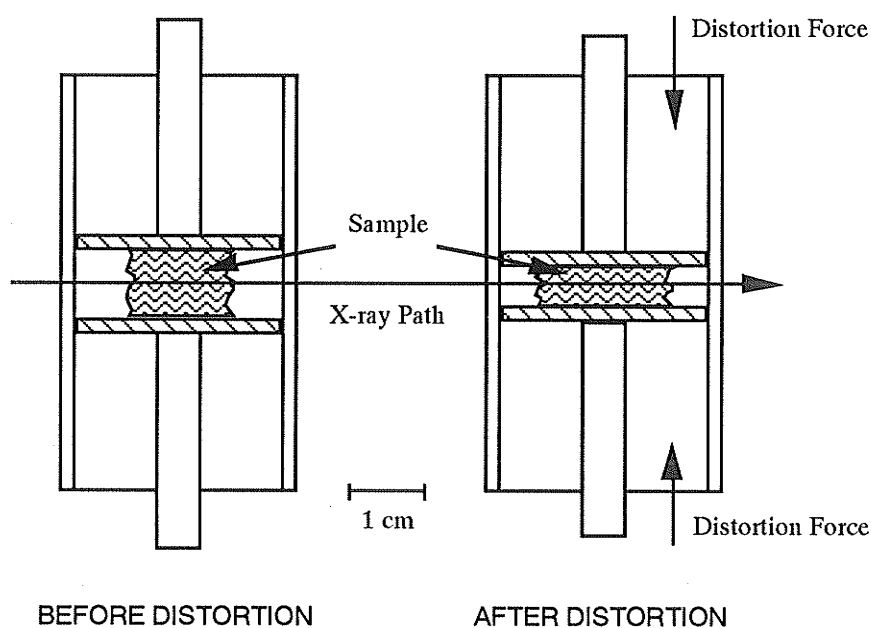
Fig. 3.3.1. A miniature breast tissue compression apparatus.

each image is reconstructed from 2000 projections using a convolution-and-backprojection algorithm.

Our unwarping calculations were performed on a Macintosh II computer using a digital image processing package written in C. In order to make the CT images comply with formatting requirements of this system, the parts of the images covering the tissue samples were compressed to 128 x 128 pixels with 8-bit density resolution. Each pixel then represented 0.2 x 0.2 mm^2 in the slice plane of the breast tissue specimen.

3.3.2. Method of Evaluating Unwarping Tests

Visual evaluation of the unwarped images against the reference images is straightforward, but subjective. For quantitative evaluation, two types of error measures are used: one for intensity and one for geometry. The intensity error measures I used are:

$$\text{correlation coefficient} \quad \varepsilon_1 = \frac{\sum\limits_{i=1}^{N} (f_i - \bar{f})(f_i^* - \bar{f^*})}{\left[\left(\sum\limits_{i=1}^{N} (f_i - \bar{f})^2\right)\left(\sum\limits_{i=1}^{N} (f_i^* - \bar{f^*})^2\right)\right]^{1/2}}$$

$$\text{Euclidean distance} \quad \varepsilon_2 = \left[\frac{1}{N} \sum\limits_{i=1}^{N} (f_i - f_i^*)^2\right]^{1/2}$$

$$\text{maximum difference} \quad \varepsilon_3 = \max_{1 \le i \le N} \left| f_i - f_i^* \right|$$

$$\text{average difference} \quad \varepsilon_4 = \bar{d} = \frac{1}{N} \sum\limits_{i=1}^{N} d_i$$

$$\text{standard deviation} \quad \varepsilon_5 = \left[\frac{1}{N-1} \sum\limits_{i=1}^{N} (d_i - \bar{d})^2\right]^{1/2}$$

$$\text{grey level entropy} \quad \varepsilon_6 = -\sum\limits_{i=0}^{L-1} h_i \log_2 h_i$$

(3.3.1)

where N is the total number of pixels in either image; f_i and f^*_i represent the pixel intensity in the reference and unwarped images, respectively; $d_i = |f_i - f^*_i|$ is the intensity difference; and h_i, $i = 0, 1,..., L\text{-}1$, are the frequencies of occurrence of the L grey levels [3.31].

For the tests in which the distorted image is generated analytically from the reference image, the true unwarping function is known exactly and we are able to calculate the geometric error measures. The following error measures give a reasonable description of the geometric performance of unwarping procedures:

$$\text{correlation coefficient} \quad \delta_1 = \frac{\sum_{i=1}^{N} (r_i - \bar{r})(r^*_i - \bar{r^*})}{\left[\left(\sum_{i=1}^{N} (r_i - \bar{r})^2\right)\left(\sum_{i=1}^{N} (r^*_i - \bar{r^*})^2\right)\right]^{1/2}}$$

$$\text{Euclidean distance} \quad \delta_2 = \left[\frac{1}{N}\sum_{i=1}^{N} (r_i - r^*_i)^2\right]^{1/2} \quad\quad (3.3.2)$$

$$\text{average difference} \quad \delta_3 = \frac{1}{N}\sum_{i=1}^{N} \left|r_i - r^*_i\right|$$

$$\text{maximum difference} \quad \delta_4 = \max_{1 \le i \le N} \left|r_i - r^*_i\right|$$

where N is the total number of pixels in the unwarped image; $r_i = (x_i^2 + y_i^2)^{1/2}$ and $r^*_i = (x^{*2}_i + y^{*2}_i)^{1/2}$ are the distances from the origin to points (x_i, y_i), and (x^*_i, y^*_i), respectively; and (x_i, y_i) and (x^*_i, y^*_i) represent coordinates of pixels in the unwarped image which are determined by the analytic, known unwarping functions, and numerical approaches, respectively. We will also examine the horizontal and vertical geometric error measures, which are defined by substituting r_i and r^*_i in (3.3.2) by x_i and x^*_i, and by y_i and y^*_i, respectively.

Note that these measures emphasize different aspects of image quality. The *correlation coefficient* ε_1 measures the extent to which two images are similar to each other. The

number ε_2 is the Euclidean distance criterion. The measure ε_3 yields the largest difference between the reference and the unwarped images. While the mean value ε_4 gives a shift of mean value after each subtraction, the *standard deviation* ε_5 measures the magnitudes of the intensity deviations from the mean value. The measure ε_6 reveals the *grey level entropy* or average information per grey level by the average value of the information contained in each possible level [3.31]. The δ_1, δ_2, δ_3, and δ_4 measures have similar explanations to those for ε_1, ε_2, ε_3, and ε_4 measures.

The correlation coefficient measure takes the highest possible value of 1 if two images are exactly the same. Other measures tend toward zero as the two images approach each other. However, the warning must be heeded that rank-ordering algorithm performances based upon a single measure can be very misleading, since a single number or even a set of numbers cannot possibly measure all the aspects in which two images may differ from each other.

3.3.3. Results with Simulated Images of Distorted Breast Tissue

Two types of tests were made with our CT images. In both classes of tests, one of the images taken before mechanical distortion was chosen as a reference image. In the first class of tests, a warped image of the same tissue after "simulated distortion" was made from the reference image by an analytic transformation. The advantage of this test is that our precise knowledge of the transformation allows an exact analysis of the geometric accuracy of any unwarping algorithm. In the second type of test, unwarping algorithms are applied to a real warped image taken after mechanical distortion of the tissue for comparison with its reference image. This test is more difficult and more realistic.

A reference image of a mastectomy sample (Fig. 3.3.2) was transformed by using the following piecewise functions

$$u(x) = \frac{u_{i+1} - u_i}{2} \sin\left[\frac{\pi}{x_{i+1} - x_i}\left(x - \frac{x_{i+1} + x_i}{2}\right)\right] + \frac{u_{i+1} + u_i}{2}, \text{ for } x_i \le x \le x_{i+1}$$

$$v(y) = \frac{v_{i+1} - v_i}{2} \sin\left[\frac{\pi}{y_{i+1} - y_i}\left(y - \frac{y_{i+1} + y_i}{2}\right)\right] + \frac{v_{i+1} + v_i}{2}, \text{ for } y_i \le y \le y_{i+1} \quad (3.3.3)$$

GEOMETRIC COORDINATES
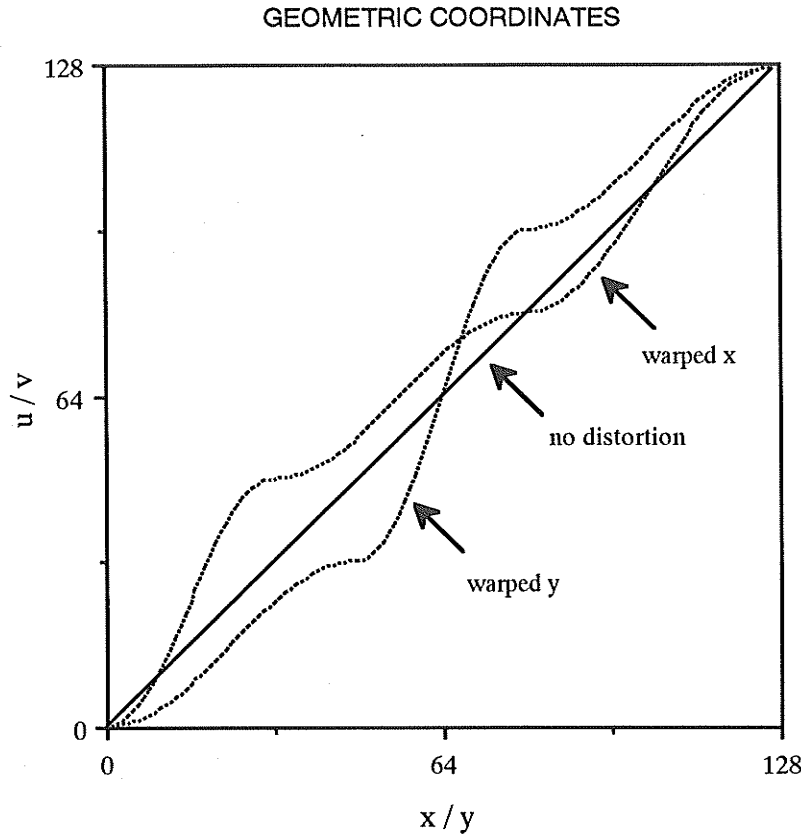
Fig. 3.3.2. Simulated geometric warping functions (3.3.3): warped x coordinates along the central horizontal line, and warped y coordinates along the central vertical line.

with known node parameters $\{(x_i, y_i), (u_i, v_i)\}$ for $i = 1, 2, ..., p$, where p is the number of node parameters used to generate the warping functions. With this set of functions we can generate warping transformation functions with specified complexity and considerable local variation in the transformation. Coordinates of control points in the reference image were chosen manually, approximately on an equilateral, triangular grid, and those in the

warped image were calculated by the above functions. The analytic unwarping functions derived from (3.3.3) are as follows:

$$x^*(u) = \frac{x^*_{i+1} - x^*_i}{\pi} \sin^{-1}\left[\frac{2}{u_{i+1} - u_i}\left(u - \frac{u_{i+1} + u_i}{2}\right)\right] + \frac{x^*_{i+1} + x^*_i}{2}, \text{ for } u_i \leq u \leq u_{i+1}$$

$$y^*(v) = \frac{y^*_{i+1} - y^*_i}{\pi} \sin^{-1}\left[\frac{2}{v_{i+1} - v_i}\left(v - \frac{v_{i+1} + v_i}{2}\right)\right] + \frac{y^*_{i+1} + y^*_i}{2}, \text{ for } v_i \leq v \leq v_{i+1}.$$

(3.3.4)

The reference and warped images from the above set of warping functions (see Fig. 3.3.2) are shown in Fig. 3.3.3. The unwarped image was obtained by the local quintic unwarping procedure using 81 pairs of control points in the reference and warped images for Fig. 3.3.4(b), which shows the difference image that is obtained by subtracting the unwarped image from the reference image. The difference image with unwarping by the local linear unwarping method is given in Fig. 3.3.4(c). For comparison we show in Figs. 3.3.4(a) and (g) the difference images of the reference and unwarped image by the analytical method, and of the reference and warped image only, respectively.

(a)

(b)
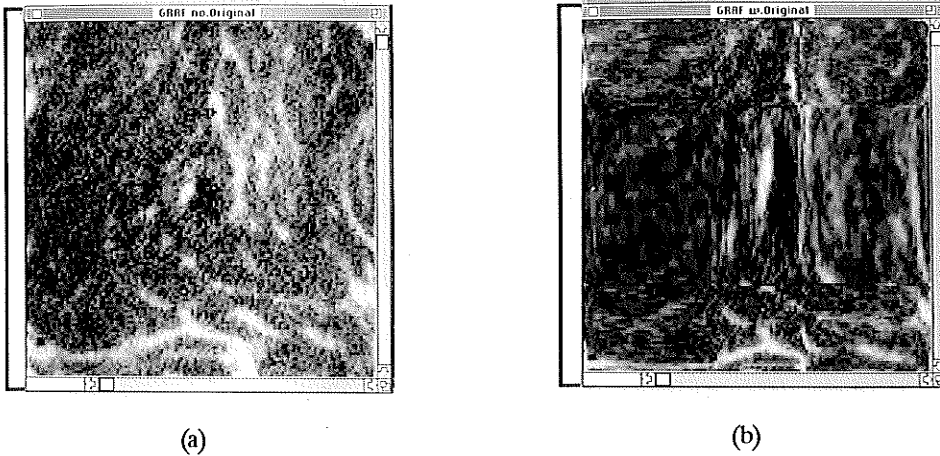
Fig. 3.3.3. (a) A reference image. (b) An artificially warped version of the reference, obtained by using analytical warping functions (Fig. 3.3.2) and linear intensity interpolation.
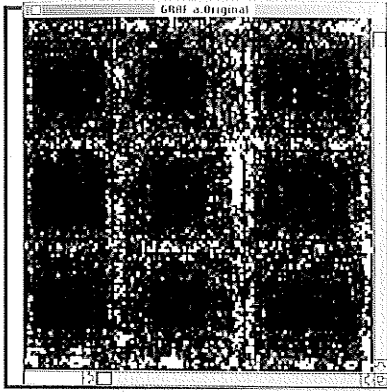
(a)
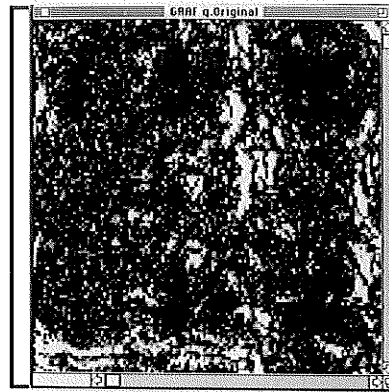
(b)

(c)
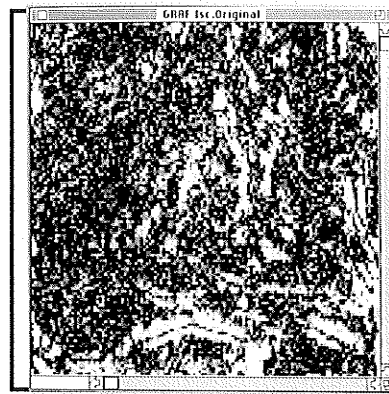
(d)
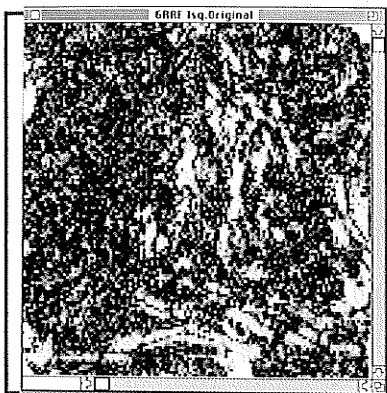
(e)
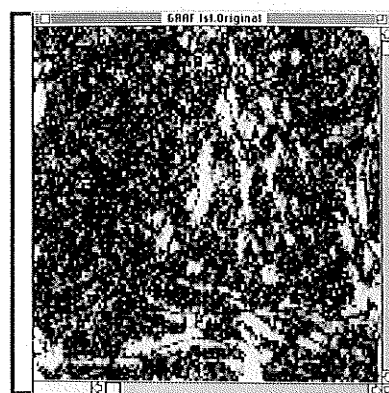
(f)
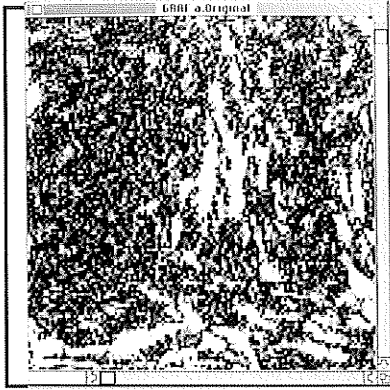
(g)

Fig. 3.3.4. Difference images of the reference image (Fig. 3.3.3(a)) and unwarped image obtained by (a) analytical unwarping functions, (b) local piecewise quintic, (c) local piecewise linear, (d) global least squares cubic, (e) global least squares quadratic, and (f) global least squares linear unwarping methods, respectively. The warped image is Fig. 3.3.3(b). Resampling of the warped image was done by linear interpolation. (g) Difference image of the reference image and warped image only (i.e., no attempt at unwarping). Pixel values in all difference images are absolute differences with black for 0 and white for a maximum difference of 83. Thus the full grey scale range is used, without clipping.

For global, polynomial interpolation methods parameters of cubic, quadratic and linear polynomials were obtained by using the least squares technique. The resultant difference images are shown in Figs. 3.3.4(d)-(f). The profile plots associated with these unwarping procedures are given in Fig. 3.3.5. The intensity and geometric measures for the unwarping procedures above are shown in Tables 3.3.1 and 3.3.2, respectively. The effect of different choices of control points on the unwarping procedure is illustrated in Tables 3.3.3 and 3.3.4.

UNWARPED COORDINATES

$$10 \log (1 + |x - x^*|)$$

(a)

UNWARPED COORDINATES

$$10 \log (1 + |y - y^*|)$$

(b)
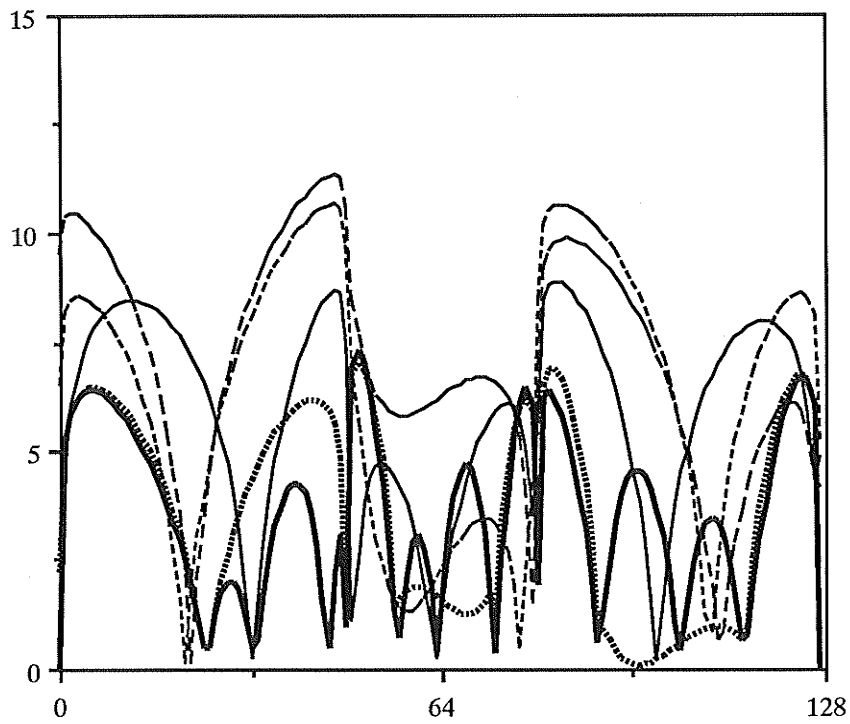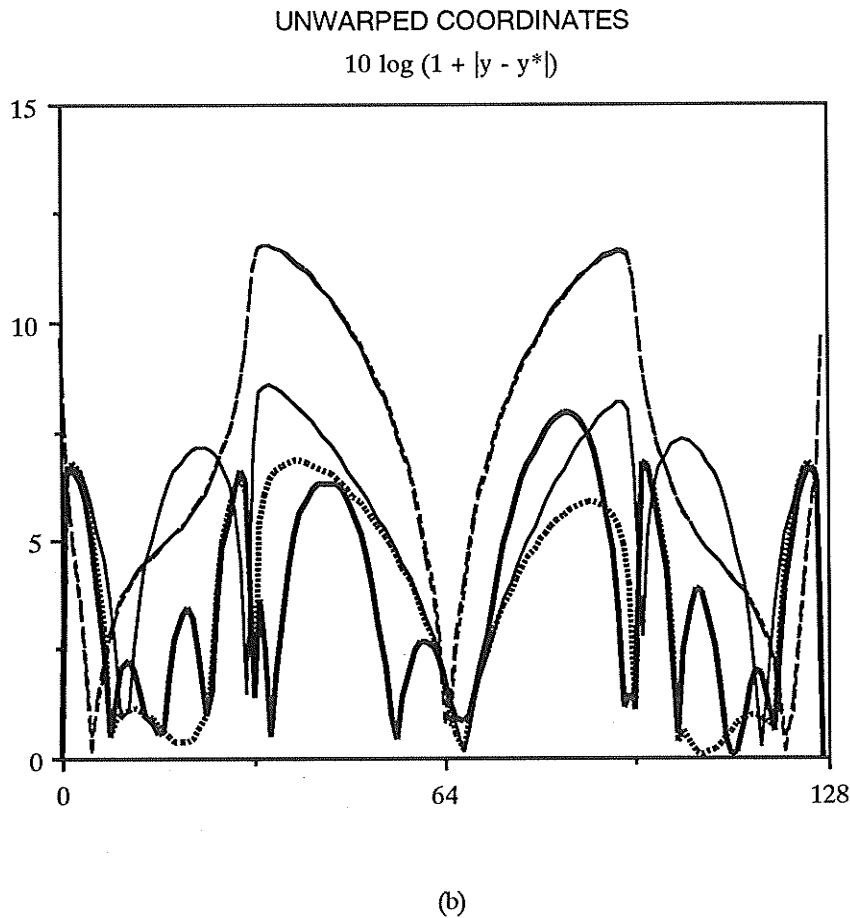
Fig. 3.3.5. Differences between the geometric unwarping functions and reference functions are displayed as the functions (a) $10 \log_{10} [1 + |x(u, v) - x^*(u, v)|]$ along the central horizontal line, and (b) $10 \log_{10} [1 + |y(u, v) - y^*(u, v)|]$ along the central vertical line, where $x(u, v)$ and $y(u, v)$ are calculated by the analytical unwarping functions, and $x^*(u, v)$ and $y^*(u, v)$ by five different unwarping methods with 81 control points. The use of nonlinear measure emphasizes the small differences.

Table 3.3.1. Intensity error measures (3.3.1) for simulated data (Fig. 3.3.3) with 81 control points

Unwarping Methods	Intensity Error Measures					
	ε_1	ε_2	ε_3	ε_4	ε_5	ε_6
Analytical	0.8983	19.54	153.0	13.02	14.57	5.174
Local Piecewise Quintic	0.6330	35.05	246.0	25.90	24.54	6.135
Local Piecewise Linear	0.5948	36.84	238.0	26.92	25.86	6.194
Global Least Squares Cubic	0.4409	42.75	220.0	32.15	28.95	6.436
Global Least Squares Quadratic	0.3878	42.33	260.0	32.16	29.28	6.391
Global Least Squares Linear	0.3569	42.80	265.0	32.71	30.16	6.382
None (warped only)	0.1994	47.65	253.0	37.48	35.46	6.658

Table 3.3.2. Geometric error measures (3.3.2) for simulated data (Fig. 3.3.3) with 81 control points

Unwarping Methods	Geometric Error Measures			
	δ_1	δ_2	δ_3	δ_4
Analytical	1.000000	0.000	0.000	0.000
Local Piecewise Quintic	0.999856	1.852	1.417	6.849
(horizontal*)	0.999698	1.895	1.417	5.106
(vertical**)	0.999606	2.168	1.550	6.304
Local Piecewise Linear	0.999796	2.227	1.654	8.569
(horizontal*)	0.999616	2.144	1.625	5.135
(vertical**)	0.999440	2.591	1.706	7.602
Global Least Squares Cubic	0.999163	4.463	3.517	13.83
(horizontal*)	0.998931	3.594	3.024	6.705
(vertical**)	0.997671	5.278	3.914	12.53
Global Least Squares Quadratic	0.998168	6.639	5.312	18.84
(horizontal*)	0.997498	5.431	4.386	10.70
(vertical**)	0.994824	7.910	6.354	16.56
Global Least Squares Linear	0.998237	6.565	5.238	19.24
(horizontal*)	0.997334	5.611	4.714	11.28
(vertical**)	0.994834	7.906	6.353	16.39

Note: * Horizontal error measures are defined by substituting r and r^* in 3.3.2 by x and x^*, respectively.

** Vertical ones are, however, defined by substituting r and r^* in 3.3.2 by y and y^*, respectively.

Table 3.3.3. Intensity error measures (3.3.1) for simulated data (Fig. 3.3.3) with different numbers of control points

Unwarping Methods		Intensity Error Measures					
(number of control points)		ε_1	ε_2	ε_3	ε_4	ε_5	ε_6
Analytical		0.8983	19.54	153.0	13.02	14.57	5.174
Local Piecewise Quintic	(7x7)	0.4264	43.06	236.0	32.32	29.96	6.447
	(9x9)	0.6330	35.05	246.0	25.90	24.54	6.135
	(10x10)	0.7563	29.16	199.0	21.12	20.49	5.846
Local Piecewise Linear	(7x7)	0.4495	42.34	235.0	31.58	29.25	6.415
	(9x9)	0.5948	36.84	238.0	26.92	25.86	6.194
	(10x10)	0.6936	32.25	238.0	23.32	22.89	5.997
Global Least Squares Cubic	(7x7)	0.4681	41.61	203.0	31.35	28.07	6.402
	(9x9)	0.4409	42.75	220.0	32.15	28.95	6.436
	(10x10)	0.4315	42.66	227.0	32.21	29.16	6.438
Global Least Squares Quadratic	(7x7)	0.3616	43.03	270.0	32.79	30.02	6.349
	(9x9)	0.3878	42.33	260.0	32.16	29.28	6.391
	(10x10)	0.3897	42.19	253.0	31.98	29.28	6.427
Global Least Squares Linear	(7x7)	0.3263	43.93	245.0	33.37	30.99	6.489
	(9x9)	0.3569	42.80	265.0	32.71	30.16	6.382
	(10x10)	0.3595	42.86	266.0	32.58	30.19	6.375
None (warped only)		0.1994	47.65	253.0	37.48	35.46	6.658

Table 3.3.4. Geometric error measures (3.3.2) for simulated data (Fig. 3.3.3) with different numbers of control points

Unwarping Methods		Geometric Error Measures			
(number of control points)		δ_1	δ_2	δ_3	δ_4
Analytical		1.000000	0.000	0.000	0.000
Local Piecewise Quintic	(7x7)	0.999498	3.491	2.701	12.46
	(9x9)	0.999856	1.852	1.417	6.849
	(10x10)	0.999964	0.938	0.726	4.026
Local Piecewise Linear	(7x7)	0.999439	3.728	2.799	13.03
	(9x9)	0.999796	2.227	1.654	8.569
	(10x10)	0.999923	1.391	1.010	5.377
Global Least Squares Cubic	(7x7)	0.999139	4.553	3.543	14.24
	(9x9)	0.999163	4.463	3.517	13.83
	(10x10)	0.999180	4.425	3.463	13.48
Global Least Squares Quadratic	(7x7)	0.998129	6.763	5.438	19.18
	(9x9)	0.998168	6.639	5.312	18.84
	(10x10)	0.998177	6.633	5.291	19.29
Global Least Squares Linear	(7x7)	0.998195	6.730	5.400	19.63
	(9x9)	0.998237	6.565	5.238	19.24
	(10x10)	0.998242	6.551	5.223	19.42

3.3.4. Results with Actual Images of Distorted Breast Tissue

We applied the geometric unwarping procedures to a true image of mechanically distorted breast tissue, which is shown in Fig. 3.3.6. Because of some out-of-plane warping, some texture features in one image are missing in the corresponding distorted image. This makes our test of real geometric unwarping more difficult than the above test

with the simulated data set. (This problem should vanish when we go to 3D unwarping.) We manually chose 42 pairs of corresponding texture features from the reference and warped images as the control points. The differences between the reference image and unwarped image made with different unwarping algorithms are shown in Fig. 3.3.7. In Table 3.3.5 we also present the intensity measures for these unwarping results.

(a)

(b)

(c)

(d)
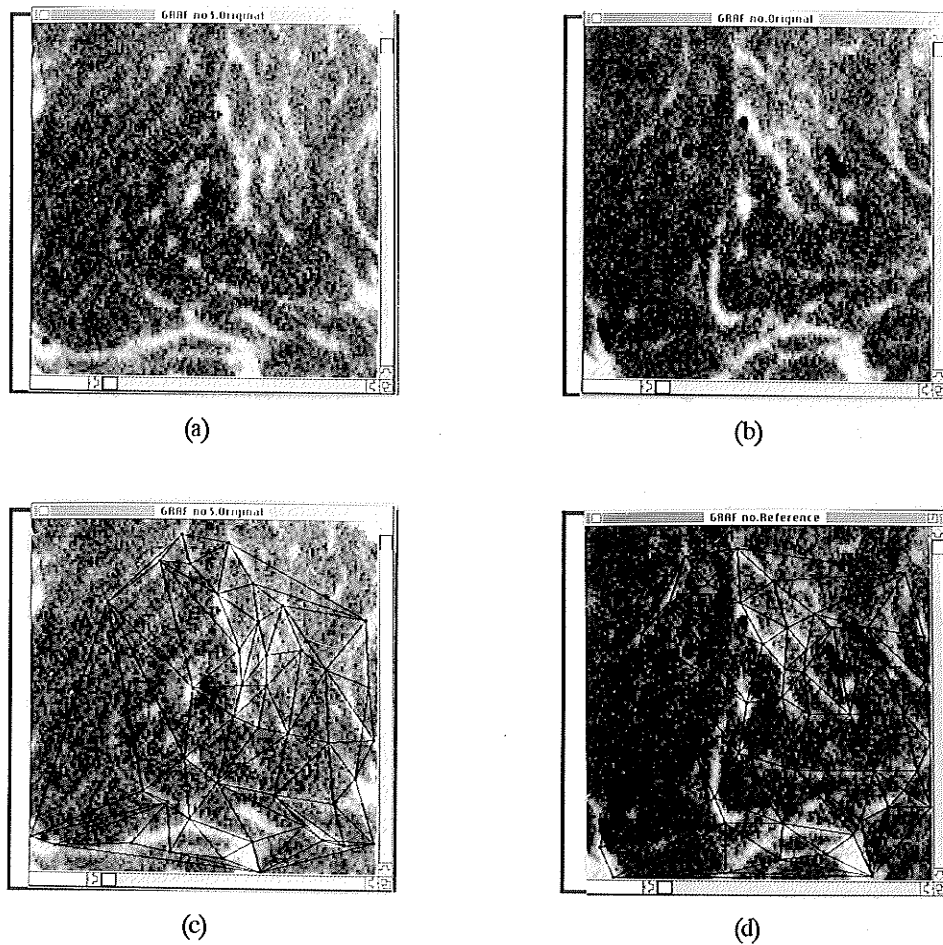
Fig. 3.3.6. (a) The reference image. (b) The image of mechanically distorted tissue. These images are obtained by reconstructing a mastectomy sample scanned with the AS&E Micro-CT scanner. In (c) and (d) 42 control points estimated by eye are shown, along with the triangles generated by Lawson's triangulation algorithm. The outermost edges of the triangular mesh in the reference image (c) form a convex hull.
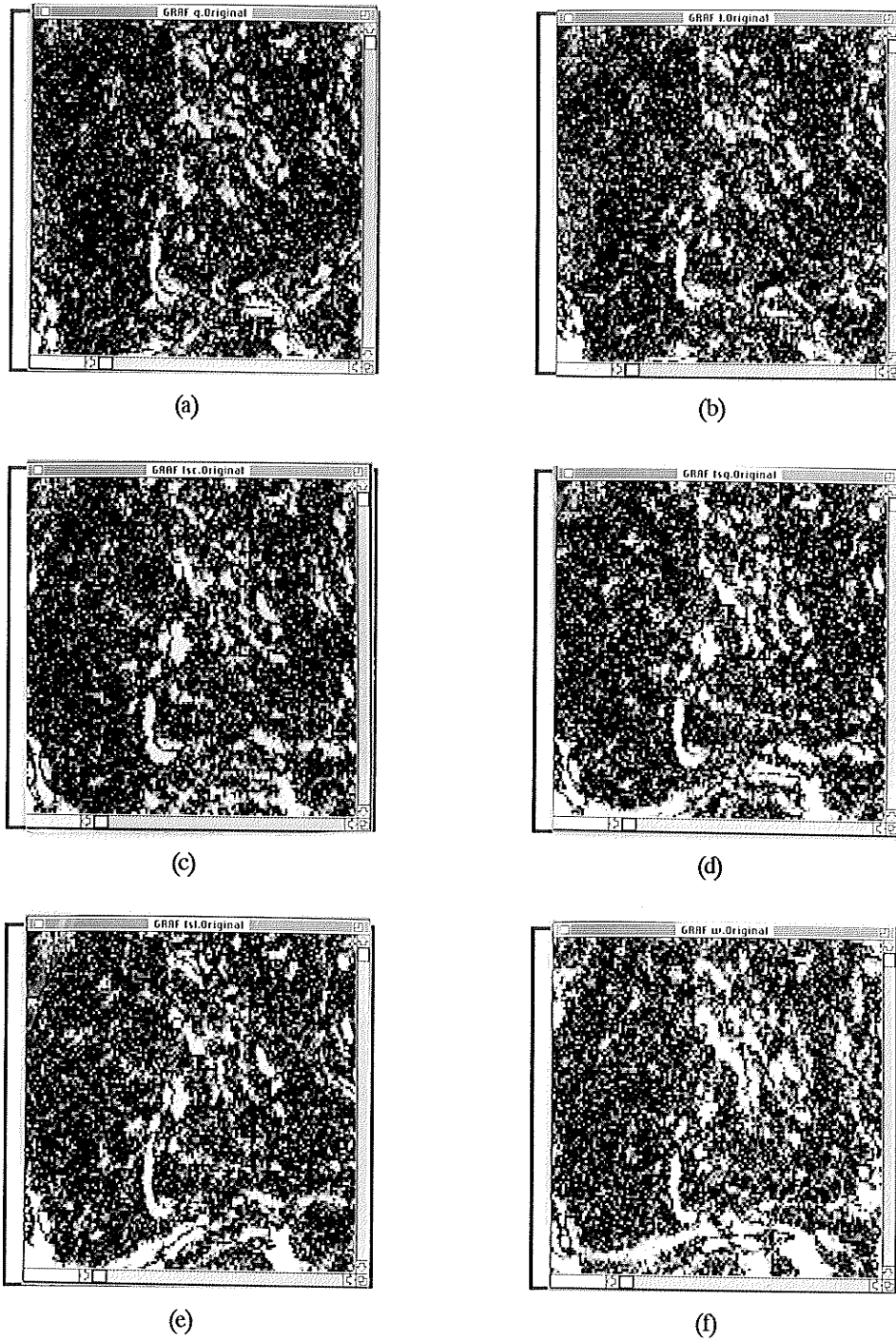
Fig. 3.3.7. The difference images of the reference image (Fig. 3.3.6(a)) and unwarped image obtained by (a) local piecewise quintic, (b) local piecewise linear, (c) global least squares cubic, (d) global least squares quadratic, and (e) global least squares linear unwarping methods, respectively. Resampling of the warped image was done by linear interpolation. (f) Difference image of the reference image and warped image only. Pixel values in all difference images are absolute differences with black for 0 and white for a maximum observed difference of 105, using the full grey scale range, without clipping.

Table 3.3.5. Intensity error measures (3.3.1) for mechanically distorted data (Fig. 3.3.6) with 42 control points

Unwarping Methods	Intensity Error Measures					
	ε_1	ε_2	ε_3	ε_4	ε_5	ε_6
Local Piecewise Quintic	0.5230	43.96	266.0	34.88	30.85	6.456
Local Piecewise Linear	0.5127	44.07	273.0	35.31	31.48	6.427
Global Least Squares Cubic	0.4662	45.45	367.0	36.69	34.06	6.015
Global Least Squares Quadratic	0.4145	47.46	315.0	37.71	35.48	6.283
Global Least Squares Linear	0.3977	45.90	288.0	37.67	35.50	6.433
None (warped only)	0.1806	53.66	312.0	46.54	42.83	6.602

3.4. Discussion and Conclusions

In building toward a system for detecting early breast cancers, we have investigated five different geometric unwarping methods for representing the transformation between an image and its warped version. We have evaluated each of these algorithms for accuracy in recovering a known test transformation and unwarping a real image taken after mechanical distortion.

It has been shown that for warping functions which do not have much local geometric distortion, the global cubic least squares method may produce better unwarping results than the local linear method [3.58]. However, for the warping functions used here, which have considerable local geometric distortion, we conclude that local unwarping techniques (even the local linear method) can produce better results than the global methods in terms of both intensity (Table 3.3.1) and geometric measures (Table 3.3.2). With all evaluation measures we used, the local quintic method is the best among these approaches.

From the point of view of intensity error measures, the local quintic algorithm does not necessarily produce better results than the local linear one, when the number of control points is less than a case-dependent number (between 49 and 81 in our first test example) (Table 3.3.3). In terms of geometric error measures, local methods with more control points produce much better results than those with fewer ones, and the local quintic algorithm meets evaluation criteria better than the local linear one (Table 3.3.4). For the global polynomial methods, however, the results obtained with more control points show no significant improvements at all, either in intensity or geometric error measures, and are not consistent from one measure to another (Tables 3.3.3 and 3.3.4). The entropy error measure is small when an unwarping algorithm produces good results, because it measures the information per grey level by the average value of information contained in each grey level. In other words, we need fewer numbers of bits to present better difference images. It is interesting and inexplicable to us that local unwarping methods produce smaller entropy measures with a higher order of polynomial but global ones have the reverse results (Tables 3.3.1 and 3.3.3). This effect may be produced by ripples (spatial undulations) in the higher order global polynomials.

The performance of different unwarping algorithms for mechanically distorted data, in terms of error measures, is consistent with that for simulated warping data, except for the entropy measure: for an unknown reason the local unwarping methods have larger entropy error measures than the global ones (Table 3.3.5), which is exactly the reverse of simulated data. Most features that are not aligned are actually those present in either reference or warped image, but not in both (Fig. 3.3.7). Because of this problem, no corresponding features (control points) for these structures are identified. The lack of alignment in these regions also results in larger evaluation measures. However, the local methods are generally better than global approaches, as we concluded above in testing with simulated warping.

At this time much effort in computational geometry has been given to the 2D point-inclusion (or point-location) problems, and they are well understood; very little is known about solving the point-inclusion problem in 3D and even less for a higher number of dimensions [3.44]. More efficient point-inclusion algorithms than we used could be incorporated to speed up the point locating procedure, which is a pre-processing step for surface fitting and interpolation. Research on 3D interpolation from arbitrarily located data has been reported [3.4],[3.10],[3.11],[3.23],[3.40],[3.45],[3.50]. These advances are expected to facilitate further investigations on 3D image registration. Triangular spline interpolants and multi-stage methods for 2D and 3D surface approximation need testing for geometric unwarping problems.

The prospective applications of this image registration approach reported here go beyond mammography, and may be equally applicable to other 2D problems such as those encountered in the analysis of growth and development. They may also make clear the limits of usefulness of currently available hardware for geometric warping, and suggest that more flexible and powerful hardware could be designed.

References

[3.1]   J. Adams, C. Patton, C. Reader and D. Zamora, "Hardware for geometric warping," *Electronic Imaging,* April issue, 1984.

[3.2]   H. Akima, "A method of bivariate interpolation and smooth surface fitting for irregularly distributed data points," *ACM Trans. Math. Software,* vol. 4, pp. 148-164, 1978.

[3.3]   H. Akima, "On estimating partial derivatives for bivariate interpolation of scattered data," *Rocky Mountain J. Math.,* vol. 14, pp. 41-52, 1984.

[3.4]   P. Alfeld, "A discrete C^1 interpolant for tetrahedral data," *Rocky Mountain J. Math.,* vol. 14, pp. 5-16, 1984.

[3.5]   R. E. Barnhill, "Representation and approximation of surfaces," In *Mathematical Software III,* J. R. Rice, Ed., New York: Academic Press, 1977, pp. 69-120.

[3.6]   R. E. Barnhill, "A survey of the representation and design of surfaces," *IEEE Comput. Graphics Appl.,* vol. 3, pp. 9-16, 1983.

[3.7] R. E. Barnhill, "Surfaces in computer aided geometric design: A survey with new results," *Comput. Aided Geom. Design,* vol. 2, pp. 1-17, 1985.

[3.8] R. E. Barnhill, G. Birkhoff and W. J. Gordon, "Smooth interpolation in triangles," *J. Approx. Theory,* vol. 8, pp. 114-128, 1973.

[3.9] R. E. Barnhill and G. Farin, "C^1 quintic interpolation over triangles: two explicit representations," *Inter. J. Num. Meth. Eng.,* vol. 17, pp. 1763-1778, 1981.

[3.10] R. E. Barnhill and F. F. Little, "Three- and four-dimensional surfaces," *Rocky Mountain J. Math.,* vol. 14, pp. 77-102, 1984.

[3.11] R. E. Barnhill and S. E. Stead, "Multistage trivariate surfaces," *Rocky Mountain J. Math.,* vol. 14, pp. 103-118, 1984.

[3.12] L. W. Bassett and R. H. Gold, Eds., *Breast Cancer Detection: Mammography and Other Methods in Breast Imaging,* 2nd ed., Orlando, FL: Grune and Stratton, 1987.

[3.13] W. Boehm, "The de Boor algorithm for triangular splines," In *Surfaces in Computer Aided Geometric Design,* R. E. Barnhill and W. Boehm, Eds., Amsterdam, Holland: North-Holland Publishing Co., 1983, pp. 109-120.

[3.14] W. Boehm, "Generating the Bezier points of triangular splines," In *Surfaces in Computer Aided Geometric Design,* R. E. Barnhill and W. Boehm, Eds., Amsterdam, Holland: North-Holland Publishing Co., 1983, pp. 77-91.

[3.15] F. L. Bookstein, *The Measurement of Biological Shape and Shape Change,* Berlin: Springer-Verlag, 1978.

[3.16] F. L. Bookstein, B. Chernoff, R. L. Elder, J. M. Humphries Jr., G. R. Smith and R. E. Strauss, *Morphometrics in Evolutionary Biology, The Geometry of Size and Shape Change, With Examples from Fishes,* Philidelphia: The Academy of Natural Sciences of Philidelphia, 1985.

[3.17] F. L. Bookstein, "Principal warps: Thin-plate splines and the decomposition of deformations," *IEEE Trans. Pattern Anal. Machine Intell.,* vol. PAMI-11, no. 6, pp. 567-585, 1989.

[3.18] F. L. Bookstein, "Distortion correction," In *Three-Dimensional Neuroimaging,* A. E. Toga, Ed., New York, NY: Raven Press, 1990, pp. 235-249.

[3.19] K. R. Castleman, *Digital Image Processing,* Englewood Cliffs, NJ: Prentice-Hall, 1979.

[3.20] J. M. Cheverud, "Phenotypic, genetic, and environmental morphological integration in the cranium, " *Evolution,* vol. 36, no. 3, pp. 499-516, 1982.

[3.21] J. M. Cheverud, "Quantitative genetics and developmental constraints on evolution by selection," *J. Theor. Biol.,* vol. 110, pp. 155-171, 1984.

[3.22] B. Delaunay, "Sur la sphère vide," *Bulletin of the Academy of Sciences of the U.S.S.R., Classe des Sciences Mathématiques et Naturelles,* vol. 8, pp. 793-800, 1934.

[3.23] I. P. Dubey and S. K. Upadhyay, "A trivariate interpolation method developed on the basis of Akima's bivariate interpolation procedure," *Comput. Phys. Commun.,* vol. 54, pp. 23-29, 1989.

[3.24] G. Farin, "Smooth interpolation to scattered 3D data," In *Surfaces in Computer Aided Geometric Design,* R. E. Barnhill and W. Boehm, Eds., Amsterdam, Holland: North-Holland, 1983, pp. 43-63.

[3.25] T. A. Foley, "Three-stage interpolation to scattered data," *Rocky Mountain J. Math.*, vol. 14, pp. 141-150, 1984.

[3.26] R. H. J. Gmelig Meyling, "Approximation by cubic C^1 - splines on arbitrary triangulations," *Numer. Math.*, vol. 51, pp. 65-85, 1987.

[3.27] R. Gordon, "Toward robotic x-ray vision: new directions for computed tomography," *Appl. Opt.*, vol. 24, pp. 4124-4133, 1985.

[3.28] A. Goshtasby, "Piecewise linear mapping functions for image registration," *Pattern Recog.*, vol. 19, pp. 459-466, 1986.

[3.29] A. Goshtasby, "Piecewise cubic mapping functions for image registration," *Pattern Recog.*, vol. 20, pp. 525-533, 1987.

[3.30] P. J. Green and R. Sibson, "Computing Dirichlet tessellations in the plane," *Computer J.*, vol. 21, pp. 168-173, 1978.

[3.31] E. L. Hall, *Computer Image Processing and Reconstruction*, New York, NY: Academic Press, 1979.

[3.32] J. R. Jensen, *Introductory Digital Image Processing: A Remote Sensing Perspective*, Englewood Cliffs, NJ: Prentice-Hall, 1986.

[3.33] I. M. Klucewicz, "A piecewise C^1 interpolant to arbitrarily spaced data," *Comput. Graph. Image Process.*, vol. 8, pp. 92-112, 1978.

[3.34] C. L. Lawson, "Software for C^1 surface interpolation," In *Mathematical Software III*, J. R. Rice, Ed., New York: Academic Press, 1977, pp. 161-194.

[3.35] D. G. Leckie, "Use of polynomial transformations for registration of airborne digital line scan image," *Proc. Fourteenth Int. Sym. Remote Sensing Environment*, 1980, pp. 635-641.

[3.36] D. T. Lee and B. J. Schachter, "Two algorithms for constructing a Delaunay triangulation," *Int. J. Comput. Info. Sci.*, vol. 9, pp. 219-242, 1980.

[3.37] B. A. Lewis and J. S. Robinson, "Triangulation of planar regions with applications," *Computer J.*, vol. 21, pp. 324-332, 1978.

[3.38] M. L. Nack, "Rectification and registration of digital images and the effect of cloud detection," *Proc. Machine Process. Remotely Sensed Data*, 1977, pp. 12-23.

[3.39] G. M. Nielson and R. Franke, "Surfaces construction based upon triangulations," In *Surfaces in Computer Aided Geometric Design*, R. E. Barnhill and W. Boehm, Eds., Amsterdam, Holland: North-Holland Publishing Co., 1983, pp. 163-177.

[3.40] T. F. Oostendorp, A. van Oosterom and G. Huiskamp, "Interpolation on a triangulated 3D surface," *J. Comput. Phys.*, vol. 80, pp. 331-343, 1989.

[3.41] P. Percell, "On cubic and quartic Clough-Tocher finite elements," *SIAM J. Numer. Anal.*, vol. 13, pp. 100-103, 1976.

[3.42] M. J. D. Powell and M. A. Sabin, "Piecewise quadratic approximation on triangles," *ACM Trans. Math. Software*, vol. 3, pp. 316-325, 1977.

[3.43]   W. K. Pratt, *Digital Image Processing*, New York, NY: John Wiley & Sons, 1978.

[3.44]   F. P. Preparata and M. I. Shamos, *Computational Geometry: An Introduction*, New York, NY: Springer-Verlag, 1985.

[3.45]   R. J. Renka, "Multivariate interpolation of large sets of scattered data," *ACM Trans. Math. Software*, vol. 14, pp. 139-148, 1988.

[3.46]   R. A. Schowengerdt, *Techniques for Image Processing and Classification in Remote Sensing*, New York, NY: Academic Press, 1983.

[3.47]   L. L. Schumaker, "Fitting surfaces to scattered data," In *Approximation Theory II*, G. G. Lorentz, C. K. Chui and L. L. Schumaker, Eds., 1976, pp. 203-268.

[3.48]   F. H. Séguin and P. J. Bjorkholm, "Optimization of parameters for high-resolution X-ray computed tomography," In *Review of Progress in Quantitative Nondestructive Evaluation*, D. O. Thompson and D. E. Chimenti, Eds., NewYork, NY: Plenum Publishing Co., 1989, pp. 373-380.

[3.49]   F. H. Séguin, P. Burstein, P. J. Bjorkholm, F. Homburger and R. A. Adams, "X-ray computed tomography with 50-μm resolution," *Appl. Opt.*, vol. 24, pp. 4117-4123, 1985.

[3.50]   M. C. Spruill, "Optimal designs for multivariate interpolation," *J. Multivariate Anal.*, vol. 34, pp. 141-155, 1990.

[3.51]   S. E. Stead, "Estimation of gradients from scattered data," *Rocky Mountain J. Math.*, vol. 14, pp. 265-280, 1984.

[3.52]   D. Steiner and M. E. Kirby, "Geometrical referencing of Landsat images by affine transformation and overlaying of map data," *Photogrametria*, vol. 33, pp. 41-75, 1977.

[3.53]   J. K. Stevens and J. T. Trogadis, "Computer-assisted reconstruction from serial electron micrographs: a tool for the systematic study of neuronal form and function," *Adv. Cell. Neurobiol.*, vol. 5, pp. 341-369, 1984.

[3.54]   J. K. Stevens and J. T. Trogadis, "Reconstructive three-dimensional electron microscopy: A routine biologic tool," *Anal. Quant. Cytol. Histol.*, vol. 8, pp. 102-107, 1986.

[3.55]   D. W. Thompson, *On Growth and Form*, 2nd ed., Cambridge: Cambridge University Press, 1942.

[3.56]   G. Voronoi, "Nouvelles applications des paramètres continus à la théorie des formes quadratiques, deuxième mémoire, recherches sur les parallellohèdres primitifs," *Journal für die Reine und angewandte Mathematik*, vol. 134, pp. 198-287, 1908.

[3.57]   P. van Wie and M. Stein, "A Landsat digital image rectification system," *IEEE Trans. Geosci. Electron.*, vol. GE-15, pp. 130-137, 1977.

[3.58]   X. Zhou and R. Gordon, "Geometric unwarping for digital subtraction mammography," In *Proc. Vision Interface '88*, Edmonton, Canada, June 6-10, 1988, pp. 25-30.

[3.59]   X. Zhou and R. Gordon, "3D digital subtraction mammography," In *Proc. 16th Canadian Med. and Biol. Eng. Soc. Conf.*, Winnipeg, Canada, June 9-12, 1990, pp. 29-30.

CHAPTER 4
GREY LEVEL RESAMPLING IN GEOMETRIC UNWARPING

4.1. Introduction

As described in Section 3.2, the second requirement for the geometric unwarping operation is an algorithm for the interpolation of intensity values (grey levels), which is usually referred to as *resampling*. That is, if we designate the intensities of the reference and unwarped images as $f(x, y)$ and $f^*(x^*, y^*)$, then we also require, at corresponding points, that

$$f(x, y) \approx f^*(x^*, y^*). \tag{4.1.1}$$

In the warped image, the intensity values, designated by $g(u, v)$, are defined only at integer values of u and v. Equation (4.1.1), however, will in general dictate that the intensity value for $f^*(x^*, y^*)$ be taken from the corresponding $g(u, v)$ at noninteger coordinates. If the geometric unwarping is considered as a mapping from g to f^*, pixels in g can map to positions between pixels in f^* and vice versa.

There are two approaches for implementation of the geometric unwarping algorithm. First, we may think of the procedure as transferring the grey levels from the warped image to unwarped image pixel by pixel. If a pixel in the warped image maps to a position between four pixels in the unwarped image, then its grey level is divided among the four pixels according to the interpolation rule (or more pixels, if higher order interpolation used). We may call this the *pixel transfer* approach [Fig. 4.1.1(a)]. The second approach is the *pixel fill* technique [Fig. 4.1.1(b)]. In this case, the unwarped pixels are mapped onto the warped image one at a time to establish their grey levels. If the unwarped pixel falls

between four warped pixels, its grey level is determined by the interpolation algorithm (more pixels are needed for more accurate interpolation). We note that pixel transfer could be wasteful, because many pixels may map to positions outside the border of the unwarped image, and each unwarped pixel could be addressed several times. With pixel fill, however, the grey level of each unwarped pixel is uniquely determined by one interpolation between warped pixels.

PIXEL TRANSFER

warped $g(u, v)$ unwarped $f^*(x^*, y^*)$

u, v INTEGERS x^*, y^* NON-INTEGERS

(a)

PIXEL FILL

warped $g(u, v)$ unwarped $f^*(x^*, y^*)$

u, v NON-INTEGERS x^*, y^* INTEGERS

(b)
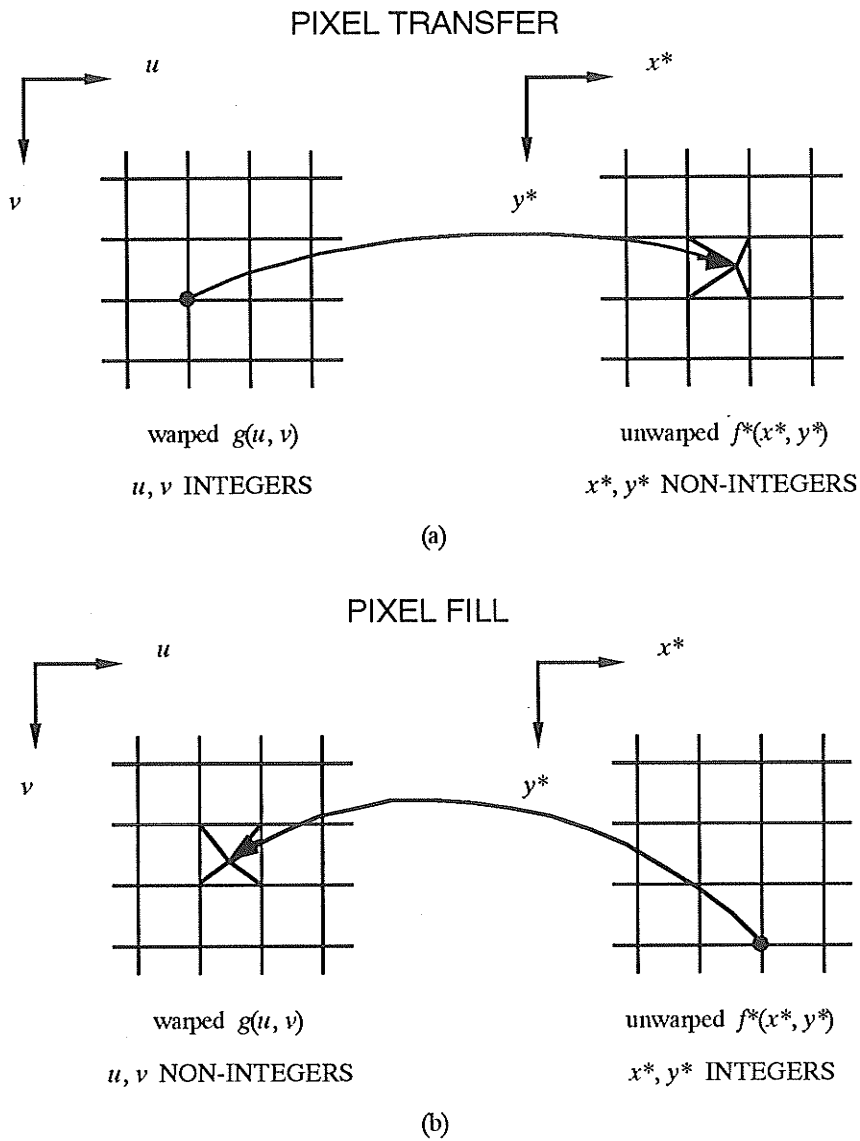
Fig. 4.1.1. Implementations of geometric unwarping transformations: (a) pixel transfer, and (b) pixel fill.

Hou and Andrews [4.12] proposed an interpolation algorithm for image processing and digital filtering by cubic spline functions. Interpolation by a cubic convolution method has been developed by Bernstein [4.6], modified by Keys [4.13], and analyzed by Park and Schowengerdt [4.15]. Surface fitting approximation methods have been used in edge detection techniques [4.9],[4.10],[4.14]. There are some other interpolation methods such as nearest neighbor and bilinear interpolation [4.26]. Approaches by C^0, C^1 and C^2 continuous rectangular and non-rectangular interpolants for surface representation and approximation have been studied extensively and are currently used in the field of computer aided geometric design [4.2]-[4.4],[4.25]. It is our purpose here to investigate and test the interpolation and approximation techniques above as well as other approaches by using real CT (X-ray computed tomography) images for intensity resampling in geometric unwarping for digital subtraction mammography. Among the interpolation techniques I used are truncated sinc, Lagrange polynomials, cubic splines, and cubic convolution interpolations. The least squares approximations include the least squares technique with and without distance weighting, and surface fitting by orthogonal functions.

4.2. Grey Level Interpolation

We will restrict ourselves to interpolations only from equally spaced data, because we assume pixels have the same sampling intervals in each dimension. Since the 2D (and likewise 3D) interpolation may be accomplished by performing 1D interpolation in each dimension, in the following discussion of interpolation methods, therefore, our analysis pertains to only the 1D problem: Given a set of sampled data, $\{f(x_i) = f_i, i = 0, 1, 2,..., n - 1\}$, determine an interpolated function $f^*(x)$ such that $f^*(x_i) = f(x_i)$ at all data points.

It has been pointed out that many interpolation functions, for equally spaced data, can be presented in the form [4.26]

$$f^*(x) = \sum_{i=0}^{n-1} c_i \, s\!\left(\frac{x - x_i}{h}\right) \tag{4.2.1}$$

where s is the *interpolation function*, f^* is the interpolated function, h is the sampling interval, n is the number of data points, x_i is the ith data point, and x is a point $x_0 < ... < x < ... < x_{n-1}$ at which interpolation is to be performed. In this work, it will be useful to represent the indices of data points $\{0, 1, ..., n - 1\}$ by an equivalent set of integers $\{n_{LO}, n_{LO} + 1, ..., -1, 0, 1, ..., n_{HI} - 1, n_{HI}\}$, where

$$n_{LO} = \begin{cases} -\dfrac{n-1}{2}, & n \text{ odd} \\[2mm] -\dfrac{n-2}{2}, & n \text{ even} \end{cases} \quad \text{and} \quad n_{HI} = \begin{cases} \dfrac{n-1}{2}, & n \text{ odd} \\[2mm] \dfrac{n}{2}, & n \text{ even.} \end{cases} \tag{4.2.2}$$

It is noted that an index in the latter set is closest to 0 than that in any other set of n integers. By using this notation, (4.2.1) becomes

$$f^*(x) = \sum_{i=n_{LO}}^{n_{HI}} c_i \, s\!\left(\frac{x - x_i}{h}\right) \tag{4.2.3}$$

where $x_i = x_0 + ih$, and $x = x_0 + ph$, and p is the distance of an interpolation point x to the data point x_0, which we call the *base* point of the interpolation.

We require that $f^*(x)$ has certain properties, and each of these properties results in a condition on the interpolation function $s(x)$. We would like to "preserve area" by the condition that the integral of the interpolated data equals the trapezoidal rule approximation to the integral, i.e.,

$$\int_{-\infty}^{\infty} f^*(x)dx = h \sum_{i=n_{LO}}^{n_{HI}} c_i. \tag{4.2.4}$$

This implies that

$$\int_{-\infty}^{\infty} s(x)dx = 1. \tag{4.2.5}$$

We will also require that the coefficients c_i's are to be determined from the sampled data so that the interpolation condition, $f^*(x_i) = f_i$ for each x_i, is satisfied. This gives rise to the following condition

$$f_i = \sum_{k = n_{LO}}^{n_{HI}} c_k \, s(i - k).$$
(4.2.6)

One possible choice of the interpolation function is that $s(0) = 1$ and $s(k) = 0$ for all integers $k \neq 0$. While it is not necessary, this specific condition has an important computing significance. That is, the coefficients c_i's are simply replaced by the sampled data, or $c_i = f_i$, for $i = n_{LO}, \ldots, -1, 0, 1, \ldots, n_{HI}$, significantly reducing computer time.

We will analyze the behavior of each intensity interpolation method considered below through the use of Fourier transforms. That is, by taking the Fourier transform of an interpolated function we can see how the frequencies present in the original data are modified by the interpolation process. By the linearity of the Fourier transform and convolution theorem [4.8], we find that the Fourier transform of $f^*(x)$ is given by

$$[F f^*](X) = h\,[Fs](hX) \sum_{i = n_{LO}}^{n_{HI}} c_i \exp(-j2\pi i hX).$$
(4.2.7)

The summation term in (4.2.7) is the discrete Fourier transform of the sampled data. The function $[Fs](hX)$ acts as a low-pass filter. An analysis of various interpolation methods may be made by comparing the Fourier transforms of their interpolation functions (*cf.* [4.8]). The explicit expressions for some interpolation functions and their Fourier transforms are presented in Appendix 2.

4.2.1. Truncated Sinc Interpolation

If the function $f^*(x)$ is band-limited and sufficiently sampled, then it can be reconstructed exactly by using the ideal sinc interpolation function [4.17]

$$sinc(x) = \frac{sin(\pi x)}{\pi x}.$$
(4.2.8)

The sinc (or band limiting) interpolation function and its Fourier transform, a $\prod$ function [4.8], are given in Fig. 4.2.1. Such an interpolation function will pass every frequency component of a band-limited function without change, provided that the sampling interval is sufficiently small.
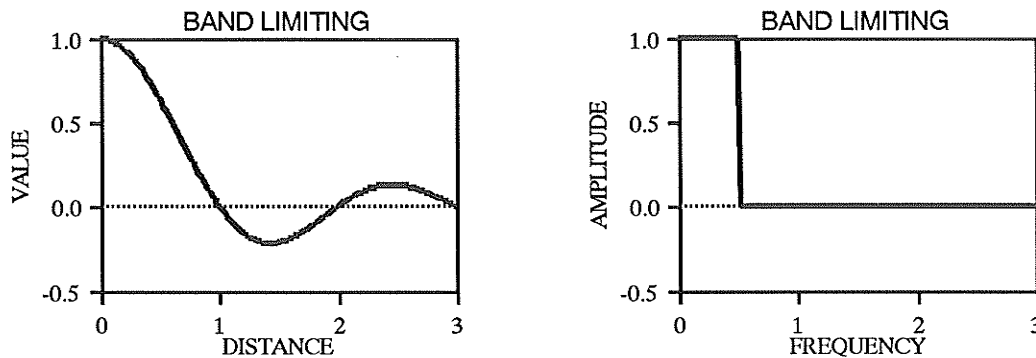
Fig. 4.2.1. Sinc (band limiting) interpolation function and its Fourier transform.

Because the ideal sinc interpolation function is not spatially limited, a truncated form of the sinc function must be used instead. Some truncated sinc interpolation functions and their Fourier transforms with different truncation widths are shown in Fig. 4.2.2. Note that I have obtained these Fourier transforms by using a special numerical integration technique [4.18] because of the singularity of the Fourier integral of the sinc function. When the truncation width is greater than 2.0, the spectra also have some undesirable overshoots in the region $X < 0.5$. For truncated sinc functions having widths of 1, 3, 5, etc., the spectra have more high frequency components than those with widths of 2, 4, 6, etc. This is because of the discontinuities of the function and the slope at the end points. One method of suppressing these ripples is to construct the interpolation function as a smooth, spatially limited one which approximates the sinc function and eliminates the discontinuities at the end points at the same time. Obviously the truncated sinc formulas will approximate the

sinc function as the number of points increases, and their Fourier transforms will also approach the $\prod$ function.

(a)

(b)

(c)
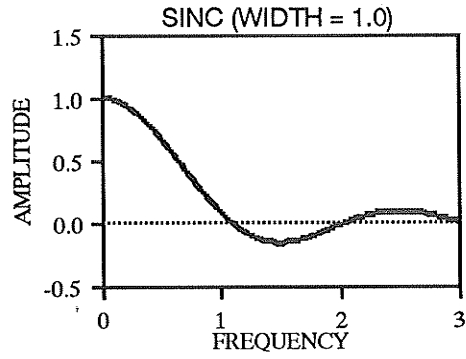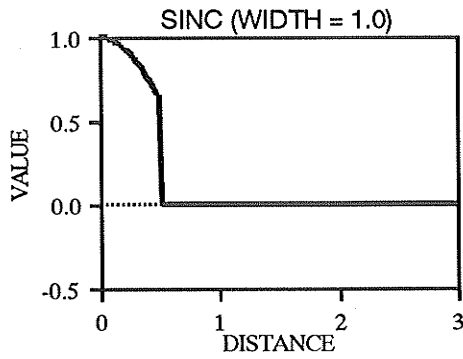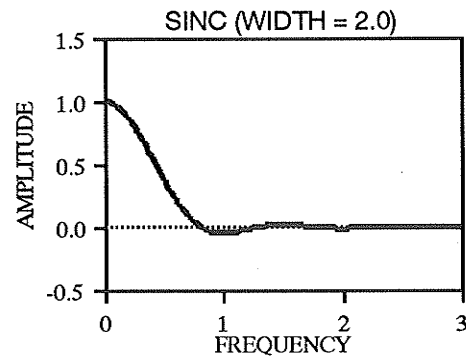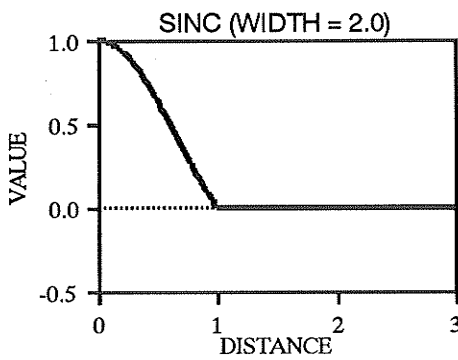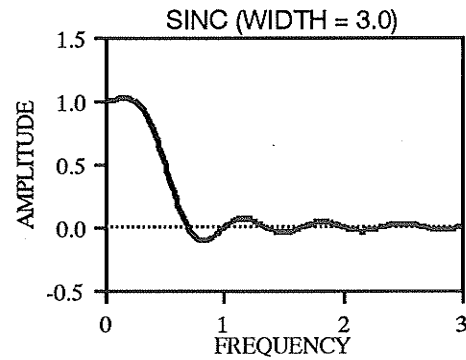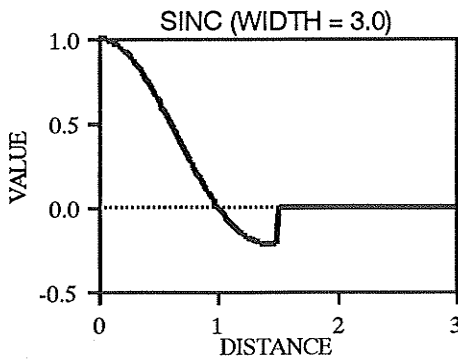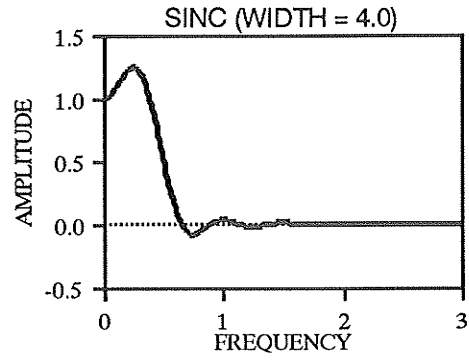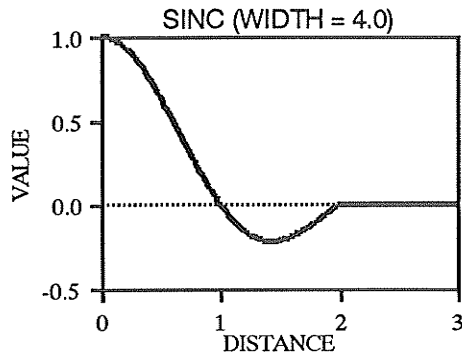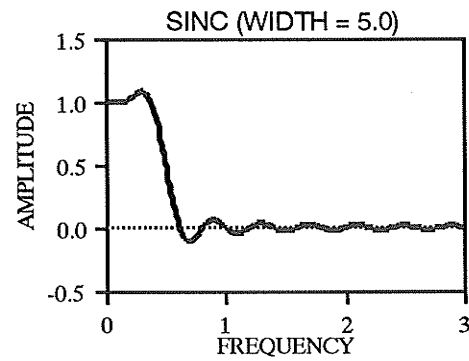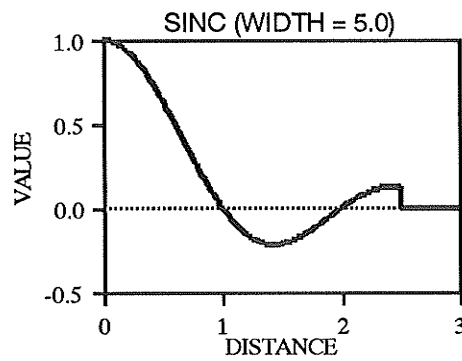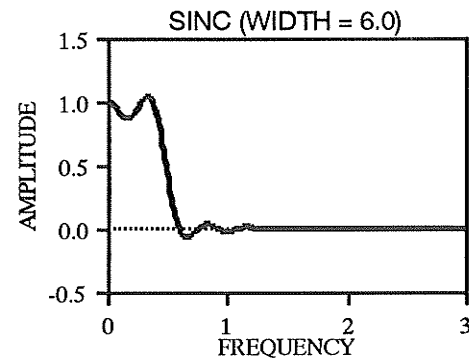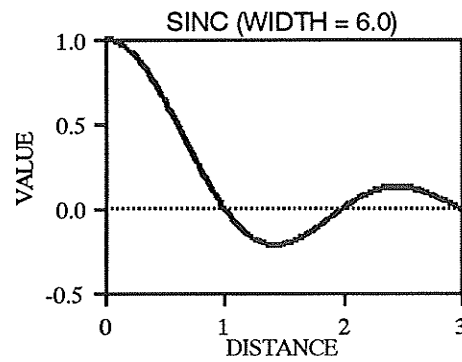
Fig. 4.2.2. Truncated sinc interpolation functions and their Fourier transforms. (a) Width of 1, (b) width of 2, (c) width of 3, (d) width of 4, (e) width of 5, and (f) width of 6.

4.2.2. Lagrange Interpolation

The simplest interpolation scheme, which coarsely approximates the ideal sinc interpolation approach, is the so-called zero-order or nearest neighbor interpolation. In this case, the intensity is taken to be that of the warped pixel nearest to the position to which it maps. In other words, nearest-neighbor interpolation is equivalent to convolving the warped image with a uniform window function which is one pixel size wide. The significant advantage of nearest-neighbor interpolation over other algorithms is that no calculations are required to derive the unwarped pixel intensity value.

An improved approximation of the sinc function can be obtained by a first-order or linear function. First-order interpolation produces more desirable results with a slight increase in programming complexity and computing time. It is noted that first-order interpolation on a rectangular grid requires a bilinear function because fitting a plane through four points is an overconstrained problem. That is, it can be done by fitting a hyperbolic paraboloid, defined by a bilinear equation $a_{00} + a_{10}x + a_{01}y + a_{11}xy$, through the four known data points. The four coefficients are to be chosen so that the resultant hyperbolic paraboloid fits the known values at the four corners.

The extra computing effort of high order interpolation may be justified in some applications. By analogy to the bilinear approach, we propose a set of higher order intensity interpolation methods. That is, we may interpolate first in one coordinate n times and then interpolate the n values obtained in another coordinate once, where n is the number of data points for the Lagrange interpolation of order $n - 1$. From the above discussion, we note that for the n point Lagrange interpolation, when such a complete polynomial of $(n - 1)$ order plus some higher order terms is used, all $n \times n$ data points are used up. For instance, we fit by biquadratic interpolation a quadratic polynomial plus $a_{12}xy^2 + a_{21}x^2y + a_{22}x^2y^2$; by bicubic interpolation a cubic polynomial plus $a_{31}x^3y + a_{22}x^2y^2 + a_{13}xy^3 + a_{32}x^3y^2 + a_{23}x^2y^3 + a_{33}x^3y^3$, etc.

The Lagrange interpolation formulas $s(x)$ can be presented as

$$s(x) = \begin{cases} A_k^n(p), & n_{LO} \le k \le n_{HI} \\ 0, & \text{otherwise} \end{cases} \qquad (4.2.9)$$

where A_k^n are the polynomials given by Abramowitz and Stegun [4.1]:

$$A_k^n(p) = \begin{cases} \dfrac{(-1)^{\frac{n}{2}+k} \prod\limits_{t=1}^{n} \left(p + \frac{n}{2} - t\right)}{\left(\frac{n-2}{2}+k\right)! \left(\frac{n}{2}-k\right)! (p-k)}, & n \text{ even} \\[4em] \dfrac{(-1)^{\frac{n-1}{2}+k} \prod\limits_{t=0}^{n-1} \left(p + \frac{n-1}{2} - t\right)}{\left(\frac{n-1}{2}+k\right)! \left(\frac{n-1}{2}-k\right)! (p-k)}, & n \text{ odd}, \end{cases} \qquad (4.2.10)$$

$x = p - k$ and p is in $[-0.5, 0.5)$ if n is odd or p is in $[0, 1)$ if n is even. The selection of an $n \times n$ neighborhood of a pixel for 2D Lagrange interpolation is shown schematically in Fig. 4.2.3. That is, the base point of the interpolation $P_0(x_0, y_0)$ must be restricted in the dotted region in order to obtain a unique interpolated value at that point. Fig. 4.2.4 shows graphs of Lagrange interpolation functions and their Fourier transforms with n up to 6. Lagrange functions with an odd number of data points suppress high frequencies less effectively but approximate the sinc function better as far as low frequency components are concerned than those with an even number of points.

(a)

(b)
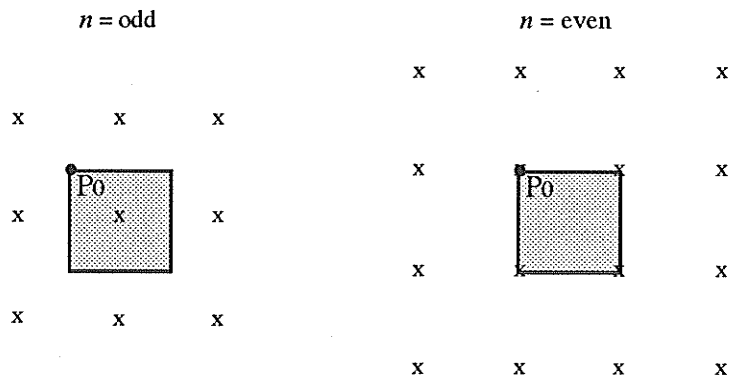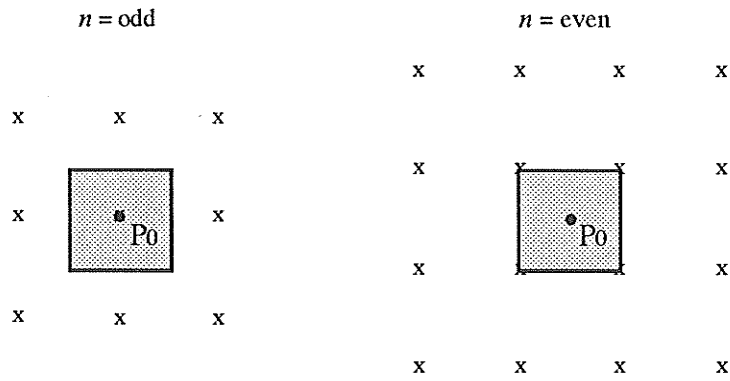
Fig. 4.2.3. The selection of a pixel's neighborhood.

(a)

(b)

(c)
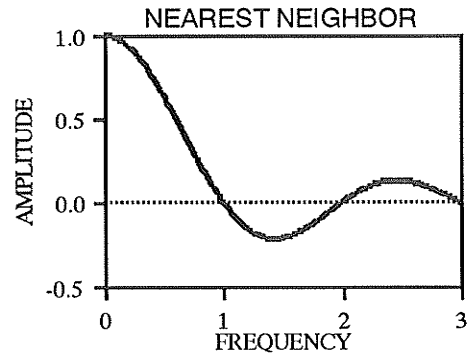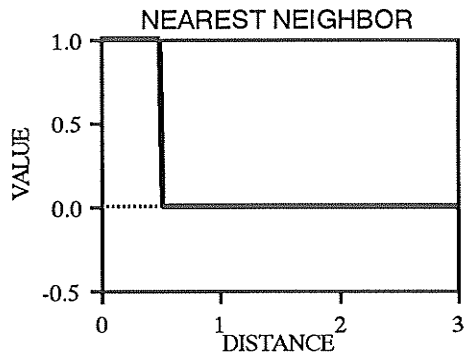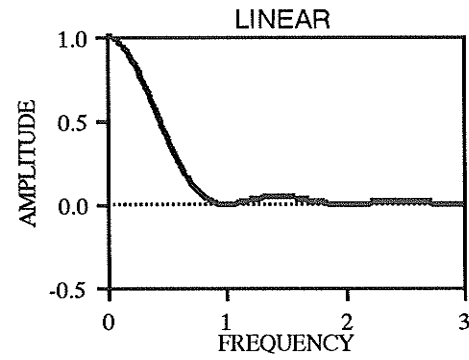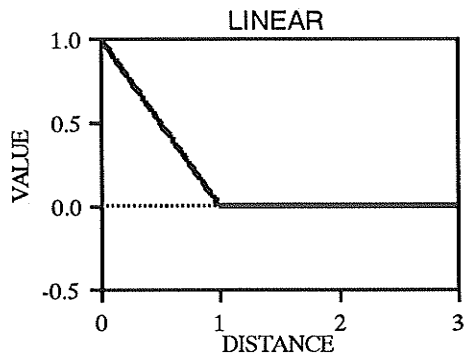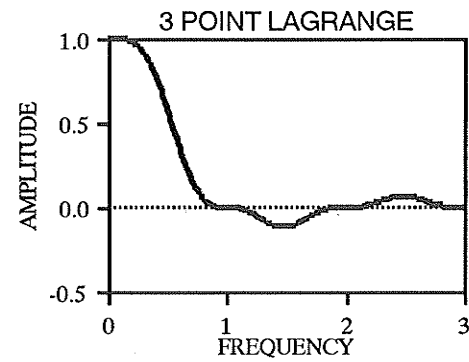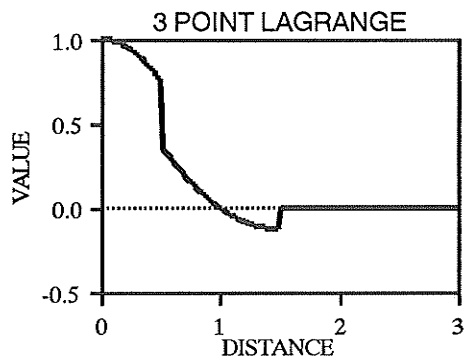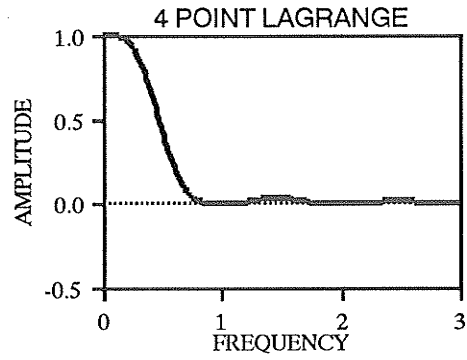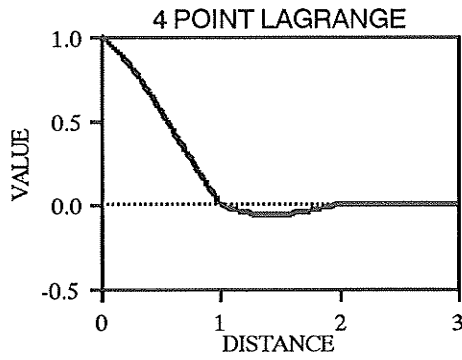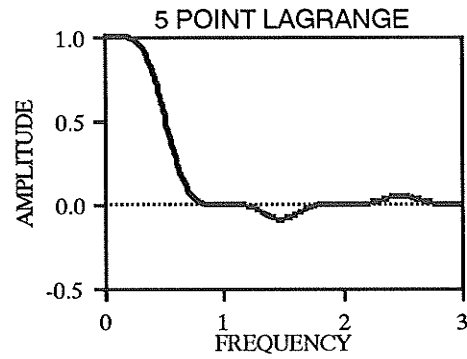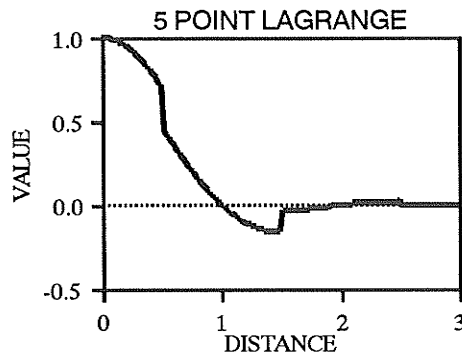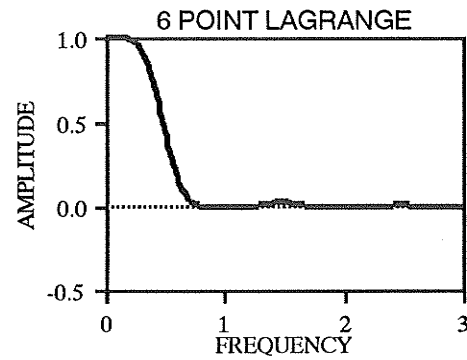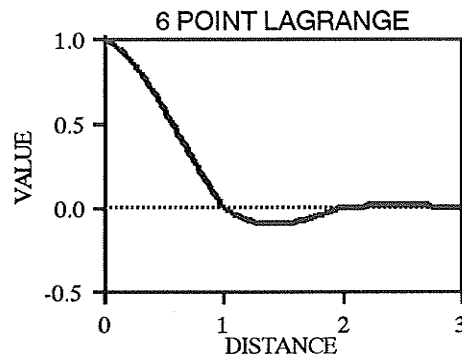
Fig. 4.2.4. Lagrange interpolation functions and their Fourier transforms. (a) Nearest neighbor interpolation, (b) linear interpolation, (c) 3 point Lagrange, (d) 4 point Lagrange, (e) 5 point Lagrange, and (f) 6 point Lagrange.

4.2.3. Cubic Splines Interpolation

Spline interpolation [4.21],[4.23] has been widely used in numerous fields. For instance, interpolating noisy data by splines was investigated by Pavlidis [4.16]. Hou and Andrews have adopted spline interpolation for image restoration, and for image interpolation and digital filtering [4.11],[4.12]. Boundary elements based on cubic spline functions have been developed for use in the solution of boundary value problems [4.7]. Spline functions have superior properties in connecting curve segments or surface patches smoothly in computer graphics [4.5] and computer aided geometric design [4.27].

Spline interpolation not only alleviates the difficulties suffered by the classical polynomial approach, but also minimizes the least squares errors of the function values and its derivatives at the interpolation points [4.21]. In other words, among interpolation functions which produce results passing through the data points, only spline interpolation gives the smoothest and best approximation (in a least squares sense). In this thesis *B-spline* functions [4.21],[4.27] are used because of their smoothness and local, finite support. Therefore, they can be used as interpolation functions in (4.2.3).

Let $x_0 < x_1 < ... < x_n < x_{n+1}$ be a partition of the interval $[a, b]$, where $a = x_0$, and $b = x_{n+1}$. A *B*-spline of order n is defined by the following piecewise polynomial:

$$B_n(x; x_0,x_1,...,x_{n+1}) = (n + 1) \sum_{i=0}^{n} \frac{(x - x_i)^n \, U(x - x_i)}{W(x_i)} \qquad (4.2.11)$$

where

$$U(x - x_i) = \begin{cases} (x - x_i)^0, & x \geq x_i \\ 0, & \text{otherwise} \end{cases}$$

and

$$W(x_i) = \prod_{\substack{j=0 \\ j \neq i}}^{n+1} (x_i - x_j). \qquad (4.2.12)$$

Spline functions of zero and first orders are simply the nearest neighbor and linear interpolation functions, respectively. While the interpolation by quadratic spline function is composed of a set of parabolas which join at the data points continuously, together with their slopes, the interpolation by cubic spline function is a sequence of third order polynomials which join at the data points together with their slopes and curvatures as well. In the rest of this thesis we only consider the cubic B-spline functions.

Note that the cubic B-spline function is shift-invariant for equally spaced data. From (4.2.11) and by a simple rearrangement of terms, we have the cubic B-spline function for equally spaced data points explicitly given by

$$
s(x) = \begin{cases}
\frac{1}{6}x^3 + x^2 + 2x + \frac{4}{3}, & -2 \le x < -1 \\[2mm]
-\frac{1}{2}x^3 - x^2 + \frac{2}{3}, & -1 \le x < 0 \\[2mm]
\frac{1}{2}x^3 - x^2 + \frac{2}{3}, & 0 \le x < 1 \\[2mm]
-\frac{1}{6}x^3 + x^2 - 2x + \frac{4}{3}, & 1 \le x < 2 \\[2mm]
0, & \text{otherwise}
\end{cases}
\tag{4.2.13}
$$

The cubic B-spline function and its Fourier transform are shown in Fig. 4.2.5. The Fourier transform is given by $\text{sinc}^4(X)$. It is nonnegative, and it can be shown that as $X \to \infty$ the function $\text{sinc}^4(X) \to X^{-4}$. This implies that it suppresses high frequency components more effectively than the truncated sinc and Lagrange functions above. Note that it suppresses more low frequencies than other methods as well.

Special care has to be taken into account in the interpolation by spline functions. Consider $f^*(x)$ at any point $x = x_k + ph$, $0 \le p < 1$, where x_k is the kth data point, and h is the sampling interval. Interpolation of $f^*(x)$ by cubic spline functions becomes
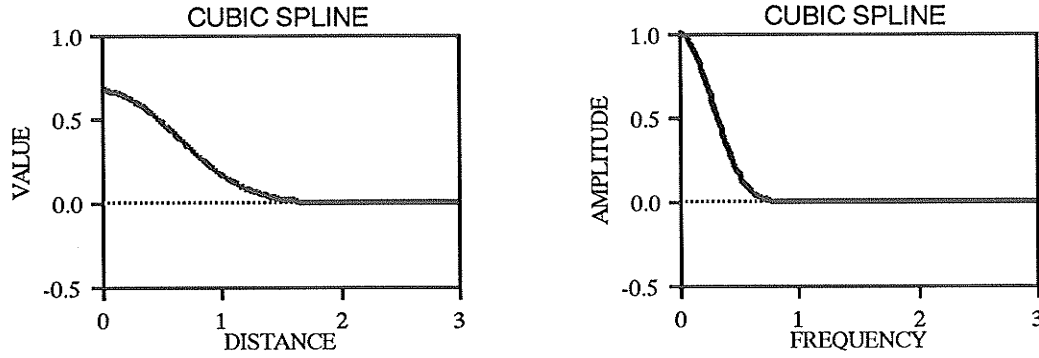
Fig. 4.2.5. Cubic B-spline function and its Fourier transform.

$$f^*(x_k + ph) = \sum_{i=k-1}^{k+2} c_i \, s(p + k - i)$$

$$= \frac{1}{6h} \Big\{ c_{k-1} \big[-(p+1)^3 + 6(p+1)^2 - 12(p+1) + 8 \big]$$

$$+ c_k \big[3p^3 - 6p^2 + 4 \big] + c_{k+1} \big[-3(p-1)^3 - 6(p-1)^2 + 4 \big] \qquad (4.2.14)$$

$$+ c_{k+2} \big[(p-2)^3 + 6(p-2)^2 + 12(p-2) + 8 \big] \Big\}$$

$$= \frac{1}{6h} \sum_{i=0}^{3} b_i \, p^{3-i}$$

where

$$\begin{bmatrix} b_0 \\ b_1 \\ b_2 \\ b_3 \end{bmatrix} = \begin{bmatrix} -1 & 3 & -3 & 1 \\ 3 & -6 & 3 & 0 \\ -3 & 0 & 3 & 0 \\ 1 & 4 & 1 & 0 \end{bmatrix} \begin{bmatrix} c_{k-1} \\ c_k \\ c_{k+1} \\ c_{k+2} \end{bmatrix}. \qquad (4.2.15)$$

The coefficients c_k can be determined as follows. Equation (4.2.14) allows us to find an interpolation value at any point between data points. In particular, at a data point $x = x_k$, i.e., $p = 0$, we have

$$f^*(x_k) = \frac{1}{6h} (c_{k-1} + 4c_k + c_{k+1}). \qquad (4.2.16)$$

From (4.2.15) and (4.2.16), and noting that $f^*(x_k)$ at all data points are exactly the given sampled data $f(x_k)$, we obtain

$$f = E\, c \qquad (4.2.17)$$

where E is an $N \times N$ symmetric matrix

$$E = \frac{1}{6h} \begin{bmatrix} 4 & 1 & & & & \\ 1 & 4 & 1 & & & \\ & 1 & 4 & 1 & & \\ & & \ddots & \ddots & \ddots & \\ & & & 1 & 4 & 1 \\ & & & & 1 & 4 \end{bmatrix}$$

$$f = [f(x_1) \ f(x_2) \cdots f(x_N)]^T$$

and

$$c = [c_1 \ c_2 \cdots c_N]^T. \tag{4.2.18}$$

The matrix E is strictly diagonally dominant with positive, real diagonal elements. The inversion of E is easy to find. So are the coefficients c.

4.2.4. Cubic Convolution Interpolation

As discussed in Section 4.2.1, truncating the sinc function to a small width could introduce undesirable ripples in the spectrum of the resultant interpolator because of the function and slope discontinuities at the end points. Therefore, one method of suppressing these ripples is to construct the interpolation function as a smooth, spatially limited one which approximates the sinc function and eliminates the slope discontinuity at the end points in the same time. The cubic convolution interpolation is just an implementation of such an approach.

Cubic convolution interpolation was originally developed for the processing of Landsat digital images [4.6]. It has been widely used, particularly in remote sensing where it is necessary to use resampling techniques to provide accurate radiometry in a coordinate system different from that of the original image. It has been generally acknowledged as providing a good compromise between computing complexity and accuracy [4.22].

The cubic convolution kernel is composed of piecewise cubic polynomials defined over the subintervals [-2, -1], [-1, 0], [0, 1], and [1, 2]. The kernel must be symmetric with respect to the origin. In addition to these conditions, the kernel must be continuous and have a continuous first derivative. Let $s(0) = 1$ and $s(k) = 0$ for any nonzero integers k [see discussion on (4.2.6)]. In addition to these conditions, the kernel must be continuous and have a continuous first derivative. The following cubic convolution kernel with parameter α is thus obtained [4.6]:

$$s(x) = \begin{cases} -\alpha x^3 - 5\alpha x^2 - 8\alpha x - 4\alpha, & -2 \le x < -1 \\ -(\alpha + 2)x^3 - (\alpha + 3)x^2 + 1, & -1 \le x < 0 \\ (\alpha + 2)x^3 - (\alpha + 3)x^2 + 1, & 0 \le x < 1 \\ \alpha x^3 - 5\alpha x^2 + 8\alpha x - 4\alpha, & 1 \le x < 2 \\ 0, & \text{otherwise} \end{cases} \qquad (4.2.19)$$

The common value of the parameter α, which is the slope of $s(x)$ at $x = 1$, is $\alpha = -1$. This duplicates the slope of the ideal sinc function at $x = 1$. However, Keys [4.13] has proven that the choice of $\alpha = -0.5$ provides better interpolation in terms of convergence properties. It can be shown that the choice of $\alpha = -0.75$ produces continuity of the second derivative at $x = 1$.

Fig. 4.2.6 shows graphs of the cubic convolution interpolation functions and their Fourier transforms with different values of α. The parameter α provides an ability to control the frequency characteristics of the interpolation process. For $\alpha < -0.5$, it is a low-pass filter which enhances low frequencies while for $\alpha > -0.5$ it suppresses low frequencies. The choice of $\alpha = -0.5$ provides an excellent high frequency approximation to that of the ideal sinc function (cf. Figs. 4.2.1 and 4.2.6). That is, the cubic convolution kernel with $\alpha = -0.5$ is more effective at suppressing aliasing errors.

CUBIC CONV (ALPHA = -2.0)

CUBIC CONV (ALPHA = -2.0)

(a)

CUBIC CONV (ALPHA = -1.0)

CUBIC CONV (ALPHA = -1.0)

(b)

CUBIC CONV (ALPHA = -0.75)

CUBIC CONV (ALPHA = -0.75)
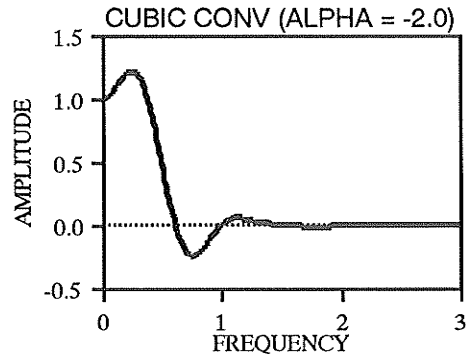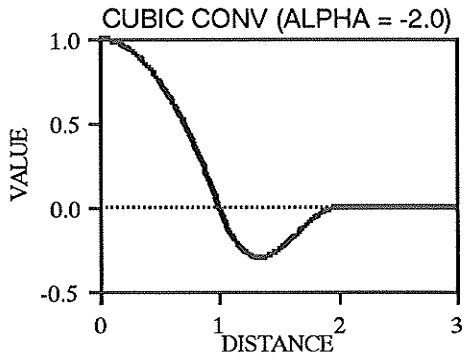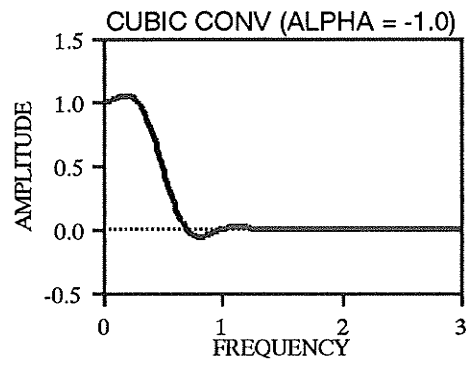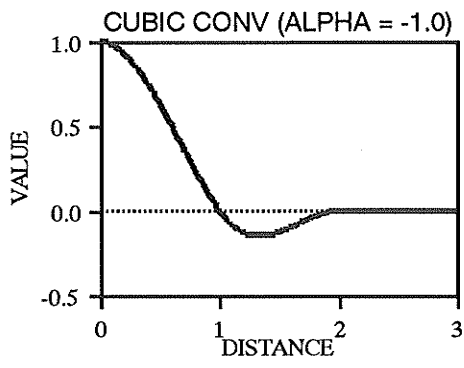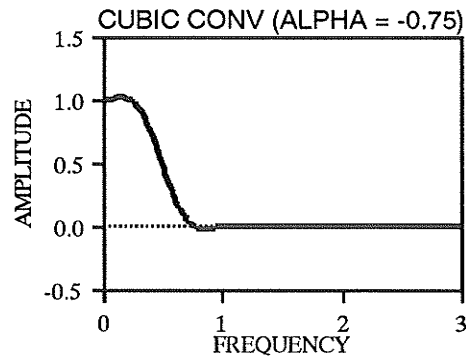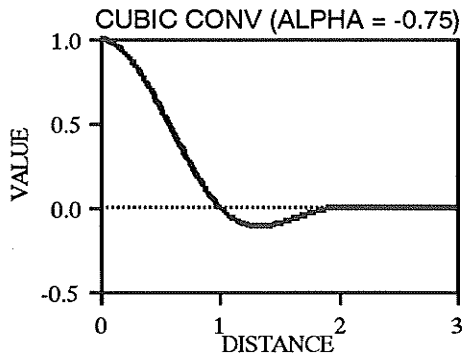
(c)
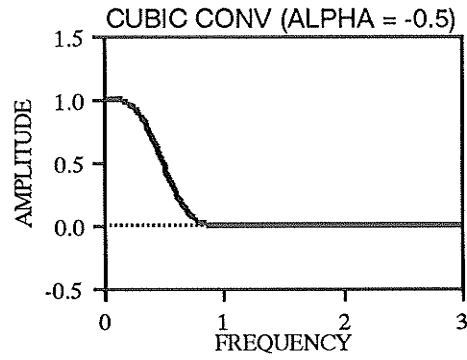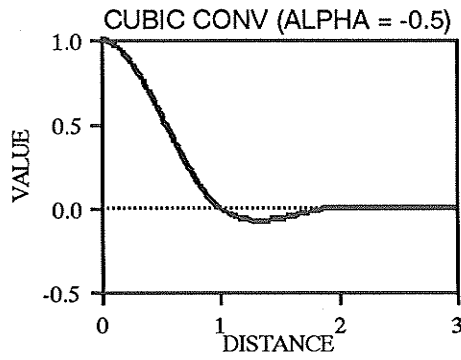
(d)
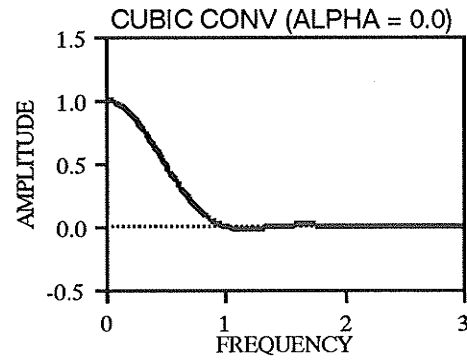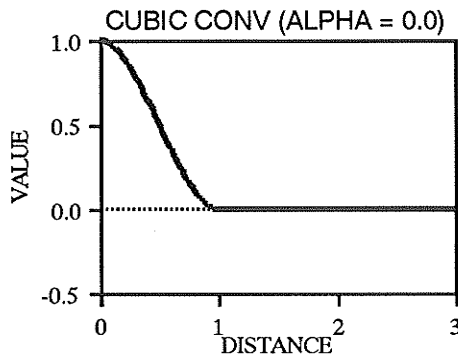
(e)
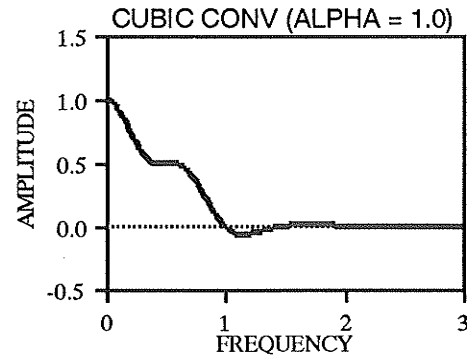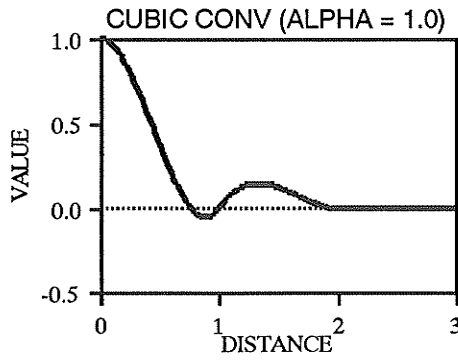
(f)

Fig. 4.2.6. Cubic convolution interpolation functions and their Fourier transforms. (a) $\alpha = -2.0$, (b) $\alpha = -1.0$, (c) $\alpha = -0.75$, (d) $\alpha = -0.5$, (e) $\alpha = 0.0$, and (f) $\alpha = 1.0$.

4.3. Grey Level Approximation

Interpolation may be viewed as a special case of the approximation of functions and data. In approximation, we do as well as possible within certain limits; approximation becomes interpolation when the limits allow us to have exact fitting values at all data points.

Approximations are generally made with respect to some measures of "closeness" or *norms*. Assume that we want to approximate the function $f(x, y)$ over the region R by some function of the form $F(a; x, y)$, where a denotes the parameters or coefficients of the approximation and F may be polynomials, splines, etc. The most widely used measure of distance is the L_2 or least squares norm.

When a large number of data points are involved, it is not normally advisable to use an interpolation method for fitting a polynomial of high enough order to provide an exact fit at all data points. Apart from the difficulty of specifying such a polynomial (which terms in $x^r y^s$ should be included?), the resulting surface will be almost always extremely undulatory. Among other reasons for preferring approximations other than interpolation is that in some applications the sampled data themselves are not accurate, so there is no point to try to find an "accurate" value based on such inaccurate sampled data.

4.3.1. Distance Weighted Least Squares Approximation

The problem of distance weighted least squares approximation can be stated as follows: Suppose we wish to estimate the function $f(x, y)$ at any point $P_0(x_0, y_0)$ for a given set of data points $\{f_i = f(x_i, y_i), i = 1, 2, ..., m\}$. Our aim is to find a polynomial $f^*(x, y)$, which we illustrate by the polynomial of order two:

$$f^*(x, y) = a_{00} + a_{10}x + a_{01}y + a_{20}x^2 + a_{11}xy + a_{02}y^2 \qquad (4.3.1)$$

that will be as accurate a fit as possible, in the least squares sense, to the data points $P_i(x_i, y_i)$. Unlike the ordinary least squares approximation, however, weights are

introduced into the least squares norm here. It has been shown that the introduction of weight functions into the norms for function approximation does not affect the methods or theory of approximation provided that they are positive [4.20]. Specifically we choose the coefficients a_{rs} to minimize the squared error

$$\varepsilon^2 = \sum_{i=1}^{m} \left(a_{00} + a_{10}x_i + a_{01}y_i + a_{20}x_i^2 + a_{11}x_iy_i + a_{02}y_i^2 - f(x_i, y_i)\right)^2 \cdot w\left(d_i^2\right) \qquad (4.3.2)$$

where $w(d_i^2)$ is a weight function and $d_i^2 = (x_i - x_0)^2 + (y_i - y_0)^2$. Taking the partial derivatives of ε^2 with respect to the coefficients a_{rs}, setting them to zero, and solving the resultant system of linear equations (six, in our example here), we immediately obtain the distance weighted least squares estimated coefficients a_{rs}, which are then used to calculate the function value at the point $P_0(x_0, y_0)$ as $f^*(x_0, y_0)$. If we choose $w(d_i^2) = 1$ for all data points, the distance weighted least squares method becomes ordinary least squares.

There is considerable flexibility over the selection of the weight function $w(d^2)$. If the function $f(x, y)$ is reasonably smooth, it is natural for us to require data points close to $P_0(x_0, y_0)$ to carry more weight than more remote points. The simplest choice for a weight function is the reciprocal function, $1/d^2$, or $1/(d^2 + \delta)$ with small δ to avoid overflow. Among other choices is the exponentially decreasing function $w(d^2) = \exp(-\beta d^2)$ for some constant β of the order of the inverse of the square of the average distances between neighboring data points. If the data are exact, then when $P_0(x_0, y_0)$ is very close to some data point we should expect that point to dominate absolutely. A function such as $w(d^2) = \exp(-\beta d^2)/(d^2 + \delta)$ may be another choice.

If we choose the weighting function

$$w\left(d_i^2\right) = \begin{cases} \delta_{ij}, & (x_0, y_0) = (x_j, y_j) \text{ for some } j \\ 1/d_i^2, & \text{otherwise} \end{cases} \qquad (4.3.3)$$

and zero-order polynomial (i.e., a constant) for the intensity approximation, the distance weighted least squares method becomes the Shepard's patch for the representation and approximation of a surface [4.24].

By analogy to the Lagrange interpolation, $n \times n$ surrounding pixels selected with the same configuration are used for the least squares approximations and the base point $P_0(x_0, y_0)$ also falls in the same region as in the Lagrange interpolation (*cf.* Fig. 4.2.3).

Referring to the selection configuration, it can be shown that, because of the symmetry of the region, the square of the average distance takes on the minimum value of $(n^2-1)/6$ when $P_0(x_0, y_0)$ is in the centre of that region [Fig. 4.2.3(a)], and the maximum value of $(n^2+2)/6$ when $P_0(x_0, y_0)$ is in one of the corners of that region [Fig. 4.2.3(b)]. So the decay parameter β for the exponential weight function, in the range from $6/(n^2+2)$ to $6/(n^2-1)$, may be a reasonable choice. The range of the decay parameter decreases significantly ($\propto 1/n^4$) as the number of data points n increases. In other words, the impact of the selection of different β on the approximation results is insignificant as long as n is not very small, say $n > 1$. Therefore, for a given n the minimum possible β is arbitrarily used in our testing here.

4.3.2. Surface Fitting Approximation

Prewitt [4.19] introduced a method of defining edge detection operators on digital images by fitting a surface in the least squares sense to a neighborhood of each pixel, and taking the magnitude of the gradient of the surface as an estimate of the rate of change of grey level in the image at that pixel. Surface fitting approximation methods have been used on multidimensional images for edge and line detection [4.9],[4.10],[4.14].

Surface fitting by orthogonal basis functions for the 2D intensity interpolation problem can be stated as follows (this statement can be easily generalized to n-dimensions): Let $x = (x_1, x_2)$ be a point, and r_0 be a rectangular region in the 2D image space. Without loss of generality, the coordinate system is chosen in such a way that the centre of the region r_0 is at the origin. Let $\{S_i(x), 0 \le i \le N\}$ be a set of 2D orthogonal basis functions defined

over the region r_0, and $f(x)$ be the digital image function. The approximation $f^*(x)$ can then be estimated as a weighted sum of the basis functions:

$$f^*(x) = \sum_{i=0}^{N} a_i \, S_i(x) \tag{4.3.4}$$

where $\{a_i, \, 0 \leq i \leq N\}$ is a set of coefficients. The total squared approximation error, ε^2, can be written as

$$\varepsilon^2 = \sum_{x \in r_0} [f(x) - f^*(x)]^2. \tag{4.3.5}$$

By the orthogonal properties of the basis functions, it can be shown that the coefficients a_i which minimize ε^2 are obtained as

$$a_i = \frac{\displaystyle\sum_{x \in r_0} f(x) \, S_i(x)}{\displaystyle\sum_{x \in r_0} S_i^2(x)}. \tag{4.3.6}$$

Let χ_i be the support of x_i and $\{P_{ij}(x_i), \, 0 \leq j \leq M\}$ be a set of discrete orthogonal polynomials (up to Mth order) on χ_i, $i = 1, 2$. The set of 2D orthogonal basis functions $\{S_i(x), \, 0 \leq i \leq N\}$ can be constructed by the 1D discrete orthogonal polynomials $P_{ij}(x_i)$ as follows [4.10]:

$$\{P_{10}(x_1)P_{20}(x_2), \, P_{11}(x_1)P_{20}(x_2), \, P_{10}(x_1)P_{21}(x_2), ..., \, P_{1i_1}(x_1)P_{2i_2}(x_2)\} \tag{4.3.7}$$

where $i = i_1 + i_2$, $0 \leq i, i_1, i_2 \leq N$.

One possible approach of generating the 1D discrete orthogonal polynomials $\{P_k(x), \, 0 \leq k \leq m\}$ is given as follows [4.9]:

$$P_k(x) = x \, P_{k-1}(x) - C_k \, P_{k-2}(x) \tag{4.3.8}$$

where

$$C_k = \frac{\displaystyle\sum_{x \in \chi} P_{k-1}(x) \, P_{k-2}(x)}{\displaystyle\sum_{x \in \chi} P_{k-2}^2(x)} \tag{4.3.9}$$

and $P_k(x)$ is a polynomial of order k. A few discrete orthogonal polynomials created from (4.3.8) and (4.3.9) are:

$$P_{i0}(x_i) = 1, \ P_{i1}(x_i) = x_i, \ P_{i2}(x_i) = x_i^2 - \frac{m_{i2}}{m_{i0}}, \ P_{i3}(x_i) = x_i^3 - \frac{m_{i4}}{m_{i2}} x_i \qquad (4.3.10)$$

where

$$m_{ik} = \sum_{x \in \chi} x_i^k \qquad (4.3.11)$$

which is the kth moment of x_i over the support χ_i.

Let us develop, as an example, the cubic surface fitting algorithm. In terms of the 1D discrete orthogonal polynomials, by (4.3.4), the cubic surface can be formed as:

$$f^*(x) = a_0 + \sum_{i=1}^{2} a_i P_{i1}(x_i) + \sum_{i=1}^{2} a_{ii} P_{i2}(x_i) + \sum_{\substack{i,j=1 \\ i<j}}^{2} a_{ij} P_{i1}(x_i)P_{j1}(x_j)$$

$$+ \sum_{i=1}^{2} a_{iii} P_{i3}(x_i) + \sum_{\substack{i,j=1 \\ i \neq j}}^{2} a_{iij} P_{i2}(x_i)P_{j1}(x_j). \qquad (4.3.12)$$

From (4.3.6) and (4.3.12), the coefficients, which minimize the squared error, are found as follows:

$$a_0 = \frac{\displaystyle\sum_{x \in r_0} f(x)}{\displaystyle\sum_{x \in r_0} (1)}$$

$$a_i = \frac{\displaystyle\sum_{x \in r_0} P_{i1}(x_i) f(x)}{\displaystyle\sum_{x \in r_0} P_{i1}^2(x_i)}, \ a_{ii} = \frac{\displaystyle\sum_{x \in r_0} P_{i2}(x_i) f(x)}{\displaystyle\sum_{x \in r_0} P_{i2}^2(x_i)}, \ a_{iii} = \frac{\displaystyle\sum_{x \in r_0} P_{i3}(x_i) f(x)}{\displaystyle\sum_{x \in r_0} P_{i3}^2(x_i)}, \ 1 \le i \le 2 \qquad (4.3.13)$$

$$a_{ij} = \frac{\displaystyle\sum_{x \in r_0} P_{i1}(x_i)P_{j1}(x_j) f(x)}{\displaystyle\sum_{x \in r_0} P_{i1}^2(x_i)P_{j1}^2(x_j)}, \ a_{iij} = \frac{\displaystyle\sum_{x \in r_0} P_{i2}(x_i)P_{j1}(x_j) f(x)}{\displaystyle\sum_{x \in r_0} P_{i2}^2(x_i)P_{j1}^2(x_j)}, \ 1 \le i < j \le 2.$$

In terms of the coordinates (x_1, x_2), the cubic surface can be written as:

$$f^*(x) = b_0 + \sum_{i=1}^{2} b_i x_i + \sum_{i=1}^{2} b_{ii} x_i^2 + \sum_{\substack{i,j=1 \\ i<j}}^{2} b_{ij} x_i x_j + \sum_{i=1}^{2} b_{iii} x_i^3 + \sum_{\substack{i,j=1 \\ i \neq j}}^{2} b_{iij} x_i^2 x_j. \qquad (4.3.14)$$

From (4.3.12), (4.3.13), and (4.3.14), we find that the a's and b's are related through the following:

$$b_0 = a_0 - \sum_{i=1}^{2} \frac{m_{i2}}{m_{i0}} a_{ii}$$

$$b_i = a_i - \frac{m_{i4}}{m_{i2}} a_{iii} - \sum_{\substack{j=1 \\ j \neq i}}^{2} \frac{m_{j2}}{m_{j0}} a_{jji}, \quad b_{ii} = a_{ii}, \quad b_{iii} = a_{iii}, \quad 1 \leq i \leq 2 \qquad (4.3.15)$$

$$b_{ij} = a_{ij}, \quad b_{iij} = a_{iij}, \quad 1 \leq i < j \leq 2.$$

For different neighborhood sizes from 1 x 1 up to 8 x 8, these coefficients b's can be represented through *local linear image operators*. These local operators have been derived for surface fitting methods of orders up to 3 and are presented in Appendix 3.

4.4. Grey Level Resampling Tests Using Breast Tissue Images

We tested the geometric unwarping algorithms with the above proposed grey level interpolation and approximation techniques using CT images of real breast tissue. The reasons for using such images, and the method for obtaining them, as well as a brief description of the used image processing system can be found in Section 3.3.1. The evaluation for these resampling tests was carried out by using the intensity error measures ε_1 to ε_4 in (3.3.1).

Two types of tests with our CT images were conducted in this study. In both classes, one of the images taken before distortion was chosen as a reference image. A warped image of the same tissue with "simulated distortion" was made from the reference image by an analytic transformation in the first type of tests. This is simply because the known transformation allows an exact analysis of the geometric accuracy of the unwarping algorithm, and allows us to distinguish the grey level resampling errors from the geometric ones. In the second type of tests, intensity resampling algorithms were applied to a real

warped image taken after mechanical distortion of the tissue for comparison with its reference image.

4.4.1. Results with Simulated Images of Distorted Breast Tissue

The reference and warped images from a set of known warping functions (see Section 3.3.3 for details) are shown in Fig. 3.3.3. The selection of control points can also be found in Section 3.3.3.

Difference images obtained by using the known, simulated analytic, and local quintic unwarping transformations and linear grey level interpolation, and the difference image of the reference image and warped image only (or no attempt at unwarping) as well are shown in Figs. 3.3.4(a), (b), and (g), respectively. The intensity measures for geometric unwarping with truncated sinc, Lagrange, cubic splines, and cubic convolution interpolation procedures are plotted in Figs. 4.4.1 - 4.4.4, respectively. Noted that, in Fig. 4.4.3, we have also used the (incorrect) original warped image pixels in lieu of the correct coefficients c in (4.2.17). We present in Figs. 4.4.5 and 4.4.6 the results by using the distance weighted least squares and surface fitting approximations, respectively.
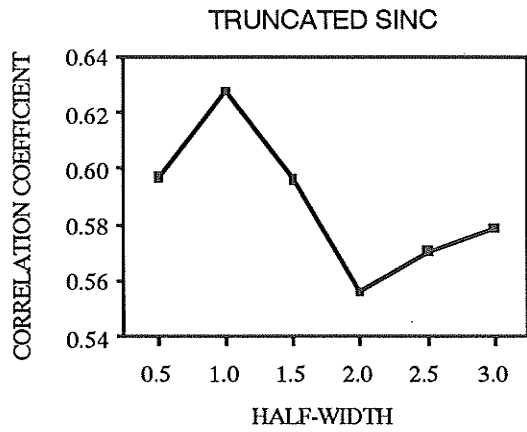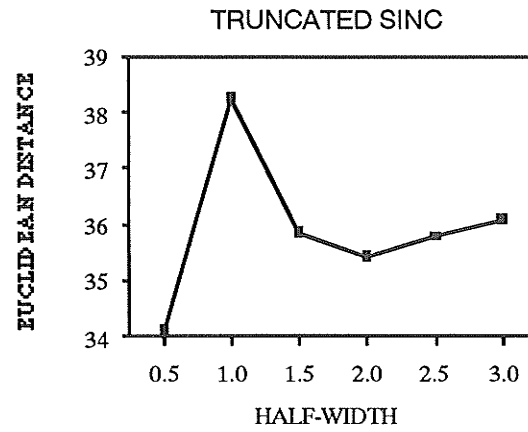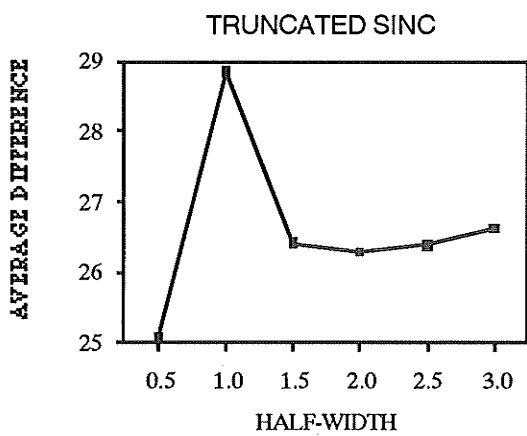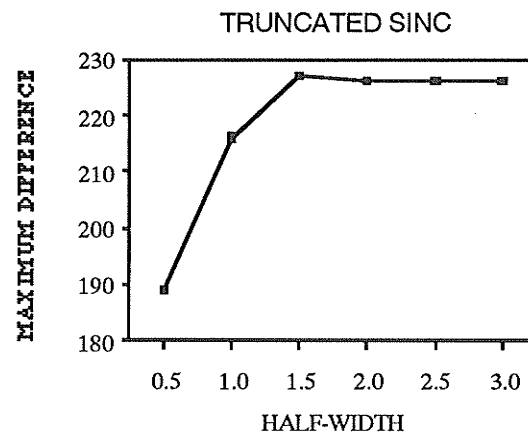
Fig. 4.4.1. Intensity error measures (3.3.1) obtained by local quintic unwarping transformation and truncated sinc grey level interpolation (4.2.8).

Fig. 4.4.2. Intensity error measures (3.3.1) obtained by local quintic unwarping transformation and Lagrange grey level interpolation (4.2.9).

CUBIC SPLINE (a)

CUBIC SPLINE (b)

CUBIC SPLINE (c)
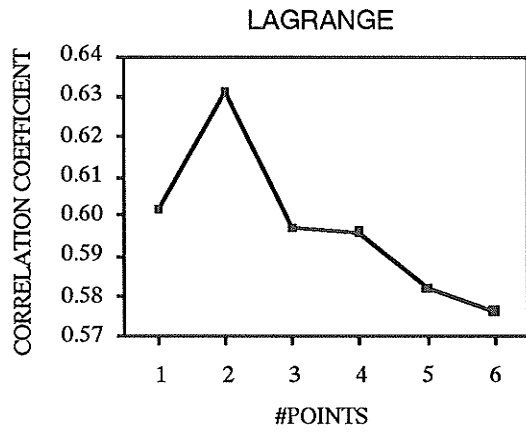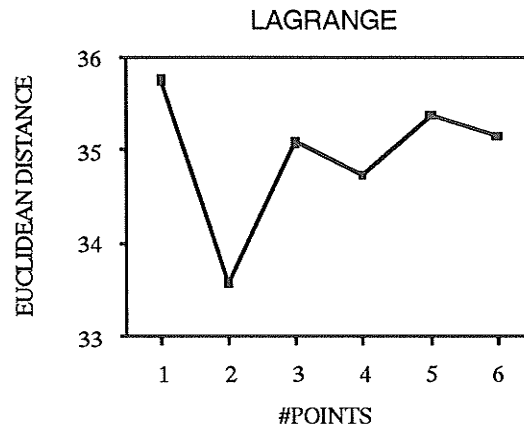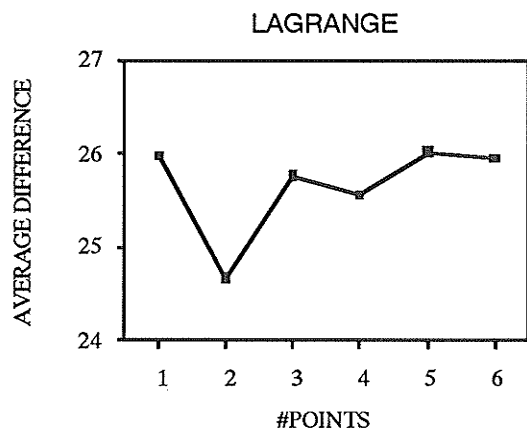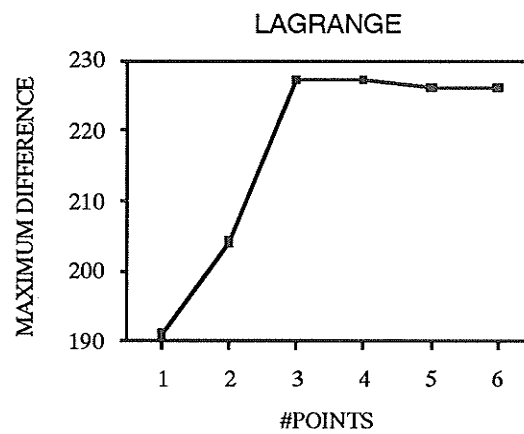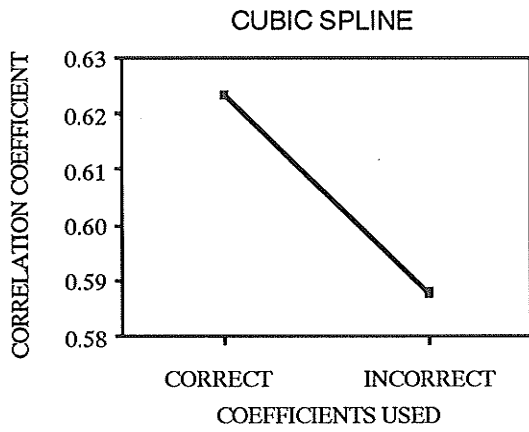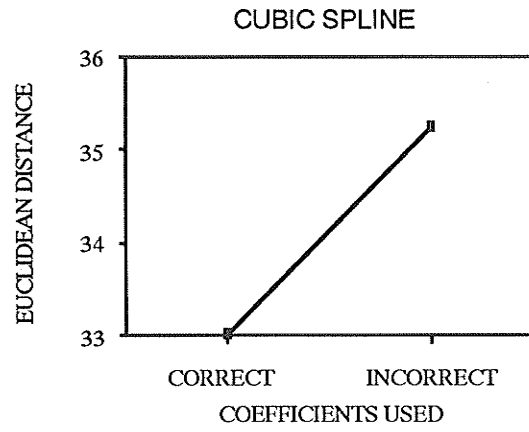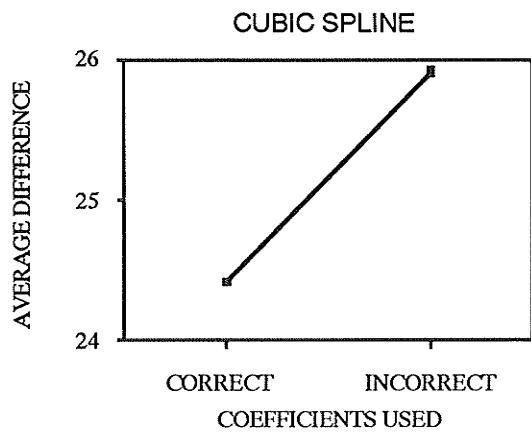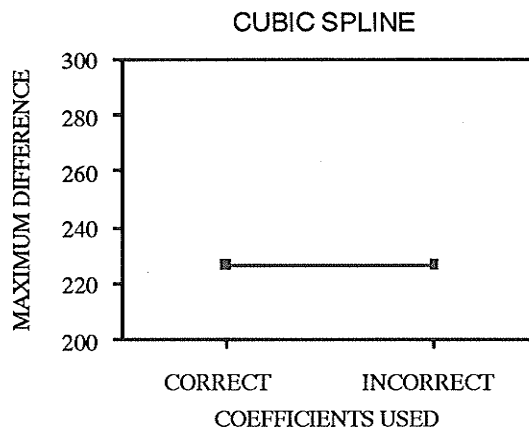
CUBIC SPLINE (d)

Fig. 4.4.3. Intensity error measures (3.3.1) obtained by local quintic unwarping transformation and cubic splines grey level interpolation (4.2.13).
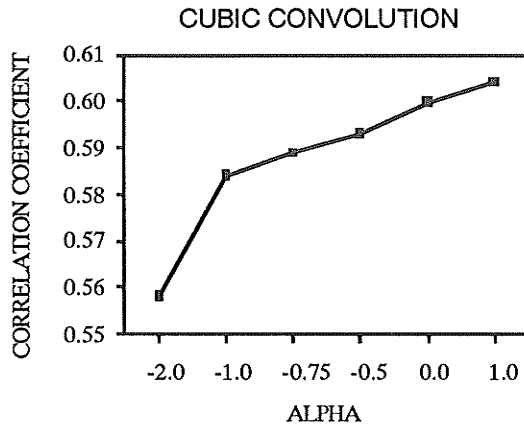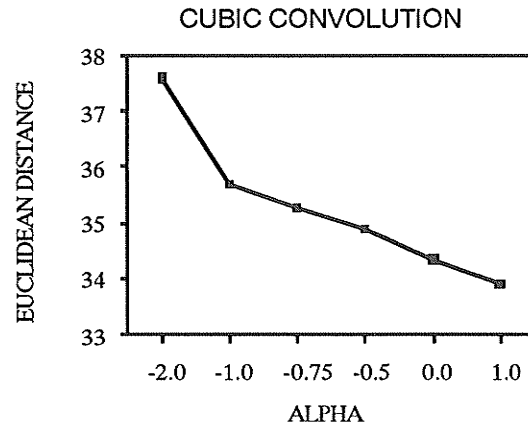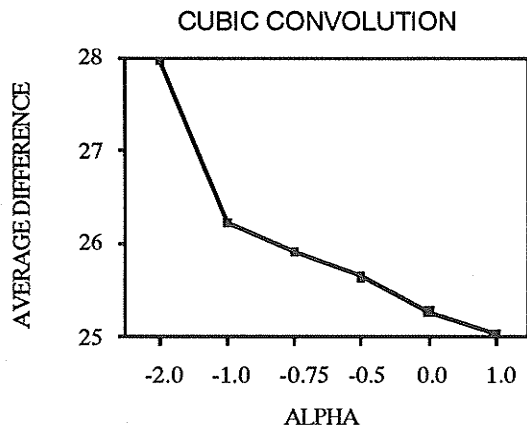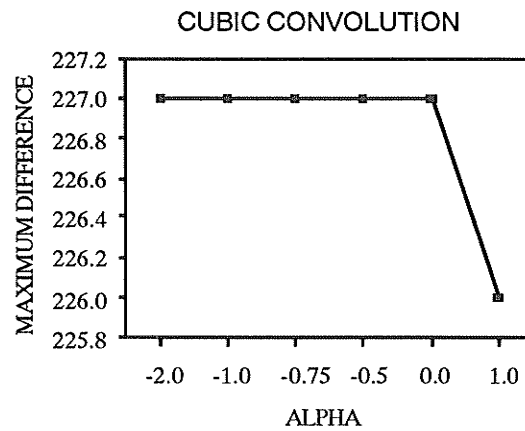
Fig. 4.4.4. Intensity error measures (3.3.1) obtained by local quintic unwarping transformation and cubic convolution grey level interpolation (4.2.19).

(a)

(b)

(c)

(d)

(e)

(f)

(g)

(h)

(i)

(j)

(k)

(l)

DWLS (THIRD ORDER)

(m)

DWLS (THIRD ORDER)

(n)

DWLS (THIRD ORDER)

(o)

DWLS (THIRD ORDER)

(p)
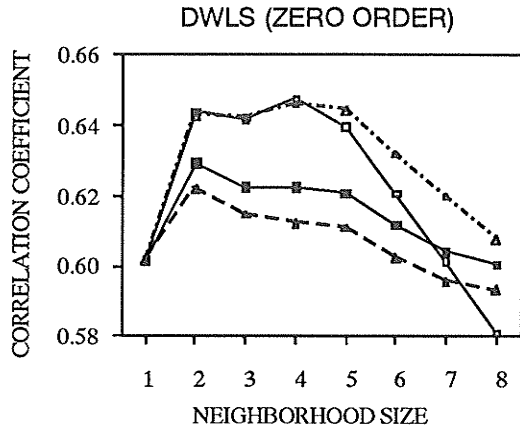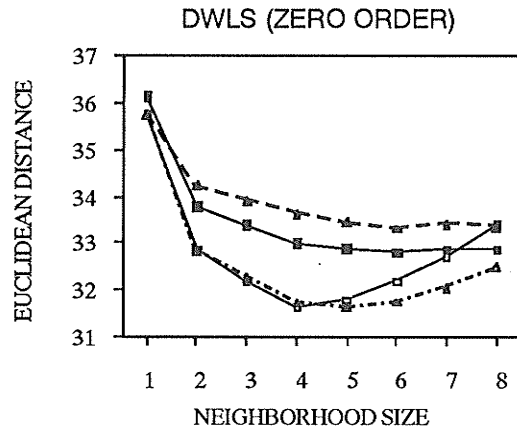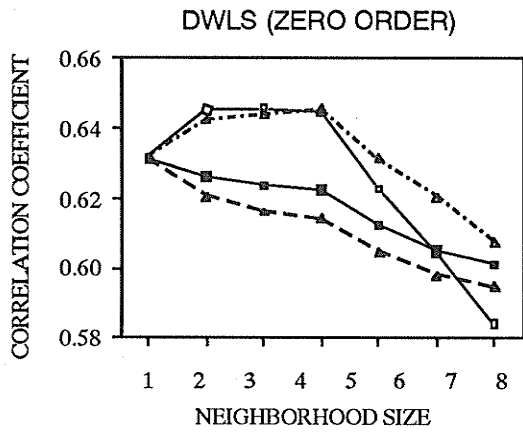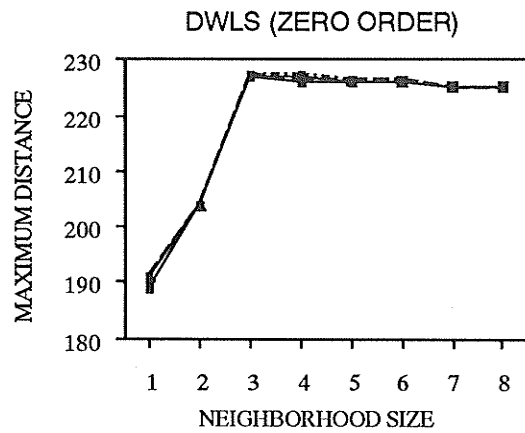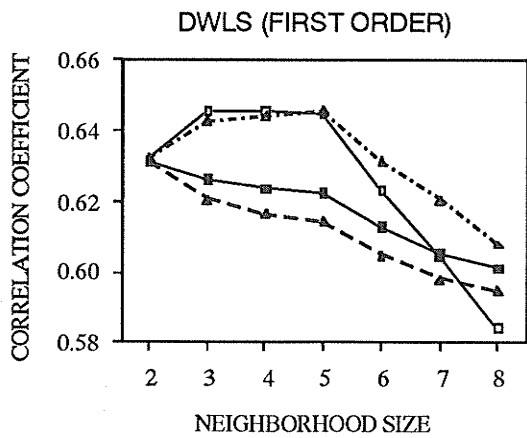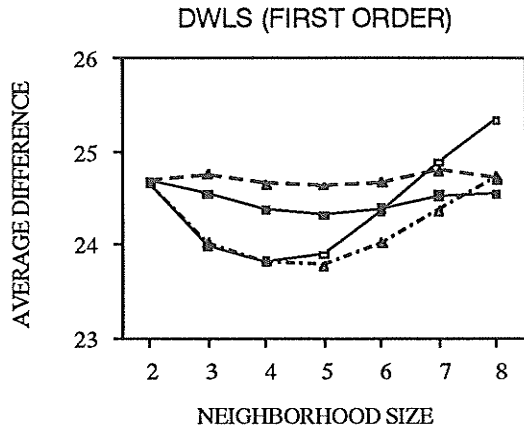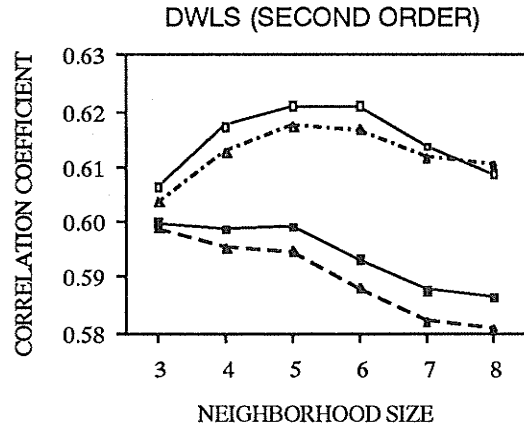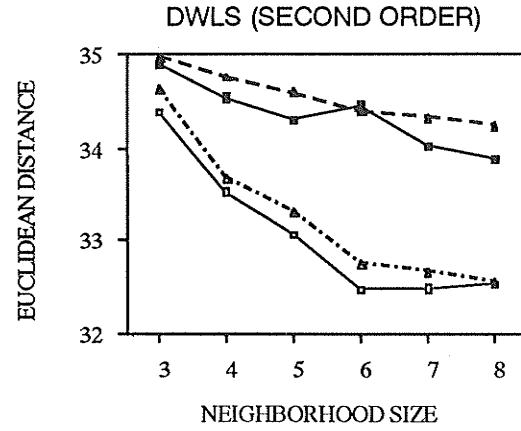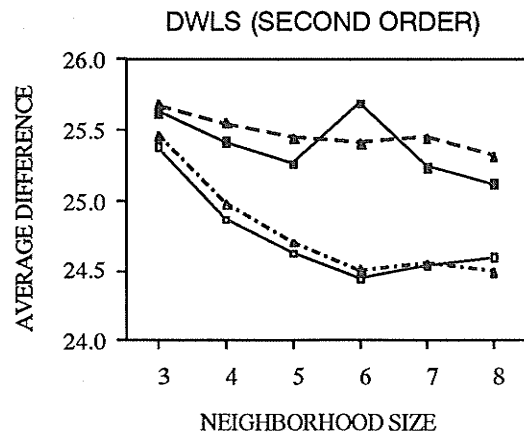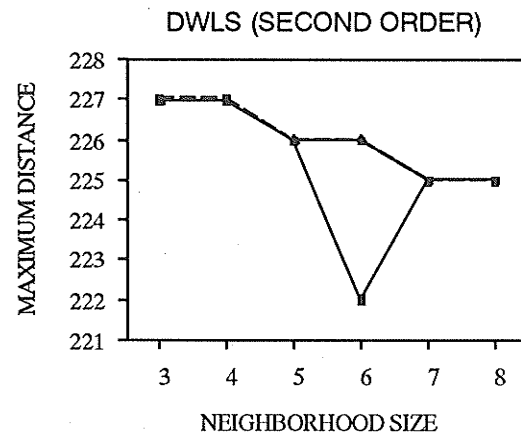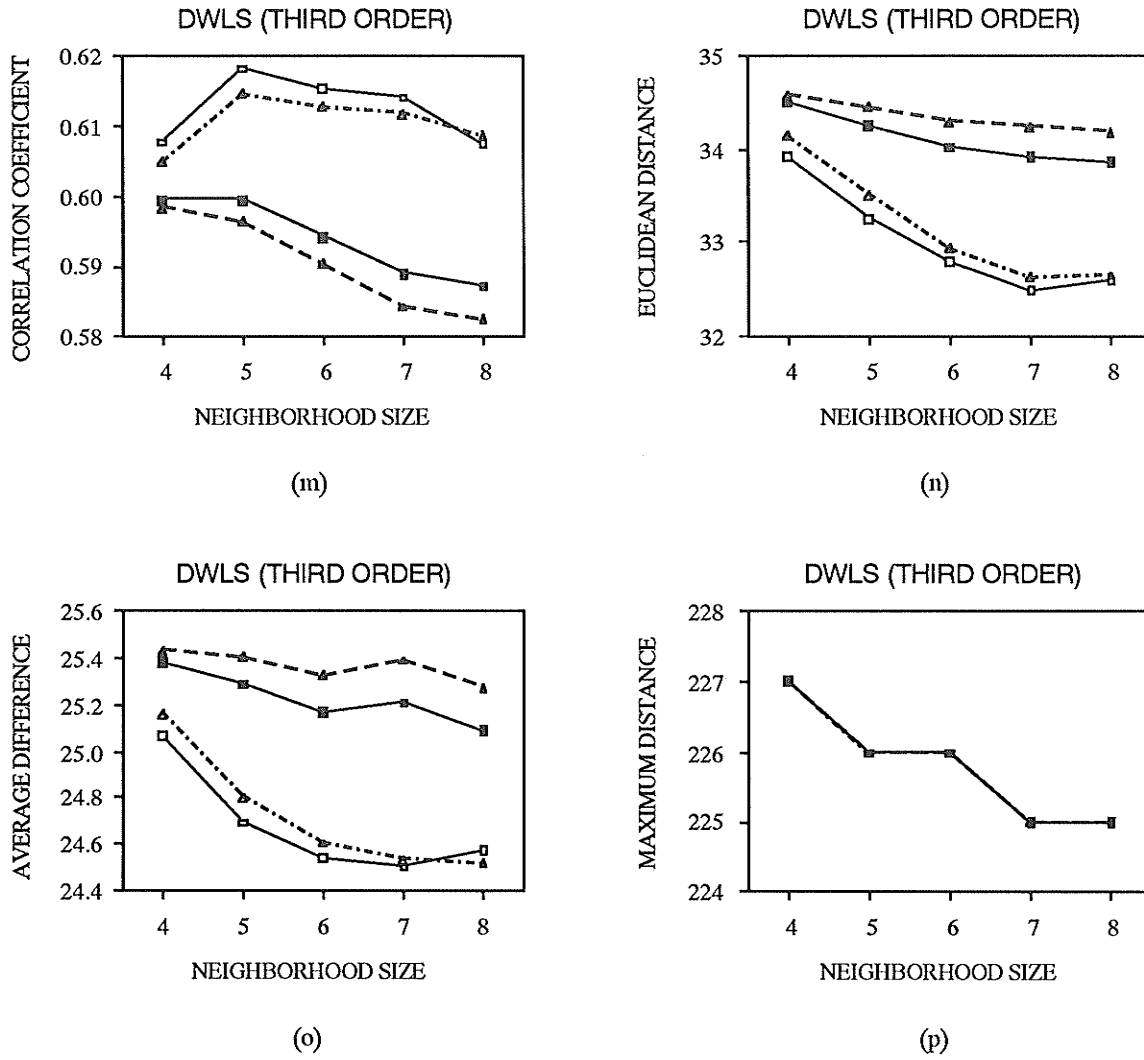
Fig. 4.4.5. Intensity error measures (3.3.1) obtained by local quintic unwarping transformation and distance weighted least squares (DWLS) grey level approximation with weighting function $w(d^2)$ of 1 (———□———), $1/d^2$ (— — ▨— —), $\exp(-\beta d^2)$ (· —△· —), and $\exp(-\beta d^2)/d^2$ (— ▲ —) .

SURFACE FITTING (FIRST ORDER)

(a)

SURFACE FITTING (FIRST ORDER)

(b)

SURFACE FITTING (FIRST ORDER)

(c)

SURFACE FITTING (FIRST ORDER)

(d)

SURFACE FITTING (SECOND ORDER)

(e)

SURFACE FITTING (SECOND ORDER)

(f)
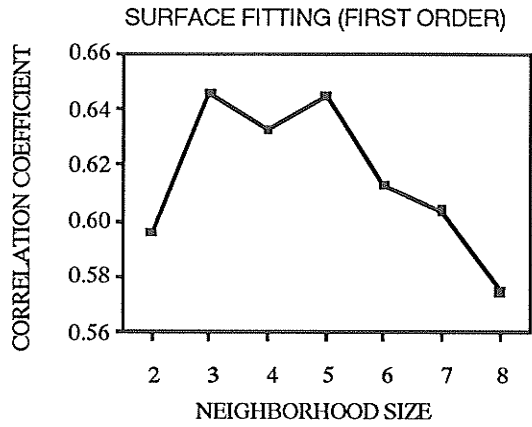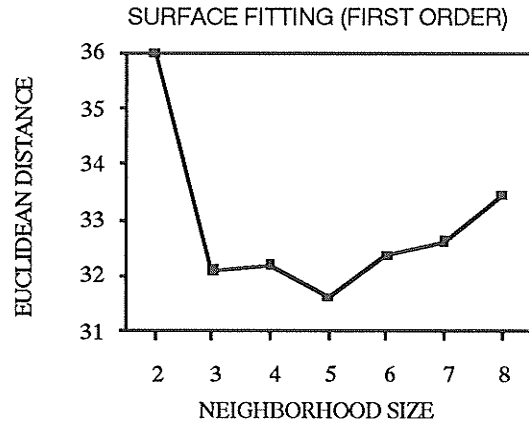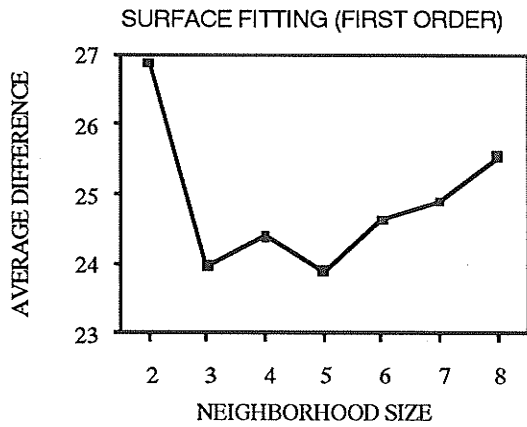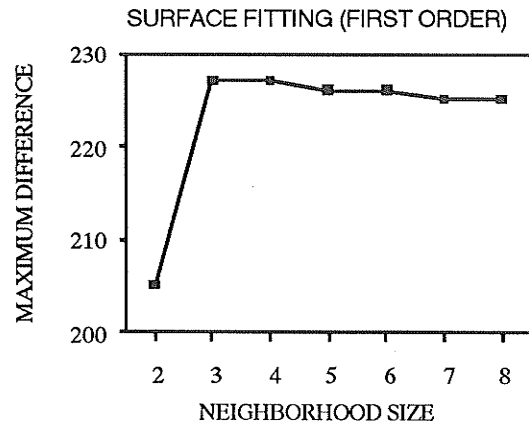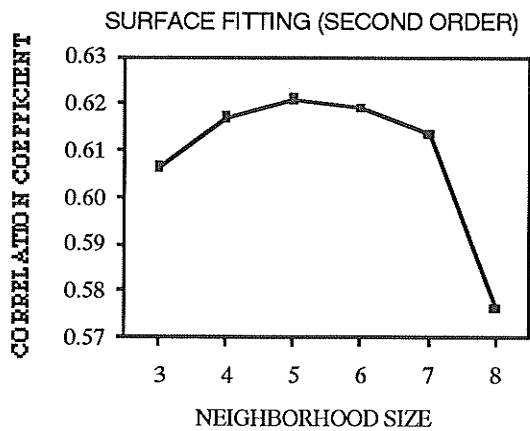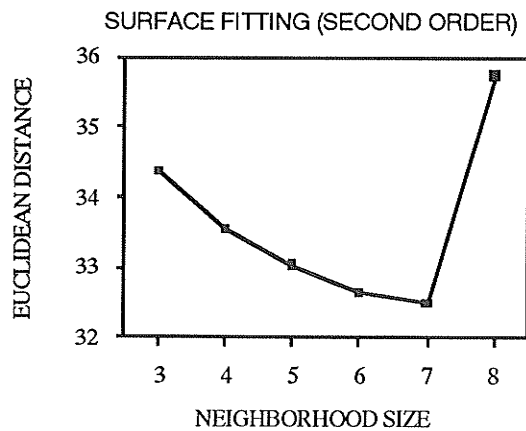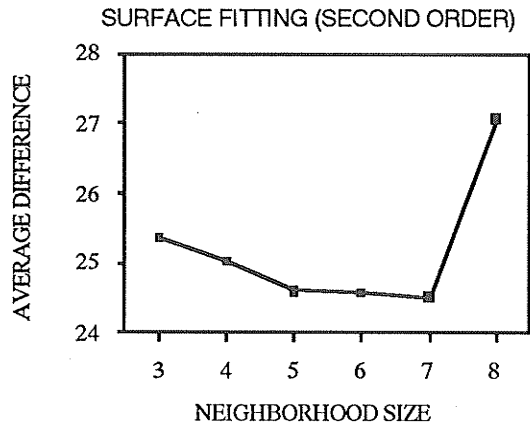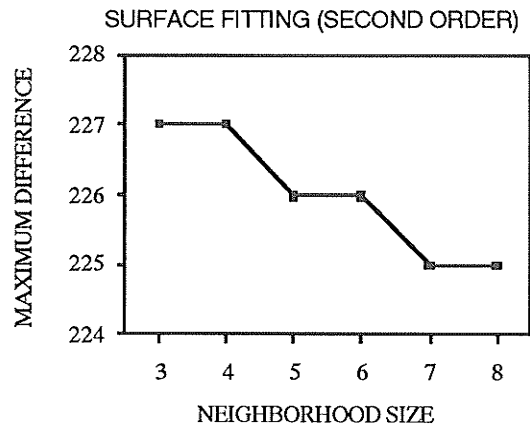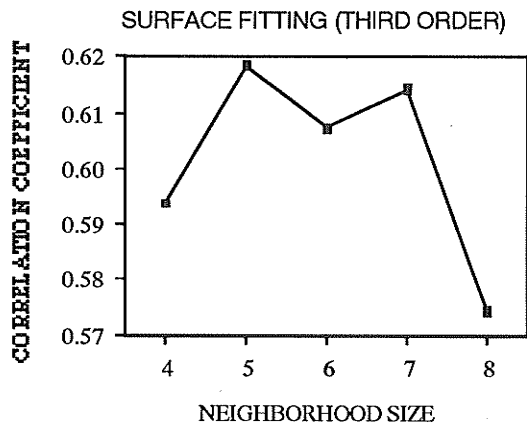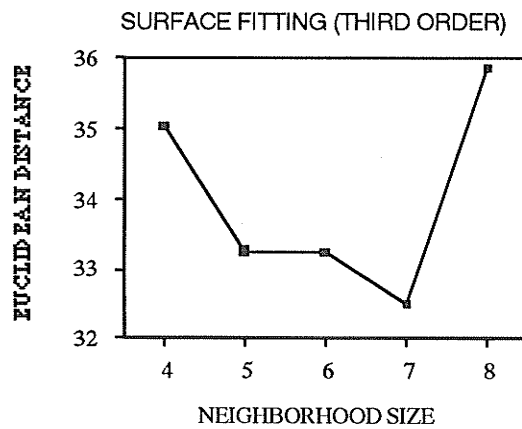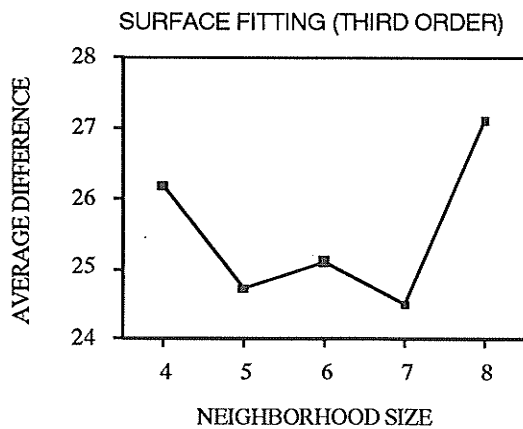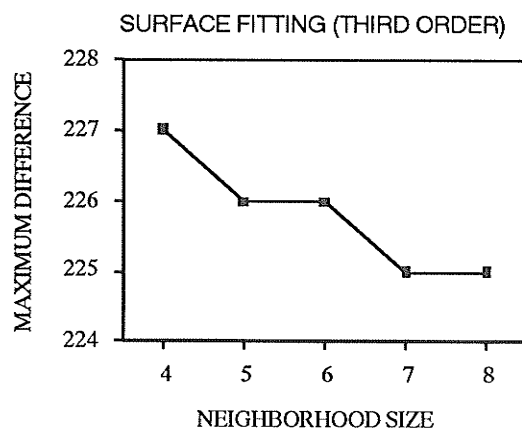
Fig. 4.4.6. Intensity error measures (3.3.1) obtained by local quintic unwarping transformation and surface fitting grey level approximation. Results from the surface fitting of zero order, not shown here, are the same as those in Figs. 4.4.5(a)-(d) with weighting function $w(d^2)$ of 1 (————□————).

4.4.2. Results with Actual Images of Distorted Breast Tissue

We applied the intensity resampling procedures to an image of mechanically distorted breast tissue, which is shown in Fig. 3.3.6. Some structures in one image are missing in the other because structures sometimes move out of a given slice plane after distortion. This makes geometric unwarping more difficult than the above test with the simulated data set. (This problem will disappear when our methods are generalized to 3D.)

Forty-two pairs of corresponding texture features from the reference and warped images were manually chosen as the control points. See Figs. 3.3.7(a) and (f), respectively, for the difference image obtained by using the local quintic unwarping transformation and linear grey level interpolation, and the difference image of the reference image and warped image only (or no attempt at unwarping). In Figs. 4.4.7 - 4.4.12 we present the intensity measures for these unwarping results from local quintic unwarping transformation, and different grey level interpolation and approximation algorithms.
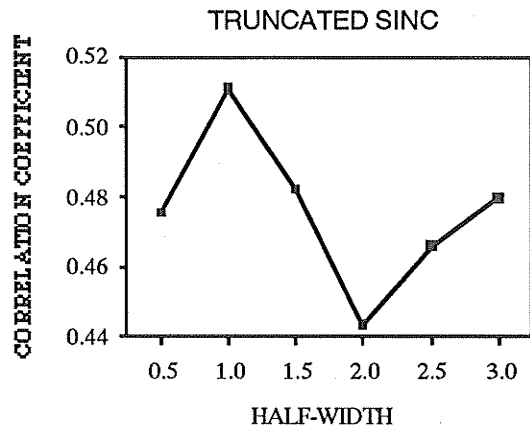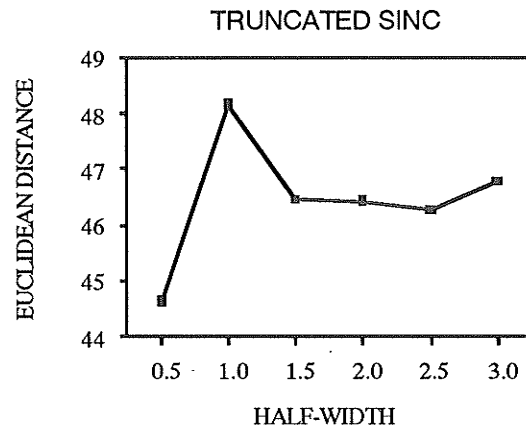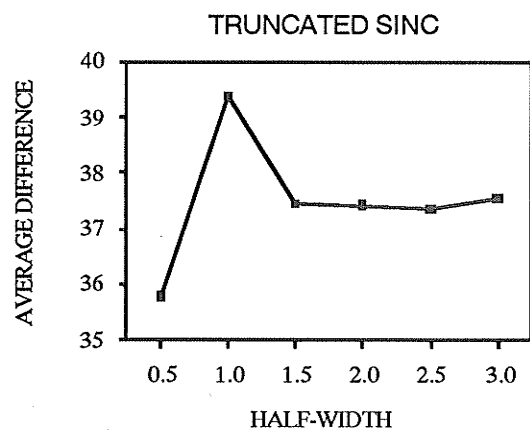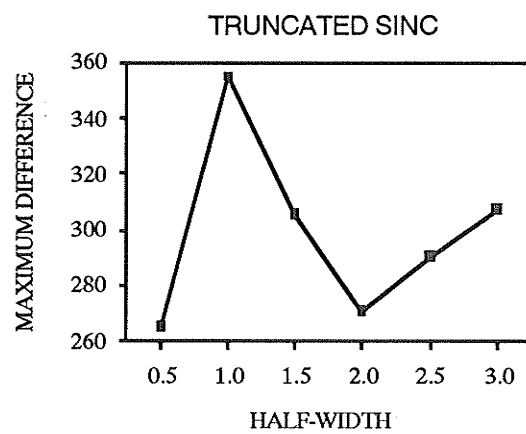
Fig. 4.4.7. Intensity error measures (3.3.1) obtained by local quintic unwarping transformation and truncated sinc grey level interpolation (4.2.8).
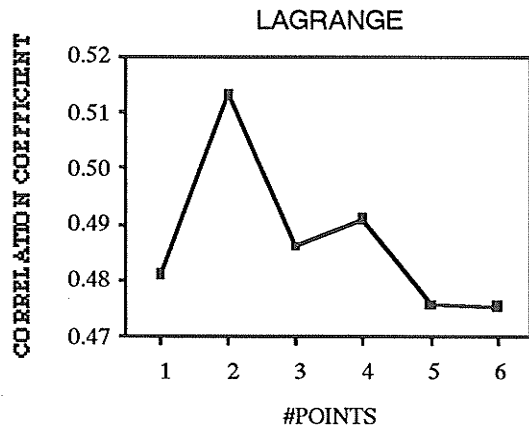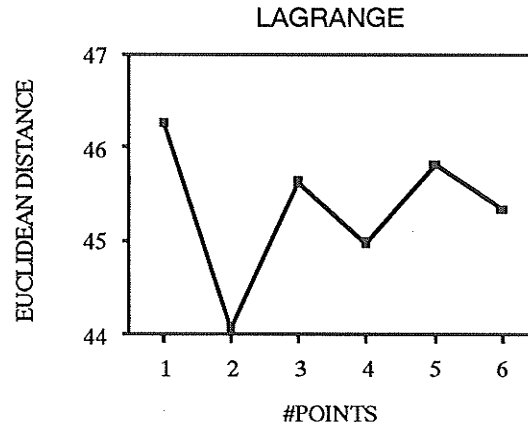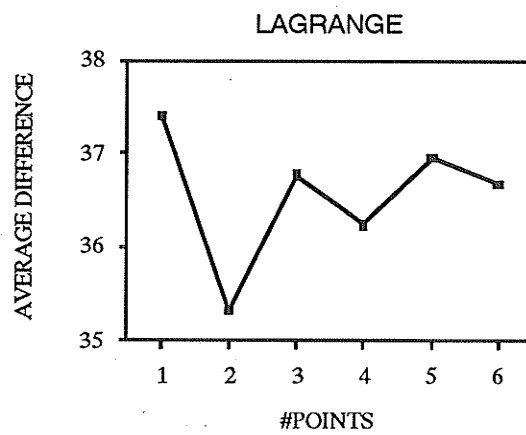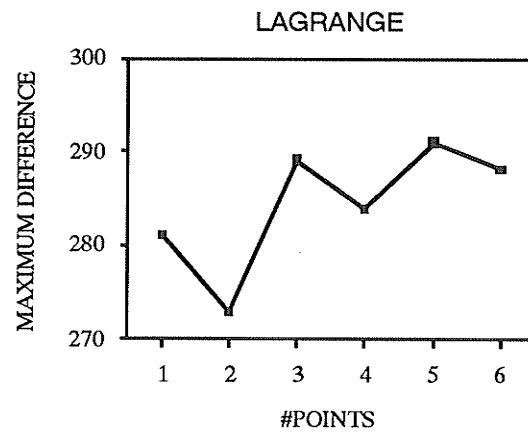
Fig. 4.4.8. Intensity error measures (3.3.1) obtained by local quintic unwarping transformation and Lagrange grey level interpolation (4.2.9).
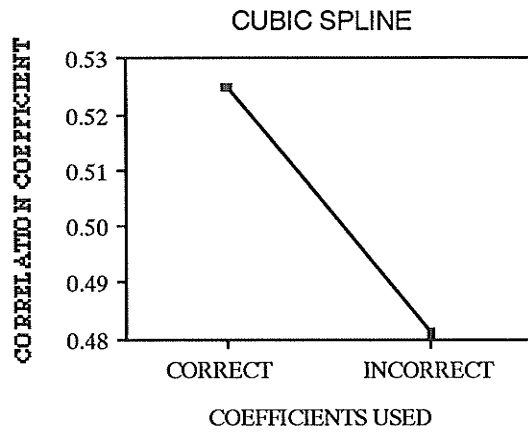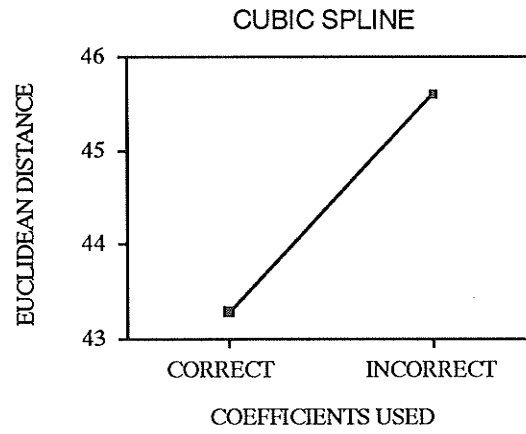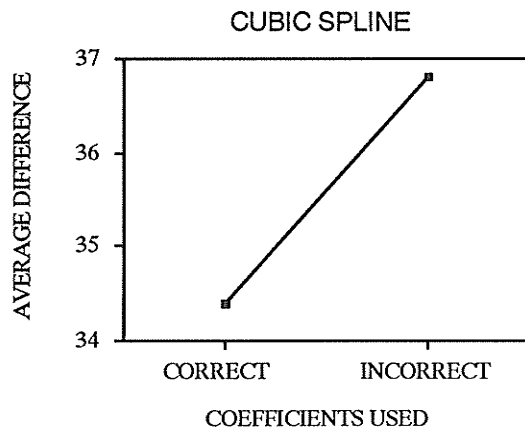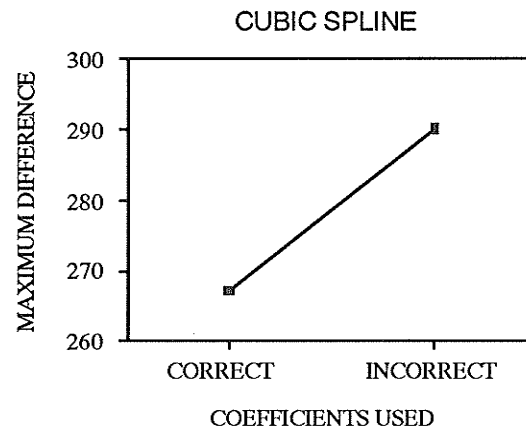
Fig. 4.4.9. Intensity error measures (3.3.1) obtained by local quintic unwarping transformation and cubic splines grey level interpolation (4.2.13).
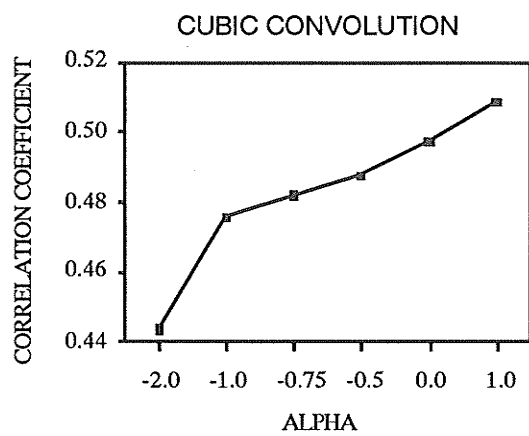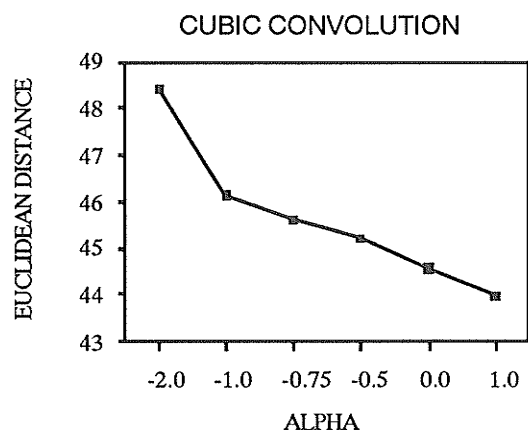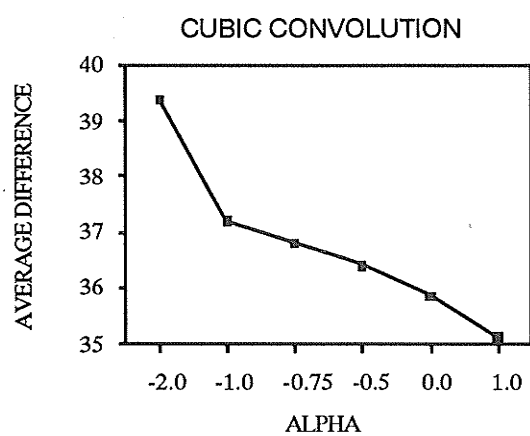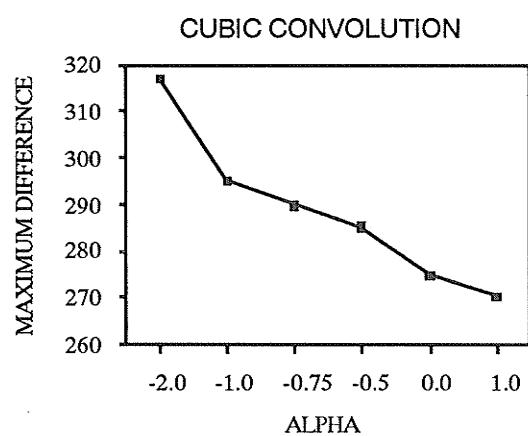
Fig. 4.4.10. Intensity error measures (3.3.1) obtained by local quintic unwarping transformation and cubic convolution grey level interpolation (4.2.19).

(a)

(b)

(c)

(d)

(e)

(f)

DWLS (FIRST ORDER)

(g)

DWLS (FIRST ORDER)

(h)

DWLS (SECOND ORDER)

(i)

DWLS (SECOND ORDER)

(j)

DWLS (SECOND ORDER)

(k)

DWLS (SECOND ORDER)
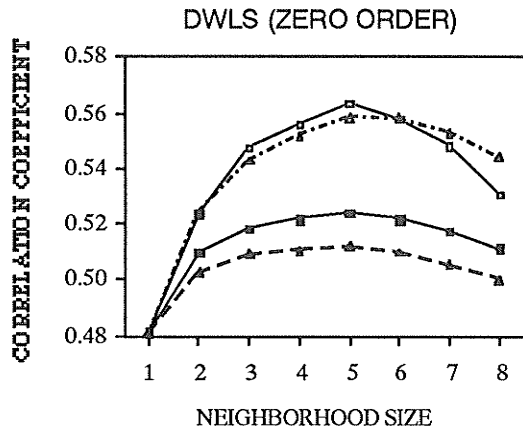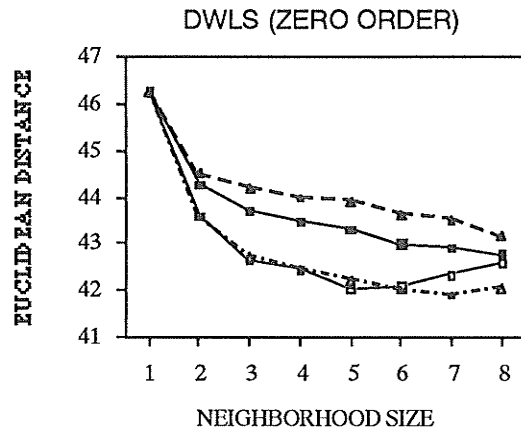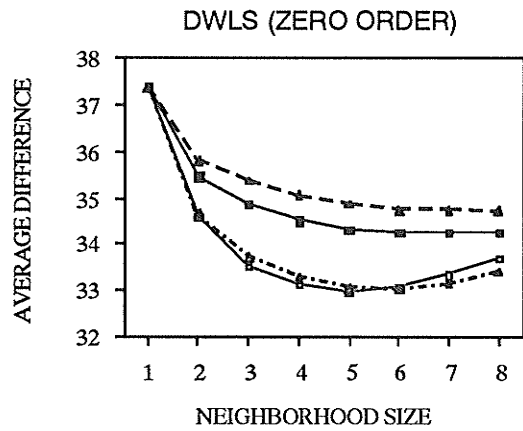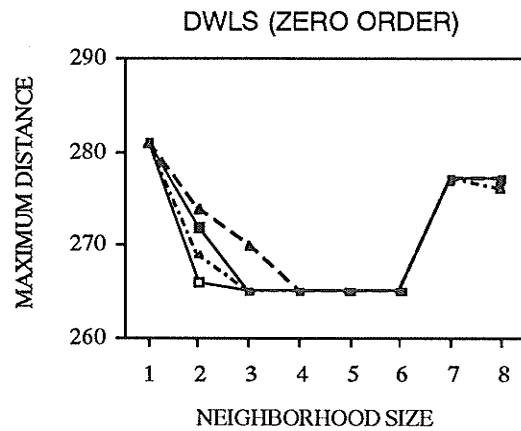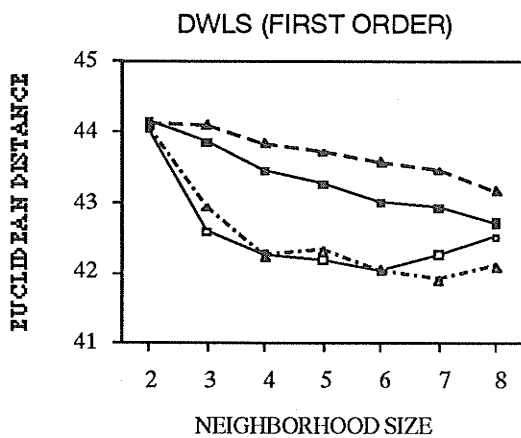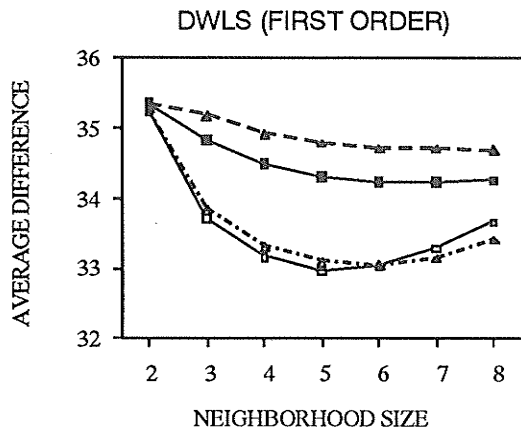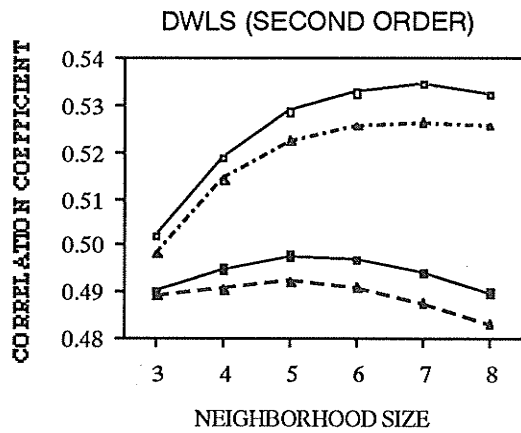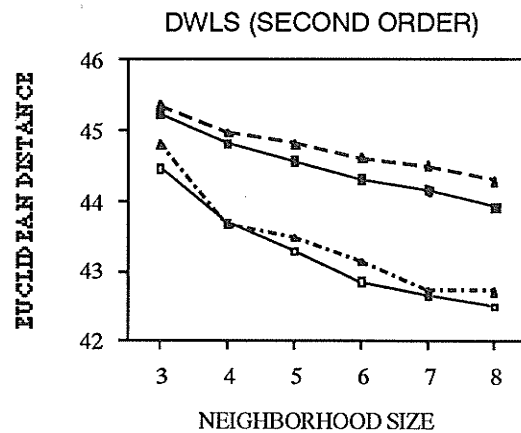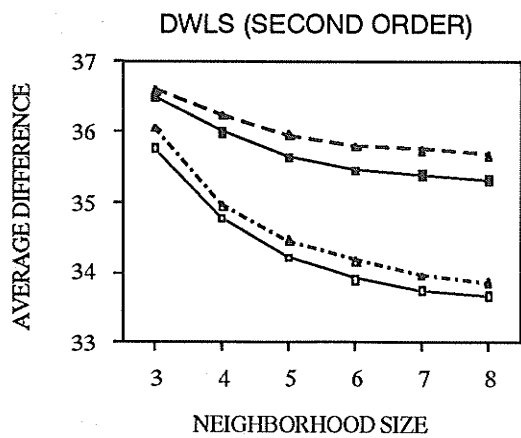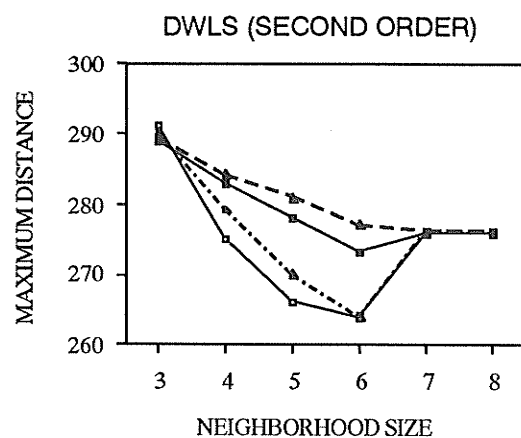
(l)
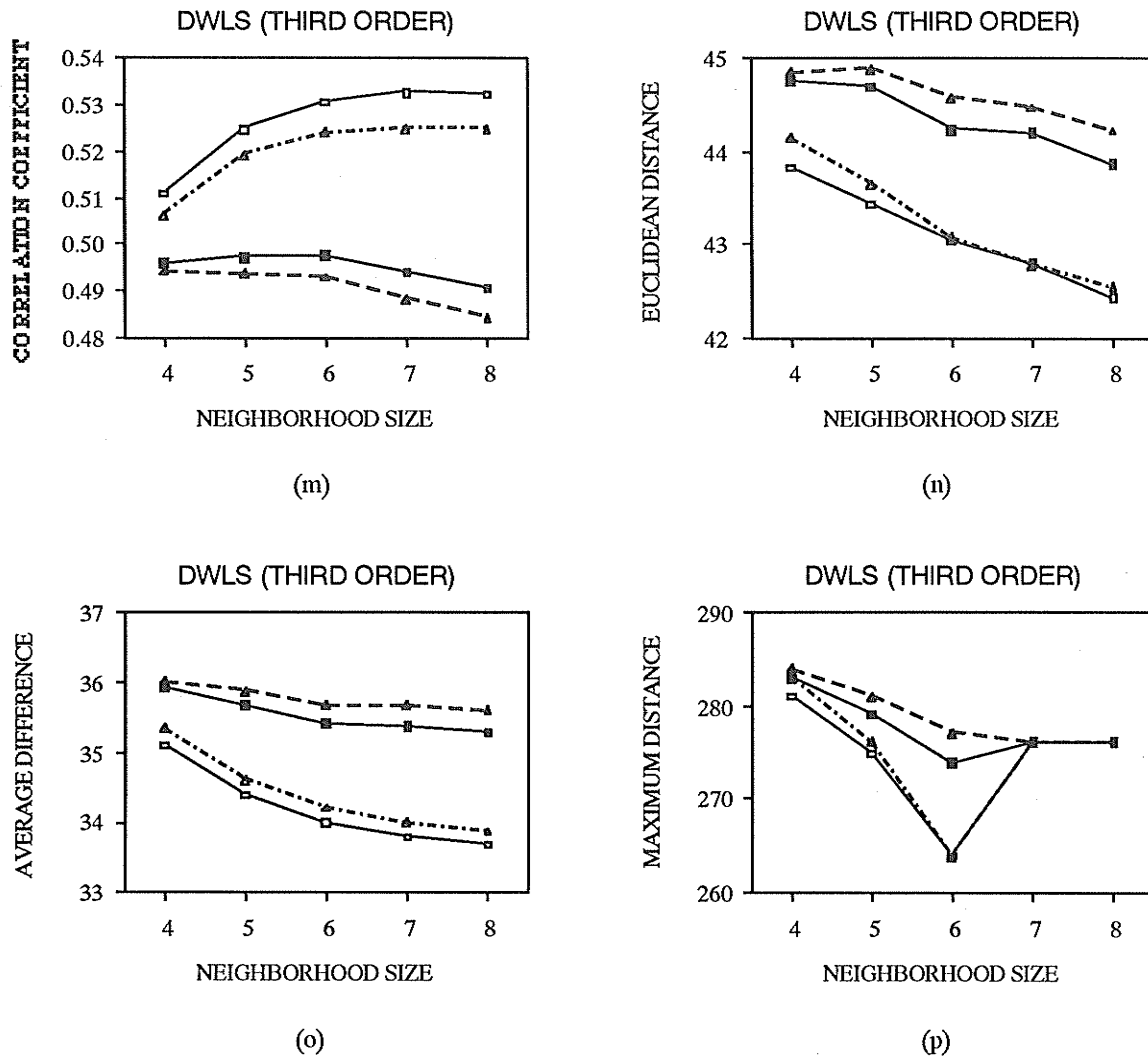
Fig. 4.4.11. Intensity error measures (3.3.1) obtained by local quintic unwarping transformation and distance weighted least squares grey level approximation with weighting function $w(d^2)$ of 1 (———□———), $1/d^2$ (— — ▨— —), $\exp(-\beta d^2)$ (· —△· —), and $\exp(-\beta d^2)/d^2$ (— ▲ —) .

SURFACE FITTING (FIRST ORDER)

(a)

SURFACE FITTING (FIRST ORDER)

(b)

SURFACE FITTING (FIRST ORDER)

(c)

SURFACE FITTING (FIRST ORDER)

(d)

SURFACE FITTING (SECOND ORDER)

(e)

SURFACE FITTING (SECOND ORDER)
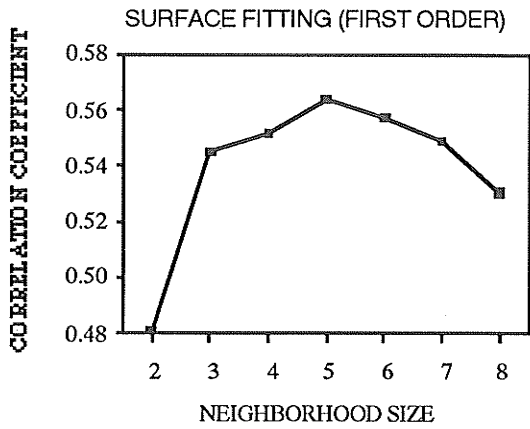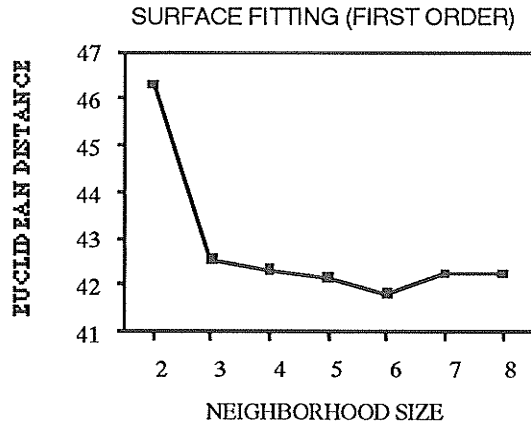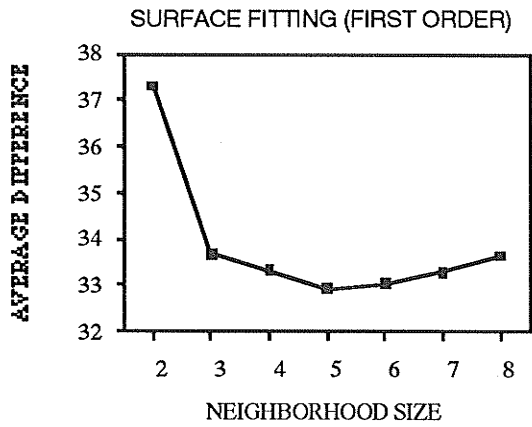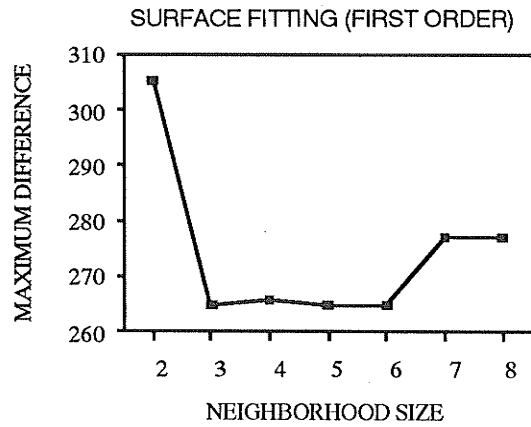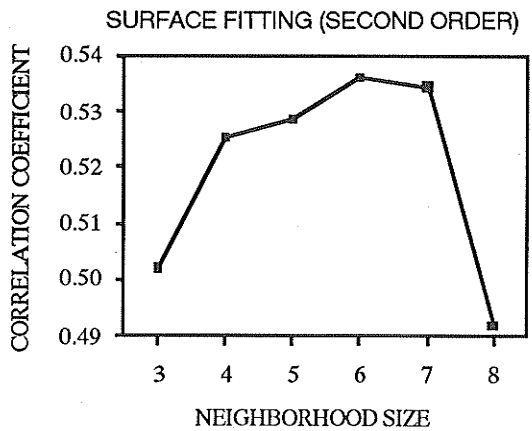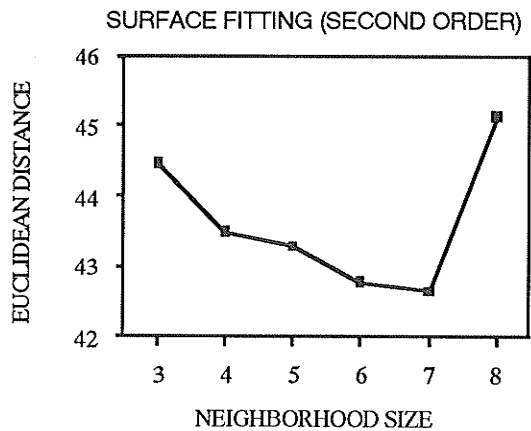
(f)
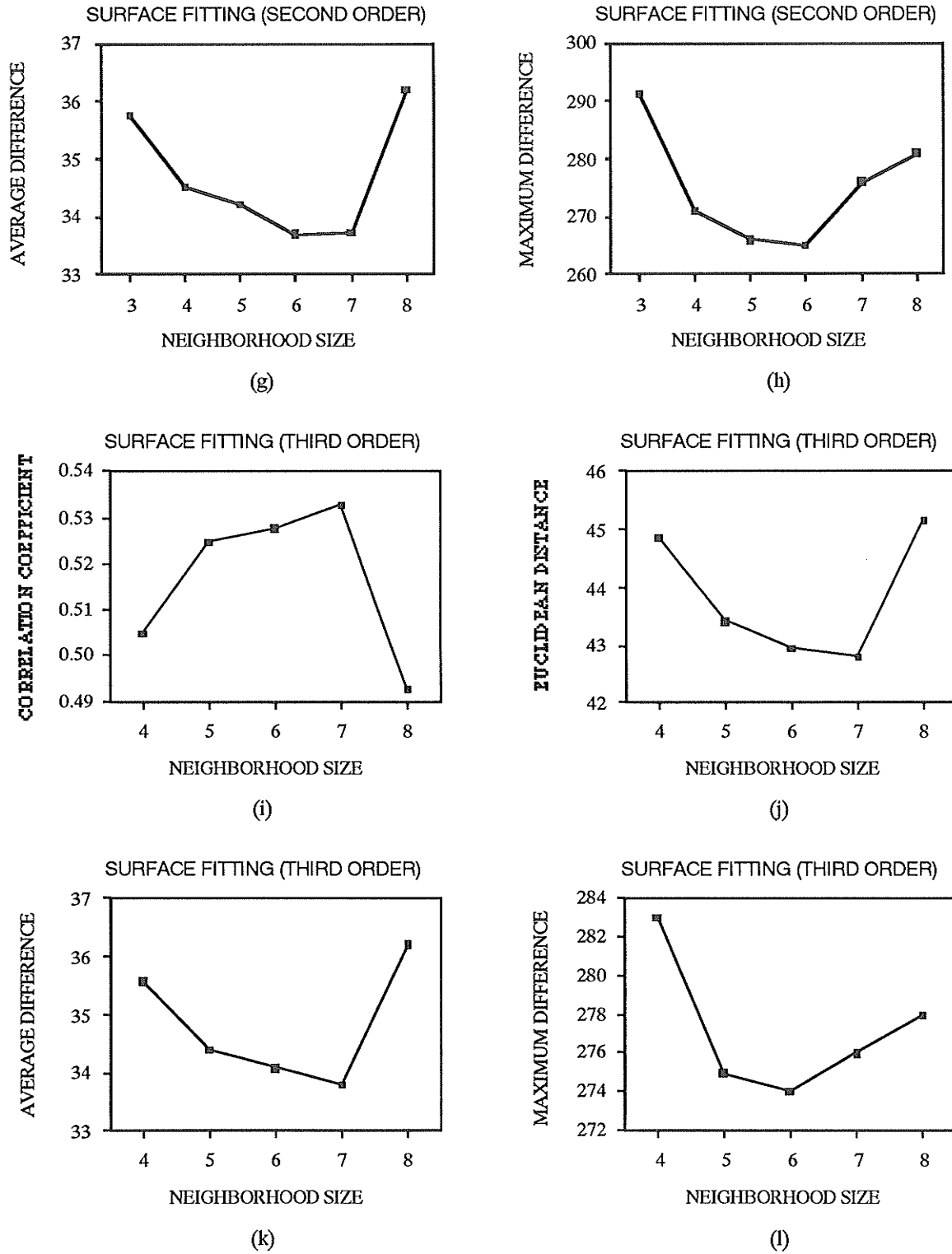
Fig. 4.4.12. Intensity error measures (3.3.1) obtained by local quintic unwarping transformation and surface fitting grey level approximation. Results from the surface fitting of zero order, not shown here, are the same as those in Figs. 4.4.11(a)-(d) with weighting function $w(d^2)$ of 1 (——□——).

4.5. Discussion and Conclusions

If an image is band-limited and sufficiently sampled, then it can be recovered exactly by using the sinc interpolation function. In practice, however, it is impossible to use such a spatially unlimited function, and a truncated form of the sinc function must be used. The discontinuities of the function value and the slope at the end points result in undesirable ripples and overshoots in the frequency domain. From the test results in this work (Figs. 4.4.1 and 4.4.7), the width of the truncated sinc function around 3.0 seems to give the best compromise as far as all measures are concerned.

Lagrange interpolation formulas will better approximate the sinc function as the number of points increases, and their Fourier transforms will also approach the $\prod$ function. Lagrange interpolations with an odd number of data points approximate the sinc function for low frequency components better but suppress high frequencies less effectively than those with an even number of points. The significant advantage of nearest-neighbor interpolation is that no calculations are required to derive the intensity value, but linear interpolation yields the best results among all Lagrange methods used with different numbers of data points.

Because of its smoothness, local support and shift-invariant properties, the cubic B-spline function offers very significant advantages for different fields. Our study on geometric unwarping of breast tissue images has shown that cubic B-spline interpolation is superior to other interpolation methods for this problem. The major concern about the cubic splines procedure is its computing complexity.

The cubic convolution algorithm provides a good compromise between computing complexity and accuracy. In other words, it is more efficient than the cubic splines and it produces more accurate results than truncated sinc and Lagrange interpolations do. As demonstrated in this thesis, the parameter α provides the ability to control the frequency characteristics of the interpolation process. Although theoretical arguments predict that

$\alpha = -0.5$ represents a good default value for general purpose implementation [4.13], [4.15], we noted that the optimal choice of α is image dependent. For instance, the choice of $\alpha = 1$ yields the best interpolation measure numbers for images with simulated distortion and mechanically distorted images of breast tissue (Figs. 4.4.4 and 4.4.10).

When a large set of data points is given, it is not necessarily appropriate to use an interpolation method to find a polynomial of high enough order for an exact fit at all data points. The resultant polynomial is almost always extremely undulatory (see Lagrange interpolation in Figs. 4.4.2 and 4.4.8 for an example). In some applications the sampled data themselves are not accurate, so there is no point at all to try to find an "accurate" value based on such inaccurate sampled data.

By using 2 x 2 to 5 x 5 neighborhoods, zero and first order least squares methods provide better intensity approximation than other neighborhood sizes. This is probably because the least squares methods act as local smoothing operators, and this smoothing effect is just more dominant for larger neighborhood sizes. There might exist some neighborhood sizes $n > 8$ with which the second and third order least squares could produce better results, although lower order least squares seem better than higher order ones for neighborhood sizes up to 8 x 8. These conclusions imply that in order to obtain reasonably accurate results it is necessary to use higher order polynomials to fit a surface over larger neighborhood sizes. As expected, results obtained by the surface fitting approach are fairly similar to those obtained by the least squares technique. This is simply because both methods do fit a polynomial over a specific neighborhood, except that power functions are adopted for least squares and orthogonal polynomials are used for surface fitting. Not surprisingly, the surface fitting procedure is more efficient computationally than the least squares. This is, of course, due to the facts that all coefficients for surface fitting are pre-calculated and stored in the memory and that a system of linear equations (the number of unknowns is dependent on the order of the fitting polynomial used) has to be solved for each pixel to be unwarped.

As discussed in Section 4.3.1, it may be appropriate for us to require data points close to the point to be interpolated to carry more weight than those more remote points, especially when a large number of data points is involved. From Figs. 4.4.5 and 4.4.11 this can be observed clearly for the zero and first order distance weighted least squares as the neighborhood size approaches 6 x 6. We expect that this is also true for the second and third order distance weighted least squares algorithms when the neighborhood is larger than some specific size. The decreasing rate of the weight function with distance also has a significant impact on the approximation performance. For example, distance weighted least squares with weight function $\exp(-\beta d^2)$ yields better results than that with either $1/d^2$ or $\exp(-\beta d^2)/d^2$ (Figs. 4.4.5 and 4.4.11).

We have presented a general discussion of the intensity resampling problem for the geometric unwarping procedure. Intensity interpolation and approximation techniques for geometric unwarping in 2D have been formulated and tested using high resolution CT mammograms. This study confirms that linear interpolation produces better results than other interpolation methods with less computing complexity. Our most accurate interpolation can be obtained by using cubic splines at the expense of longer computing time. We conclude that least squares and surface fitting approximations of zero and first orders are more useful for small neighborhood sizes (3 x 3 to 5 x 5) with an acceptable computational complexity.

References

[4.1]   M. Abramowitz and I. A. Stegun, *Handbook of Mathematical Functions with Formulas, Graphs, and Mathematical Tables,* Washington, D.C.: U.S. Department of Commerce, 1965.

[4.2]   R. E. Barnhill, "A survey of the representation and design of surfaces," *IEEE Comput. Graphics Appl.,* vol. 3, pp. 9-16, 1983.

[4.3]   R. E. Barnhill, "Surfaces in computer aided geometric design: A survey with new results," *Comput. Aided Geom. Design,* vol. 2, pp. 1-17, 1985.

[4.4]   R. E. Barnhill and W. Boehm, Eds., *Surfaces in Computer Aided Geometric Design*, Amsterdam, Holland: North-Holland Publishing, 1983.

[4.5]   R. H. Bartels, J. C. Beatty and B. A. Barsky, *An Introduction to Splines for Use in Computer Graphics and Geometric Modeling*, Los Altos, CA: Morgan Kaufmann Publishers, 1987.

[4.6]   R. Bernstein, "Digital image processing of earth observation sensor data," *IBM J. R and D*, vol. 20, pp. 40-57, 1976.

[4.7]   S. Bilgen, *Cubic Spline Elements for Boundary Integral Equations*, (Ph. D. Thesis), Department of Electrical Engineering, University of Manitoba, Winnipeg, Canada, 1982.

[4.8]   R. N. Bracewell, *The Fourier Transform and Its Applications*, 2nd Rev. ed., New York, NY: McGraw-Hill, 1986.

[4.9]   C. B. Chittineni, "Multidimensional edge and line detection by hypersurface fitting using basis functions," In *Proc. International Symposium on Machine Processing of Remotely Sensed Data at LARS*, Purdue University, West Lafayette, IN, July 1982, pp. 245-254.

[4.10] R. M. Haralick, "The digital edge," In *Proc. Pattern Recognition and Image Processing Conf.*, Dallas, TX, August 3-5, 1981, pp. 285-291.

[4.11] H. S. Hou and H. C. Andrews, "Least squares image restoration using spline basis functions," *IEEE Trans. Comput.*, vol. C-26, pp. 856-873, 1977.

[4.12] H. S. Hou and H. C. Andrews, "Cubic spline for image interpretation and digital fitting," *IEEE Trans. Acoust. Speech Signal Process.*, vol. ASSP-26, pp. 508-516, 1978.

[4.13] R. G. Keys, "Cubic convolution interpolation for digital image processing," *IEEE Trans. Acoust. Speech Signal Process.*, vol. ASSP-29, pp. 1153-1160, 1981.

[4.14] D. S. Morgenthaler and A. Rosenfeld, "Multidimensional edge by hypersurface fitting," *IEEE Trans. Pattern Anal. Machine Intell.*, vol. PAMI-3, pp. 482-286, 1981.

[4.15] S. K. Park and R. A. Schowengerdt, "Image reconstruction by parametric cubic convolution," *Comput. Vision Graphics Image Process.*, vol. 23, pp. 258-272, 1983.

[4.16] T. Pavlidis, "Optimal piecewise polynomial L_2 approximation of functions of one and two variables," *IEEE Trans. Comput.*, vol. C-24, pp. 98-102, 1975.

[4.17] W. K. Pratt, *Digital Image Processing*, New York, NY: John Wiley & Sons, 1978.

[4.18] W. H. Press, B. P. Flannery, S. A. Teukolsky and W. T. Vetterling, *Numerical Recipes: The Art of Scientific Computing*, Cambridge, England: Cambridge University Press, 1986.

[4.19] J. M. Prewitt, "Object enhancement and restoration," In *Picture Processing and Psychopictorics*, B. S. Lipkin and A. Rosenfeld, Eds., New York, NY: Academic Press, 1970, pp. 75-149.

[4.20] J. R. Rice, *Numerical Methods, Software, and Analysis*, New York, NY: McGraw-Hill Book, 1983.

[4.21] I. J. Schoenberg, *Cardinal Spline Interpolation*, Philadelphia, PA: Society for Industrial and Applied Mathematics Press, 1973.

[4.22] R. A. Schowengerdt, *Techniques for Image Processing and Classification in Remote Sensing*, New York, NY: Academic Press, 1983.

[4.23]   L. L. Schumaker, *Spline Functions: Basic Theory*, New York, NY: John Wiley & Sons, 1981.

[4.24]   D. Shepard, "A two-dimensional interpolation function for irregularly-spaced data," *Proc. ACM National Conf.*, 1968, pp. 517-524.

[4.25]   Special Issue on Representation and Approximation of Surfaces, *Rocky Mountain Journal of Mathematics*, vol. 14, 1984.

[4.26]   P. Stucki, "Image processing for document reproduction," In *Advances in Digital Image Processing: Theory, Applications, Implementation* ed. P. Stucki, Ed., New York: Plenum Press, 1979, pp. 177-218.

[4.27]   F. Yamaguchi, *Curves and Surfaces in Computer Aided Geometric Design*, Berlin: Springer-Verlag, 1988.

CHAPTER 5
MAMMOGRAPHIC FEATURE MATCHING USING ZERNIKE MOMENTS

5.1. Introduction

An essential part of the geometric unwarping problem in subtraction mammography is to identify a set of corresponding mammographic features between the warped and reference images. In this chapter, we will show how pairs of *control points*, i.e., features which are visible or can be defined unambiguously, and whose coordinates can be determined in both images, could be extracted from two images by local mammographic feature matching. Because of the nature of the approaches, as demonstrated in Chapter 3, local geometric unwarping transformations are very effective in correcting a variety of distortions in mammographic images. If we can identify the control points regardless of their position and orientation, local geometric unwarping technique using such a set of control points can be a powerful tool in registering severely distorted images.

One general class of pattern recognition problems is called *scene matching*: That is, given a pictorial description of a region of a scene, determine which region in another image is similar [5.36]. The simplest approach to this scene matching problem is called *template matching*, i.e., given an image of a template, we desire to determine all locations of the template in another image. For different applications, one element that makes template matching algorithms differ from each other is the selection of a measure of similarity, which must be decided first at each test location in order to determine the translation offset parameters. In our study, we assume that mammographic structures in

small areas are virtually intact, so a measure of similarity that has a rotational invariance property seems to be an appropriate candidate.

A fundamental element of pattern recognition procedures is to define a set of features for image representation. Moment methods are thus proposed in this study to solve the feature matching problem in the following two aspects: (1) by using moments to normalize the image, i.e., transform it into a standard form, and then extracting suitable features to classify the normalized image; and (2) by using moments or moment invariants as features of the image that remain unchanged when the image is translated, scaled, or rotated.

As pattern features in scene analysis and pattern recognition, moment descriptors have been extensively studied [5.1],[5.3],[5.12],[5.18],[5.21],[5.34],[5.35]. The utility of image moments derives from [5.20]: (1) moments have very convenient properties when an image undergoes a geometric transformation such as translation, size change, rotation, or reflection; and (2) an image has a unique approximate reconstruction in terms of a finite set of its moments (inverse moment problem [5.38]). Hu [5.25] published the first significant paper on the use of moment invariants for 2D pattern recognition applications. Maitra [5.31] proposed some possible improvements on these moment invariants. Dudani *et al.* [5.15] used moment invariants in automatic aircraft identification. Bamieh and de Figueiredo [5.6] presented a set of general moment invariants of affine transformations for 2D images, and a general moment-invariants/attributed-graph method for the identification of 3D objects. Khotanzad and Lu [5.27] applied the neural network techniques to the classification problem by using invariant moment features. The inverse moment problem of image reconstruction from a finite number of moments has been investigated (e.g., [5.32],[5.38]), through which some issues concerning the sensitivity to noise, image representation capability, selection of an optimal number of moments, etc., were studied.

Other approaches to shape/pattern recognition include boundary-based analysis via Fourier descriptors [5.29],[5.33],[5.46], and image representation by circular harmonic

expansion [5.5],[5.22],[5.23],[5.24],[5.43],[5.44]. However, the circular harmonic expansion of an image function may not be unique [5.4],[5.13].

The definition of classical moments

$$m_{pq} = \iint_{-\infty}^{\infty} x^p y^q f(x, y) \, dx \, dy \qquad (5.1.1)$$

has the form of a projection of the image function onto the monomial set $\{x^p y^q\}$, which is not orthogonal. Consequently, the recovery of an image from these moments is computationally expensive and strongly ill-posed [5.8],[5.9],[5.38],[5.42]. The fundamental reason for the ill-posedness of the inverse moment problem is the lack of orthogonality of the set $\{x^p y^q\}$, and some regularization approach has been taken to resolve this deficiency [5.38]. By applying the theory of orthogonal polynomials, Teague [5.39] suggested the use of orthogonal moments to overcome the problems associated with the classical moments. Furthermore, the orthogonality implies the linear independence of the corresponding moments, and the reconstruction procedure does not require a regularization. That is, it simply adds individual contributions from each moment to generate the reconstructed image.

Zernike moments are a class of such orthogonal moments [5.39]. Besides the above mentioned general advantages of orthogonal moments, Zernike moments also possess a property of rotational invariance: the magnitude of moments remains unchanged when the image is rotated. Thus, the magnitudes of Zernike moments can be used as rotation invariant features for image representation.

5.2. Geometric Normalization

5.2.1. Introduction

Picture normalization by moments plays an important role in the derivation of moment invariants for picture analysis and pattern recognition [5.20],[5.36]. Hu [5.25] proposed the moment approach as a solution to pattern recognition problems by using moments up through the second order to normalize the picture, and by extracting moment invariants from the normalized picture as classification features regardless of its position, orientation and size. Teague [5.39] discussed the properties of lower order moments through an equivalent "image ellipse" model for two-dimensional picture analysis. Abu-Mostafa and Psaltis [5.2] proposed a general class of 2D picture normalization procedures based on higher order complex moments, and established the relationship between normalization and invariance properties of moments. Leu [5.30] recently suggested a 2D picture normalization procedure to correct shape skewing to achieve view-independence in processes such as computer vision.

However, we have found that in the past work picture normalization procedures either were proposed without substantial theoretical analyses or were given with some incorrect parameters. It is, thus, our purpose here to present a thorough study of the picture normalization problem. We give the normalization procedure in terms of the 3D case, which might be used in conjunction with the 3D moment invariants derived by Sadjadi and Hall [5.37] for recognition of objects independent of position, orientation, and size. We also discuss the normalization process in n-dimensions with a straightforward generalization of the 3D results.

Normalization is a process of transforming a picture function $f_1(x_1, x_2, x_3)$ into another function $f_2(x_1, x_2, x_3)$ so that it retains all the relevant information of the original picture and also satisfies a set of conditions that we call the normalization criteria. There are

generally two types of picture normalizations: one concerns the gray level and the other the geometry. In this work, we shall consider only the geometric normalization. Picture reflection is also excluded in our study. Therefore, the normalization process of translation, rotation and scaling can be described by the following relationship:

$$
\begin{bmatrix} x_1' \\ x_2' \\ x_3' \end{bmatrix} = \begin{bmatrix} s_1^{-1} & 0 & 0 \\ 0 & s_2^{-1} & 0 \\ 0 & 0 & s_3^{-1} \end{bmatrix} \begin{bmatrix} l_1 & m_1 & n_1 \\ l_2 & m_2 & n_2 \\ l_3 & m_3 & n_3 \end{bmatrix} \left\{ \begin{bmatrix} x_1 \\ x_2 \\ x_3 \end{bmatrix} - \begin{bmatrix} t_{x_1} \\ t_{x_2} \\ t_{x_3} \end{bmatrix} \right\} \qquad (5.2.1)
$$

where (l_i, m_i, n_i) are the direction cosines of the new coordinates x_i' with respect to the x_i coordinate system.

5.2.2. Definitions and Notations

Given an arbitrary picture function $f(x_1, x_2, x_3)$, the three-dimensional moments of order (p_1, p_2, p_3), $m_{p_1 p_2 p_3}$, of the function f, are defined as (cf. [5.14])

$$
m_{p_1 p_2 p_3} = \iiint_{-\infty}^{\infty} x_1^{p_1} x_2^{p_2} x_3^{p_3}\, f(x_1, x_2, x_3)\, dx_1 dx_2 dx_3 \qquad (5.2.2)
$$

where $p_1, p_2, p_3 = 0, 1, 2, \ldots$. The uniqueness of the 3D moments can be determined from the following theorem (cf. [5.14]): if $f(x_1, x_2, x_3)$ is piecewise continuous and has nonzero values only in a finite part of the R^3 space, then moments of all orders exist and the moment sequence $\{m_{p_1 p_2 p_3}\}$ is uniquely determined by $f(x_1, x_2, x_3)$ and conversely $\{m_{p_1 p_2 p_3}\}$ uniquely determines $f(x_1, x_2, x_3)$. In other words, the triple sequence of moments constitutes a complete picture description, and partial picture descriptions can be obtained by using subsets of them.

A related set of moments are the *central moments* of the function $f(x_1, x_2, x_3)$, defined by

$$
\mu_{p_1 p_2 p_3} = \iiint_{-\infty}^{\infty} (x_1 - \overline{x_1})^{p_1} (x_2 - \overline{x_2})^{p_2} (x_3 - \overline{x_3})^{p_3}\, f(x_1, x_2, x_3)\, dx_1 dx_2 dx_3 \qquad (5.2.3)
$$

where

$$\overline{x_1} = \frac{m_{100}}{m_{000}}, \quad \overline{x_2} = \frac{m_{010}}{m_{000}}, \quad \text{and } \overline{x_3} = \frac{m_{001}}{m_{000}}. \tag{5.2.4}$$

This merely amounts to a change of coordinate systems that centres the x_1, x_2, and x_3 axes at the centroid $(\overline{x_1}, \overline{x_2}, \overline{x_3})$ of the picture. The first central moments μ_{100}, μ_{010} and μ_{001} of a picture are zero. The central moments do not change under translation of the coordinate system because the centroid of the picture also translates by the same amount. From now on, for the sake of simplicity, we assume that the origin coincides with the centroid $(\overline{x_1}, \overline{x_2}, \overline{x_3})$, and consider only the central moments expressed as

$$\mu_{p_1 p_2 p_3} = \iiint_{-\infty}^{\infty} x_1^{p_1} x_2^{p_2} x_3^{p_3} \, f(x_1, x_2, x_3) \, dx_1 dx_2 dx_3. \tag{5.2.5}$$

The set of moments are in fact the coefficients in a series expansion of some complete description of the picture, the *moment generating function* $M(u_1, u_2, u_3)$ of a picture function $f(x_1, x_2, x_3)$, defined by (*cf.* [5.14])

$$M(u_1, u_2, u_3) = \iiint_{-\infty}^{\infty} f(x_1, x_2, x_3) \exp(u_1 x_1 + u_2 x_2 + u_3 x_3) \, dx_1 dx_2 dx_3. \tag{5.2.6}$$

We shall refer to the space (x_1, x_2, x_3) in which the picture $f(x_1, x_2, x_3)$ is defined as the *picture space* and the space (u_1, u_2, u_3) in which the moment generating function $M(u_1, u_2, u_3)$ is defined as the *parameter space*. Under our assumption that f is well-behaved, the moment generating function can be expanded in a power series as

$$M(u_1, u_2, u_3) = \iiint_{-\infty}^{\infty} f(x_1, x_2, x_3) \sum_{p_1, p_2, p_3 = 0}^{\infty} \frac{(u_1 x_1)^{p_1}}{p_1!} \frac{(u_2 x_2)^{p_2}}{p_2!} \frac{(u_3 x_3)^{p_3}}{p_3!} \, dx_1 dx_2 dx_3$$

$$= \sum_{p_1, p_2, p_3 = 0}^{\infty} \frac{u_1^{p_1}}{p_1!} \frac{u_2^{p_2}}{p_2!} \frac{u_3^{p_3}}{p_3!} \iiint_{-\infty}^{\infty} f(x_1, x_2, x_3) \, x_1^{p_1} x_2^{p_2} x_3^{p_3} \, dx_1 dx_2 dx_3$$

$$= \sum_{p_1, p_2, p_3 = 0}^{\infty} \mu_{p_1 p_2 p_3} \frac{u_1^{p_1}}{p_1!} \frac{u_2^{p_2}}{p_2!} \frac{u_3^{p_3}}{p_3!}. \tag{5.2.7}$$

In other words, the expansion coefficients of M are precisely the moments $\mu_{p_1 p_2 p_3}$ of f. It follows that an appropriately selected form of the moment generating function M offers an approximate description of the picture f. It is possible to define a function, which is closely related to such an approximate description of f, on which the picture normalization process is based.

5.2.3. The Associated Ellipsoid Model

If moments only up through second order are considered, the moment generating function M is approximated by

$$M(u_1,\ u_2,\ u_3) \approx \mu_{000} + \frac{1}{2}\mu_{200}u_1^2 + \frac{1}{2}\mu_{020}u_2^2 + \frac{1}{2}\mu_{002}u_3^2 + \mu_{110}u_1 u_2 + \mu_{101}u_1 u_3 + \mu_{011}u_2 u_3$$

$$= \mu_{000} + \frac{1}{2}\,\mathbf{u}^{\mathrm{T}}\mathbf{A}\mathbf{u} \tag{5.2.8}$$

with $\mu_{100} = \mu_{010} = \mu_{001} = 0$, where $\mathbf{u}^{\mathrm{T}}$ is the transpose of $\mathbf{u}$, and $\mathbf{A}$ and $\mathbf{u}$ are defined, respectively, by

$$\mathbf{A} = \begin{bmatrix} \mu_{200} & \mu_{110} & \mu_{101} \\ \mu_{110} & \mu_{020} & \mu_{011} \\ \mu_{101} & \mu_{011} & \mu_{002} \end{bmatrix} \text{ and } \mathbf{u} = \begin{bmatrix} u_1 \\ u_2 \\ u_3 \end{bmatrix}. \tag{5.2.9}$$

From (5.2.6), (5.2.8) and (5.2.9) we see that the moment generating function M has a minimum μ_{000} at $\mathbf{u} = \mathbf{0}$ provided that the picture function f is non-negative. Therefore, the quadratic form $\mathbf{u}^{\mathrm{T}}\mathbf{A}\mathbf{u} > 0$. In other words, the form $\mathbf{u}^{\mathrm{T}}\mathbf{A}\mathbf{u}$, hence the symmetric matrix $\mathbf{A}$, is positive definite.

From the truncated moment generating function M (5.2.8), we are able to define a *quadric surface* as follows

$$\mu_{200}u_1^2 + \mu_{020}u_2^2 + \mu_{002}u_3^2 + 2\mu_{110}u_1 u_2 + 2\mu_{101}u_1 u_3 + 2\mu_{011}u_2 u_3 - \mu_{000} = 0 \quad (5.2.10)$$

or

$$\mathbf{u}^{\mathrm{T}}\mathbf{A}\mathbf{u} - \mu_{000} = 0 \tag{5.2.11}$$

where $\mathbf{A}$ and $\mathbf{u}$ are the same as defined in (5.2.9). When the *characteristic* quadratic form

$$M_0(u_1, u_2, u_3) = \mathbf{u^T A u} \qquad (5.2.12)$$

corresponding to (5.2.11) is positive definite, as shown above, the surface is an *ellipsoid* [5.28]. We call the ellipsoid (5.2.11) an *associated ellipsoid* of the picture f. Because the moment generating function M gives a complete description of the picture f, the ellipsoid defined from M can be regarded as a surface that in a sense "best fits" f (up through the second order). Therefore, given f's best-fitting ellipsoid e, we can attempt to perform "picture normalization" on f by transforming coordinates so that e becomes some type of standard surface, say, a sphere. The steps of picture normalization will be worked out in this and the next two sections.

If we rotate the ellipsoid with respect to the origin (the centroid of the picture), so that each principal axis of the ellipsoid is directed along one of the coordinate axes, it is possible to reduce the equation (5.2.11) to the following form

$$\lambda_1 u_1^2 + \lambda_2 u_2^2 + \lambda_3 u_3^2 = \mu_{000}. \qquad (5.2.13)$$

In matrix notation, this can be rewritten in the following way. For a quadratic form

$$\mathbf{u^T A u} = \mu \qquad (5.2.14)$$

we would like to introduce a linear transformation representing a rotation

$$\mathbf{u = R u'} \qquad (5.2.15)$$

so that

$$\mathbf{u'^T D u'} = \mu \qquad (5.2.16)$$

where

$$\mu = [\mu_{000}], \quad \mathbf{u'} = \begin{bmatrix} u_1' \\ u_2' \\ u_3' \end{bmatrix}, \quad \mathbf{R} = \begin{bmatrix} l_1 & l_2 & l_3 \\ m_1 & m_2 & m_3 \\ n_1 & n_2 & n_3 \end{bmatrix}, \quad \text{and } \mathbf{D} = \begin{bmatrix} \lambda_1 & 0 & 0 \\ 0 & \lambda_2 & 0 \\ 0 & 0 & \lambda_3 \end{bmatrix}. \qquad (5.2.17)$$

On substituting (5.2.15) for $\mathbf{u}$ in (5.2.14), we have

$$\mathbf{u'^T(R^T A R)u'} = \mu. \qquad (5.2.18)$$

A comparison of (5.2.18) with (5.2.16) indicates that

$$\mathbf{R^T A R = D} \qquad (5.2.19)$$

i.e., **R** is a matrix that transforms **A** to diagonal form.

A more general term of this diagonalization problem is the *singular value decomposition* (SVD) [5.16]: If $A \in \mathfrak{R}^{m \times n}$ then there exist orthogonal matrices

$$U = [u_1, ..., u_m] \in \mathfrak{R}^{m \times m} \text{ and } V = [v_1, ..., v_n] \in \mathfrak{R}^{n \times n} \qquad (5.2.20)$$

such that

$$U^T A V = \begin{bmatrix} \sigma_1 & & & 0 \\ & \sigma_2 & & \\ & & \ddots & \\ 0 & & & \sigma_p \end{bmatrix} \qquad (5.2.21)$$

where $p = \min\{m, n\}$ and $\sigma_1 \geq \sigma_2 \geq ... \geq \sigma_p \geq 0$.

The σ_i are the singular values of **A**, and the vectors u_i and v_i are the *i*-th left singular vector and the *i*-th right singular vector, respectively. In other words, we have

$$A v_i = \sigma_i u_i$$
$$A^T u_i = \sigma_i v_i. \qquad i = 1, ..., p \qquad (5.2.22)$$

When $A \in \mathfrak{R}^{n \times n}$ is symmetric and positive definite, then for $U, V \in \mathfrak{R}^{n \times n}$, $U = V$. Furthermore, the σ_i are the eigenvalues of **A** and u_i (or v_i) are the corresponding eigenvectors.

In the present case the matrix **R** in (5.2.17) is orthogonal. On premultiplying both sides of (5.2.19) by **R**, and setting $R = [r_1, r_2, r_3]$, we have

$$A[r_1, r_2, r_3] = [\lambda_1 r_1, \lambda_2 r_2, \lambda_3 r_3] \qquad (5.2.23)$$

or

$$A r_1 = \lambda_1 r_1, \quad A r_2 = \lambda_2 r_2, \quad A r_3 = \lambda_3 r_3. \qquad (5.2.24)$$

In other words, λ_1, λ_2 and λ_3 are indeed the eigenvalues of **A**, and r_1, r_2 and r_3 are the corresponding eigenvectors.

Because of the positive definiteness of $\mathbf{A}$ the eigenvalues λ_1, λ_2 and λ_3 are positive, so equation (5.2.13) represents an ellipsoid. This is also why we use a minus sign in (5.2.11). By comparing it with the standard form

$$\frac{u_1^2}{a_1^2} + \frac{u_2^2}{a_2^2} + \frac{u_3^2}{a_3^2} = 1 \tag{5.2.25}$$

we see that the principal axis parameters a_1, a_2, a_3 of the ellipsoid (5.2.13) are determined by

$$a_1 = \sqrt{\frac{\mu_{000}}{\lambda_1}}, \ a_2 = \sqrt{\frac{\mu_{000}}{\lambda_2}}, \text{ and } a_3 = \sqrt{\frac{\mu_{000}}{\lambda_3}}. \tag{5.2.26}$$

5.2.4. Relationship between Transformations in the Picture Space and the Parameter Space

In the above, we suggested that picture normalization be performed on the picture f by transforming its coordinates to make the best-fitting moment generating function M some type of standard shape. In this subsection we shall examine the relationship between the transformations in the picture space and those in the parameter space.

Since the central moments are used in the normalization process and the centroid of the picture is placed at the origin, the centre of the corresponding associated ellipsoid is accordingly at the origin in the parameter space. Therefore, there is no need to further perform a translation transformation.

When the picture function $f(x_1, x_2, x_3)$ rotates, i.e., $f'(x_1', x_2', x_3') = f(x_1, x_2, x_3)$ subject to the following transformation

$$\begin{bmatrix} x_1' \\ x_2' \\ x_3' \end{bmatrix} = \begin{bmatrix} l_1 & m_1 & n_1 \\ l_2 & m_2 & n_2 \\ l_3 & m_3 & n_3 \end{bmatrix} \begin{bmatrix} x_1 \\ x_2 \\ x_3 \end{bmatrix} \tag{5.2.27}$$

or

$$\mathbf{x'} = \mathbf{R}^{-1}\mathbf{x} \tag{5.2.28}$$

where

$$\mathbf{x} = \begin{bmatrix} x_1 \\ x_2 \\ x_3 \end{bmatrix}, \quad \mathbf{x}' = \begin{bmatrix} x_1' \\ x_2' \\ x_3' \end{bmatrix}, \quad \mathbf{R} = \begin{bmatrix} l_1 & l_2 & l_3 \\ m_1 & m_2 & m_3 \\ n_1 & n_2 & n_3 \end{bmatrix} \qquad (5.2.29)$$

and (l_i, m_i, n_i) are the direction cosines of the new coordinates x_i'. In matrix notation the moment generating function $M(u_1, u_2, u_3)$ becomes as

$$
\begin{aligned}
M'(u_1, u_2, u_3) &= \iiint_{-\infty}^{\infty} f'(x_1, x_2, x_3)\exp(\mathbf{u}^T\mathbf{x})\, dx_1 dx_2 dx_3 \\
&= \iiint_{-\infty}^{\infty} f(x_1', x_2', x_3')\exp(\mathbf{u}^T\mathbf{R}\mathbf{x}')\, dx_1' dx_2' dx_3' \\
&= \iiint_{-\infty}^{\infty} f(x_1', x_2', x_3')\exp\left[(\mathbf{R}^{-1}\mathbf{u})^T\mathbf{x}'\right] dx_1' dx_2' dx_3' \\
&= \iiint_{-\infty}^{\infty} f(x_1', x_2', x_3')\exp\left[(\mathbf{u}')^T\mathbf{x}'\right] dx_1' dx_2' dx_3' \\
&= M(u_1', u_2', u_3')
\end{aligned}
\qquad (5.2.30)
$$

where

$$\mathbf{u}' = \mathbf{R}^{-1}\mathbf{u}$$

$$\mathbf{u} = \begin{bmatrix} u_1 \\ u_2 \\ u_3 \end{bmatrix}, \quad \text{and } \mathbf{u}' = \begin{bmatrix} u_1' \\ u_2' \\ u_3' \end{bmatrix}. \qquad (5.2.31)$$

A comparison of (5.2.31) with (5.2.28) shows that, when the picture $f(x_1, x_2, x_3)$ rotates about a certain rotation axis by a certain angle, the function $M(u_1, u_2, u_3)$ will rotate about the same rotation axis by the same amount of angle and *vice versa*.

When the picture function $f(x_1, x_2, x_3)$ is scaled by a factor s_i in each axis, i.e., $f'(x_1', x_2', x_3') = f(x_1, x_2, x_3)$ with the following relationship

$$\begin{bmatrix} x_1' \\ x_2' \\ x_3' \end{bmatrix} = \begin{bmatrix} s_1^{-1} & 0 & 0 \\ 0 & s_2^{-1} & 0 \\ 0 & 0 & s_3^{-1} \end{bmatrix} \begin{bmatrix} x_1 \\ x_2 \\ x_3 \end{bmatrix} \qquad (5.2.32)$$

or

$$\mathbf{x}' = \mathbf{S}^{-1}\mathbf{x} \qquad (5.2.33)$$

where

$$\mathbf{x} = \begin{bmatrix} x_1 \\ x_2 \\ x_3 \end{bmatrix}, \quad \mathbf{x'} = \begin{bmatrix} x_1' \\ x_2' \\ x_3' \end{bmatrix}, \quad \mathbf{S} = \begin{bmatrix} s_1 & 0 & 0 \\ 0 & s_2 & 0 \\ 0 & 0 & s_3 \end{bmatrix} \tag{5.2.34}$$

the moment generating function $M(u_1, u_2, u_3)$ becomes as

$$
\begin{aligned}
M'(u_1, u_2, u_3) &= \iiint_{-\infty}^{\infty} f'(x_1, x_2, x_3) \exp(\mathbf{u}^T\mathbf{x}) \, dx_1 dx_2 dx_3 \\
&= \left(\frac{1}{s_1 s_2 s_3}\right) \iiint_{-\infty}^{\infty} f(x_1', x_2', x_3') \exp(\mathbf{u}^T\mathbf{S}\mathbf{x'}) \, dx_1' dx_2' dx_3' \\
&= \left(\frac{1}{s_1 s_2 s_3}\right) \iiint_{-\infty}^{\infty} f(x_1', x_2', x_3') \exp\left[(\mathbf{S}^{-1}\mathbf{u})^T\mathbf{x'}\right] \, dx_1' dx_2' dx_3' \\
&= \left(\frac{1}{s_1 s_2 s_3}\right) \iiint_{-\infty}^{\infty} f(x_1', x_2', x_3') \exp\left[(\mathbf{u'})^T\mathbf{x'}\right] \, dx_1' dx_2' dx_3' \\
&= \left(\frac{1}{s_1 s_2 s_3}\right) M(u_1', u_2', u_3')
\end{aligned}
\tag{5.2.35}
$$

where

$$\mathbf{u'} = \mathbf{S}^{-1}\mathbf{u}$$

$$\mathbf{u} = \begin{bmatrix} u_1 \\ u_2 \\ u_3 \end{bmatrix}, \quad \text{and} \quad \mathbf{u'} = \begin{bmatrix} u_1' \\ u_2' \\ u_3' \end{bmatrix}. \tag{5.2.36}$$

This indicates that, when $f(x_1, x_2, x_3)$ is enlarged by a factor of s_i in each axis, $M(u_1, u_2, u_3)$ is reduced by the same factors (and its function value is reduced by a factor of $s_1 s_2 s_3$), and *vice versa*.

5.2.5. Three-Dimensional Geometric Normalization

We have studied the relationship between the central moments and the moment generating function, established the associated ellipsoid model, and examined the relationship between transformations in the picture space and those in the parameter space.

We are now able to conclude this section by stating the following picture normalization procedure:

(1) A translation of the coordinate origin to the centroid, which is determined by (5.2.4), of the picture $f(x_1, x_2, x_3)$ is performed. Central moments up to the second order $\{\mu_{p_1 p_2 p_3}, p_1 + p_2 + p_3 = 0, 1, 2 \text{ and } p_1, p_2, p_3 = 0, 1, 2\}$ are obtained from (5.2.5).

(2) The associated ellipsoid of f, which is centred at the origin in the parameter space, can be formed from the central moments obtained in (1), according to (5.2.11). The lengths of the principal axes are calculated by (5.2.26) from the eigenvalues λ_i of the symmetric, positive definite matrix $\mathbf{A}$ (5.2.9), and the principal axes are directed along the corresponding eigenvectors $\mathbf{r_i}$. (In other words, their direction cosines are the components of the eigenvectors $\mathbf{r_i}$.)

(3) In the parameter space, the associated ellipsoid is rotated in such a way that its principal axes are directed along the coordinate axes. That is, it is reduced to the form (5.2.25) with principal axis parameters of (5.2.26). The picture undergoes a rotation about the same rotation axis and of the same angle in the picture space.

(4) The rotated associated ellipsoid obtained in (3) is then scaled so that it becomes a sphere. This amounts to enlarging the picture by factors of the principal axis parameters (5.2.26) in the corresponding coordinate axes in the picture space.

5.2.6. *N*-Dimensional Geometric Normalization

In this section we simply state the picture normalization procedure in n-dimensional pictures from the results obtained in the 3D case above. Higher dimensional pictures are of some biomedical interest, as in the formation of multimodal images [5.17]. The n-dimensional moments of order $(p_1, p_2, ..., p_n)$, $m_{p_1 p_2 ... p_n}$, of the function $f(x_1, x_2, ..., x_n)$, could be defined as

$$m_{p_1 p_2 \ldots p_n} = \iint \ldots \int_{-\infty}^{\infty} x_1{}^{p_1} x_2{}^{p_2} \ldots x_n{}^{p_n} f(x_1, x_2, \ldots, x_n) \, dx_1 dx_2 \ldots dx_n \qquad (5.2.37)$$

where $p_1, p_2, \ldots, p_n = 0, 1, 2, \ldots$ The n-dimensional central moments with the *hyper-centroid*

$$\overline{x_1} = \frac{m_{10\ldots0}}{m_{00\ldots0}}, \quad \overline{x_2} = \frac{m_{01\ldots0}}{m_{00\ldots0}}, \quad \ldots, \text{ and } \overline{x_n} = \frac{m_{00\ldots1}}{m_{00\ldots0}} \qquad (5.2.38)$$

coinciding with the origin could be defined as

$$\mu_{p_1 p_2 \ldots p_n} = \iint \ldots \int_{-\infty}^{\infty} x_1{}^{p_1} x_2{}^{p_2} \ldots x_n{}^{p_n} f(x_1, x_2, \ldots, x_n) \, dx_1 dx_2 \ldots dx_n. \qquad (5.2.39)$$

We define the *associated hyper-ellipsoid* of the picture $f(x_1, x_2, \ldots, x_n)$ as

$$\mathbf{u}^T \mathbf{A} \mathbf{u} - \mu_{00\ldots0} = 0 \qquad (5.2.40)$$

where

$$\mathbf{A} = \begin{bmatrix} \mu_{20\ldots0} & \mu_{11\ldots0} & \cdots & \mu_{10\ldots1} \\ \mu_{11\ldots0} & \mu_{02\ldots0} & \cdots & \mu_{01\ldots1} \\ \vdots & \vdots & \ddots & \vdots \\ \mu_{10\ldots1} & \mu_{01\ldots1} & \cdots & \mu_{00\ldots2} \end{bmatrix} \text{ and } \mathbf{u} = \begin{bmatrix} u_1 \\ u_2 \\ \vdots \\ u_n \end{bmatrix}. \qquad (5.2.41)$$

Diagonalizing the definite positive matrix $\mathbf{A}$ in (5.2.40) reduces the hyper-ellipsoid (5.2.40) to the following form

$$\lambda_1 u_1^2 + \lambda_2 u_2^2 + \ldots + \lambda_n u_n^2 = \mu_{00\ldots0} \qquad (5.2.42)$$

which can be further standardized as

$$\frac{u_1^2}{a_1^2} + \frac{u_2^2}{a_2^2} + \ldots + \frac{u_n^2}{a_n^2} = 1 \qquad (5.2.43)$$

where λ_i are the eigenvalues of the matrix $\mathbf{A}$, and

$$a_1 = \sqrt{\frac{\mu_{00\ldots0}}{\lambda_1}}, \ a_2 = \sqrt{\frac{\mu_{00\ldots0}}{\lambda_2}}, \ \ldots, \text{ and } a_n = \sqrt{\frac{\mu_{00\ldots0}}{\lambda_n}}. \qquad (5.2.44)$$

Therefore, the picture normalization in n-dimensions can be stated as follows.

(1) A translation of the coordinate origin to the centroid, which is determined by (5.2.37) and (5.2.38), of the picture $f(x_1, x_2, \ldots, x_n)$ is performed. Central moments up

to the second order $\{\mu_{p_1 p_2 \ldots p_n}, p_1 + p_2 + \ldots + p_n = 0, 1, 2$ and $p_1, p_2, \ldots, p_n = 0, 1, 2\}$ are obtained from (5.2.39).

(2) The associated hyper-ellipsoid of f, which is centred at the origin in the parameter space, can be formed from the central moments obtained in (1), according to (5.2.40). The lengths of the principal axes are calculated by (5.2.44) from the eigenvalues λ_i of the symmetric, positive definite matrix $\mathbf{A}$ (5.2.41), and the principal axes are directed along the corresponding eigenvectors $\mathbf{r_i}$. (In other words, their direction cosines are the components of the eigenvectors $\mathbf{r_i}$.)

(3) In the parameter space, the associated hyper-ellipsoid is rotated in such a way that its principal axes are directed along the coordinate axes. That is, it is reduced to the form (5.2.43) with principal axis parameters of (5.2.44). The picture undergoes a rotation about the same rotation axis and of the same angle in the picture space.

(4) The rotated associated hyper-ellipsoid obtained in (3) is then scaled so that it becomes a hyper-sphere. This amounts to enlarging the picture by factors of the principal axis parameters (5.2.44) in the corresponding coordinate axes in the picture space.

5.3. Definition of Zernike Moments

Zernike polynomials are a set of complex polynomials which form a complete orthogonal set over the interior of the unit circle [5.10],[5.11],[5.45]:

$$V_{nl}(x, y) = V_{nl}(\rho \sin\theta, \rho \cos\theta) = R_{nl}(\rho) \exp(il\theta) \qquad (5.3.1)$$

where (ρ, θ) are the polar coordinates of a point (x, y), $n = 0, 1, 2, \ldots$, l takes on positive and negative integer values subject to the constraints

$$n - |l| \text{ is even}, \quad |l| < n \qquad (5.3.2)$$

and the radial polynomial is defined as follows:

$$R_{nl}(\rho) = \sum_{s=0}^{(n-|l|)/2} (-1)^s \frac{(n-s)!}{s!\left(\frac{n+|l|}{2} - s\right)!\left(\frac{n-|l|}{2} - s\right)!} \rho^{n-2s}. \qquad (5.3.3)$$

Note that $R_{n,-l}(\rho) = R_{nl}(\rho)$. These polynomials are orthogonal and satisfy

$$\iint_{x^2+y^2 \leq 1} V_{nl}^*(x, y)V_{mk}(x, y)dxdy = \frac{\pi}{n+1}\delta_{mn}\delta_{kl} \qquad (5.3.4)$$

where the asterisks denotes the complex conjugate and δ_{ij} is the Kronecker symbol

$$\delta_{ij} = \begin{cases} 1 & i = j, \\ 0 & \text{otherwise.} \end{cases} \qquad (5.3.5)$$

By the orthogonality and completeness of the Zernike polynomials [5.10],[5.11], any continuous image function $f(x, y)$ that vanishes outside the unit circle can be uniquely expanded as follows:

$$f(x, y) = \sum_{n=0}^{\infty} \sum_{l} A_{nl}V_{nl}(x, y) \qquad (5.3.6)$$

where the complex coefficient A_{nl} is referred to as Zernike moment of order n with angular dependence l [5.10]

$$A_{nl} = \frac{n+1}{\pi}\iint_{x^2+y^2 \leq 1} f(x, y)V_{nl}^*(x, y)dxdy. \qquad (5.3.7)$$

Note that $A_{nl}^* = A_{n,-l}$. To calculate the Zernike moments of an image, the centre of the image is taken as the origin and pixel coordinates are mapped to the range of the unit circle, i.e., $x^2 + y^2 \leq 1$. Those pixels falling outside the unit circle are not used in the calculation. The number of pixels falling inside the unit circle can be set arbitrarily by assigning any desired width to the pixel.

The function $R_{nl}(\rho)$ is real valued, and since the image function $f(x, y)$ is also real, it is often convenient to work with real expansions and real-valued Zernike moments. By noting that $V_{nl}^*(\rho, \theta) = V_{n,-l}(\rho, \theta)$ and making some rearrangements of the terms, we have the real expansion corresponding to (5.3.6)

$$\hat{f}(x, y) = \sum_{n=0}^{n_{max}} \sum_{l} (C_{nl}\cos l\theta + S_{nl}\sin l\theta)R_{nl}(\rho) \qquad (5.3.8)$$

where l now takes on only positive integral values subject to (5.3.2). As n_{max} approaches infinity $\hat{f}(x, y)$ will approach $f(x, y)$ [5.39]. The real Zernike moments can be rewritten as follows

$$C_{nl} = \frac{2n + 2}{\pi} \iint_{x^2+y^2\leq1} f(x, y)R_{nl}(\rho)\cos l\theta \; dxdy$$

$$S_{nl} = \frac{2n + 2}{\pi} \iint_{x^2+y^2\leq1} f(x, y)R_{nl}(\rho)\sin l\theta \; dxdy \tag{5.3.9}$$

for l not zero and

$$C_{n0} = \frac{n + 1}{\pi} \iint_{x^2+y^2\leq1} f(x, y)R_{n0}(\rho) \; dxdy \tag{5.3.10}$$

$$S_{n0} = 0.$$

The relationship between real and complex Zernike moments is ($l > 0$)

$$C_{nl} = 2\text{Re}(A_{nl}),$$
$$S_{nl} = -2\text{Im}(A_{nl}), \tag{5.3.11}$$
$$A_{nl} = \frac{1}{2}(C_{nl} - iS_{nl}) = A^*_{n, -l}.$$

Two examples of the reconstruction of an image from its Zernike moments are shown in Fig. 5.3.1. From the illustrative point of view, we have simply taken binary images of the capitalized characters E and F as the input $f(x, y)$. Note that the reconstructed function $\hat{f}(x, y)$, obtained by including increasingly higher-order moments, is actually continuous-valued (over 256 grey levels) across the unit disk. However, the reconstructed images generated by using (5.3.8) are followed by a binarization with a threshold of 0.5 (grey level 128) to facilitate viewing the results. It is apparent that lower order moments capture gross shape information and higher order moments contribute to high frequency details.

5.4. Rotation Invariant Features

Consider a rotation of the image through angle θ_0. If the rotated image is denoted by f', the relationship between the original and rotated images in the same polar coordinates is
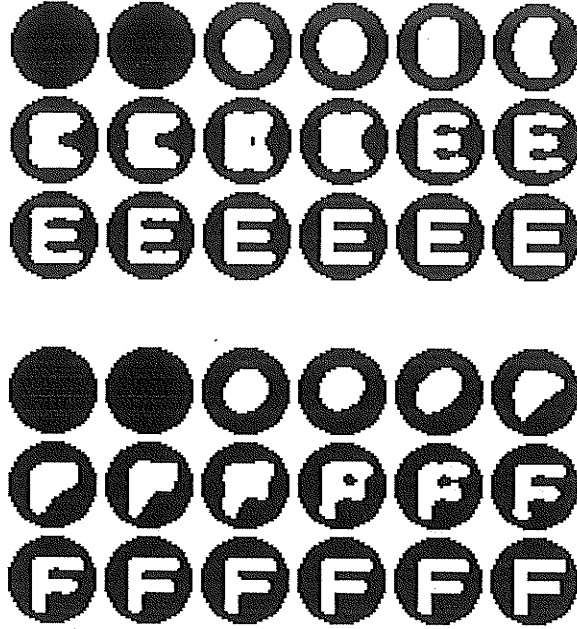
Fig. 5.3.1. The reconstructed images of the characters E and F. From top row and left to right: reconstructed images with up to zero order moment through up to sixteenth order moment. For comparison, the original images are given at the bottom-right corners.

$$f'(\rho, \theta) = f(\rho, \theta - \theta_0). \tag{5.4.1}$$

By changing the variables in double integral form of (5.3.7), we obtain the Zernike moment expression in polar coordinates:

$$A_{nl} = \frac{n+1}{\pi} \int_0^1 \int_0^{2\pi} f(\rho, \theta) V_{nl}^*(\rho, \theta) \, d\theta \rho d\rho$$

$$= \frac{n+1}{\pi} \int_0^1 \int_0^{2\pi} f(\rho, \theta) R_{nl}(\rho) \exp(-il\theta) \, d\theta \rho d\rho. \tag{5.4.2}$$

The Zernike moment of the rotated image in the same coordinates is, on the other hand,

$$(A_{nl})' = \frac{n+1}{\pi} \int_0^1 \int_0^{2\pi} f(\rho, \theta - \theta_0) R_{nl}(\rho) \exp(-il\theta) \, d\theta \rho d\rho. \tag{5.4.3}$$

By a change of variable $\varphi = \theta - \theta_0$, we obtain

$$(A_{nl})' = \frac{n+1}{\pi} \int_0^1 \int_0^{2\pi} f(\rho, \varphi) R_{nl}(\rho) \exp\left(-il(\varphi + \theta_0)\right) d\varphi \rho d\rho$$

$$= \left[\frac{n+1}{\pi} \int_0^1 \int_0^{2\pi} f(\rho, \varphi) R_{nl}(\rho) \exp(-il\varphi) \, d\varphi \rho d\rho \right] \exp(-il\theta_0) \qquad (5.4.4)$$

$$= A_{nl} \exp(-il\theta_0).$$

Equation (5.4.4) shows that Zernike moments have a simple rotational transformation property, i.e., each Zernike moment merely acquires a phase shift on rotation. This implies that the magnitudes of the Zernike moments of a rotated image function remain identical to those before rotation. Thus $|A_{nl}|$, the magnitude of the Zernike moment, can be taken as a rotation invariant feature of the underlying image function [5.26]. As far as the constructed Zernike moment features are concerned, we can concentrate on $|A_{nl}|$ with $l \geq 0$. This is because $A_{n, -l} = A_{nl}^*$, thus $|A_{nl}| = |A_{n, -l}|$.

This rotational invariance property is demonstrated as follows. In Fig. 5.4.1 we show binary images of the characters A, B, and C, and five rotated version of them (with rotation angles of 30°, 60°, 150°, 180°, and 300°). Figs. 5.4.2, 5.4.3. and 5.4.4 show graphs of the sample mean μ, standard deviation σ, and σ/μ for 81 Zernike moments (from order 0 through order 16) calculated from the characters A, B, and C, respectively. The σ/μ ratio measures the percentage of spread of the $|A_{nl}|$ values from their corresponding means. In these examples, for instance, there are only a few (out of 81) moments at which the σ/μ values are higher than 10%. The correlation coefficients between the original and its rotated
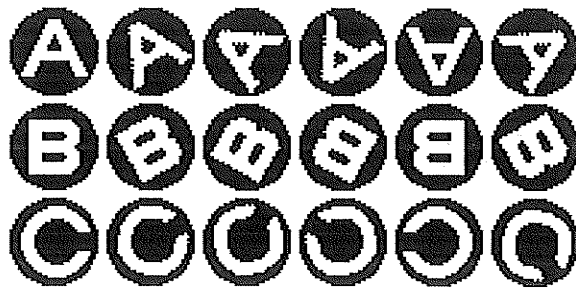
Fig. 5.4.1. Binary images of the characters A, B, C, and their rotated versions with rotation angles of 30°, 60°, 150°, 180°, and 300°.

images (Fig. 5.4.5) calculated from (5.4.1) are also a good measure of invariance. All these measures indicate that the rotation invariance is nearly attained. The only reason for not obtaining exact invariance is that the discrete form of the image function rather than its continuous form has been used in the calculation of Zernike moments. (The ratio σ/μ could, in fact, be used to monitor the loss of image quality when an image undergoes consecutive digital rotations.)

(a)

(b)

(c)
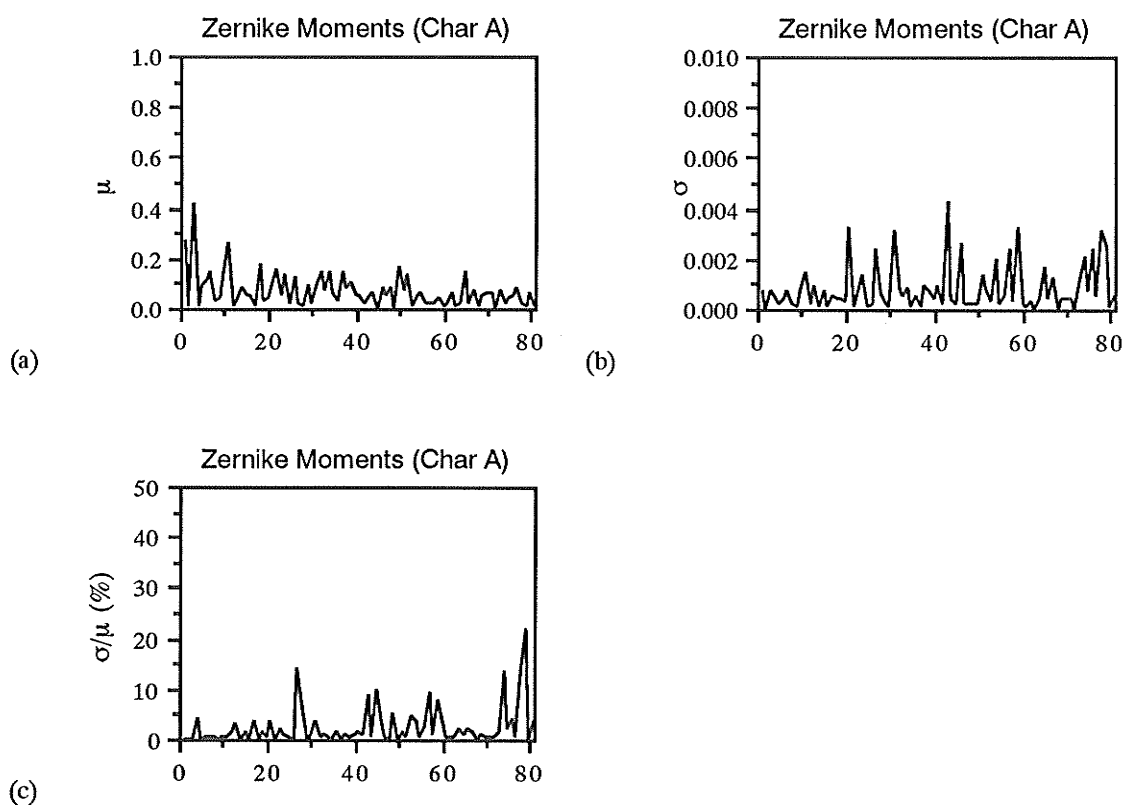
Fig. 5.4.2. Zernike moments (up to order 16) sample mean μ (a), standard deviation σ (b), and σ/μ value (c) for the character A.
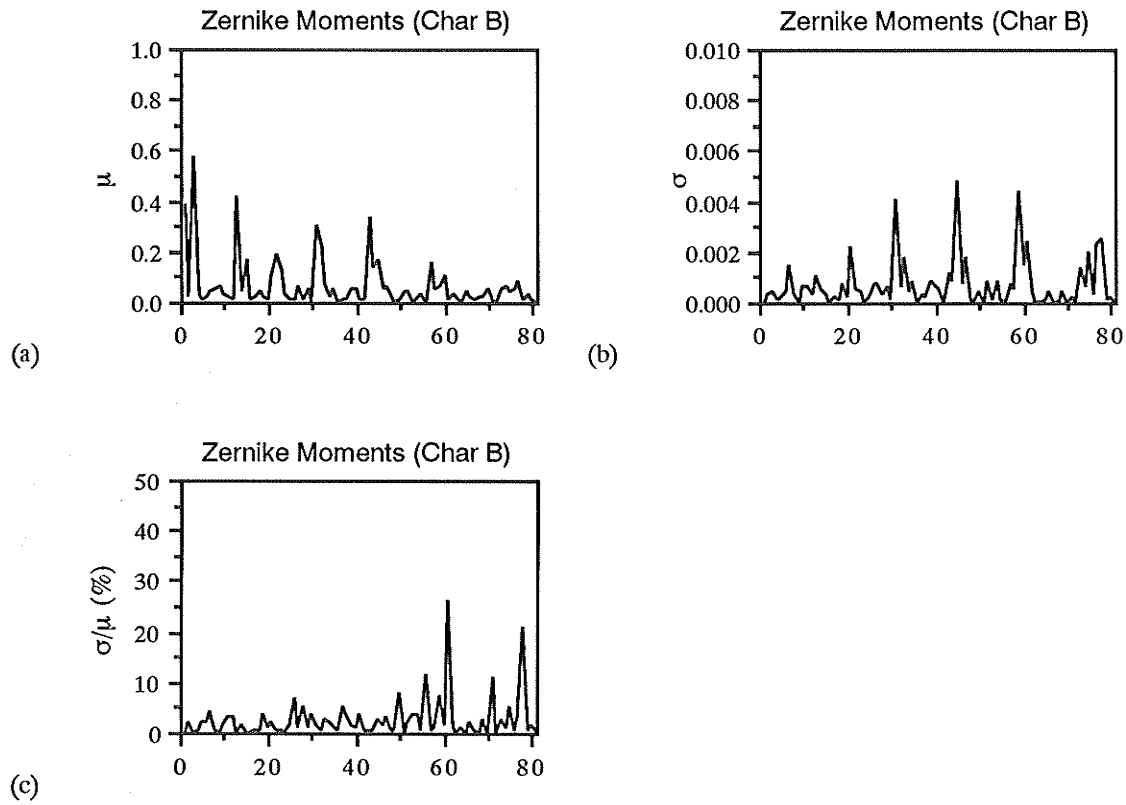
Fig. 5.4.3. Zernike moments (up to order 16) sample mean μ (a), standard deviation σ (b), and σ/μ value (c) for the character B.

(a)

(b)

(c)
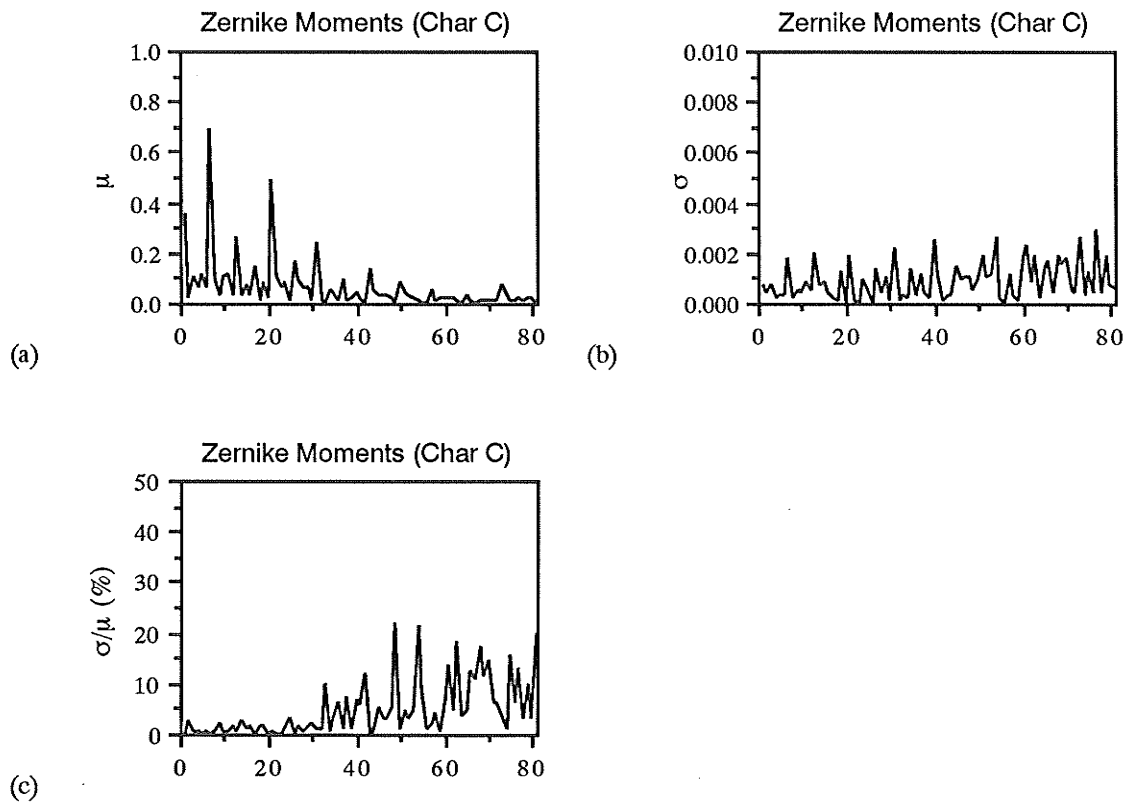
Fig. 5.4.4. Zernike moments (up to order 16) sample mean μ (a), standard deviation σ (b), and σ/μ value (c) for the character C.

Correlation from Zernike Moments
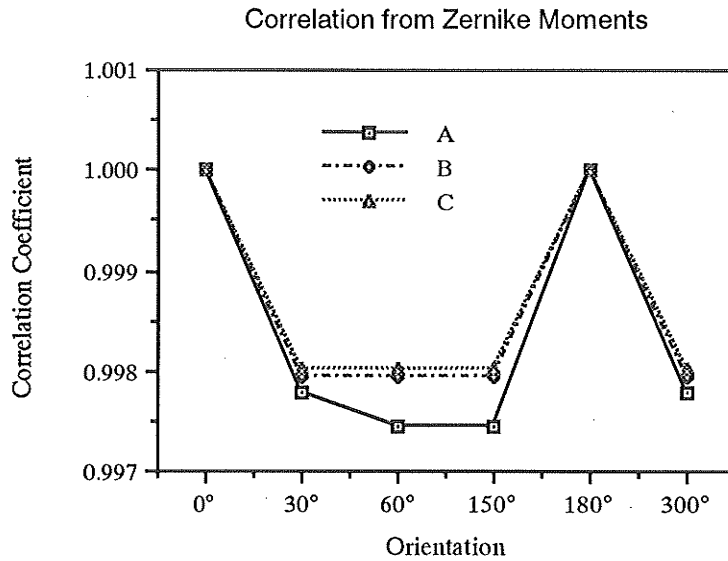
Fig. 5.4.5. Correlation measures from Zernike moments (up to order 16) for the characters A, B, and C.

A fundamental problem in pattern recognition has been the question of between-class discrimination versus within-class invariance. In other words, the challenge is always to extract features for image representation that are invariant to transformations which remain unchanged in "unimportant" ways (the variations within the class), yet at the same time that are sensitive to transformations which change the figures in "important" ways (the identity of a class) [5.14]. Figure 5.4.6 shows the images of characters A, B, C, D, E, F, N, and O, and the cross-correlation coefficients between each pair of these characters. This indicates that image representation using Zernike moments is capable of discriminating between similar, but different objects.

(a)
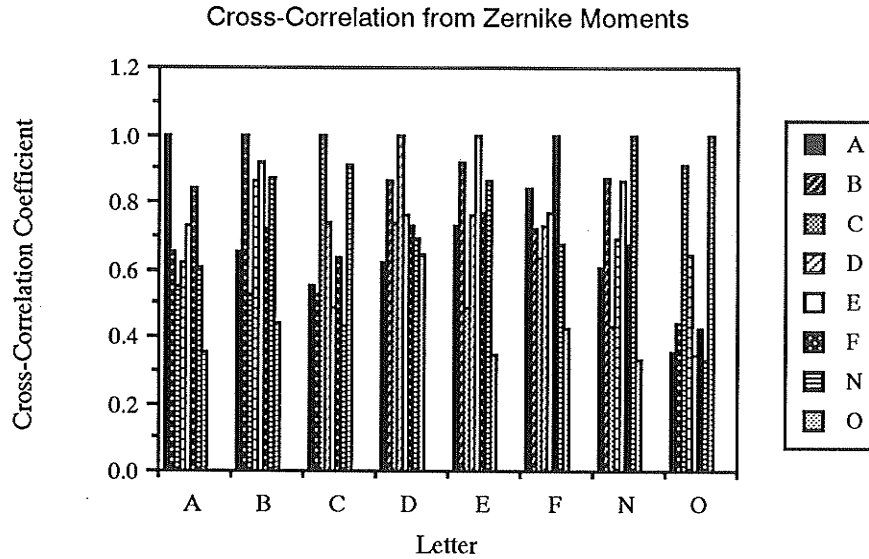
(b)

Fig. 5.4.6. Cross-correlation measures from Zernike moments (up to order 16) for the characters A, B, C, D, E, F, N, and O. (a) The characters, and (b) the cross-correlation coefficients.

5.5. Mammographic Feature Matching

5.5.1. Introduction

A class of image processing problems called *scene matching* is often encountered in image processing tasks such as feature/edge detection, image registration, etc. The brute force approach to this kind of problem is *template matching*. That is, given an image of a template, it is desired to determine all locations of the template in another image [5.36]. As far as a digital image is concerned, a *template* (also called a *mask* or *window*) is an array of

any numbers designed to detect certain regional property. That is, the template may be simply the grey levels of an object, or some features derived from the object.

From the point of view of pattern recognition, moment invariants are considered reliable features if their values are insensitive to the presence of different types of noise. The effects of sampling, digitizing, and quantization noise on moment invariants were addressed in [5.40]. Teh and Chin [5.41] studied the effect of image noise on various types of moments by using stochastic images. It has been shown that orthogonal moments, e.g. Zernike moments, are better than other types of moments in terms of information redundancy [5.41]. They concluded that Zernike moments are superior to other moments in terms of overall performance. The superiority of Zernike moment features over regular moments and moment invariants in terms of image representation ability and noise sensitivity in pattern recognition problems was demonstrated experimentally by Khotanzad and Hong [5.26]. The rotational invariance and image representation ability of Zernike moments are explored in this study to solve the mammographic feature matching problem.

5.5.2. Matching Measures

There are many possible ways of measuring the degree of similarity (or match) or dissimilarity (or mismatch) between two images f and g over certain region. Distance measures or norms (see Section 6.2.2), for instance, can be used as dissimilarity measures.

In template matching, a measure of similarity (or match) at each test location must be first decided in order to determine the translation offset parameters. The basic correlation method consists of forming a correlation measure between image functions and determining the location of correspondence by finding the location of the maximum correlation [5.19].

Thus the following formula is used to correlate Zernike moments of the feature template with those computed at each of the test locations in the image:

$$R(x, y) = \frac{\sum_{i=1}^{N_n} A_{nl}^{(i)} B_{nl}^{(i)}(x, y)}{\left[\left(\sum_{i=1}^{N_n} A_{nl}^{(i)}\right)\left(\sum_{i=1}^{N_n} B_{nl}^{(i)}(x, y)\right)\right]^{1/2}} \qquad (5.5.1)$$

where $R(x, y)$ is the moment correlation at test location (x, y) (i.e., the top left corner of the image is located at the coordinates (x, y) of the picture), $A_{nl}^{(i)}$ is the ith Zernike moment of the feature template and $B_{nl}^{(i)}(x, y)$ is the ith Zernike moment of the picture at test location (x, y), and N_n is the total number of Zernike moments up to a given order n.

5.5.3. Feature Matching Using Zernike Moments

Two examples of feature matching are presented in this section. In both cases, the template is shifted over all the possible locations in the test image, and the correlation coefficient is calculated from the grey levels and Zernike moments at each location. For the sake of display, the resultant correlation functions (in the range 0 to 1) are mapped to the range of 0 to 255. When using the correlation of Zernike moments as the similarity measure, we take the total number of Zernike moments as 81 (for orders 0 through 16).

In Figs. 5.5.1(a) and (b) we show a test image consisting of various characters including the character E in various orientations, and the template E, respectively. Figure 5.5.1(c) shows the results of template matching by using correlation of grey level values as the measure of similarity. The results after thresholding at level of 250 (out of 255: ~98%) is given in Fig. 5.5.1(d). By using grey level values we are able to locate only the object with the same orientation. We present in Fig. 5.5.1(e) the results of template matching by using correlation of Zernike moments of the objects as the measure of similarity. We use the same threshold value of 250 to Fig. 5.5.1(e) and obtain the results in Fig. 5.5.1(f). The character E with different orientations is correctly identified.
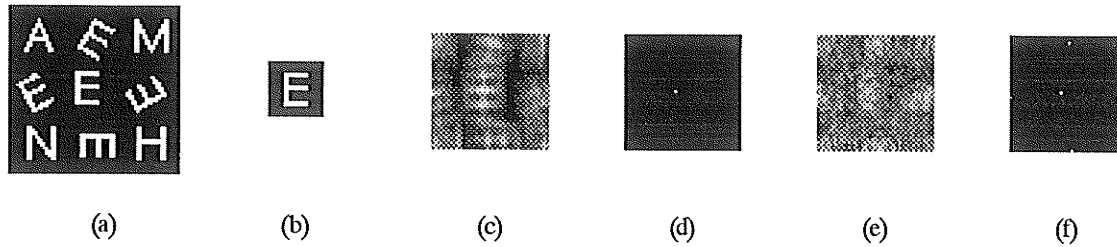
Fig. 5.5.1. Template matching by correlation measures on simulated data: (a) The test image; (b) the template; matching results (0-255) from grey levels, (c) before and (d) after thresholding; matching results (0-255) from Zernike moments, (e) before and (f) after thresholding. Thresholding was set at grey level 250 in both cases.

We also tested the template matching procedure by using a mammographic image [Fig. 5.5.2(a)] and a rotated structure from a small area [Fig. 5.5.2(b)]. The matching results by using grey level values and Zernike moments are shown in Figs. 5.5.2(c) and (e), respectively. The thresholded versions of these results [at the highest possible value of 239 (~94%) for the grey level method, and 250(~98%) for the Zernike moments method] are given in Figs. 5.5.2(d) and (f), respectively. The Zernike moment method correctly locates the desired structure, but the grey level approach fails to do so.
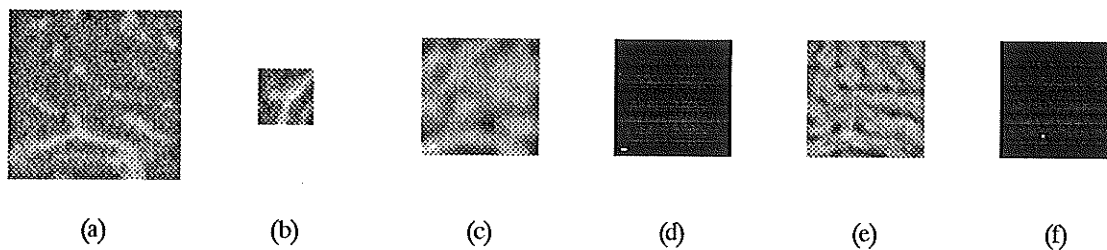
Fig. 5.5.2. Template matching by correlation measures on mammographic data: (a) The test image; (b) the template; matching results (213-239) from grey levels, (c) before and (d) after thresholding at 239 (94%); matching results (220-250) from Zernike moments, (e) before and (f) after thresholding at 250 (98%).

5.6. Discussion and Conclusions

A study of the picture normalization problem from the point of view of moments has been presented. We have studied the relationship between (central) moments of a picture function and its corresponding moment generating function, proposed the associated ellipsoid model, and examined the relationship between transformations in the picture space and those in the parameter space. The normalization procedure is illustrated in terms of the 3D case. Generalization of this 3D procedure to n-dimensions is also presented. Image normalization may be applied as a pre-processing step in image analysis and recognition procedures, such as in extracting features for feature matching.

In our calculations of Zernike moments, rotations of the test patterns are obtained digitally, i.e., the original, digitized patterns are rotated. This process has introduced a certain amount of noise in the images, and is responsible for the imperfect rotational invariance from Zernike moments. Experiments show that such digitization noise is tolerable as far as our local feature matching is concerned. Other investigators have shown that Zernike moments are much better than other moments or moment invariants in terms of the insensitivity to different types of noise [5.40],[5.41].

In the test on mammographic images (Fig. 5.5.2), we obtained fairly high correlation coefficients (0.84 - 0.94 for the grey level measure and 0.86 - 0.98 for the Zernike moment measure) over the whole image. This is probably because the template feature and the test image have some redundant information which is highly correlated. If we can eliminate redundant information in these images, for instance, through segmentation/thinning (see discussion below and Section 7.2.1), we may obtain a correlation coefficient function with much narrower peaks at those matching locations.

Since our objective is to identify the corresponding mammographic structures in both the reference and warped images, it is reasonable to first segment/binarize the original mammographic images, (a pre-processing step of thinning to the binary images may be

useful in some cases) and then apply an appropriate template matching technique to the resultant binary images. Advantages of this approach include at least the following (1) computing time is reduced considerably, and (2) some unimportant, redundant, or "noisy" structures can be removed. An optimal choice of segmentation and thinning techniques for application in mammographic feature matching may be further studied in the future (see Section 7.2.1).

In template matching, as discussed in Section 5.5, cross-correlation of the desired template with the image is calculated at each test location. For large templates, this requires a large amount of computing time, even though it may be done in the Fourier domain. One approach to reduce the computing time is to use a cumulative measure of mismatch, say the sum of absolute differences of the Zernike moments, instead of the correlation measure of match. In this way, those locations at which a good match cannot possibly exist are rapidly eliminated [5.7]. A useful extension to this *sequential approach* may be one of using a sequential algorithm to discard gross mismatch locations followed by a correlation measure for the remaining test locations. Another approach, *hierarchical* one, is to create a set of multi-resolution images from the image and template, and incorporate a hierarchical search for a possible match location in these multi-resolution images starting at a lower resolution. The decision rules are designed to select the most promising test locations at each search level. Only the selected locations are tested at the next level, so that only the most promising test locations are examined at the higher resolution levels.

We have proposed a new method for rotation invariant template matching. The rotation invariance property of the magnitudes of Zernike moments has been used as the similarity measure in the matching procedure. Experiments have shown that our approach using Zernike moments correctly locates the desired objects regardless of their position and orientation.

References

[5.1] Y. S. Abu-Mostafa and D. Psaltis, "Recognitive aspects of moment invariants," *IEEE Trans. Pattern Anal. Machine Intell.,* vol. PAMI-6, pp. 698-706, 1984.

[5.2] Y. S. Abu-Mostafa and D. Psaltis, "Image normalization by complex moments," *IEEE Trans. Pattern Anal. Machine Intell.,* vol. PAMI-7, pp. 46-55, 1985.

[5.3] F. L. Alt, "Digital pattern recognition by moments," *J. ACM,* vol. 9, pp. 240-258, 1962.

[5.4] H. H. Arsenault, "Rotation-invariant digital pattern recognition using circular harmonic expansion: author's reply to comments," *Appl. Opt.,* vol. 28, pp. 1614-1615, 1989.

[5.5] H. H. Arsenault and Y.-N. Hsu, "Rotation-invariant discrimination between almost similar objects," *Appl. Opt.,* vol. 22, pp. 130-132, 1983.

[5.6] B. Bamieh and R. J. P. de Figueiredo, "A general moment-invariants/attributed-graph method for three-dimensional object recognition from a single image," *IEEE J. Robotics Automation,* vol. RA-2, pp. 31-41, 1986.

[5.7] D. I. Barnea and H. F. Silverman, "A class of algorithms for fast digital image registration," *IEEE Trans. Comput.,* vol. C-21, pp. 179-186, 1972.

[5.8] M. Bertero, C. DeMol and E. R. Pike, "Linear inverse problems with discrete data I: General formulation and singular system analysis," *Inverse Problems,* vol. 1, pp. 301-330, 1985.

[5.9] M. Bertero, T. A. Poggio and V. Torre, "Ill-posed problems in early vision," *Proc. IEEE,* vol. 76, pp. 865-885, 1988.

[5.10] A. B. Bhatia and E. Wolf, "On the circle polynomials of Zernike and related orthogonal sets," *Proc. Cambridge Philosophical Soc.,* vol. 50, pp. 40-48, 1954.

[5.11] M. Born and E. Wolf, Eds., *Principles of Optics: Electromagnetic Theory of Propagation, Interference and Diffraction of Light,* 5th ed. Oxford, England: Pergamon Press, 1975, pp. 464-466, 767-771.

[5.12] J. F. Boyce and W. J. Hossack, "Moment invariants for pattern recognition," *Pattern Recog. Lett.,* vol. 1, pp. 451-456, 1983.

[5.13] P.-E. Danielsson, "Rotation-invariant digital pattern recognition using circular harmonic expansion: a comment," *Appl. Opt.,* vol. 28, pp. 1613-1614, 1989.

[5.14] R. O. Duda and P. E. Hart, *Pattern Classification and Scene Analysis,* New York, NY: John Wiley & Sons, 1973.

[5.15] S. A. Dudani, K. J. Breeding and R. B. McGhee, "Aircraft identification by moment invariants," *IEEE Trans. Comput.,* vol. C-26, pp. 39-45, 1977.

[5.16] G. H. Golub and C. F. Van Loan, *Matrix Computations.* Baltimore, Maryland: Johns Hopkins University Press, 1983.

[5.17] R. Gordon and J. Coumans, "Combining multiple imaging techniques for in vivo pathology: a quantitative method for coupling new imaging modalities," *Med. Phys.,* vol. 11, pp. 79-80, 1984.

[5.18] L. Gupta and M. D. Srinath, "Contour sequence moments for the classification of closed planar shapes," *Pattern Recog.*, vol. 20, pp. 267-272, 1987.

[5.19] E. L. Hall, *Computer Image Processing and Reconstruction*, New York, NY: Academic Press, 1979.

[5.20] B. K. P. Horn, *Robot Vision*, New York, NY: MIT Press, 1986.

[5.21] T. C. Hsia, "A note on invariant moments in image processing," *IEEE Trans. Syst. Man Cybern.*, vol. SMC-11, pp. 831-834, 1981.

[5.22] Y. Hsu and H. H. Arsenault, "Optical pattern recognition using circular harmonic expansion," *Appl. Opt.*, vol. 21, pp. 4016-4019, 1982.

[5.23] Y. Hsu and H. H. Arsenault, "Pattern discrimination by multiple circular harmonic components," *Appl. Opt.*, vol. 23, 841-844, 1984.

[5.24] Y. Hsu, H. H. Arsenault and G. April, "Rotation-invariant digital pattern recognition using circular harmonic expansion," *Appl. Opt.*, vol. 21, pp. 4012-4015, 1982.

[5.25] M. K. Hu, "Visual pattern recognition by moment invariants," *IRE Trans. Inform. Theory*, vol. IT-8, pp. 179-187, 1962.

[5.26] A. Khotanzad and Y. H. Hong, "Invariant image recognition by Zernike moments," *IEEE Trans. Pattern Anal. Machine Intell.*, vol. PAMI-12, pp. 489-497, 1990.

[5.27] A. Khotanzad and J. Lu, "Classification of invariant image representations using a neural network," *IEEE Trans. Acoust. Speech Signal Process.*, vol. ASSP-38, pp. 1028-1038, 1990.

[5.28] G. A. Korn and T. M. Korn, *Mathematical Handbook for Scientists and Engineers: Definitions, Theorems, and Formulas for Reference and Review*, Second (enlarged, and revised) ed. New York, NY: McGraw-Hill Book, 1968.

[5.29] A. Krzyzak, S. Y. Leung and C. Y. Suen, "Reconstruction of two-dimensional patterns by Fourier descriptors," In *Proc. 9th ICPR*, Rome, Italy, Nov. 1988, pp. 555-558.

[5.30] J. Leu, "Shape normalization through compacting," *Pattern Recog. Lett.*, vol. 10, pp. 243-250, 1989.

[5.31] S. Maitra, "Moment invariants," *Proc. IEEE*, vol. 67, pp. 697-699, 1979.

[5.32] M. Pawlak, "On the reconstruction aspects of moment descriptors," In *Proc. IEEE Info. Theory Conf.*, San Diego, CA, 1990.

[5.33] E. Persoon and K. S. Fu, "Shape discrimination using Fourier descriptors," *IEEE Trans. Syst. Man Cybern.*, vol. SMC-7, pp. 170-179, 1977.

[5.34] S. S. Reddi, "Radial and angular moment invariants for image identification," *IEEE Trans. Pattern Anal. Machine Intell.*, vol. PAMI-3, pp. 240-242, 1981.

[5.35] A. P. Reeves, R. J. Prokop, S. E. Andrews and F. Kuhl, "Three-dimensional shape analysis using moments and Fourier descriptors," *IEEE Trans. Pattern Anal. Machine Intell.*, vol. PAMI-10, pp. 937-943, 1988.

[5.36] A. Rosenfeld and A. C. Kak, *Digital Picture Processing*, 2nd ed. New York, NY: Academic Press, 1982.

[5.37]   F. A. Sadjadi and E. L. Hall, "Three-dimensional moment invariants," *IEEE Trans. Pattern Anal. Machine Intell.,* vol. PAMI-2, pp. 127-136, 1980.

[5.38]   G. Talenti, "Recovering a function from a finite number of moments," *Inverse Problems,* vol. 3, pp. 501-517, 1987.

[5.39]   M. R. Teague, "Image analysis via the general theory of moments," *J. Opt. Soc. Am.,* vol. 70, pp. 920-930, 1980.

[5.40]   C. Teh and R. T. Chin, "On digital approximation of moment invariants," *Comput. Vision Graph. Image Process.,* vol. 33, pp. 318-326, 1986.

[5.41]   C. Teh and R. T. Chin, "On image analysis by the methods of moments," *IEEE Trans. Pattern Anal. Machine Intell.,* vol. PAMI-10, pp. 496-513, 1988.

[5.42]   A. N. Tikhonov and V. Y. Arsenin, *Solutions of Ill-Posed Problems,* New York, NY: John Wiley & Sons, 1977.

[5.43]   R. Wu and H. Stark, "Rotation-invarinat pattern recognition using a vector reference," *Appl. Opt.,* vol. 23, pp. 838-840, 1984.

[5.44]   R. Wu and H. Stark, "Rotation-invarinat pattern recognition using optimum feature extraction," *Appl. Opt.,* vol. 24, pp. 179-184, 1985.

[5.45]   F. von Zernike, "Beugungstheorie des schneidenver-fahrens und seiner verbesserten form, der phasenkontrastmethode," *Physica,* vol. 1, pp. 689-704, 1934.

[5.46]   C. T. Zhan and C. T. Roskies, "Fourier descriptors for plane closed curves," *IEEE Trans. Comput.,* vol. C-21, pp. 269-281, 1972.

CHAPTER 6
PHASE INFORMATION DERIVED FROM ZERNIKE MOMENTS

6.1. Introduction

Even though the geometric distortion in mammograms, due to breast compression, etc., is created in a nonhomogeneous manner, it is still reasonable to assume that most mammary structures in a small region remain intact. More information extracted from the local structures can be incorporated in the matching algorithms to further facilitate solving the mammographic feature matching problem.

In Chapter 5, we have seen that Zernike moments have a nice property: only a phase change occurs when the object rotates. While the invariance of the magnitude of Zernike moments under rotation has shown its usefulness for automatic recognition of objects regardless of their orientation (e.g., [6.5]), the phase information in Zernike moments has been entirely discarded in the past. By making use of the phase information, we propose a new algorithm for recognizing the orientation of a planar object and a new algorithm for finding the axes of symmetry of a planar object. The development of these algorithms are of significance in pattern recognition and computational geometry as well.

6.2. Recognition of Orientation

6.2.1. Introduction

The recognition of an object's orientation is an important problem in image analysis and pattern recognition. In many machine vision problems, there are a variety of model-based inspection tasks which require the coordinate system of an object to be aligned with that of a set of observations before the actual inspection judgements can be made. To determine whether each object is in its correct position and orientation, the relationship between these two coordinate systems has to be established, which usually is given by a two-dimensional translation and rotation [6.4]. In the image registration for rigid objects, such as the registration of portal images in the cancer treatment verification process, the determination of the object's orientation will yield the desired rotation transformation [6.14]. In the image registration for nonrigid objects (via local geometric unwarping), e.g., the registration of digital mammograms, the determination of local features' orientation may result in an optimal geometric transformation. The recognition of orientation may also present an optimal solution for texture matching by using finite element methods. That is, there is not only the match between selected features, but also the spatial rotation that has occurred between them is taken into account.

From (5.4.4), it is straightforward to find that under rotation the real-valued Zernike moments become

$$
\begin{aligned}
(A_{nl})' = (C_{nl})' + i\,(S_{nl})' &= A_{nl}\exp(-il\theta_0) \\
&= (C_{nl} + i\,S_{nl})(\cos l\theta_0 - i\sin l\theta_0) \\
&= (C_{nl}\cos l\theta_0 + S_{nl}\sin l\theta_0) + i(S_{nl}\cos l\theta_0 - C_{nl}\sin l\theta_0).
\end{aligned}
\tag{6.2.1}
$$

Expressing this in matrix form, we have

$$
\begin{bmatrix} (C_{nl})' \\ (S_{nl})' \end{bmatrix} = \begin{bmatrix} C_{nl} & S_{nl} \\ S_{nl} & -C_{nl} \end{bmatrix} \begin{bmatrix} \cos l\theta_0 \\ \sin l\theta_0 \end{bmatrix}.
\tag{6.2.2}
$$

As long as the magnitude of the moment $|A_{nl}| = [(C_{nl})^2 + (S_{nl})^2]^{1/2} \neq 0$, we find that

$$\begin{bmatrix} \cos l\theta_0 \\ \sin l\theta_0 \end{bmatrix} = \frac{1}{(C_{nl})^2 + (S_{nl})^2} \begin{bmatrix} C_{nl} & S_{nl} \\ S_{nl} & -C_{nl} \end{bmatrix} \begin{bmatrix} (C_{nl})' \\ (S_{nl})' \end{bmatrix}. \tag{6.2.3}$$

It is then possible to solve these equations to find the relative orientation θ_0 of the object with respect to the other one in the same class.

We present here a new method for recognizing the orientation of a planar object by making use of the phase information in Zernike moments. This can be done by minimizing a specially defined function to obtain the orientation of the object with respect to a standard, reference object (or model) of the same class. The performance of the proposed method is not significantly affected by the presence of noise in the images due to the nature of the minimization procedure.

6.2.2. L_p-Norms

Before further considering the specific problem of symmetry detection, it is helpful to discuss the concept of *norm*. For the purpose of quantitatively discussing errors, it is convenient to be able to associate with any approximation error function a nonnegative scalar that in some sense measures its magnitude. The geometrical concept of the length of a vector has many natural applications in connection with function spaces and approximation. Just as in 2D or 3D Euclidean space we have a way of measuring the distance between two vectors, we would like to use length to measure the goodness or closeness of an approximation (or the "length" of a certain error function).

A family of norms, the L_p-norms, for a continuous function f on a closed interval $[a, b]$ are defined by (*cf.* [6.12])

$$\|f\|_p = \left(\int_a^b |f(x)|^p dx \right)^{1/p}, p \geq 1. \tag{6.2.4}$$

The most commonly used norms are the following special cases of the L_p-norms:

L_1 norm:

$$\|f\|_1 = \left(\int_a^b |f(x)| dx \right)$$

(6.2.5)

L_2 (or Euclidean) norm:

$$\|f\|_2 = \left(\int_a^b |f(x)|^2 dx \right)^{1/2}$$

(6.2.6)

L_∞ (or maximum) norm:

$$\|f\|_\infty = \max_{x \in [a, b]} |f(x)|.$$

(6.2.7)

6.2.3. An Angular Error Function

Because of the errors in the numerical calculation of Zernike moments and the noise from digitization of images, a single or a few pairs from the set of Zernike moments $\{C_{nl}, S_{nl}\}$, where $n=0,1,...,n_{max}$ and l takes on integral values subject to (5.3.2), cannot be reliably used in (6.2.3) to find the orientation $\theta = \theta_0$. Thanks to the rotational invariance of the magnitude of Zernike moments, we can solve this problem by minimizing some norms of the following angular error function

$$d(n, l) = \left\{ \left[(C_{nl})' - (C_{nl} \cos l\theta + S_{nl} \sin l\theta) \right]^2 + \left[(S_{nl})' - (S_{nl} \cos l\theta - C_{nl} \sin l\theta) \right]^2 \right\}^{1/2}.$$

(6.2.8)

In other words, the recognition of orientation amounts to an optimization problem.

For the error evaluation of discrete data, there are direct analogs of the continuous L_p-norms. The difference $d(n, l)$ just defines a vector, so we can use the vector norms:

$$\|d\|_1 = \sum |d(n, l)|$$

(6.2.9)

$$\|d\|_2 = \left[\sum |d(n, l)|^2 \right]^{1/2}$$

(6.2.10)

$$\|d\|_\infty = \max |d(n, l)|$$

(6.2.11)

where $n = 0, 1, ..., n_{max}$, n_{max} is the maximum Zernike moment order used, and l takes on positive integral values subject to (5.3.2).

Note that the difference function $d(n, l)$ in (6.2.8) is the magnitude of the change in Zernike moment under a rotation θ. It is, therefore, possible to normalize this error function with respect to the magnitude of Zernike moments in order to obtain a "normalized" measure for the optimization procedure. The error function using normalized norms are thus given as follows:

$$\|d\|_1 = \frac{\sum |d(n, l)|}{\sum |A_{nl}|} \tag{6.2.12}$$

$$\|d\|_2 = \left[\frac{\sum |d(n, l)|^2}{\sum |A_{nl}|^2}\right]^{1/2} \tag{6.2.13}$$

$$\|d\|_\infty = \frac{\max |d(n, l)|}{\max |A_{nl}|}. \tag{6.2.14}$$

6.2.4. Recognition of Orientation

An algorithm for recognition of orientation of planar objects using Zernike moments may thus be formulated as follows.

(1) A translation of the origin of the coordinate system to the centroid of the images is first performed. Zernike moments of the images up to order n are then calculated using (5.3.9) and (5.3.10).

(2) The correlation coefficient of these two sets of Zernike moments, which measures the similarity between these objects, is calculated. (We may also use other similarity measures, e.g., distance measures [6.11], for this purpose.) If the correlation coefficient is higher than a certain threshold value (say 0.99), we move to next step; otherwise, these two objects do not belong to the same class at all, and we stop here. This is because, if the objects are from the same class, by the rotational invariance of Zernike moments, the correlation coefficient of these two sets of Zernike moments must be high.

(3) By minimizing the specially defined angular error functions (6.2.12) - (6.2.14), we obtain the required orientation of these objects for a given error threshold value.

In the following, we demonstrate the orientation recognition algorithm outlined above with some examples. The images of characters A, B, and C shown in Fig. 5.4.1 were used as the test images, and a procedure of minimization by golden section search was used [6.9]. From Fig. 5.4.5 we see that for each case the correlation coefficients between the characters and their rotated versions are very close to the highest possible value of 1. The error functions for orientation recognition in characters A, B, and C and their rotated versions (rotations of 0°, 30°, 60°, 150°, 180°, and 300°) are presented in Figs. 6.2.1 - 6.2.3, respectively. The orientations and the corresponding minimum errors for each case are shown in Tables 6.2.1 - 6.2.3, respectively. [The orientation between an image and its rotation of 0° (itself) is exactly recognized, so the orientation (0°) and error (0.00) are not given in Tables 6.2.1 - 6.2.3.]

Another approach to the recognition of orientation is to define as an object's orientation the principal axis of its "associated ellipse" model. Note that the orientation of the principal axis from (5.2.15) and (5.2.17) may be subject to some errors due to the numerical nature of the moment calculation. A test was carried out on images of characters A, B, C, D, E, F, and N [Fig. 5.4.6(a)] and their rotated versions with rotation angles of 0°, 30°, 60°, 150°, 180°, and 300°. The results are shown in Table 6.2.4. [The orientation between an image and itself (rotation of 0°) is exactly detected, so the orientation (0°) is not given in Table 6.2.4.] Because there is no unique (or infinite) principal axis in rotationally symmetric objects, e.g., character O, this approach fails to obtain any orientation information.
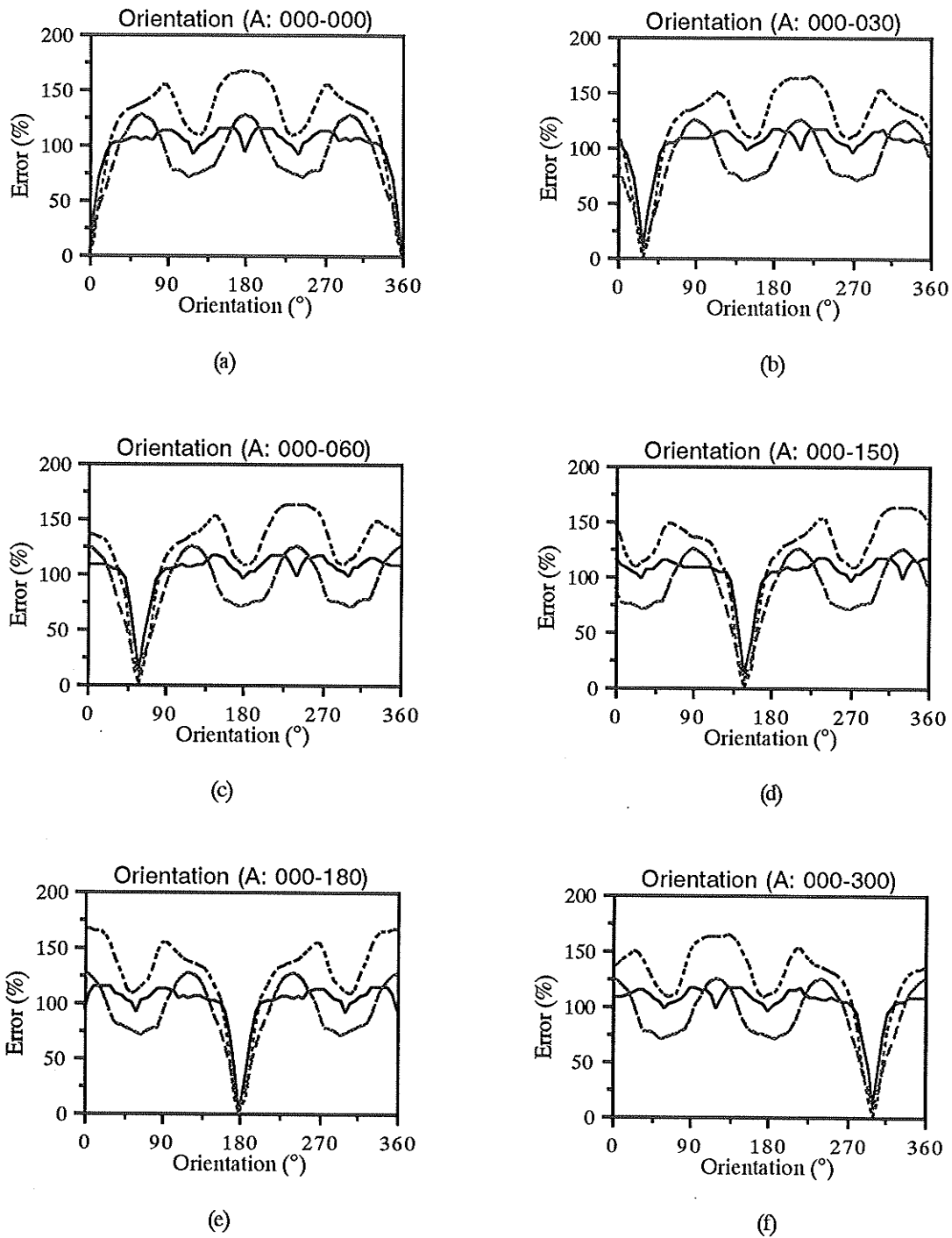
Fig. 6.2.1. The error functions with respect to the L_1 (———), Euclidean (- - - -), and maximum (— — -) norms for orientation recognition in character A and its rotations: (a) 0°, (b) 30°, (c) 60°, (d) 150°, (e) 180°, and (f) 300°.
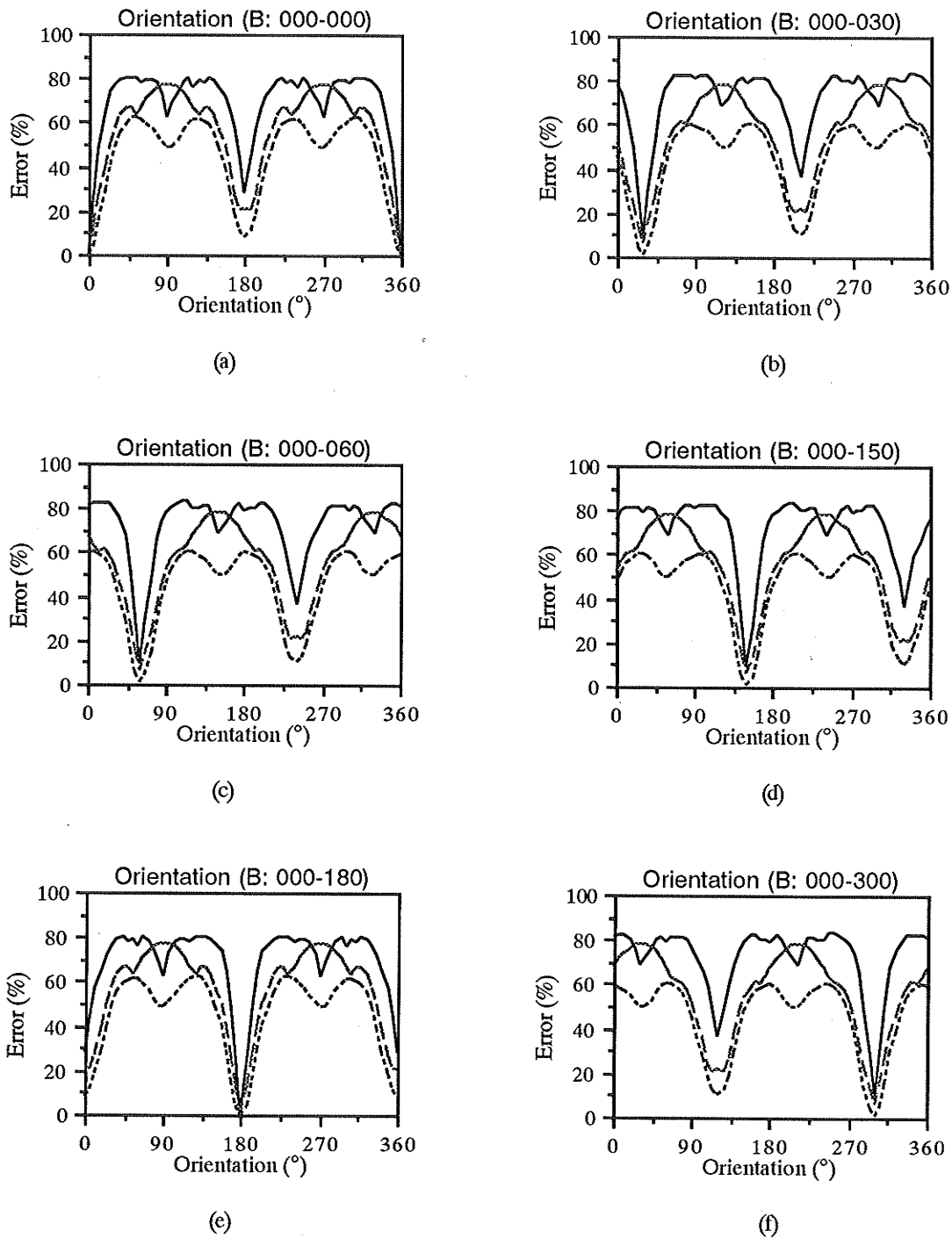
Fig. 6.2.2. The error functions with respect to the L_1 (———), Euclidean (- - - -), and maximum (— — -) norms for orientation recognition in character B and its rotations: (a) 0°, (b) 30°, (c) 60°, (d) 150°, (e) 180°, and (f) 300°.
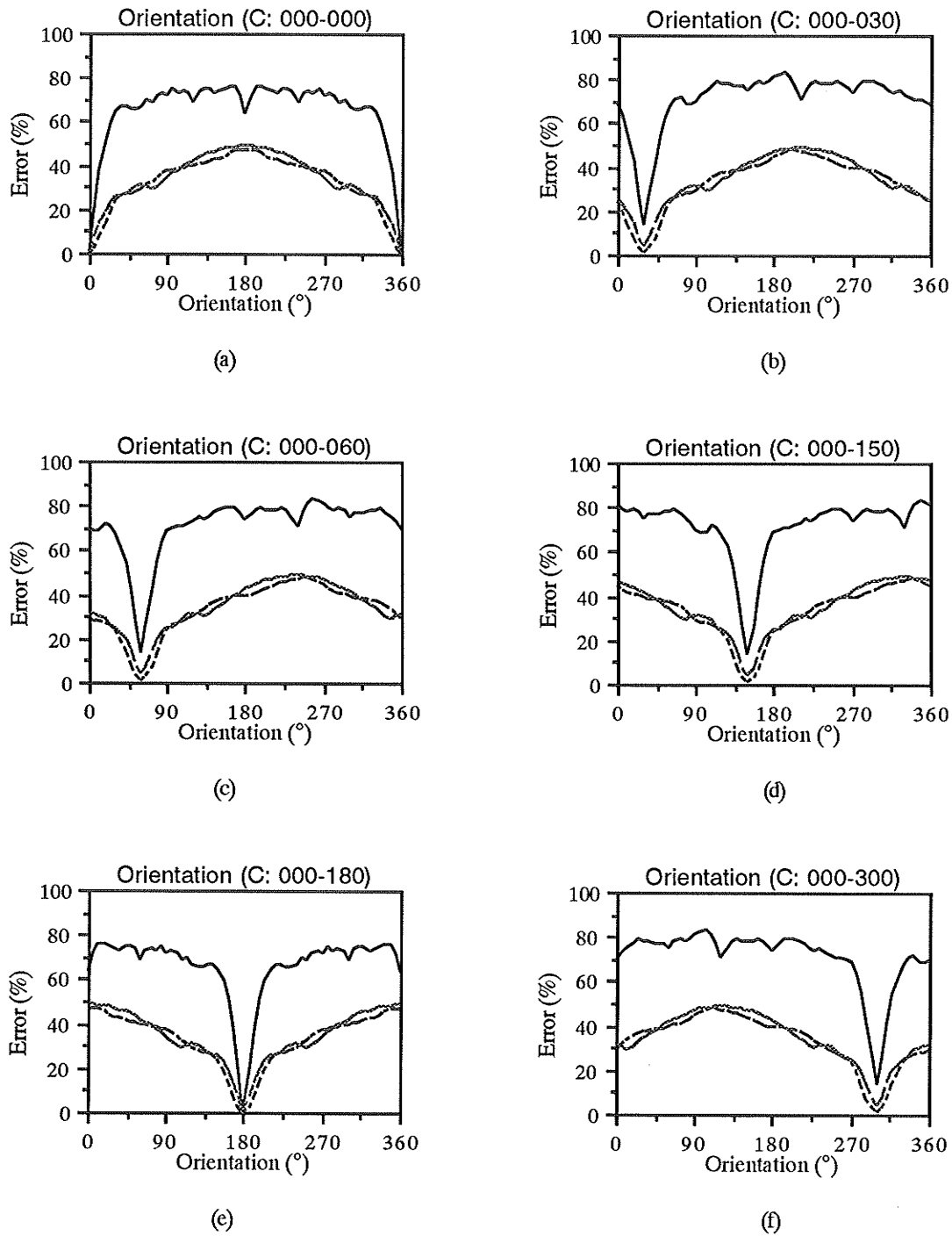
Fig. 6.2.3. The error functions with respect to the L_1 (———), Euclidean (- - - -), and maximum (— — -) norms for orientation recognition in character C and its rotations: (a) 0°, (b) 30°, (c) 60°, (d) 150°, (e) 180°, and (f) 300°.

Table 6.2.1. The orientations and the corresponding minimum errors (in parentheses) for character A

Orientation	L_1 Norm	Euclidean Norm	Max Norm
30°	30.29 (0.1013)	30.21 (0.0079)	29.65 (0.0519)
60°	59.80 (0.1144)	59.86 (0.0093)	60.23 (0.0528)
150°	149.80 (0.1144)	149.86 (0.0093)	150.23 (0.0528)
180°	180.01 (0.0006)	180.01 (0.0000)	180.01 (0.0004)
300°	300.29 (0.1013)	300.21 (0.0079)	299.66 (0.0519)

Table 6.2.2. The orientations and the corresponding minimum errors (in parentheses) for character B

Orientation	L_1 Norm	Euclidean Norm	Max Norm
30°	29.82 (0.0893)	29.83 (0.0053)	29.17 (0.0562)
60°	60.18 (0.0893)	60.17 (0.0053)	60.83 (0.0562)
150°	150.19 (0.0893)	150.18 (0.0053)	150.83 (0.0562)
180°	180.01 (0.0004)	180.01 (0.0000)	180.01 (0.0002)
300°	299.81 (0.0893)	299.83 (0.0053)	299.17 (0.0562)

Table 6.2.3. The orientations and the corresponding minimum errors (in parentheses) for character C

Orientation	L_1 Norm	Euclidean Norm	Max Norm
30°	29.96 (0.1378)	29.99 (0.0069)	29.16 (0.0347)
60°	60.04 (0.1378)	60.00 (0.0069)	60.84 (0.0347)
150°	150.04 (0.1378)	150.00 (0.0069)	150.84 (0.0347)
180°	180.01 (0.0003)	180.01 (0.0000)	180.01 (0.0001)
300°	299.96 (0.1378)	300.00 (0.0069)	299.16 (0.0347)

Table 6.2.4. The orientations detected by using "associated ellipse" model for different images

Orientation (°)	Orientation from "associated ellipse" models						
	A	B	C	D	E	F	N
30	11.95	28.46	30.21	29.40	30.15	30.51	31.66
60	77.11	61.54	59.79	60.60	60.44	60.23	55.55
150	167.11	151.54	149.79	150.60	150.44	150.23	145.55
180	180.00	180.00	180.00	180.00	180.00	180.00	180.00
300	281.95	298.46	300.21	299.40	300.15	300.51	301.66

The sensitivity of the orientation recognition algorithm to image noise is examined by applying it to some noisy images with noise of controlled signal-to-noise ratio (SNR) values. A procedure for generation of noise in binary images has been developed (Appendix 4). The images of character A and its rotated versions with rotation angles of 30°, 60°, 150°, 180°, and 300°, contaminated with different amount of noise, are given in Fig. 6.2.4. The noiseless images of A are also shown in Fig. 6.2.4(a) for the purpose of comparison. Correlation coefficients between these images and their rotations are presented in Fig. 6.2.5. Ten noisy images for each SNR value are generated for each rotation angle (including 0°). We show in Fig. 6.2.6 only the error functions for orientation recognition between character A and its rotated version with rotation angle of 30°, both having noise with different SNR values. The orientations, the corresponding minimum errors, and their standard deviations for character A and its different rotations with SNR values of 15dB, 10dB, and 5dB are given in Tables 6.2.5 - 6.2.7, respectively.
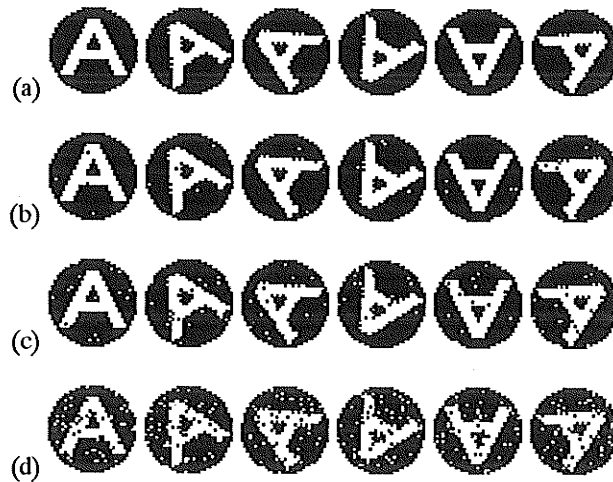
Fig. 6.2.4. The images of character A and its rotated versions with different SNR values: (a) noiseless, (b) 15dB, (c) 10dB, and (d) 5dB.

Correlation from Zernike Moments
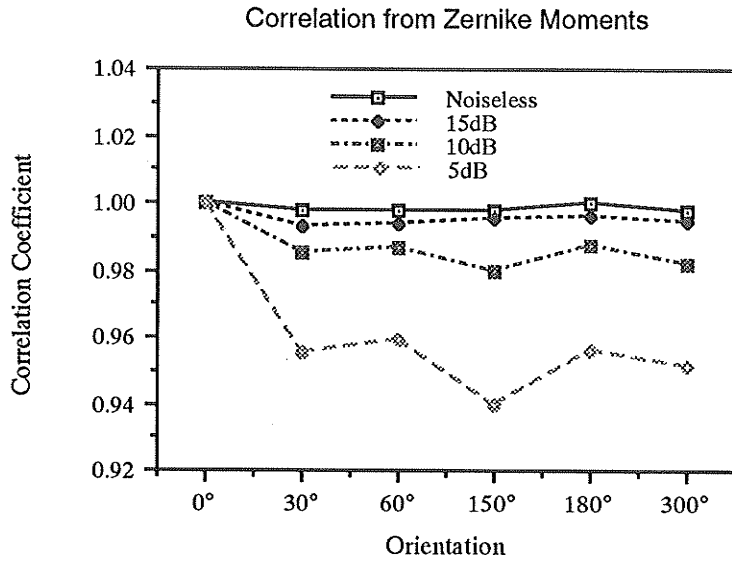
Fig. 6.2.5. Correlation measures from Zernike moments (up to order 16) for character A with SNR values of 15dB, 10dB, and 5dB.

(a)

(b)

(c)

(d)
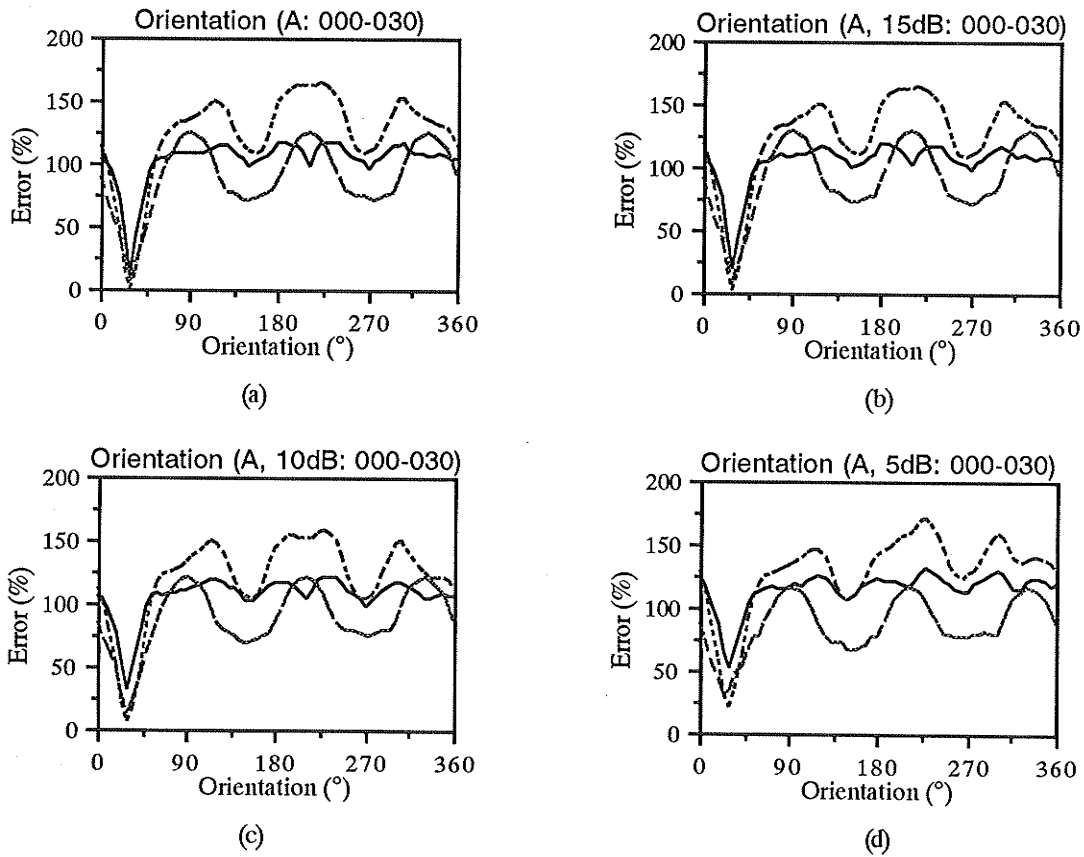
Fig. 6.2.6. The error functions with respect to the L_1 (———), Euclidean (- - - -), and maximum (— — -) norms for orientation recognition in character A and a rotated version (30°) with different SNR values: (a) noiseless, (b) 15dB, (c) 10dB, and (d) 5dB.

Table 6.2.5. The average orientations, the average minimum errors, and their standard deviations (in parentheses) for character A with SNR of 15dB

Orientation (°)	L_1 Norm		Euclidean Norm		Maximum Norm	
	Orientation	Error	Orientation	Error	Orientation	Error
0	0.02 (0.0902)	0.1607 (0.0383)	0.00 (0.1008)	0.0186 (0.0081)	-0.19 (0.5372)	0.0740 (0.0112)
30	30.16 (0.1901)	0.1866 (0.0265)	30.20 (0.1675)	0.0245 (0.0068)	30.29 (1.1366)	0.0881 (0.0142)
60	59.76 (0.2293)	0.2027 (0.0282)	59.80 (0.1548)	0.0285 (0.0079)	59.67 (1.3647)	0.0926 (0.0153)
150	149.83 (0.1293)	0.1925 (0.0264)	149.83 (0.0877)	0.0265 (0.0069)	149.75 (1.1404)	0.0903 (0.0050)
180	180.02 (0.0946)	0.1664 (0.0396)	180.02 (0.1360)	0.0203 (0.0093)	179.81 (1.1983)	0.0828 (0.0187)
300	300.25 (0.1535)	0.1926 (0.0292)	300.22 (0.1453)	0.0267 (0.0073)	299.66 (1.3041)	0.0998 (0.0083)

Table 6.2.6. The average orientations, the average minimum errors, and their standard deviations (in parentheses) for character A with SNR of 10dB

Orientation (°)	L_1 Norm		Euclidean Norm		Maximum Norm	
	Orientation	Error	Orientation	Error	Orientation	Error
0	-0.01 (0.2385)	0.2836 (0.0385)	-0.03 (0.2445)	0.0581 (0.0159)	-0.29 (1.6100)	0.1298 (0.0184)
30	30.22 (0.3573)	0.3059 (0.0302)	30.25 (0.3265)	0.0677 (0.0148)	29.07 (1.9750)	0.1604 (0.0281)
60	59.94 (0.4259)	0.3272 (0.0322)	59.85 (0.3466)	0.0786 (0.0195)	60.10 (0.8333)	0.1531 (0.0276)
150	149.77 (0.3859)	0.3159 (0.0302)	149.77 (0.3367)	0.0716 (0.0125)	150.05 (1.8286)	0.1445 (0.0226)
180	180.09 (0.3501)	0.2796 (0.0192)	180.02 (0.2481)	0.0565 (0.0077)	179.11 (1.4355)	0.1357 (0.0180)
300	300.29 (0.4143)	0.3001 (0.0202)	300.38 (0.4239)	0.0649 (0.0098)	299.96 (1.7697)	0.1426 (0.0271)

Table 6.2.7. The average orientations, the average minimum errors, and their standard deviations (in parentheses) for character A with SNR of 5dB

Orientation ($^{\circ}$)	L_1 Norm		Euclidean Norm		Maximum Norm	
	Orientation	Error	Orientation	Error	Orientation	Error
0	-0.10 (0.7363)	0.4980 (0.0903)	0.1279 (0.6017)	0.1961 (0.0623)	0.86 (2.5166)	0.2622 (0.0466)
30	29.67 (0.8212)	0.5119 (0.0299)	29.91 (0.7117)	0.1983 (0.0212)	29.25 (2.4812)	0.2463 (0.0229)
60	59.97 (0.9125)	0.5356 (0.0384)	60.00 (0.8615)	0.2211 (0.0334)	59.66 (3.8066)	0.2671 (0.0421)
150	149.91 (0.5522)	0.5161 (0.0229)	149.87 (0.4762)	0.2050 (0.0211)	148.75 (4.6265)	0.2739 (0.0695)
180	179.93 (0.8004)	0.5171 (0.0334)	179.73 (0.7031)	0.2028 (0.0259)	178.34 (2.4911)	0.2669 (0.0357)
300	300.24 (0.5529)	0.5336 (0.0304)	300.26 (0.4105)	0.2155 (0.0237)	300.01 (3.5502)	0.2665 (0.0416)

6.3. Detection of Axes of Symmetry

6.3.1. Introduction

An axis of symmetry of a planar image is such a straight line that the image is invariant to reflection with respect to that line. Without lose of generality, we assume that the axis of symmetry passes through the origin and it is denoted by $\theta = \theta_0$. The straight line $\theta = \theta_0$ is apparently equivalent to $\theta = \pi + \theta_0$. In what follows, therefore, we restrict the angle θ_0 to the range of $[0, \pi)$.

The detection of axes of symmetry of a planar image is of significance in both computational geometry and pattern recognition. Atallah [6.1] described an algorithm for symmetry detection by enumerating all the axes of symmetry of a planar image which is

made up of segments, circles, points, etc. The method proposed by Friedberg [6.3] is able to detect both lateral symmetry and skew (affine transformed) symmetry. Marola [6.6] suggested an algorithm for finding all the axes of symmetry of symmetric and almost symmetric planar images. This method is based on the identification of the centroids of the given image and other related sets of points, followed by a maximization of a specially designed coefficient of symmetry. Extraction of local symmetry features was suggested for general tasks in image processing and analysis [6.2]. It is of specific interest to us that symmetry information from local mammographic structures may provide auxiliary information in the process of feature matching. A template matching procedure based on symmetry detection of planar images was presented in [6.7]. Nalwa [6.8] studied the implications of symmetry in line drawings. By describing simple objects in terms of their local axes of symmetry, Seitz [6.13] proposed a different approach for object recognition in complex scenes. For a more comprehensive bibliography, see Friedberg [6.3].

This problem may be not difficult if the image consists of a finite or infinite set of points placed in perfect symmetry [6.1]. In most cases, however, the presence of noise, the nature of digitization, etc., reduce the appropriateness and reliability of some methods. For instance, even if the original image is symmetric, its digitized version generally may not be symmetric.

We take a different approach to the symmetry detection problem here. We propose a new algorithm for detecting the axes of symmetry in planar images by making use of the phase information in Zernike moments. We will show that the imaginary part of Zernike moments of a symmetric object vanishes if its axis of symmetry is taken as the x-axis. Because of the noise from image digitization and errors in numerical calculation of Zernike moments, we can find all the axes of symmetry by minimizing a specially defined function. Since the proposed method is not particularly affected by noise, due to the nature of the minimization procedure, it is applicable to almost symmetric images.

6.3.2. Zernike Moments of Symmetric Objects

Let $f(\rho, \theta)$ denote the object under consideration in the polar coordinates. Consider first the symmetry with respect to $\theta_0 = 0$. In other words, the object is symmetric about the horizontal x-axis, $f(\rho, \theta) = f(\rho, -\theta)$. Its Zernike moments are obtained as:

$$
\begin{aligned}
A_{nl} &= \frac{n+1}{\pi} \int_0^1 \int_0^{2\pi} f(\rho, \theta) R_{nl}(\rho) \exp(-il\theta) \, d\theta \rho d\rho \\
&= \frac{n+1}{\pi} \int_0^1 \left[\int_0^{\pi} f(\rho, \theta) \exp(-il\theta) \, d\theta + \int_{\pi}^{2\pi} f(\rho, \theta) \exp(-il\theta) \, d\theta \right] R_{nl}(\rho) \rho d\rho \\
&= \frac{n+1}{\pi} \int_0^1 \left[\int_0^{\pi} f(\rho, \theta) \exp(-il\theta) \, d\theta + \int_{\pi}^{0} f(\rho, 2\pi\text{-}\theta') \exp(il\theta') (-d\theta') \right] R_{nl}(\rho) \rho d\rho \\
&= \frac{n+1}{\pi} \int_0^1 \left[\int_0^{\pi} f(\rho, \theta) \exp(-il\theta) \, d\theta + \int_0^{\pi} f(\rho, -\theta') \exp(il\theta') \, d\theta' \right] R_{nl}(\rho) \rho d\rho \\
&= \frac{n+1}{\pi} \int_0^1 \left[\int_0^{\pi} f(\rho, \theta) \exp(-il\theta) \, d\theta + \int_0^{\pi} f(\rho, \theta') \exp(il\theta') \, d\theta' \right] R_{nl}(\rho) \rho d\rho \\
&= \frac{n+1}{\pi} \int_0^1 \left[\int_0^{\pi} f(\rho, \theta) (\exp(-il\theta) + \exp(il\theta)) \, d\theta \right] R_{nl}(\rho) \rho d\rho \\
&= \frac{n+1}{\pi} \int_0^1 \left[\int_0^{\pi} 2f(\rho, \theta) \cos l\theta \, d\theta \right] R_{nl}(\rho) \rho d\rho \\
&= C_{nl}
\end{aligned}
\tag{6.3.1}
$$

where C_{nl} are real-valued. The periodicity $f(\rho, \theta) = f(\rho, 2\pi\text{-}\theta)$ and the equality $2\cos x = \exp(-ix) + \exp(ix)$ have been used in the above derivation. Equation (6.3.1) means that the imaginary parts of the Zernike moments of a symmetric object will vanish if its axis of symmetry is taken as the x-axis.

From the rotational properties (5.4.4), then we obtain the Zernike moments for an object symmetric with respect to a straight line $\theta = \theta_0$ as follows

$$
A_{nl} = (A_{nl})' \exp(-il\theta_0)
\tag{6.3.2}
$$

where $(A_{nl})'$ are some real-valued numbers. Expressing the real-valued numbers $(A_{nl})'$ in terms of the Zernike moments A_{nl} in (6.3.2), we have

$$(A_{nl})' = A_{nl} \exp(il\theta_0)$$
$$= (C_{nl} + i\,S_{nl})(\cos l\theta_0 + i\,\sin l\theta_0) \qquad (6.3.3)$$
$$= (C_{nl}\cos l\theta_0 - S_{nl}\sin l\theta_0) + i(C_{nl}\sin l\theta_0 + S_{nl}\cos l\theta_0).$$

By comparing (6.3.3) with (6.3.1), therefore, we obtain

$$C_{nl}\sin l\theta_0 + S_{nl}\cos l\theta_0 = 0. \qquad (6.3.4)$$

In other words, if such an angle θ_0 can be found that (6.3.4) holds for all the Zernike moments, the straight line $\theta = \theta_0$ must be the axis of symmetry of this object. Apparently any of such axes of symmetry can be detected by using this method.

6.3.3. An Angular Error Function

As discussed in Section 6.2, because of the numerical errors and the digitization noise, a single or a few pairs of Zernike moments are not reliable enough to be used in finding the axis of symmetry $\theta = \theta_0$. We solve this problem by minimizing the following angular error function

$$d(n, l) = C_{nl}\sin l\theta_0 + S_{nl}\cos l\theta_0 \qquad (6.3.5)$$

with respect to the same vector norms as those in (6.2.9) - (6.2.11). That is, the detection of axes of symmetry becomes an optimization problem.

Note that the difference function $d(n, l)$ in (6.3.5) is also the imaginary part of the Zernike moment under a rotation θ. In other words, the change in the imaginary part of the Zernike moment is simply "transferred" to the real part because of the invariance of its magnitude. It is, therefore, reasonable to normalize this error function with respect to the magnitude of the Zernike moment in order to obtain a "normalized"measure for the minimization procedure. The normalized error functions here have the same forms as those given in (6.2.12) - (6.2.14), except that the difference $d(n, l)$ in (6.3.5) is used.

6.3.4. Detection of Axes of Symmetry

The algorithm for detection of axes of symmetry of a planar object by using Zernike moments can be stated as follows.

(1) A translation of the origin of the coordinate system to the centroid of the object is first performed. Zernike moments of the object up to order n are then calculated using (5.3.9) and (5.3.10).

(2) By minimizing the specially defined error functions (6.2.12) - (6.2.14) with $d(n, l)$ from (6.3.5), we are able to find all the axes of symmetry of the object for a given error threshold value.

We demonstrate the proposed algorithm for detection of axes of symmetry with some examples. The characters A, B, C, D, E, F, N, and O shown in Fig. 5.4.6(a) were used as test images. The same minimization procedure as that in Section 6.2.4 was used here. The error functions for symmetry detection in these images are presented in Fig. 6.3.1. The axes of symmetry and their corresponding minimum errors are shown in Tables 6.3.1 - 6.3.8.

(a)

(b)
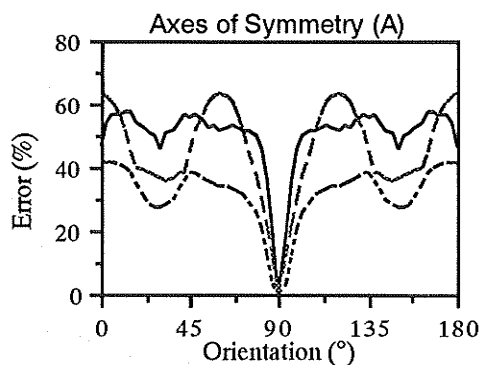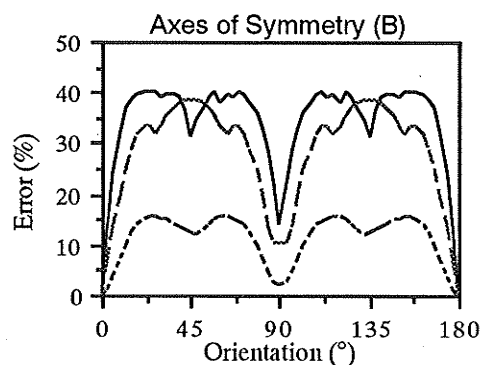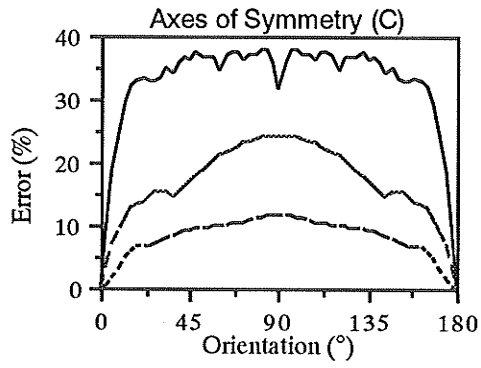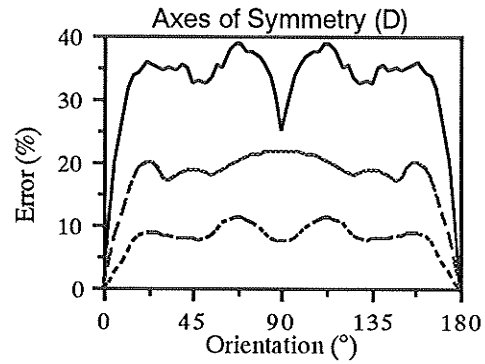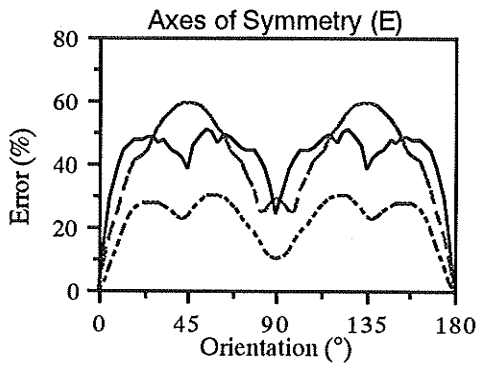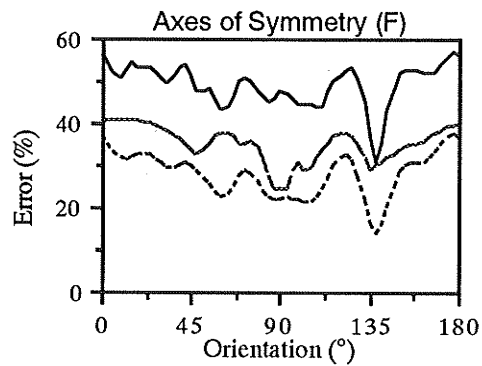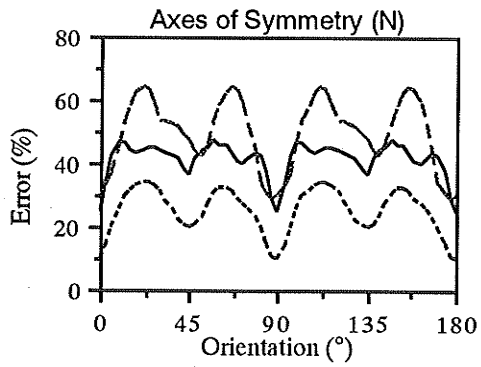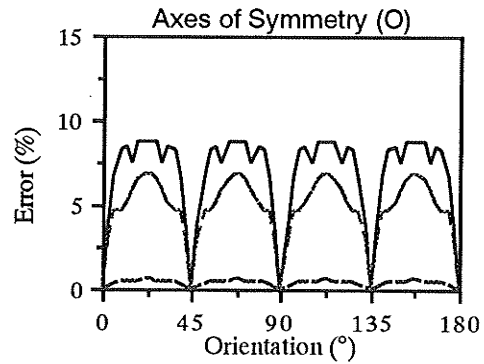
Fig. 6.3.1. The error functions with respect to the L_1 (———), Euclidean (- - - -), and maximum (— — -) norms for symmetry detection in characters A, B, C, D, E, F, N, and O.

Table 6.3.1. The axes of symmetry and the corresponding minimum errors (in parentheses) for character A

Orientation ($^\circ$)	Axis of Symmetry		
	L_1 Norm	Euclidean Norm	Max Norm
0	90.00 (0.0003)	90.00 (0.0000)	90.00 (0.0002)
30	120.25 (0.0591)	120.18 (0.0034)	119.69 (0.0366)
60	149.84 (0.0708)	149.89 (0.0048)	150.12 (0.0369)
150	59.84 (0.0708)	59.89 (0.0048)	60.12 (0.0369)
180	90.00 (0.0003)	90.00 (0.0000)	90.00 (0.0002)
300	30.26 (0.0591)	30.18 (0.0034)	29.69 (0.0366)

Table 6.3.2. The axes of symmetry and the corresponding minimum errors (in parentheses) for character B

Orientation ($^\circ$)	Axis of Symmetry		
	L_1 Norm	Euclidean Norm	Max Norm
0	0.00 (0.0000)	0.00 (0.0000)	0.00 (0.0000)
30	29.86 (0.0356)	29.85 (0.0013)	30.75 (0.0305)
60	60.14 (0.0356)	60.15 (0.0013)	60.12 (0.0305)
150	150.15 (0.0356)	150.15 (0.0013)	149.25 (0.0305)
180	0.00 (0.0000)	0.00 (0.0000)	0.00 (0.0000)
300	119.85 (0.0356)	119.84 (0.0013)	120.75 (0.0305)

Table 6.3.3. The axes of symmetry and the corresponding minimum errors (in parentheses) for character C

Orientation (°)	Axis of Symmetry		
	L_1 Norm	Euclidean Norm	Max Norm
0	0.00 (0.0000)	0.00 (0.0000)	0.00 (0.0000)
30	29.97 (0.0773)	30.14 (0.0034)	30.49 (0.0295)
60	60.03 (0.0773)	59.85 (0.0034)	59.51 (0.0295)
150	150.03 (0.0773)	149.85 (0.0034)	149.51 (0.0295)
180	0.00 (0.0000)	0.00 (0.0000)	0.00 (0.0000)
300	119.97 (0.0773)	120.15 (0.0034)	120.49 (0.0295)

Table 6.3.4. The axes of symmetry and the corresponding minimum errors (in parentheses) for character D

Orientation (°)	Axis of Symmetry		
	L_1 Norm	Euclidean Norm	Max Norm
0	0.00 (0.0000)	0.00 (0.0000)	0.00 (0.0000)
30	30.02 (0.0508)	30.01 (0.0018)	29.77 (0.0209)
60	59.98 (0.0508)	59.99 (0.0018)	60.23 (0.0209)
150	149.98 (0.0508)	149.99 (0.0018)	150.23 (0.0209)
180	0.00 (0.0000)	0.00 (0.0000)	0.00 (0.0000)
300	120.01 (0.0508)	120.01 (0.0018)	119.77 (0.0209)

Table 6.3.5. The axes of symmetry and the corresponding minimum errors (in parentheses) for character E

Orientation (°)	Axis of Symmetry		
	L_1 Norm	Euclidean Norm	Max Norm
0	0.00 (0.0000)	0.00 (0.0000)	0.00 (0.0000)
30	30.22 (0.0437)	30.14 (0.0018)	30.31 (0.0302)
60	60.00 (0.0401)	60.12 (0.0018)	59.56 (0.0356)
150	150.00 (0.0401)	150.13 (0.0018)	149.57 (0.0356)
180	0.00 (0.0000)	0.00 (0.0000)	0.00 (0.0000)
300	120.22 (0.0437)	120.15 (0.0018)	120.31 (0.0302)

Table 6.3.6. The axes of symmetry and the corresponding minimum errors (in parentheses) for character F

Orientation (°)	Axis of Symmetry		
	L_1 Norm	Euclidean Norm	Max Norm
0	138.15 (0.3038)	138.40 (0.1397)	85.98 (0.2408)
30	168.12 (0.3043)	168.49 (0.1412)	116.37 (0.2326)
60	18.09 (0.3037)	18.42 (0.1376)	152.53 (0.2417)
150	108.09 (0.3037)	108.42 (0.1376)	62.53 (0.2417)
180	138.15 (0.3038)	138.40 (0.1397)	85.98 (0.2408)
300	78.12 (0.3043)	78.50 (0.1412)	26.36 (0.2326)

Table 6.3.7. The axes of symmetry and the corresponding minimum errors (in parentheses) for character N

Orientation (°)	Axis of Symmetry		
	L_1 Norm	Euclidean Norm	Max Norm
0	89.51 (0.2412)	89.09 (0.1016)	89.01 (0.2877)
30	29.48 (0.2421)	29.06 (0.1067)	28.47 (0.2967)
60	59.32 (0.2631)	58.71 (0.1135)	60.26 (0.2987)
150	59.32 (0.2631)	58.71 (0.1135)	60.26 (0.2987)
180	89.51 (0.2412)	89.09 (0.1016)	89.01 (0.2877)
300	29.48 (0.2421)	29.06 (0.1067)	28.47 (0.2967)

Table 6.3.8. The axes of symmetry and the corresponding minimum errors (in parentheses) for character O

Orientation (°)	Axis of Symmetry		
	L_1 Norm	Euclidean Norm	Max Norm
0	15.00 (0.0756)	0.00 (0.0000)	9.84 (0.0440)
30	25.78 (0.0341)	25.99 (0.0008)	26.99 (0.0221)
60	19.22 (0.0341)	19.01 (0.0008)	18.01 (0.0221)
150	19.22 (0.0341)	19.01 (0.0008)	18.01 (0.0221)
180	15.00 (0.0756)	0.00 (0.0000)	9.84 (0.0440)
300	25.78 (0.0341)	25.99 (0.0008)	26.99 (0.0221)

We examined the sensitivity of the symmetry detection algorithm to image noise by applying it to noisy images with different SNR values. The same procedure as that in Section 6.2 for generation of noise in binary images was used (Appendix 4). The noisy images of character A and its rotated versions (Fig. 6.2.4) were used. The error functions for symmetry detection in noisy image A with different SNR values are shown in Fig. 6.3.2. The axes of symmetry and their corresponding minimum errors are shown in Table 6.3.9.

(a)

(b)

(c)

(d)
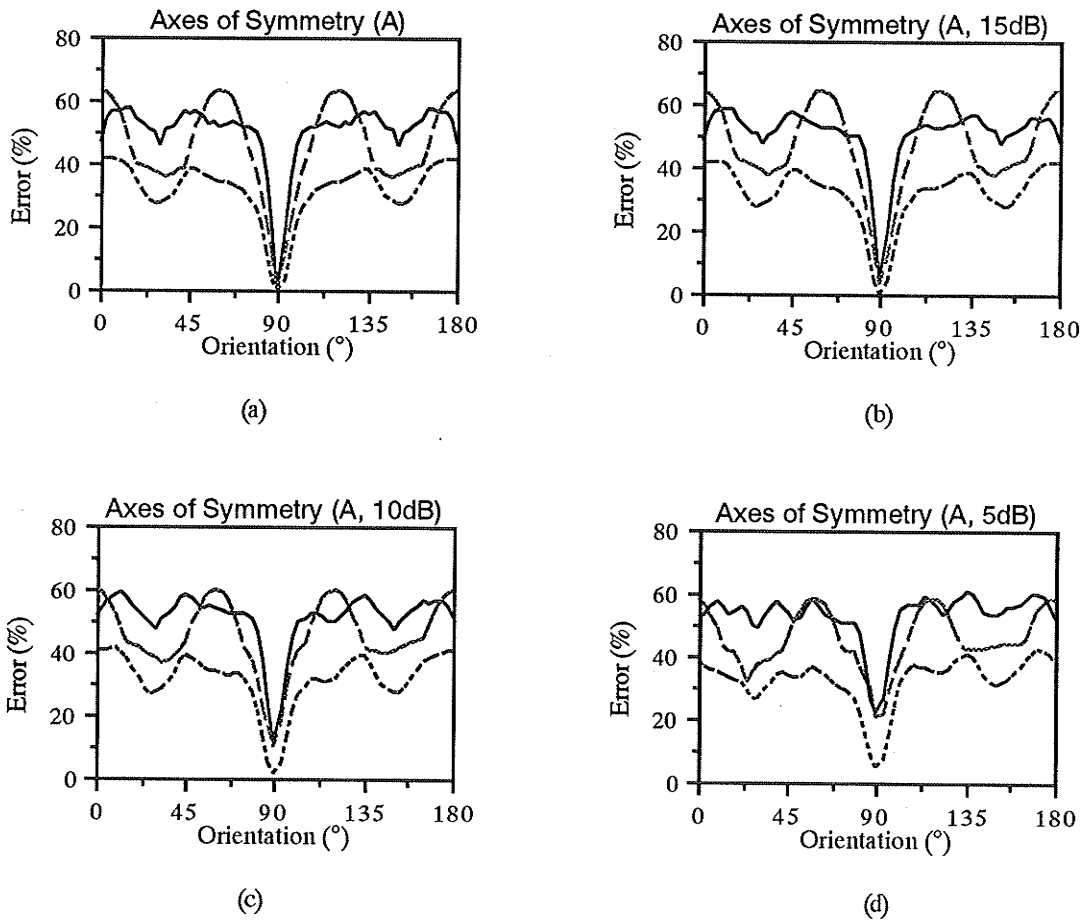
Fig. 6.3.2. The error functions with respect to the L_1 (———), Euclidean (- - - -), and maximum (— — -) norms for symmetry detection in character A with different SNR values: (a) noiseless, (b) 15dB, (c) 10dB, and (d) 5dB.

Table 6.3.9. The average symmetric axes, the average minimum errors, and their standard deviations (in parentheses) for character A with SNR of 15dB

Orientation (°)	L_1 Norm		Euclidean Norm		Maximum Norm	
	Symm.Axis	Error	Symm.Axis	Error	Symm.Axis	Error
0	90.03 (0.0903)	0.0634 (0.0245)	90.00 (0.0768)	0.0042 (0.0033)	90.18 (0.5322)	0.0430 (0.0139)
30	120.25 (0.1198)	0.0753 (0.0107)	120.18 (0.1792)	0.0056 (0.0016)	119.91 (0.6466)	0.0509 (0.0096)
60	149.77 (0.1762)	0.0970 (0.0175)	149.83 (0.1351)	0.0094 (0.0036)	150.04 (0.8450)	0.0643 (0.0187)
150	59.81 (0.1403)	0.0911 (0.0150)	59.88 (0.0779)	0.0082 (0.0022)	59.96 (0.2979)	0.0554 (0.0092)
180	90.05 (0.1417)	0.0663 (0.0279)	90.02 (0.0915)	0.0049 (0.0040)	90.20 (0.3817)	0.0417 (0.0124)
300	30.26 (0.1456)	0.0880 (0.0125)	30.20 (0.1209)	0.0075 (0.0020)	30.25 (0.4729)	0.0537 (0.0064)

Table 6.3.10. The average symmetric axes, the average minimum errors, and their standard deviations (in parentheses) for character A with SNR of 10dB

Orientation (°)	L_1 Norm		Euclidean Norm		Maximum Norm	
	Symm.Axis	Error	Symm.Axis	Error	Symm.Axis	Error
0	90.00 (0.1378)	0.1218 (0.0159)	89.97 (0.2381)	0.0146 (0.0039)	90.09 (0.9843)	0.0806 (0.0149)
30	120.05 (0.3091)	0.1311 (0.0185)	120.13 (0.1431)	0.0171 (0.0045)	119.49 (0.8251)	0.0869 (0.0117)
60	149.91 (0.2782)	0.1486 (0.0262)	149.87 (0.2698)	0.0224 (0.0089)	149.58 (1.3875)	0.0949 (0.0203)
150	59.79 (0.2772)	0.1411 (0.0213)	59.78 (0.2107)	0.0197 (0.0054)	60.35 (0.8394)	0.0911 (0.0163)
180	89.98 (0.1560)	0.1108 (0.0198)	90.00 (0.1562)	0.0127 (0.0033)	89.36 (0.7754)	0.0788 (0.0133)
300	30.35 (0.2611)	0.1296 (0.0101)	30.35 (0.2597)	0.0169 (0.0030)	30.30 (1.3962)	0.0857 (0.0185)

Table 6.3.11. The average symmetric axes, the average minimum errors, and their standard deviations (in parentheses) for character A with SNR of 5dB

Orientation (°)	L_1 Norm		Euclidean Norm		Maximum Norm	
	Symm.Axis	Error	Symm.Axis	Error	Symm.Axis	Error
0	89.92 (0.3045)	0.2150 (0.0210)	89.98 (0.3101)	0.0474 (0.0097)	89.97 (1.8301)	0.1513 (0.0298)
30	120.15 (0.4794)	0.2124 (0.0275)	120.10 (0.3939)	0.0468 (0.0113)	119.54 (0.9881)	0.1479 (0.0246)
60	149.94 (0.4718)	0.2230 (0.0191)	150.14 (0.5039)	0.0559 (0.0094)	150.13 (1.5236)	0.1752 (0.0191)
150	59.91 (0.3944)	0.2166 (0.0197)	59.76 (0.3453)	0.0495 (0.0100)	59.79 (0.8227)	0.1457 (0.0194)
180	89.82 (0.5185)	0.2099 (0.0180)	89.76 (0.4498)	0.0461 (0.0097)	89.83 (1.8983)	0.1518 (0.0270)
300	30.03 (0.5274)	0.2232 (0.0248)	30.15 (0.3519)	0.0522 (0.0110)	29.89 (0.9256)	0.1477 (0.0235)

6.4. Discussion and Conclusions

By making use of the phase information in Zernike moments, we have formulated two new algorithms: one for recognizing the orientation of a planar object, and the other one for finding the axes of symmetry of a planar object. We have demonstrated these methods by computer experiments. We have also examined the performance of these techniques with the presence of noise in the images under consideration.

Because of the digitization noise and numerical errors in moment calculations, we resolve the orientation and symmetry detection problems by adopting an approximation approach, i.e., minimizing some specially defined error functions with respect to some norms. As discussed in Section 4.3, many approximation methods are based on the principle of minimizing some norm of the error function $y = f^* - f$, where f^* is to

approximate f and has some predetermined form. Indeed, even if f^* has been computed by some other method, e.g., Taylor expansion, it is of interest to measure how good the approximation is with some norm. The selection of norms is less critical but still important [6.10].

Three commonly used norms are used: the L_1, L_2 (or Euclidean), and L_∞ (or maximum) norms. The main advantage of using the L_1 norm is that it is remarkably insensitive to random errors, wild points, and other uncertainties. In other words, it emphasizes the importance of many small errors rather than a few large errors. The Euclidean norm, however, will be large, if large errors occur in a few places. The maximum norm is unsuitable when uncertainty is present in the data because it often magnifies the effect of a single uncertainty or random error.

From Figs. 6.2.1 - 6.2.3 we see that the orientation of an object with respect to a reference one from the same class can be clearly defined and determined by using the phase information in their Zernike moments. The specially defined error functions simply shift the same amount in angle as the object is rotated. [If the objects are symmetric or almost symmetric with respect to more than one axis, e.g., the image of character B, we may find out such axes of symmetry (Fig. 6.2.2). The problem of symmetry detection is thoroughly discussed in Section 6.3.]

Because of the digitization noise in obtaining rotated versions of the images, we do not normally expect a perfect recognition of the orientation. Different norms have different characteristics in representing such noise. It appears that using the Euclidean norm produces the least error compared to the other two norms for the examples in Figs. 6.2.1 - 6.2.3 (Tables 6.2.1 - 6.2.3). It is norm-dependent on how to select a threshold value for the minimum error, and the angle at which the errors are less than this threshold is defined the orientation. For instance, the threshold values for our examples in Figs. 6.2.1 - 6.2.3 may be chosen as 15% (the L_1 norm), 1% (Euclidean norm), and 5-10% (maximum norm). Note that the shape of the error functions for different amount of noise (Fig. 6.2.6)

is basically the same and that the minimum error increases as the SNR value decreases. So, the selection of threshold value is also problem-dependent: higher threshold value for noisier images.

The "associated ellipse" approach for orientation recognition seems to be very sensitive to numerical errors and image noise (Table 6.2.4). This is because in building the associated ellipse model only a few lower order moments (up to second order) are used, which may be affected by various sources of noise. With our orientation recognition method, however, the problem of orientation detection becomes an optimization (or minimization) problem, i.e., the impact of noise can be lessened considerably. For example, noise from digitization, numerical integration, etc., affects the accuracy of Zernike moments, especially higher order moments. The error functions show that only small errors (maybe many) have occurred in the moments obtained, i.e., larger L_1 errors and smaller Euclidean errors (Figs. 6.2.1-6.2.3 and Tables 6.2.1 - 6.2.3). The point is that by applying an optimization procedure to many noisy moments we are still able to estimate the orientations reliably, but using the "associated ellipse" approach we have much less flexibility because there are only a few noisy moments to be manipulated.

We have shown that the proposed algorithm can correctly detect the axes of symmetry for symmetric images with high confidence (small error). It is norm- and problem-dependent on how to select a threshold value for the minimum error, and the angles at which the errors are less than this threshold are declared the axes of symmetry. For the noiseless images, for example, the threshold values of 10% (the L_1 norm), 1% (Euclidean norm), and 5% (maximum norm) may be used (*cf.* Fig. 6.3.1 and Tables 6.3.1 - 6.3.5 and Table 6.3.8). From Fig. 6.3.1 and Tables 6.3.1 - 6.3.8 we have made a similar observation as in the case of orientation recognition that minimization based on the Euclidean norm results in the least error compared to two other norms.

The inaccuracy in the case of character O (see Table 6.3.8) results basically from the errors in obtaining these digital images . If the same threshold value as the above is applied

to the error functions for character O [Fig. 6.3.1(h)], we can be assured that this object is angularly symmetric, i.e., infinite number of axes of symmetry. In the case of character F, there is approximately an axis of symmetry at about 135°, so a minimum appears in the error functions (except that based on maximum norm). Because the minimum errors (30-40% for the L_1 norm, 10-15% for Euclidean norm, and 25-30% for maximum norm) for characters F and N [Figs. 6.3.1(f) and 6.3.1(g)] are substantially high, it is certain that these images are either unsymmetrical or too noisy. We also note from this case [Fig. 6.3.1(f) and Table 6.3.6] that use of the maximum norm did not correctly detect such "wild" axes of symmetry.

As in the case of orientation recognition, different norms in the detection of symmetric axes have different sensitivities to noise in images, but the shape of the error functions for different amount of noise (Fig. 6.3.2) is virtually the same and the minimum error increases as the SNR value decreases.

From Tables 6.2.5 - 6.2.7 and 6.3.9 - 6.3.11 we see that orientations and axes of symmetry from noisy images detected by using the Euclidean norm appear to have less deviations than those obtained using two other norms. For the minimization errors we have similar observations. The maximum norm produces the largest deviation in the detected orientations. We conclude that the proposed orientation recognition and symmetry detection algorithms are capable of finding the correct orientations and axes of symmetry in very noisy cases (Tables 6.2.7 and 6.3.11).

References

[6.1]   M. J. Atallah, "On symmetry detection," *IEEE Trans. Comput.*, vol. C-34, pp. 663-666, 1985.

[6.2]   J. Bigün, "Local symmetry features in image processing," *Signal Process.*, vol. 15, pp. 219, 1988.

[6.3]   S. A. Friedberg, "Finding axes of skewed symmetry," *Comput. Vision Graph. Image Process.*, vol. 34, pp. 138-155, 1986.

[6.4]   R. M. Haralick, H. Joo, C.-N. Lee, X. Zhuang, V. G. Vaidya and M. B. Kim, "Pose estimation from corresponding point data," In *Machine Vision for Inspection and Measurement*, H. Freeman, ed., Boston, MA: Academic Press, 1989, pp. 1-84.

[6.5]   A. Khotanzad and Y. H. Hong, "Invariant image recognition by Zernike moments," *IEEE Trans. Pattern Anal. Machine Intell.*, vol. PAMI-12, pp. 489-497, 1990.

[6.6]   G. Marola, "On the detection of the axes of symmetry of symmetric and almost symmetric planar images," *IEEE Trans. Pattern Anal. Machine Intell.*, vol. PAMI-11, pp. 104-108, 1989.

[6.7]   G. Marola, "Using symmetry for detecting and locating objects in a picture," *Comput. Vision Graph. Image Process.*, vol. 46, pp. 179-195, 1989.

[6.8]   V. S. Nalwa, "Line-drawing interpretation: Bilateral symmetry," *IEEE Trans. Pattern Anal. Machine Intell.*, vol. PAMI-11, pp. 1117-1120, 1989.

[6.9]   W. H. Press, B. P. Flannery, S. A. Teukolsky and W. T. Vetterling, *Numerical Recipes: The Art of Scientific Computing*, Cambridge, England: Cambridge University Press, 1986.

[6.10]   J. R. Rice, *Numerical Methods, Software, and Analysis*, New York, NY: McGraw-Hill Book, 1983.

[6.11]   A. Rosenfeld and A. C. Kak, *Digital Picture Processing*, 2nd ed., New York, NY: Academic Press, 1982.

[6.12]   H. R. Schwarz and J. Waldvogel, *Numerical Analysis: A Comprehensive Introduction*, New York, NY: John Wiley & Sons, 1989.

[6.13]   P. Seitz, "The robust recognition of object primitives using local axes of symmetry," *Signal Process.*, vol. 18, pp. 89-108, 1989.

[6.14]   S. Shalev, X. Ding, K. McGee, S. Ryder and X. Zhou, "Analysis of portal beam displacements," Presented at *Radiation Protection Symposium and Joint Conference*, June 16-22, 1991, Winnipeg, Canada, 1991.

CHAPTER 7
CONCLUSIONS AND FUTURE WORK

7.1. Conclusions

A comprehensive review on the detection of early breast cancer, and developments in mammography and other breast imaging modalities has been carried out. We concluded that detection and treatment of breast cancer at early stages is the only method with proven potential for lowering the death rate from this disease. Detection of early breast cancer is promoted by many medical care and health organizations by encouraging the regular use of three types of screening: breast self-examination, clinical breast examination, and X-ray mammography. We must detect smaller tumors than ordinary projection mammography does to improve the survival rate for breast cancer. Digital mammography and digital image processing techniques applied to breast imaging have promised to be more sensitive to small malignant changes and merit further investigation.

In this thesis digital subtraction mammography via geometric unwarping has been studied for detection of early breast cancer. We have formulated a method by using local geometric unwarping for estimating the geometric transformation between reference and warped mammographic images. We have also proposed and implemented a template matching procedure by using the correlation of Zernike moments as the measure of similarity. In this way a set of corresponding control points for derivation of the geometric unwarping transformation can be extracted from some local mammographic structures regardless of their position and orientation. A pre-processing procedure of geometric normalization may be applied to such local structures to improve the within-class invariance and between-class sensitivity of the classification features. Methods for extracting phase

information from an object's Zernike moments for detecting its orientation and symmetry axes, which may be incorporated to facilitate the identification of control points, are also formulated and implemented in this thesis.

7.2. Future Work

A method of image reconstruction from projections for objects that diffuse the incident radiation, such as photons, phonons, neutrons, etc., has been reported [7.62]. It is expected that this method may be applied to medical imaging, industrial imaging, and geophysical imaging. Several others have been working actively on computing the optical scatter distribution noninvasively for the breast and other soft tissue organs. The analysis of how to place these images in registration depends to a significant degree upon the imaging systems and the groups of data available. Many other investigators are currently working with 3D and 4D volume registration and the mixture of geometric and volumetric data describing the same set of physical circumstances. Also an important topic in the future work is an increase of the sensitivity and specificity of breast imaging. The work in mammography should be expanded and updated to include the important recent work with multimodality imaging, PET, time-resolved optical spectroscopy, and others.

There are a number of possible improvements to the geometric unwarping procedure presented in this thesis. Generalization of this geometric unwarping procedure to three-dimensions also needs to be addressed. A number of prospective research topics are thus proposed as follows.

7.2.1. Characterization of Mammographic Features

Mammographic images have a tremendously large number of fine structures and details. It is virtually impossible to analyze and process all these details. At the same time,

redundant information, as demonstrated in Section 5.5, usually interferes with the template matching procedure for identifying the control points. It seems important and crucial to express mammographic structures with appropriate image representations which reduce the redundant information, but still retain a minimum amount of meaningful information for further analysis and processing.

One possibility is binary image representation, which may be obtained by segmentation or thresholding of the original image. Since image segmentation techniques are problem-oriented and differ precisely in the way they emphasize one or more of the desired properties and in the way they balance and compromise one desired property against another, it is necessary to investigate specifically some segmentation methods for mammographic image processing. Comprehensive reviews on image segmentation techniques can be found in [7.22],[7.26],[7.29],[7.54].

Studies of thinning techniques with application to mammographic image processing are also worthwhile considering. Thinning may be used (1) to reduce a pattern to its medial axis form, (2) to enable patterns to be represented as simple data structures in order to speed up analysis process, or (3) to reduce data storage or transmission requirements. Ultimately, the idea is to eliminate redundant information, leaving sufficient useful information to allow topological analysis and measurement of the pattern, or in some cases regeneration of the original pattern. There exists a great volume of literature on thinning or skeletonization of patterns, e.g., [7.18]-[7.21],[7.24],[7.31],[7.40],[7.49],[7.50],[7.53], [7.63],[7.68], etc.

One other more general approach to the characterization of mammographic features is mathematical morphology. Mathematical morphological operations tend to simplify image data preserving their essential shape characteristics and eliminating irrelevancies. By mathematical morphology images are considered as sets of points and the operations come from set theory. The relations between pixels are logical relations, rather than arithmetic ones. The logical relations which are used to construct operations lend themselves to

geometric interpretations. Morphological transformations employ specific sequences of neighborhood transformations to measure useful geometric features on images. In other words, mathematical morphology provides an orderly method of decomposing global geometric measurements into sequences of local transformations. In particular, mathematical morphology starts with the local hit-or-miss transform and, through the derivative transforms of erosion/dilation, thickening/thinning, and opening/closing, builds up a useful set of image processing operations. Mathematical morphological transformations apply to sets of any dimensions. The basic formulation of the theory of mathematical morphology and applications of the theory can be found in [7.14],[7.30], [7.32],[7.37],[7.42]-[7.46],[7.57]-[7.60],[7.64],[7.69].

7.2.2. Identification of Mammographic Features by Template Matching

As discussed in Section 5.5, in identifying the control points by template matching, we have to calculate the correlation of the desired mammographic feature template with the image at each test location. The major concern is the computing time. One solution is that correlation may be carried out in Fourier domain. It is also worthwhile considering other options such as sequential approach, hierarchical search, or hybrid methods which combine some of these individual approaches. There is no clear answer to the question of how to select an optimal template size, which is probably (and should be) varying from case to case and may be mainly dependent upon the results from the characterization process of Section 7.2.1. The total number of features that are to be correlated as a measure of similarity may be reduced if Zernike moments of reasonably higher orders are used instead of the original grey level values. (For example, the total number of Zernike moments from orders 0 through 16 is 81, and the total number of pixels in a 16 x 16 template, which is normally considered fairly small, is 256.) But, it takes a great deal of time to calculate

Zernike moments at all the test locations. The choice of an optimal Zernike moment order for mammographic features in the template matching procedure also needs further studying.

7.2.3. Three-Dimensional Mammographic Feature Matching

There are several possibilities for obtaining the corresponding 3D control points: (1) pseudo-3D Zernike moment approach, (2) 3D spherical harmonics approach, and (3) 3D curve matching approach. Three-dimensional mathematical morphological analysis, more specifically, thinning (see Section 7.2.1) may be applied as a pre-processing step.

(a) As far as the pseudo-3D Zernike moment approach is concerned, the following steps may be considered:

(1) Apply the 3D geometric normalization procedure proposed in Section 5.2 to the desired feature, and find its principal axes.

(2) Slice the feature along its major principal axis, and resample these slices.

(3) Calculate Zernike moments from these resampled slices.

(4) At each test position, perform steps (1) - (3) to the sub-image. Perform template matching using Zernike moments to see if there is a match.

(5) Repeat step (4) at all possible positions.

It is possible to impose a constraint to this procedure that relative orientations in the corresponding slices must be the same. The sensitivity of the principal axes obtained in step (1) to various sources of noise may cause some problems.

(b) The Zernike polynomial is a solution of Laplace's equation in 2D [7.67]. The rotation property of the Zernike moment, which is a set of coefficients of an orthogonal expansion of a function over the unit disk by using Zernike polynomials, can be expressed as a simple phase factor. Of great interest is the fact that this set of Zernike polynomials transforms into itself by a representation of the two-dimensional rotation group [7.2].

Analogically, we expect that spherical harmonics [7.1],[7.23],[7.38],[7.41],[7.55], a solution of Laplace's equation in 3D, may possibly have a "simple" property of rotation.

(c) The 3D feature matching by characteristic curves is based on a notion of a rigidly embedded curve (*cf.* [7.10],[7.12],[7.28],[7.56]). (More precisely, the characteristic curves are parametrized by arc length as a vector-valued function.) In other words, when a structure (object) undergoes any rotation and translation, any curve defined by the geometry of the object moves in the same way as the object does. This assumption may be true if mammographic structures in small regions remain intact despite the mechanical distortion to a global extent incurred in the imaging process. The characteristic curves may include curves from glandular tissues, boundary curves separating two texturally different tissues, or other more subtly defined curves, e.g., curves of specified constant curvature on a surface (curvature contours), or lines of maximum curvature (ridges), etc. Relative insensitivity to noise is the main property that these characteristic curves must posses. To enforce such a property some preliminary curve smoothing may be needed.

7.2.4. Three-Dimensional Geometric Unwarping

The 3D geometric unwarping procedure may, in analogy to the 2D case, be outlined as follows: Given a set of 3D control points, (1) partition the 3D image space from a set of control points by 3D triangulation; and (2) apply pseudo-3D interpolation techniques, or truly 3D interpolation techniques to the control points to get the unwarping transformation. Extrapolation outside the convex hull (3D triangulated space) may be desirable.

The construction of the Voronoi diagram of a set of points, and its dual, the Delaunay tessellation (or triangulation), itself is one of the most fundamental and important problems in various disciplines [7.4]. Many algorithms have been proposed for constructing the Voronoi diagram and Delaunay tessellation in two and three dimensions, e.g., [7.3], [7.11],[7.13],[7.15],[7.27],[7.34]-[7.36],[7.39],[7.47],[7.51],[7.61],[7.66], etc. Avis

and Bhattacharya [7.7], Brown [7.16], Bowyer [7.17], and Watson [7.65] have also reported algorithms to construct the Voronoi diagram of a set of points in n dimensions. It is possible to construct the Delaunay tessellation in n dimensions from its dual Voronoi diagram even though this may be a very expensive computation [7.33].

In terms of 3D interpolation, pseudo-3D interpolation techniques (control points unevenly distributed only in planes which are not necessarily parallel to one another) may be used [7.48]. This is applicable only if the 3D images are obtained through stacking a set of 2D CT images. Truly 3D interpolation techniques have been reported [7.5],[7.6],[7.8], [7.9],[7.25],[7.52].

References

[7.1] G. Arfken, *Mathematical Methods for Physicists,* 3rd Ed., Orlando, FL: Academic Press, 1985.

[7.2] A. B. Bhatia and E. Wolf, "On the circle polynomials of Zernike and related orthogonal sets," *Proc. Cambridge Philosophical Soc.,* vol. 50, pp. 40-48, 1954.

[7.3] N. Ahuja, "Dot pattern processing using Voronoi neighborhoods," *IEEE Trans. Pattern Anal. Machine Intell.,* vol. PAMI-2, pp. 336-343, 1982.

[7.4] N. Ahuja and B. J. Schachter, *Pattern Models,* New York, NY: John Wiley & Sons, 1983.

[7.5] P. Alfeld, "A discrete C^1 interpolant for tetrahedral data," *Rocky Mountain J. Math.,* vol. 14, pp. 5-16, 1984a.

[7.6] P. Alfeld, "A trivariate Clough-Tocher scheme for tetrahedral data," *Comp. Aided Geom. Design,* vol. 1, pp. 169-181, 1984b.

[7.7] D. Avis and B. K. Bhattacharya, "Algorithms for computing d-dimensional Voronoi diagrams and their duals," In *Advances in Computing Research: Computational Geometry,* F. P. Preparata, Ed., Greenwich, Connecticut: JAI Press, 1983, pp. 159-180.

[7.8] R. E. Barnhill, "Surfaces in computer aided geometric design: A survey with new results," *Comput. Aided Geom. Design,* vol. 2, pp. 1-17, 1985.

[7.9] R. E. Barnhill and F. F. Little, "Three- and four-dimensional surfaces," *Rocky Mountain J. Math.,* vol. 14, pp. 77-102, 1984.

[7.10] C. M. Bastuscheck, "Object recognition by three-dimensional curve matching," *Int. J. Intell. Sys.,* vol. 1, pp. 105-132, 1986.

[7.11] J. L. Bentley, B. W. Weide and A. C. Yao, "Optimal expected time algorithms for closest-point problems," *ACM Trans. Math. Software,* vol. 6, pp. 563-580, 1980.

[7.12]   R. Bolles, P. Horaud and M. Hannah, "3DPO: A three-dimensional part orientation system," In *First International Symposium on Robotics Research,* Cambridge, MA, 1984, pp. 413-424.

[7.13]   K. E. Brassel and D. Rief, "A procedure to generate Thiessen polygons," *Geograph. Anal.,* vol. 11, pp. 289-303, 1979.

[7.14]   J. F. Bronskill and A. N. Venetsanopoulos, "Multidimensional shape description and recognition using mathematical morphology," *J. Intell. Robotic Sys.,* vol. 1, pp. 117-143, 1988.

[7.15]   W. Brostow, J. P. Dussault and B. L. Fox, "Construction of Voronoi polyhedra," *J. Comput. Phys.,* vol. 29, pp. 81-92, 1978.

[7.16]   K. Q. Brown, "Voronoi diagrams from convex hull," *Info. Proc. Lett.,* vol. 9, pp. 223-228, 1979.

[7.17]   A. Bowyer, "Computing Dirichlet tessellations," *Comp. J.,* vol. 24, pp. 162-166, 1981.

[7.18]   Y. S. Chen and W. H. Hsu, "A modified fast parallel algorithm for thinning digital patterns," *Pattern Recog. Lett.,* vol. 7, pp. 99-106, 1988.

[7.19]   Y. S. Chen and W. H. Hsu, "A systematic approach for designing 2-subcycle and pseudo 1-subcycle parallel thinning algorithms," *Pattern Recog.,* vol. 22, pp. 267-282, 1989.

[7.20]   Y. S. Chen and W. H. Hsu, "A comparison of some one-pass parallel thinnings," *Pattern Recog. Lett.,* vol. 11, pp. 35-41, 1990.

[7.21]   R. T. Chin, H. Wan, D. L. Stover and R. D. Iverson, "A one-pass thinning algorithm and its parallel implementation," *Comput. Vision Graph. Image Process.,* vol. 40, pp. 30-40, 1987.

[7.22]   G. B. Coleman and H. C. Andrews, "Image segmentation by clustering," *Proc. IEEE,* vol. 67, pp. 773-785, 1979.

[7.23]   J. F. Cornwell, *Group Theory in Physics,* London: Academic Press, 1984.

[7.24]   E. R. Davies and A. P. N. Plummer, "Thinning algorithms: A critique and a new methodology," *Pattern Recog.,* vol. 14, pp. 53-63, 1981.

[7.25]   I. P. Dubey and S. K. Upadhyay, "A trivariate interpolation method developed on the basis of Akima's bivariate interpolation procedure," *Comput. Phys. Commun.,* vol. 54, pp. 23-29, 1989.

[7.26]   K. S. Fu and J. K. Mui, "A survey on image segmentation," *Pattern Recog.,* vol. 13, pp. 3-16, 1980.

[7.27]   P. J. Green and R. Sibson, "Computing Dirichlet tessellations in the plane," *Comp. J.,* vol. 21, pp. 168-173, 1978.

[7.28]   W. Grimson and T. Lozano-Pérez, "Recognition and localization of overlapping parts from sparse data in two and three dimensions," In *IEEE Int. Conf. Robotics and Automation,* St. Louis, 1985, pp. 61-66.

[7.29]   R. M. Haralick and L. G. Shapiro, "Image segmentation techniques," *Comput. Vision Graphics Image Process.,* vol. 29, pp. 100-132, 1985.

[7.30]   R. M. Haralick, S. R. Sternberg and X. Zhuang, "Image analysis using mathematical morphology," *IEEE Trans. Pattern Anal. Machine Intell.,* vol. PAMI-9, pp. 532-550, 1987.

[7.31]   C. M. Holt, A. Stewart, M. Clint and R. H. Perrott, "An improved parallel thinning algorithm," *Comm. ACM,* vol. 30, pp. 156-160, 1987.

[7.32]   B. K. Jang and R. T. Chin, "Analysis of thinning algorithms using mathematical morphology," *IEEE Trans. Pattern Anal. Machine Intell.,* vol. PAMI-12, pp. 541-551, 1990.

[7.33]   V. Klee, "On the complexity of d-dimensional Voronoi diagrams," *Arch. Math.,* vol. 34, pp. 75-80, 1980.

[7.34]   C. L. Lawson, "Software for C^1 surface interpolation," In *Mathematical Software III,* J. R. Rice, Ed., New York: Academic Press, 1977, pp. 161-194.

[7.35]   D. T. Lee, "Two-dimensional Voronoi diagrams in the L_p metric," *J. ACM,* vol. 27, pp. 604-618, 1980.

[7.36]   D. T. Lee and B. J. Schachter, "Two algorithms for constructing a Delaunay triangulation," *Int. J. Comput. Info. Sci.,* vol. 9, pp. 219-242, 1980.

[7.37]   J. S. J. Lee, R. M. Haralick and L. G. Shapiro, "Morphologic edge detection," *IEEE Trans. Robotics Automat.,* vol. RA-3, pp. 142-156, 1987.

[7.38]   R. Lenz, "Group invariant pattern recognition," *Pattern Recog. Lett.,* vol. 23, pp. 199-217, 1990.

[7.39]   B. A. Lewis and J. S. Robinson, "Triangulation of planar regions with applications," *Comp. J.,* vol. 21, pp. 324-332, 1978.

[7.40]   S. Lobregt, P. W. Verbeek and F. C. A. Groen, "Three-dimensional skeletonization: Principle and algorithm," *IEEE Trans. Pattern Anal. Machine Intell.,* vol. PAMI-2, pp. 75-77, 1980.

[7.41]   T. M. MacRobert and I. N. Sneddon, *Spherical Harmonics: An Elementary Treatise on Harmonic Functions with Applications,* 3rd Ed., Oxford, England: Pergamon Press, 1967.

[7.42]   P. Maragos and R. W. Schafer, "Morphological skeleton representation and coding of binary images," *IEEE Trans. Acoust. Speech Signal Process.,* vol. ASSP-34, pp. 1228-1244, 1986.

[7.43]   P. Maragos and R. W. Schafer, "Morphological filters - Part I: Their set-theoretic analysis and relations to linear shift-invariant filters," *IEEE Trans. Acoust. Speech Signal Process.,* vol. ASSP-35, pp. 1153-1169, 1987.

[7.44]   P. Maragos and R. W. Schafer, "Morphological filters - Part II: Their relations to median, order-statistic, and stack filters," *IEEE Trans. Acoust. Speech Signal Process.,* vol. ASSP-35, pp. 1170-1184, 1987.

[7.45]   P. Maragos and R. W. Schafer, "Corrections to 'Morphological filters - Part II: Their relations to median, order-statistic, and stack filters'," *IEEE Trans. Acoust. Speech Signal Process.,* vol. ASSP-37, pp. 597, 1989.

[7.46]   G. Matheron, *Random Sets and Integral Geometry,* New York, NY: John Wiley, 1975.

[7.47]   N. N. Medvedev, "The algorithm for three-dimensional Voronoi polyhedra," *J. Comput. Phys.,* vol. 67, pp. 223-229, 1986.

[7.48]   J. K. Navlakha, "An analytical technique for 3-dimensional interpolation," *BIT,* vol. 24, pp. 119-122, 1984.

[7.49]   H. Ogawa and K. Taniguchi, "Thinning and stroke segmentation for handwriting Chinese character recognition," *Pattern Recog.*, vol. 15, pp. 299-308, 1982.

[7.50]   T. Pavlidis, "A thinning algorithm for discrete binary images," *Comput. Graph. Image Process.*, vol. 13, pp. 142-157, 1980.

[7.51]   F. P. Preparata and S. J. Hong, "Convex hulls of finite sets of points in two and three dimensions," *Comm. ACM*, vol. 20, pp. 87-93, 1977.

[7.52]   R. J. Renka, "Multivariate interpolation of large sets of scattered data," *ACM Trans. Math. Software*, vol. 14, pp. 139-148, 1988.

[7.53]   S. Riazanoff, B. Cervelle and J. Chorowicz, "Parametrisable skeletonization of binary and multi-level images," *Pattern Recog. Lett.*, vol. 11, pp. 25-33, 1990.

[7.54]   A. Rosenfeld and L. S. Davis, "Image segmentation and image models," *Proc. IEEE*, vol. 67, pp. 764-772, 1979.

[7.55]   G. Sansone, *Orthogonal Functions*, New York, NY: Interscience Publishers, 1959.

[7.56]   J. T. Schwartz and M. Sharir, "Identification of partially obscured objects in two and three dimensions by matching of noisy characteristic curves," *The Int. J. Robotics Research*, vol. 6, pp. 29-44, 1987.

[7.57]   J. Serra, *Image Analysis and Mathematical Morphology*, New York, NY: Academic Press, 1982.

[7.58]   J. Serra, "Introduction to mathematical morphology," *Comput. Vision Graphics Image Process.*, vol. 35, pp. 283-305, 1986.

[7.59]   J. Serra, Ed., *Image Analysis and Mathematical Morphology, Volume 2: Theoretical Advances*, New York, NY: Academic Press, 1988.

[7.60]   F. Y.-C. Shih and O. R. Mitchell, "Threshold decomposition of gray-scale morphology into binary morphology," *IEEE Trans. Pattern Anal. Machine Intell.*, vol. PAMI-11, pp. 31-42, 1989.

[7.61]   R. Sibson, "Locally equiangular triangulations," *Comp. J.*, vol. 21, pp. 243-245, 1978.

[7.62]   J. R. Singer, F. A. Grünbaum, P. Kohn and J. P. Zubelli, "Image reconstruction of the interior of bodies that diffuse radiation," *Science*, vol. 248, pp. 990-993, 1990.

[7.63]   R. Stefanelli and A. Rosenfeld, "Some parallel thinning algorithms for digital pictures," *J. ACM*, vol. 18, pp. 255-264, 1971.

[7.64]   S. R. Sternberg, "Grayscale morphology," Comput. Vision Graphics Image Process., vol. 35, pp. 333-355, 1986.

[7.65]   D. F. Watson, "Computing the d-dimensional Delauney tessellation with aplication to Voronoi polytopes," *Comp. J.*, vol. 24, pp. 167-172, 1981.

[7.66]   D. F. Watson and G. M. Philip, "Systematic triangulations," *Comput. Graphics Image Process.*, vol. 26, pp. 217-223, 1984.

[7.67]   F. von Zernike, "Beugungstheorie des schneidenver-fahrens und seiner verbesserten form, der phasenkontrastmethode," *Physica*, vol. 1, pp. 689-704, 1934.

[7.68]   T. Y. Zhang and C. Y. Suen, "A fast parallel algorithm for thinning digital patterns," *Comm. ACM,* vol. 27, pp. 236-239, 1984.

[7.69]   X. Zhuang and R. M. Haralick, "Morphological structuring element decomposition," *Comput. Vision Graph. Image Process.,* vol. 35, pp. 370-382, 1986.

APPENDIX 1

DETECTION OF EARLY BREST CANCER: AN OVERVIEW AND FUTURE PROSPECTS

This appendix has been reprinted from *CRC Critical Reviews in Biomedical Engineering*, vol. 17, no. 4, 1989.

APPENDIX 2

INTERPOLATION FUNCTIONS AND THEIR FOURIER TRANSFORMS

Some interpolation functions $s(x)$ and their Fourier transforms $S(X)$ used are listed in the following.

A2.1. Lagrange Interpolation

(1) Nearest Neighbor:

$$s(x) = \begin{cases} 1, & -\frac{1}{2} \leq x < \frac{1}{2} \\ 0, & \text{otherwise} \end{cases}$$

$$S(X) = sinc(X). \qquad (A2.1.1)$$

(2) Linear:

$$s(x) = \begin{cases} x + 1, & -1 \leq x < 0 \\ -x + 1, & 0 \leq x < 1 \\ 0, & \text{otherwise} \end{cases}$$

$$S(X) = sinc^2(X). \qquad (A2.1.2)$$

(3) 3 point Lagrange:

$$s(x) = \begin{cases} \frac{1}{2}x^2 + \frac{3}{2}x + 1, & -\frac{3}{2} \leq x < -\frac{1}{2} \\ -x^2 + 1, & -\frac{1}{2} \leq x < \frac{1}{2} \\ \frac{1}{2}x^2 - \frac{3}{2}x + 1, & \frac{1}{2} \leq x < \frac{3}{2} \\ 0, & \text{otherwise} \end{cases}$$

$$S(X) = \begin{cases} 1, & X = 0 \\ \frac{3}{8}\left[1 + \frac{2}{(\pi X)^2}\right][sinc(X) - sinc(3X)], & X \neq 0. \end{cases}$$

(A2.1.3)

(4) 4 point Lagrange:

$$s(x) = \begin{cases} \frac{1}{6}x^3 + x^2 + \frac{11}{6}x + 1, & -2 \leq x < -1 \\ -\frac{1}{2}x^3 - x^2 + \frac{1}{2}x + 1, & -1 \leq x < 0 \\ \frac{1}{2}x^3 - x^2 - \frac{1}{2}x + 1, & 0 \leq x < 1 \\ -\frac{1}{6}x^3 + x^2 - \frac{11}{6}x + 1, & 1 \leq x < 2 \\ 0, & \text{otherwise} \end{cases}$$

$$S(X) = \begin{cases} 1, & X = 0 \\ \frac{1}{3}\left[2 + \frac{3}{(\pi X)^2}\right][sinc^2(X) - sinc^2(2X)], & X \neq 0. \end{cases}$$

(A2.1.4)

(5) 5 point Lagrange:

$$s(x) = \begin{cases} \frac{1}{24}x^4 + \frac{5}{12}x^3 + \frac{35}{24}x^2 + \frac{25}{12}x + 1, & -\frac{5}{2} \leq x < -\frac{3}{2} \\ -\frac{1}{6}x^4 - \frac{5}{6}x^3 - \frac{5}{6}x^2 + \frac{5}{6}x + 1, & -\frac{3}{2} \leq x < -\frac{1}{2} \\ \frac{1}{4}x^4 - \frac{5}{4}x^2 + 1, & -\frac{1}{2} \leq x < \frac{1}{2} \\ -\frac{1}{6}x^4 + \frac{5}{6}x^3 - \frac{5}{6}x^2 - \frac{5}{6}x + 1, & \frac{1}{2} \leq x < \frac{3}{2} \\ \frac{1}{24}x^4 - \frac{5}{12}x^3 + \frac{35}{24}x^2 - \frac{25}{12}x + 1, & \frac{3}{2} \leq x < \frac{5}{2} \\ 0, & \text{otherwise} \end{cases}$$

$$S(X) = \begin{cases} 1, & X = 0 \\ \frac{5}{384}\left[9 + \frac{20}{(\pi X)^2} + \frac{24}{(\pi X)^4}\right][2sinc(X) - 3sinc(3X) + sinc(5X)], & X \neq 0. \end{cases}$$

(A2.1.5)

(6) 6 point Lagrange:

$$s(x) = \begin{cases} \frac{1}{120}x^5 + \frac{1}{8}x^4 + \frac{17}{24}x^3 + \frac{15}{8}x^2 + \frac{137}{60}x + 1, & -3 \le x < -2 \\[2mm] -\frac{1}{24}x^5 - \frac{3}{8}x^4 - \frac{25}{24}x^3 - \frac{5}{8}x^2 + \frac{13}{12}x + 1, & -2 \le x < -1 \\[2mm] \frac{1}{12}x^5 + \frac{1}{4}x^4 - \frac{5}{12}x^3 - \frac{5}{4}x^2 + \frac{1}{3}x + 1, & -1 \le x < 0 \\[2mm] -\frac{1}{12}x^5 + \frac{1}{4}x^4 + \frac{5}{12}x^3 - \frac{5}{4}x^2 - \frac{1}{3}x + 1, & 0 \le x < 1 \\[2mm] \frac{1}{24}x^5 - \frac{3}{8}x^4 + \frac{25}{24}x^3 - \frac{5}{8}x^2 - \frac{13}{12}x + 1, & 1 \le x < 2 \\[2mm] -\frac{1}{120}x^5 + \frac{1}{8}x^4 - \frac{17}{24}x^3 + \frac{15}{8}x^2 - \frac{137}{60}x + 1, & 2 \le x < 3 \\[2mm] 0, & \text{otherwise} \end{cases}$$

$$S(X) = \begin{cases} 1, & X = 0 \\[2mm] \frac{1}{80}\left[8 + \frac{15}{(\pi X)^2} + \frac{15}{(\pi X)^4}\right]\left[5 sinc^2(X) - 8 sinc^2(2X) + 3 sinc^2(3X)\right], & X \ne 0. \end{cases}$$

(A2.1.6)

A2.2. Cubic Splines Interpolation

$$s(x) = \begin{cases} \frac{1}{6}x^3 + x^2 + 2x + \frac{4}{3}, & -2 \le x < -1 \\[2mm] -\frac{1}{2}x^3 - x^2 + \frac{2}{3}, & -1 \le x < 0 \\[2mm] \frac{1}{2}x^3 - x^2 + \frac{2}{3}, & 0 \le x < 1 \\[2mm] -\frac{1}{6}x^3 + x^2 - 2x + \frac{4}{3}, & 1 \le x < 2 \\[2mm] 0, & \text{otherwise} \end{cases}$$

$$S(X) = sinc^4(X).$$

(A2.2.1)

A2.3. Cubic Convolution Interpolation

$$s(x) = \begin{cases} -\alpha x^3 - 5\alpha x^2 - 8\alpha x - 4\alpha, & -2 \le x < -1 \\ -(\alpha + 2)x^3 - (\alpha + 3)x^2 + 1, & -1 \le x < 0 \\ (\alpha + 2)x^3 - (\alpha + 3)x^2 + 1, & 0 \le x < 1 \\ \alpha x^3 - 5\alpha x^2 + 8\alpha x - 4\alpha, & 1 \le x < 2 \\ 0, & \text{otherwise} \end{cases}$$

$$S(X) = \begin{cases} 1, & X = 0 \\ -\dfrac{3 + 4\alpha}{(\pi X)^2} sinc(2X) - \dfrac{2\alpha}{(\pi X)^2} sinc(4X) + \dfrac{3}{(\pi X)^2} sinc^2(X) + \dfrac{6\alpha}{(\pi X)^2} sinc^2(2X), & X \ne 0. \end{cases} \qquad (A2.3.1)$$

APPENDIX 3

LOCAL IMAGE OPERATORS BASED ON ORTHOGONAL POLYNOMIAL FUNCTIONS

The following operators are a set of local, 2D linear image operators $B_{x_1...x_iy_1...y_j}{}^k(n)$, which estimate in an $n \times n$ neighborhood by a polynomial of order k a value proportional to the ith and jth cross derivatives with respect to x and y, respectively. They may be used to find the local derivatives of an image. They are used here in surface fitting for intensity approximation.

A3.1. Zero Order Operators

For an $n \times n$ neighborhood, the zero order operators can be represented by the following $n \times n$ matrix of 1's

$$B_0^0(n) = \frac{1}{n^2} \begin{bmatrix} 1 & 1 & \cdots & 1 \\ 1 & 1 & \cdots & 1 \\ \vdots & \vdots & \ddots & \vdots \\ 1 & 1 & \cdots & 1 \end{bmatrix}. \tag{A3.1.1}$$

A3.2. First Order Operators

Note that the operators $B_0{}^1$, which are not shown here, are the same as those for the zero order $B_0{}^0$, respectively.

(1) 2 x 2 neighborhood:

$$B_1^1(2) = \frac{1}{2} \begin{bmatrix} -1 & 1 \\ -1 & 1 \end{bmatrix} \text{ and } B_2^1(2) = \left[B_1^1(2) \right]^T. \tag{A3.2.1}$$

(2) 3 x 3 neighborhood:

$$B_1^1(3) = \frac{1}{6} \begin{bmatrix} -1 & 0 & 1 \\ -1 & 0 & 1 \\ -1 & 0 & 1 \end{bmatrix} \quad \text{and} \quad B_2^1(3) = \left[B_1^1(3) \right]^T. \qquad \text{(A3.2.2)}$$

(3) 4 x 4 neighborhood:

$$B_1^1(4) = \frac{1}{40} \begin{bmatrix} -3 & -1 & 1 & 3 \\ -3 & -1 & 1 & 3 \\ -3 & -1 & 1 & 3 \\ -3 & -1 & 1 & 3 \end{bmatrix} \quad \text{and} \quad B_2^1(4) = \left[B_1^1(4) \right]^T. \qquad \text{(A3.2.3)}$$

(4) 5 x 5 neighborhood:

$$B_1^1(5) = \frac{1}{50} \begin{bmatrix} -2 & -1 & 0 & 1 & 2 \\ -2 & -1 & 0 & 1 & 2 \\ -2 & -1 & 0 & 1 & 2 \\ -2 & -1 & 0 & 1 & 2 \\ -2 & -1 & 0 & 1 & 2 \end{bmatrix} \quad \text{and} \quad B_2^1(5) = \left[B_1^1(5) \right]^T. \qquad \text{(A3.2.4)}$$

(5) 6 x 6 neighborhood:

$$B_1^1(6) = \frac{1}{210} \begin{bmatrix} -5 & -3 & -1 & 1 & 3 & 5 \\ -5 & -3 & -1 & 1 & 3 & 5 \\ -5 & -3 & -1 & 1 & 3 & 5 \\ -5 & -3 & -1 & 1 & 3 & 5 \\ -5 & -3 & -1 & 1 & 3 & 5 \\ -5 & -3 & -1 & 1 & 3 & 5 \end{bmatrix} \quad \text{and} \quad B_2^1(6) = \left[B_1^1(6) \right]^T. \qquad \text{(A3.2.5)}$$

(6) 7 x 7 neighborhood:

$$B_1^1(7) = \frac{1}{168} \begin{bmatrix} -3 & -2 & -1 & 0 & 1 & 2 & 3 \\ -3 & -2 & -1 & 0 & 1 & 2 & 3 \\ -3 & -2 & -1 & 0 & 1 & 2 & 3 \\ -3 & -2 & -1 & 0 & 1 & 2 & 3 \\ -3 & -2 & -1 & 0 & 1 & 2 & 3 \\ -3 & -2 & -1 & 0 & 1 & 2 & 3 \\ -3 & -2 & -1 & 0 & 1 & 2 & 3 \end{bmatrix} \quad \text{and} \quad B_2^1(7) = \left[B_1^1(7) \right]^T. \qquad \text{(A3.2.6)}$$

(7) 8 x 8 neighborhood:

$$B_1^1(8) = \frac{1}{672} \begin{bmatrix} -7 & -5 & -3 & -1 & 1 & 3 & 5 & 7 \\ -7 & -5 & -3 & -1 & 1 & 3 & 5 & 7 \\ -7 & -5 & -3 & -1 & 1 & 3 & 5 & 7 \\ -7 & -5 & -3 & -1 & 1 & 3 & 5 & 7 \\ -7 & -5 & -3 & -1 & 1 & 3 & 5 & 7 \\ -7 & -5 & -3 & -1 & 1 & 3 & 5 & 7 \\ -7 & -5 & -3 & -1 & 1 & 3 & 5 & 7 \\ -7 & -5 & -3 & -1 & 1 & 3 & 5 & 7 \end{bmatrix} \quad \text{and} \quad B_2^1(8) = \left[B_1^1(8)\right]^T. \qquad (A3.2.7)$$

A3.3. Second Order Operators

Note that the operators B_1^2, B_2^2, which are not shown here, are the same as those for the first order B_1^1, B_2^1, respectively.

(1) 3 x 3 neighborhood:

$$B_0^2(3) = \frac{1}{9} \begin{bmatrix} -1 & 2 & -1 \\ 2 & 5 & 2 \\ -1 & 2 & -1 \end{bmatrix}, \quad B_{11}^2(3) = \frac{1}{6} \begin{bmatrix} 1 & -2 & 1 \\ 1 & -2 & 1 \\ 1 & -2 & 1 \end{bmatrix}, \quad B_{12}^2(3) = \frac{1}{4} \begin{bmatrix} 1 & 0 & -1 \\ 0 & 0 & 0 \\ -1 & 0 & 1 \end{bmatrix},$$

$$\text{and } B_{22}^2(3) = \left[B_{11}^2(3)\right]^T. \qquad (A3.3.1)$$

(2) 4 x 4 neighborhood:

$$B_0^2(4) = \frac{1}{32} \begin{bmatrix} -3 & 2 & 2 & -3 \\ 2 & 7 & 7 & 2 \\ 2 & 7 & 7 & 2 \\ -3 & 2 & 2 & -3 \end{bmatrix}, \quad B_{11}^2(4) = \frac{1}{16} \begin{bmatrix} 1 & -1 & -1 & 1 \\ 1 & -1 & -1 & 1 \\ 1 & -1 & -1 & 1 \\ 1 & -1 & -1 & 1 \end{bmatrix}, \quad B_{12}^2(4) = \frac{1}{100} \begin{bmatrix} 9 & 3 & -3 & -9 \\ 3 & 1 & -1 & -3 \\ -3 & -1 & 1 & 3 \\ -9 & -1 & 3 & 9 \end{bmatrix},$$

$$\text{and } B_{22}^2(4) = \left[B_{11}^2(4)\right]^T. \qquad (A3.3.2)$$

(3) 5 x 5 neighborhood:

$$B_0^2(5) = \frac{1}{175} \begin{bmatrix} -13 & 2 & 7 & 2 & -13 \\ 2 & 17 & 22 & 17 & 2 \\ 7 & 22 & 27 & 22 & 7 \\ 2 & 17 & 22 & 17 & 2 \\ -13 & 2 & 7 & 2 & -13 \end{bmatrix}, \quad B_{11}^2(5) = \frac{1}{70} \begin{bmatrix} 2 & -1 & -2 & -1 & 2 \\ 2 & -1 & -2 & -1 & 2 \\ 2 & -1 & -2 & -1 & 2 \\ 2 & -1 & -2 & -1 & 2 \\ 2 & -1 & -2 & -1 & 2 \end{bmatrix},$$

$$B_{12}^2(5) = \frac{1}{100} \begin{bmatrix} 4 & 2 & 0 & -2 & -4 \\ 2 & 1 & 0 & -1 & -2 \\ 0 & 0 & 0 & 0 & 0 \\ -2 & -1 & 0 & 1 & 2 \\ -4 & -2 & 0 & 2 & 4 \end{bmatrix}, \text{ and } B_{22}^2(5) = \left[B_{11}^2(5) \right]^T. \qquad (A3.3.3)$$

(4) 6 x 6 neighborhood:

$$B_0^2(6) = \frac{1}{576} \begin{bmatrix} -34 & -4 & 11 & 11 & -4 & -34 \\ -4 & 26 & 41 & 41 & 26 & -4 \\ 11 & 41 & 56 & 56 & 41 & 11 \\ 11 & 41 & 56 & 56 & 41 & 11 \\ -4 & 26 & 41 & 41 & 26 & -4 \\ -34 & -4 & 11 & 11 & -4 & -34 \end{bmatrix}, \quad B_{11}^2(6) = \frac{1}{336} \begin{bmatrix} 5 & -1 & -4 & -4 & -1 & 5 \\ 5 & -1 & -4 & -4 & -1 & 5 \\ 5 & -1 & -4 & -4 & -1 & 5 \\ 5 & -1 & -4 & -4 & -1 & 5 \\ 5 & -1 & -4 & -4 & -1 & 5 \\ 5 & -1 & -4 & -4 & -1 & 5 \end{bmatrix},$$

$$B_{12}^2(6) = \frac{1}{1225} \begin{bmatrix} 25 & 15 & 5 & -5 & -15 & -25 \\ 15 & 9 & 3 & -3 & -9 & -15 \\ 5 & 3 & 1 & -1 & -3 & -5 \\ -5 & -3 & -1 & 1 & 3 & 5 \\ -15 & -9 & -3 & 3 & 9 & 15 \\ -25 & -15 & -5 & 5 & 15 & 25 \end{bmatrix}, \quad \text{and } B_{22}^2(6) = \left[B_{11}^2(6) \right]^T. \qquad (A3.3.4)$$

(5) 7 x 7 neighborhood:

$$B_0^2(7) = \frac{1}{147} \begin{bmatrix} -7 & -2 & 1 & 2 & 1 & -2 & -7 \\ -2 & 3 & 6 & 7 & 6 & 3 & -2 \\ 1 & 6 & 9 & 10 & 9 & 6 & 1 \\ 2 & 7 & 10 & 11 & 10 & 7 & 2 \\ 1 & 6 & 9 & 10 & 9 & 6 & 1 \\ -2 & 3 & 6 & 7 & 6 & 3 & -2 \\ -7 & -2 & 1 & 2 & 1 & -2 & -7 \end{bmatrix}, \quad B_{11}^2(7) = \frac{1}{588} \begin{bmatrix} 5 & 0 & -3 & -4 & -3 & 0 & 5 \\ 5 & 0 & -3 & -4 & -3 & 0 & 5 \\ 5 & 0 & -3 & -4 & -3 & 0 & 5 \\ 5 & 0 & -3 & -4 & -3 & 0 & 5 \\ 5 & 0 & -3 & -4 & -3 & 0 & 5 \\ 5 & 0 & -3 & -4 & -3 & 0 & 5 \\ 5 & 0 & -3 & -4 & -3 & 0 & 5 \end{bmatrix},$$

$$B_{12}^2(7) = \frac{1}{784} \begin{bmatrix} 9 & 6 & 3 & 0 & -3 & -6 & -9 \\ 6 & 4 & 2 & 0 & -2 & -4 & -6 \\ 3 & 2 & 1 & 0 & -1 & -2 & -3 \\ 0 & 0 & 0 & 0 & 0 & 0 & 0 \\ -3 & -2 & -1 & 0 & 1 & 2 & 3 \\ -6 & -4 & -2 & 0 & 2 & 4 & 6 \\ -9 & -6 & -3 & 0 & 3 & 6 & 9 \end{bmatrix}, \quad \text{and } B_{22}^2(7) = \left[B_{11}^2(7) \right]^T. \qquad (A3.3.5)$$

(6) 8 x 8 neighborhood:

$$B_0^2(8) = \frac{1}{128} \begin{bmatrix} -5 & -2 & 0 & 1 & 1 & 0 & -2 & -5 \\ -2 & 1 & 3 & 4 & 4 & 3 & 1 & -2 \\ 0 & 3 & 5 & 6 & 6 & 5 & 3 & 0 \\ 1 & 4 & 6 & 7 & 7 & 6 & 4 & 1 \\ 1 & 4 & 6 & 7 & 7 & 6 & 4 & 1 \\ 0 & 3 & 5 & 6 & 6 & 5 & 3 & 0 \\ -2 & 1 & 3 & 4 & 4 & 3 & 1 & -2 \\ -5 & -2 & 0 & 1 & 1 & 0 & -2 & -5 \end{bmatrix}, \quad B_{11}^2(8) = \frac{1}{1344} \begin{bmatrix} 7 & 1 & -3 & -5 & -5 & -3 & 1 & 7 \\ 7 & 1 & -3 & -5 & -5 & -3 & 1 & 7 \\ 7 & 1 & -3 & -5 & -5 & -3 & 1 & 7 \\ 7 & 1 & -3 & -5 & -5 & -3 & 1 & 7 \\ 7 & 1 & -3 & -5 & -5 & -3 & 1 & 7 \\ 7 & 1 & -3 & -5 & -5 & -3 & 1 & 7 \\ 7 & 1 & -3 & -5 & -5 & -3 & 1 & 7 \\ 7 & 1 & -3 & -5 & -5 & -3 & 1 & 7 \end{bmatrix},$$

$$B_{12}^2(8) = \frac{1}{4056} \begin{bmatrix} 49 & 35 & 21 & 7 & -7 & -21 & -35 & -49 \\ 35 & 25 & 15 & 5 & -5 & -15 & -25 & -35 \\ 21 & 15 & 9 & 3 & -3 & -9 & -15 & -21 \\ 7 & 5 & 3 & 1 & -1 & -3 & -5 & -7 \\ -7 & -5 & -3 & -1 & 1 & 3 & 5 & 7 \\ -21 & -15 & -9 & -3 & 3 & 9 & 15 & 21 \\ -35 & -25 & -15 & -5 & 5 & 15 & 25 & 35 \\ -49 & -35 & -21 & -7 & 7 & 21 & 35 & 49 \end{bmatrix}, \quad \text{and } B_{22}^2(8) = \left[B_{11}^2(8)\right]^T. \quad (A3.3.6)$$

A3.4. Third Order Operators

Note that the operators B_0^3, B_{11}^3, B_{22}^3, B_{12}^3, which are not shown here, are the same as those for the second order B_0^2, B_{11}^2, B_{22}^2, B_{12}^2, respectively.

(1) 4 x 4 neighborhood:

$$B_1^3(4) = \frac{1}{48} \begin{bmatrix} 5 & -12 & 12 & -5 \\ -4 & -15 & 15 & 4 \\ -4 & -15 & 15 & 4 \\ 5 & -12 & 12 & -5 \end{bmatrix}, \quad B_{111}^3(4) = \frac{1}{24} \begin{bmatrix} -1 & 3 & -3 & 1 \\ -1 & 3 & -3 & 1 \\ -1 & 3 & -3 & 1 \\ -1 & 3 & -3 & 1 \end{bmatrix},$$

$$B_{112}^3(4) = \frac{1}{40} \begin{bmatrix} -3 & 3 & 3 & -3 \\ -1 & 1 & 1 & -1 \\ 1 & -1 & -1 & 1 \\ 3 & -3 & -3 & 3 \end{bmatrix}, \quad B_2^3(4) = \left[B_1^3(4)\right]^T, \quad B_{222}^3(4) = \left[B_{111}^3(4)\right]^T,$$

$$\text{and } B_{221}^3(4) = \left[B_{112}^3(4)\right]^T. \quad (A3.4.1)$$

(2) 5 x 5 neighborhood:

$$B_1^3(5) = \frac{1}{420}\begin{bmatrix} 31 & -44 & 0 & 44 & -31 \\ -5 & -62 & 0 & 62 & 5 \\ -17 & -68 & 0 & 68 & 17 \\ -5 & -62 & 0 & 62 & 5 \\ 31 & -44 & 0 & 44 & -31 \end{bmatrix}, \quad B_{111}^3(5) = \frac{1}{60}\begin{bmatrix} -1 & 2 & 0 & -2 & 1 \\ -1 & 2 & 0 & -2 & 1 \\ -1 & 2 & 0 & -2 & 1 \\ -1 & 2 & 0 & -2 & 1 \\ -1 & 2 & 0 & -2 & 1 \end{bmatrix},$$

$$B_{112}^3(5) = \frac{1}{140}\begin{bmatrix} -4 & 2 & 4 & 2 & -4 \\ -2 & 1 & 2 & 1 & -2 \\ 0 & 0 & 0 & 0 & 0 \\ 2 & -1 & -2 & -1 & 2 \\ 4 & -2 & -4 & -2 & 4 \end{bmatrix}, \quad B_2^3(5) = \left[B_1^3(5)\right]^T, \quad B_{222}^3(5) = \left[B_{111}^3(5)\right]^T,$$

$$\text{and } B_{221}^3(5) = \left[B_{112}^3(5)\right]^T. \tag{A3.4.2}$$

(3) 6 x 6 neighborhood:

$$B_1^3(6) = \frac{1}{18144}\begin{bmatrix} 950 & -844 & -517 & 517 & 844 & -950 \\ 140 & -1330 & -679 & 679 & 1330 & -140 \\ -265 & -1573 & -760 & 760 & 1573 & 265 \\ -265 & -1573 & -760 & 760 & 1573 & 265 \\ 140 & -1330 & -679 & 679 & 1330 & -140 \\ 950 & -844 & -517 & 517 & 844 & -950 \end{bmatrix}, \quad B_{111}^3(6) = \frac{1}{648}\begin{bmatrix} -5 & 7 & 4 & -4 & -7 & 5 \\ -5 & 7 & 4 & -4 & -7 & 5 \\ -5 & 7 & 4 & -4 & -7 & 5 \\ -5 & 7 & 4 & -4 & -7 & 5 \\ -5 & 7 & 4 & -4 & -7 & 5 \\ -5 & 7 & 4 & -4 & -7 & 5 \end{bmatrix},$$

$$B_{112}^3(6) = \frac{1}{1960}\begin{bmatrix} -25 & 5 & 20 & 20 & 5 & -25 \\ -15 & 3 & 12 & 12 & 3 & -15 \\ -5 & 1 & 4 & 4 & 1 & -5 \\ 5 & -1 & -4 & -4 & -1 & 5 \\ 15 & -3 & -12 & -12 & -3 & 15 \\ 25 & -5 & -20 & -20 & -5 & 25 \end{bmatrix}, \quad B_2^3(6) = \left[B_1^3(6)\right]^T, \quad B_{222}^3(6) = \left[B_{111}^3(6)\right]^T,$$

$$\text{and } B_{221}^3(6) = \left[B_{112}^3(6)\right]^T. \tag{A3.4.3}$$

(4) 7 x 7 neighborhood:

$$B_1^3(7) = \frac{1}{1764} \begin{bmatrix} 67 & -37 & -43 & 0 & 43 & 37 & -67 \\ 22 & -67 & -58 & 0 & 58 & 67 & -22 \\ -5 & -85 & -67 & 0 & 67 & 85 & 5 \\ -14 & -91 & -70 & 0 & 70 & 91 & 14 \\ -5 & -85 & -67 & 0 & 67 & 85 & 5 \\ 22 & -67 & -58 & 0 & 58 & 67 & -22 \\ 67 & -37 & -43 & 0 & 43 & 37 & -67 \end{bmatrix}, B_{111}^3(7) = \frac{1}{252} \begin{bmatrix} -1 & 1 & 1 & 0 & -1 & -1 & 1 \\ -1 & 1 & 1 & 0 & -1 & -1 & 1 \\ -1 & 1 & 1 & 0 & -1 & -1 & 1 \\ -1 & 1 & 1 & 0 & -1 & -1 & 1 \\ -1 & 1 & 1 & 0 & -1 & -1 & 1 \\ -1 & 1 & 1 & 0 & -1 & -1 & 1 \\ -1 & 1 & 1 & 0 & -1 & -1 & 1 \end{bmatrix},$$

$$B_{112}^3(7) = \frac{1}{2352} \begin{bmatrix} -15 & 0 & 9 & 12 & 9 & 0 & -15 \\ -10 & 0 & 6 & 8 & 6 & 0 & -10 \\ -5 & 0 & 3 & 4 & 3 & 0 & -5 \\ 0 & 0 & 0 & 0 & 0 & 0 & 0 \\ 5 & 0 & -3 & -4 & -3 & 0 & 5 \\ 10 & 0 & -6 & -8 & -6 & 0 & 10 \\ 15 & 0 & -9 & -12 & -9 & 0 & 15 \end{bmatrix}, \quad B_2^3(7) = \left[B_1^3(7)\right]^T, \quad B_{22}^3(7) = \left[B_{111}^3(7)\right]^T,$$

$$\text{and } B_{221}^3(7) = \left[B_{112}^3(7)\right]^T. \tag{A3.4.4}$$

(5) 8 x 8 neighborhood:

$$B_1^3(8) = \frac{1}{44352} \begin{bmatrix} 1253 & -400 & -758 & -339 & 339 & 758 & 400 & -1253 \\ 560 & -895 & -1055 & -438 & 438 & 1055 & 895 & -560 \\ 98 & -1225 & -1253 & -504 & 504 & 1253 & 1225 & -98 \\ -133 & -1390 & -1352 & -537 & 537 & 1352 & 1390 & 133 \\ -133 & -1390 & -1352 & -537 & 537 & 1352 & 1390 & 133 \\ 98 & -1225 & -1253 & -504 & 504 & 1253 & 1225 & -98 \\ 560 & -895 & -1055 & -438 & 438 & 1055 & 895 & -560 \\ 1253 & -400 & -758 & -339 & 339 & 758 & 400 & -1253 \end{bmatrix},$$

$$B_{111}^3(8) = \frac{1}{3168} \begin{bmatrix} -7 & 5 & 7 & 3 & -3 & -7 & -5 & 7 \\ -7 & 5 & 7 & 3 & -3 & -7 & -5 & 7 \\ -7 & 5 & 7 & 3 & -3 & -7 & -5 & 7 \\ -7 & 5 & 7 & 3 & -3 & -7 & -5 & 7 \\ -7 & 5 & 7 & 3 & -3 & -7 & -5 & 7 \\ -7 & 5 & 7 & 3 & -3 & -7 & -5 & 7 \\ -7 & 5 & 7 & 3 & -3 & -7 & -5 & 7 \\ -7 & 5 & 7 & 3 & -3 & -7 & -5 & 7 \end{bmatrix},$$

$$B_{112}^3(8) = \frac{1}{14112} \begin{bmatrix} -49 & -7 & 21 & 35 & 35 & 21 & -7 & -49 \\ -35 & -5 & 15 & 25 & 25 & 15 & -5 & -35 \\ -21 & -3 & 9 & 15 & 15 & 9 & -3 & -21 \\ -7 & -1 & 3 & 5 & 5 & 3 & -1 & -7 \\ 7 & 1 & -3 & -5 & -5 & -3 & 1 & 7 \\ 21 & 3 & -9 & -15 & -15 & -9 & 3 & 21 \\ 35 & 5 & -15 & -25 & -25 & -15 & 5 & 35 \\ 49 & 7 & -21 & -35 & -35 & -21 & 7 & 49 \end{bmatrix},$$

$$B_2^3(8) = \left[B_1^3(8) \right]^T, \ B_{222}^3(8) = \left[B_{111}^3(8) \right]^T, \ \text{and} \ B_{221}^3(8) = \left[B_{112}^3(8) \right]^T. \tag{A3.4.5}$$

DETECTION OF EARLY BREAST CANCER: AN OVERVIEW AND FUTURE PROSPECTS

Authors: **Xiaohua Zhou**
Department of Electrical Engineering
University of Manitoba
Winnipeg, Manitoba, Canada

Richard Gordon
Departments of Botany and Radiology
University of Manitoba
Winnipeg, Manitoba, Canada

Referee: Atam P. Dhawan
Department of Electrical Engineering
University of Cincinnati
Cincinnati, Ohio

I. INTRODUCTION

The medical profession and the general public are justly concerned with the epidemic of breast cancer.[60,120,209,249,343,447,461,474] It is our purpose here to review the magnitude of the problem, the efficacy of current methods of detection, and the potential for detection of earlier carcinomas.

Approximately 1 in 12 Canadian women will develop breast cancer in the course of their lifetimes.[96] Every year some 9000 Canadian women develop breast cancer (about 74 per 100,000).[96] Although curable, particularly when detected at early stages, breast cancer kills 4300 Canadian women per year (about 33 per 100,000)[431] and is the major cause of cancer deaths among women. Because it tends to occur earlier in life than other cancers, and earlier than other major causes of death, such as cardiovascular disease, breast cancer has been shown to be the greatest cause of years of life lost by Canadian women.[96] In many Western countries the yearly incidence is between 75 and 95 cases per 100,000 women and increasing.[505] It is one of the leading causes of death in women 30 years old or older.[505] The average duration of life with untreated breast cancer is about 3 years, with a survival rate of about 40% at 3 years and 18 to 20% at 5 years.[247] The age-adjusted mortality for breast cancer in 1984 was about 28 per 100,000 population in the U.S.[545] Breast cancer is 100 times more frequent among women than among men.[130,319,610]

Long before a breast carcinoma can be detected by present technology, metastastic spread may occur, and does indeed in most cases.[247] It is also well known that detection of breast cancer at the time of no nodal involvement, when it is presumably clinically localized, carries with it an 85% 5-year survival. When nodes are involved, the figure drops to 53%, or even lower when two or three nodes show metastases.[125] Perhaps the reason for this poor showing is that in more than 90% of all breast cancer cases, the women have, as a first step, discovered symptoms or signs of breast cancer themselves and then sooner or later referred themselves to a physician.[125] However, our research interest is in the detection of very early breast cancer so we will not emphasize physical examination and breast self-examination (BSE), which detect mostly later cancers, except to review recent studies that indicate that these procedures could clearly be improved, and that their effectiveness in detection of small breast cancers could be substantially better than has been assumed.[288]

We will briefly overview such issues as understanding of breast cancer, its incidence, the

mortality and survival of patients with breast cancer, and screening programs for breast cancer. This article discusses the developments in mammography and other breast imaging modalities over the last several years. Prospects for digital mammography, image processing techniques, and three-dimensional digital subtraction mammography are also considered.

II. BREAST CANCER AND SCREENING PROGRAMS

A. ON THE UNDERSTANDING OF BREAST CANCER

Interest in cancer of the breast has begun to yield specific information as to its basic nature, dietary influences, and its hormonal and genetic determinants.[153,248] The advent of improved early detection and diagnosis has allowed the presentation to the clinician of a more favorable aspect of tumors than previously and has altered the overall clinical approach to the treatment of the disease.[163] The rewards of early diagnosis include the possibility of functional breast reconstruction, which may alter the patient's attitude to the therapy or treatment.[459]

At present there is no way of detecting *in vivo* the precise time that one or a few epithelial cells of the mammary parenchyma become neoplastic; the time of inception is, therefore, an estimated value.[363] Estimation of the growth rate has been derived from a determination of the "doubling time," i.e., the time required for a tumor to double its diameter (an eightfold increase in mass if no necrosis occurs) during a known period of time. Data obtained by this method indicate that doubling times of breast carcinomas vary extensively from one tumor to another and, in some instances, are very long.[247,342,349,546] The reported "doubling times" range from 1.2 to 900 d, depending on the locations of measured lesions.[247] Buchanan et al.[92] gave a review of cancer growth kinetics, and discussed the problem of how tumor growth rates and doubling times affect mammographic lesion detection. Apparently no one has yet taken into account this three order of magnitude range of doubling times in planning the time interval between breast examinations.

Studies using both physical examination and mammography indicate that if mammography was not performed and patients were screened by physical examination alone, most tumors would metastasize before they reach a palpable size.[186] For carcinomas less than 2 cm, only 13% metastasized to axillary nodes and only 40% were detected by physical examination. Above that size threshold, the percentage of axillary nodal involvement increased substantially. Detection rates of physical examination did not approach those of mammography until breast carcinomas had reached a size of 2 to 3 cm, but by that time 65% had spread to regional nodes. It has been suggested that when breast carcinoma is first detected by any means now available, metastastic spread has already occurred; therefore, clinically detectable breast cancer is not localized disease.[247] This conclusion is supported by the results of long-term follow-ups of breast cancer patients.[81] A major task is thus to characterize the preclinical phase of breast cancer, in particular to predict which lesion, morphologically definable only as hyperplastic, already has the potential for unrestrained growth and metastasis. It has been demonstrated that benign epithelium is transformed through hyperplasia into an *in situ* form of cancer, followed by eventual invasion into the periductal tissue.[212,213] Evidence from Gullino[247] suggests that progression from hyperplasia to neoplasia can be evaluated by determining whether the mammary tissue has acquired the capacity to induce the formation of new blood vessels in the host tissue. The present knowledge of the mechanism of metastasis suggests that a primary breast carcinoma can metastasize when it consists of a relatively small number of cells that is far below our present capacity of detection.[247] Two conclusions can be drawn from the mechanisms of breast carcinoma metastasis: the primary carcinoma may be a continuous source of neoplastic cells that spread through hematic and lymphatic vessels,[15] and manipulation of breast carcinomas may produce extensive transfer of neoplastic cells into the circulation.[193,478] Early detection and removal of the primary tumor is thus

essential, and may be effective, since generally only a few of the cells that depart a primary tumor succeed in forming a secondary tumor.[562] Hopefully, perhaps, the smallest primary tumors will have low metastasis rates. Our general inability to detect these small tumors now is a motivating factor for finding improved imaging and image processing/analysis methods.

In its earlier phases, the behavior of breast carcinoma follows a predictable sequence.[211] Once invasive growth has become established, however, behavior becomes more random. There may be secondary mass formation, intramammary lymphatic spread, extension to local structures, metastasis to regional lymph nodes, or systemic dissemination. An obvious corollary to this model of its natural history is that there exists a stage in the development of breast carcinoma in which invasion is either nonexistent or of near-microscopic dimension, and that in this stage, simple methods of treatment might be expected to provide control or even cure.[211] It was to characterize this stage that the concept of *minimal breast cancer* was proposed.[207,212,213] The term was defined histopathologically as including noninvasive carcinoma, either ductal or lobular, and invasive carcinoma having a volume no greater than that of a sphere 0.5 cm in diameter.[211] This is in contradistinction to the definition used by the Breast Cancer Detection Demonstration Projects (BCDDP), which defined a minimal cancer as one that was 1.0 cm or less in diameter.[61] The volume of a 1.0-cm mass is eight times than that of a 0.5 cm mass, and the number of patients with the larger mass who have positive axillary lymph nodes will be significantly higher.[373] The term minimal breast cancer was specifically chosen to distinguish this pathologically defined group of lesions from *early* breast cancer and *occult* breast cancer.[207] As Gallager[210] indicated, "early breast cancer, while vaguely defined, is usually understood to mean carcinoma without axillary or other metastases. Occult breast carcinoma means asymptomatic, nonpalpable breast carcinoma, detectable only by mammography. Most minimal breast cancers are both early and occult, but not all. A small percentage metastasize to axillary nodes. A few are palpable by virtue of superficial location or produce symptoms such as nipple discharge." The cure rate for intraductal or *in situ* breast lesions of 0.5 cm or less in diameter should approach 100%, assuming that the lesions are properly treated.[208] At the least, the disease-free survival rate for all evaluable patients (average follow-up of 5.3 years) was 96.8%.[211] Biopsy of such minimal breast lesions presents a challenge to the radiologist, surgeon, and pathologist to ensure that (1) the lesion is contained in the biopsy specimen, and (2) excessive breast tissue is not removed causing either unnecessary surgical deformity or difficult microscopic examination.[185] Computer-aided biopsy or even surgery may someday solve these problems.

Some evidence suggests that minimal breast cancer represents an indolent form of carcinoma and never becomes life-threatening,[68,412,445,479] though it would seem that all breast cancers must pass through a stage in which they would have been labeled as minimal breast cancer were they detected. Despite advances in mammography and mammographic screening programs, detection of minimal breast cancer remains largely a matter of chance. Most are found as a result of biopsy of some vaguely palpable abnormality that may or may not be related to the malignant process. Mammography clearly is capable of detecting some cases through indirect signs, particularly the presence of characteristic calcifications.[451,521] As methods of detection improve, it is to be expected that there will be further accumulation of experience with minimal breast cancer and that some reasonable answer to the treatment question can be supplied.

There are documented large variations in incidence of breast cancer in different ethnic and culturally and geographically diverse groups.[64,153,248] Diet is a common factor in these studies and is assuming an increasingly dominant role.[407] For example, in nonmalignant forms of breast disease and, particularly, the painful variant of chronic cystic mastopathy, the role of substances such as caffeine, chocolates, and hormonally rich cheeses is significant in pathogenesis.[620] Impressive data also show that fat and dairy products, in particular, are

closely related to the prevalence of important cocarcinogens under certain circumstances.[214] Indeed, simple obesity is an important determinant, not only of the development of breast cancer, but also for the likelihood of recurrence.[554] Gray et al.[242] demonstrated that breast cancer mortality rates are highly correlated with per capita consumption of fat ($r = 0.93$) and animal protein ($r = 0.85$). Similarly, Hirayama[286] also found that breast cancer mortality rates, in various regions of Japan, were highly correlated with fat consumption. Direct investigation of the association between nutrition and breast cancer is difficult because of problems in dietary methodology. Nevertheless, the results of a Canadian case-control study provide support to the importance of high fat intake.[402] Evidence has also shown that breast cancer mortality is associated with insufficient dietary selenium, a fat-enriched diet, and inadequate exposure to sunlight.[194] Further studies of this question are undoubtedly required, however, before specific recommendations on dietary modifications can be made.

The question whether certain groups of persons are at higher risk for the development of breast cancer has been answered adequately to some extent. Indeed, this has already been the subject of discussion from the point of view of the epidemiologist, looking at large segments of the population. Such factors as age and sex are so obvious as to be intuitive, i.e., women are at higher risk than men, and older women are at higher risk than younger women.[500] However, it might be essential to differentiate what might be considered as risks that are significant enough to influence the practice of medicine, from those factors that, although perhaps statistically important when dealing with large populations, are not enough to cause physicians to alter the advice they give patients about intervals between examinations, the need for mammograms, and so on. It is possible, therefore, to divide the various known risk factors into two groups: (1) those that might be regarded as major factors, and that, when identified, should affect follow-up and treatment; and (2) those minor factors that, although interesting and epidemiologically significant, do not carry enough risk to remand their bearers into a different follow-up category than otherwise "normal" women. Until such time as breast cancer may be prevented, the clinical efforts must be directed toward earlier detection. Women who fall into any of what have been labeled the major risk groups should, therefore, be so appraised of their status and their follow-up care.[500]

It is well established that a family history of breast cancer is an important determinant of breast cancer risk. Women who have an affected first-degree relative have, on an average, a two- to threefold increased risk of the disease.[16,36,321] Although it is not clear as to what extent this higher risk is attributable to genetic and/or environmental factors, exceptionally high incidences of breast cancer in certain families support the hypothesis of a genetic component in some families.[15,65] A recent report, however, did not find higher risks for relatives of premenopausal patients than for relatives of postmenopausal patients when the breast cancer was unilateral.[442] The familial history is also most helpful in decision-making regarding nonmalignant disease, and especially useful in helping a woman to assess honestly the likelihood of developing breast cancer.[14]

The reported associations with reproductive characteristics are of particular interest, as they imply a hormonal etiology for breast cancer.[25,126,456] Miller[398] made a comprehensive review of both the role of exogenous estrogens and the role of diet in the epidemiology of breast cancer. While nulliparous women have an approximately 50% greater risk of developing breast cancer than parous women,[82,321,443] the age at first birth is a more important determinant of breast cancer risk. In general, the younger a woman is at the time of her first birth, the lower is her risk.[37,83,95,277,403] While most researchers have concluded that the age at first birth fully explains the inverse association between high parity and breast cancer,[82,95,297,321,403,443] others have found that high parity exerts a protective effect, independent of that of age at first birth.[5,83,277] Therefore, the question of whether high parity independently reduces the risk of breast cancer has not been resolved. Although breast feeding was once thought to protect against breast cancer, a large number of studies have shown that this

association is no longer so apparent once parity or age at first birth are taken into account.[311,321,490]

Most studies show that an early age at menarche increases the risk of breast cancer.[109,45,569,598] Since the initiation of regular cycles occurs more quickly among those with an early menarche, this suggests that the early onset of ovulatory cycles may be the important factor.[26] A recent study[67] suggests that regular participation in moderate physical activity, by reducing the frequency of ovulatory cycles in adolescence, may provide an opportunity for the primary prevention of breast cancer. A late age at menopause is known to increase the risk for breast cancer.[109,443,629] It is also possible that age at menarche and age at menopause represent independent risk factors for breast cancer.[65]

It is generally accepted that relatively high doses of ionizing radiation can cause breast cancer.[345,346] Several studies revealed that women who have been exposed to high-dose radiation, say 100 rad or more, generally have a two- to fourfold increased risk of breast cancer.[78,380,515,590] According to Mole,[408] these risk estimates indicate that the female breast is more sensitive to radiation carcinogenesis than other parts of the body. The existence of low-dose risk has, however, neither been proved nor disproved. It is not known whether very low doses of radiation, such as those from current mammographic techniques, can cause breast cancer.[179] The possible existence of risk has only been inferred from the excess breast cancer incidence seen in women exposed to high dose. Unfortunately, studies on women exposed to high doses provide little or no information regarding a possible effect from low doses.[178]

Land et al.[344,345] suggested, however, that if any low-dose risk does exist, it is immeasurably small, especially when compared with the overwhelmingly large incidence of naturally occurring breast cancers. Since the mean glandular dose from a complete examination with either screen-film mammography or xeromammography is now well below 1 rad, it is considered not significant or negligible in terms of carcinogenic risk.[146,177] It was estimated that, with current low-dose technique (mean breast dose of 0.17 rad for a two-view study), a mammography examination would carry a theoretical risk of about one excess breast cancer case per year per 2 million women examined.[178] With modern low-dose mammography, even when a conservative estimate of possible reduction in mortality due to detection at an early stage is applied to the data, the estimated benefit substantially exceeds any possible hazard of low-dose radiation.[295,432] Feig[181,182] also showed that when compared in terms of years of life expectancy gained through early detection vs. years of life expectancy possibly lost from radiation, the benefits of mammographic screening appear to be considerable. "A single mammographic examination with an average dose of less than 1 rad should increase the risk of developing breast cancer by much less than 1% of the natural risk (from 7.0 to 7.07%) at age 35, and by progressively smaller percentages with increasing age".[164] No other technique, known at present, has proven to be better or equally informative for the detection of early breast cancer.[381,401] The success of mammography in the detection of and screening for breast cancer is clearly demonstrated.[292,524,582] Continuing technological improvements have thus led the American Cancer Society (ACS) to conclude that: "modern technology has reduced the radiation exposure of low-dose mammography to the point of negligible risk, if risk exists at all, and has increased its diagnostic capabilities at the same time".[289] Therefore, just as it is important to avoid needless risks, it is imperative to avoid needless cancer deaths due to delayed diagnosis and an unreasonable fear of mammography. The medical profession and the public must recognize that the proper application of mammography can save lives.[10]

Blood testing has the potential of forming a portion of a routine checkup for breast cancer, similar to the PAP test for uterine cancer.[495] More importantly, it could become an important tool for following high-risk patients, and those already treated for breast cancer. This technique relies on the as yet undemonstrated possibility that breast cancer cells have unique

surface antigens.[376] If such tumor-specific antigens are identified, monoclonal antibodies could be produced and labeled with radionuclide tracers. Administered intravenously, these labeled antibodies hopefully would have access to and adhere to breast cancer cells. With a sufficient concentration of radionuclei and sensitive imaging systems, detection of small lesions at an early stage may be a possibility. Numerous investigators have reported the existence of human mammary tumor-associated antigens.[293,512,623] Studies on breast cancer imaging with monoclonal antibodies have also been reported.[324,486]

While progress continues to be made in providing leads to various factors associated with the development of breast cancer, its biological complexities are still not fully understood, nor has any one factor or group of variables been identified that explains or predicts more than a minority of the cases of this disease.[498,506] Most of the risk factors do not readily lead to the implementation of preventive methods. However, current and future research in such areas as diet, physical exercise, and hormones may help find preventable causes, or at the least lead to a better understanding of the pathogenesis of breast cancer.[322]

It should be emphasized that mammography or any other clinical imaging modality is not an independent procedure.[290,434] It is part of the total evaluation of the patient, which includes clinical information, physical findings, and possibly laboratory data. The collaboration of patient, clinician, surgeon, radiologist, pathologist, and oncologist has been one of the intellectually and professionally rewarding aspects of mammography. This on-going experience can materially improve confidence, competence, and accuracy of the diagnosis. It can also result in a sharing of responsibility in the management of the individual patient.

B. INCIDENCE, MORTALITY, AND SURVIVAL OF PATIENTS WITH BREAST CANCER

With the exception of skin cancer, the breast is the most common site of cancer among American women. According to the U.S. National Cancer Institute (NCI) Surveillance, Epidemiology, and End Results Program, which covers slightly more than 10% of the U.S. population, the average annual age-adjusted incidence rate for breast cancer was 85 per 100,000 women for the years 1977 to 1979.[505] Combining the incidence figures for both men and women, only lung cancer and colon-rectum cancer accounted for more new cases in 1984 to 1987 than were seen in that period for female breast cancer alone.[542-545] Theoretically, the incidence of cancer connotes the number of cases that originate during a given period of time (annually, most often), but as a matter of practicality it is usually defined as the number of cases first diagnosed during the period. However, the number of women who are diagnosed at any point in time as having a disease is dependent on several factors. Among them are the technologies available for detection and diagnosis, the number of cases already in a detectable state, and the number of persons presenting themselves for examination. Data relevant to these considerations have been reported from the BCDDP.[40]

The probabilities of a newly born girl developing invasive cancer of various sites at some point during her lifetime have been computed.[505,507] For breast cancer, the probability was calculated to be 9.1%: about 1 out of every 11 women will develop this disease during her life. The number of breast cancer cases occurring annually in any age group depends on the number of persons at risk and the annual rate of developing this disease.[545]

In the U.S. and other Western countries, incidence rates increase rapidly with age until the menopausal period (45 to 55), during which they tend to level off, and after which they increase at a slower rate.[505] However, the number of women at risk, relative to the total number of women in the same age group, falls off at older ages.[505] The difference in the patterns of pre- and postmenopausal incidence rates tends to lend support to the hypothesis that these are two distinct diseases. This hypothesis of two etiologic types is still being debated.[17,135,368,369,410] Premenopausal breast cancer may have more familial determinants, whereas postmenopausal breast cancer may be more influenced by environmental conditions.

Such differences have led epidemiologists to try to identify the various environmental conditions responsible for the development of breast cancer.[402]

Of interest are the worldwide distributions of breast cancer incidence and the patterns of changes in these rates. Generally, incidence rates tend to be low in most Asian and developing countries, intermediate in southern European countries, and high in North America, Scandinavian countries, and other Westernized areas.[477] Studies of Japanese and Chinese migrants to the U.S. provide further evidence that environmental influences, such as an Americanized diet, rather than genetic factors, may explain the internationally variations in breast cancer distribution.[93,327,356] Similar conclusions were also arrived at by other investigators.[396] De Waard et al.[137] also found that in the Netherlands and Japan, the incidence rates tended to plateau or decline after age 50 to 55 among lighter weight women but increased with age among heavier women. Differences in body mass, and perhaps breast mass in particular, may account for some of these international variations in breast cancer rates.

As Seidman and Mushinski[505] indicated, overall breast cancer incidence rates are higher in whites than in blacks in the U.S. However, incidence rates have increased somewhat in both black and white women in recent years, although the change is more pronounced among blacks. This gap is thus narrowing. Perhaps the greater incidence is the result of an improved standard of living that has led either to real increases in the disease or to better detection and reporting, or both. This issue is still under investigation.

In the U.S., women in urban areas are more likely to be affected than are those in rural areas, although this differential has been decreasing over time.[77,392] Women with higher income and higher educational level are more likely to be affected with breast cancer than are women in lower categories.[133] There is also concern that recent reproductive trends, specifically the decrease in fertility rates and the postponement of childbearing until after the age of 30, may result in even higher rates, since nulliparity and a late age at first birth are known to increase the risk of breast cancer.[320,599,609] Women who have never been married have a higher risk for breast cancer than those who have been married.[82,322] This effect may be due to progesterone in semen.[589] It also has been reported that nuns have an excess mortality for breast cancer, a finding that is believed to be related to their nulliparous status.[200]

Overall mortality rates have remained relatively stable for the past several decades.[27,460,505] In 1984 to 1987, breast cancer was estimated to account for 18% of all cancer deaths among women in the U.S.[542-545] For 1987, the number of estimated deaths from breast cancer was 41,300 in the U.S. Of these deaths, 41,000 were among females.[545] In general, the reported age-adjusted death rates are high in developed countries (with the notable exception of Japan) and low in the developing countries.[505]

Survival of cancer of the breast has usually been analyzed according to such cancer characteristics as extent of metastases, size of tumor, histologic type, anatomic location, and grade of malignancy.[505] The number of positive axillary nodes was found to have an important effect on survival. The clinical size of tumors also correlated well with survival. Other factors found to affect prognosis are the age and race of the patients,[65] though the factor of race may be related to less vigorous treatment of, for instance, black women on the average than white women.[390] In a study estimating the prognosis for patients with breast cancer, Bjurstam[74] concluded that about 5 to 10% of patients with tumors less than 1.5 cm in diameter would die of this disease over a 10-year period, and only half of the symptomatic patients with tumors of 2 to 3 cm would survive 10 years. This suggests the importance of diagnosis of breast cancer at an early stage before it becomes clinically manifest.

According to a 1978 national survey by the American College of Surgeons,[433] 5-year survival rates were 72.8% for localized disease and 49.1% for regional disease. According to data provided by the American Cancer Society,[545] relative 5-year survival rates have risen from 63% for white women and 46% for black women for cases diagnosed from 1960 to 1963 to 75% for white women and 62% for black women for cases diagnosed from 1977

to 1983. But these survival trends are difficult to explain because their improvement might reflect earlier diagnosis or detection of lesions of low malignancy.[65] Modest gains in survival have, nevertheless, also been reported according to clinical stage, with patients having regional and distant disease showing greater improvement in 5-year survival rates than those with localized disease.[505] Lower survival of black patients with breast cancer relative to white patients has been reported by several investigators.[476,622] Several factors have been suggested as contributing to this racial survival difference. Black patients have been diagnosed at a more advanced clinical stage.[433] Bassett and Kreiger[53] report that socioeconomic factors account in part for this racial difference. The differences in initial breast cancer treatment and their implications for survival have been investigated by McWhorter and Mayer.[390] The NCI is currently sponsoring a multicenter investigation of black/white cancer differences.[390] This will obviously contribute to further understanding of this racial difference.

The relatively stable overall mortality rates indicate that the increasing survival rates are being offset by an increasingly probability of developing breast cancer. Since prevention of breast cancer is not yet well understood, we should thus realize that there is much work ahead of us to further improve the survival rates for patients with breast cancer through early detection, diagnosis, and treatment.

C. SCREENING FOR BREAST CANCER

Screening is predicated on the assumption that with the detection of a disease in an early or asymptomatic state, the probability of cure is greater than that if the disease were permitted to progress and present with later symptoms. Screening is presumed to lead to appropriate treatment that, in turn, will lead to reduced mortality from the disease.[352] This approach is particularly appealing for cancer sites at which it is known that a high proportion of persons will eventually die of their disease. The benefits of detection of breast cancer at early stages are still in debate, but the 30-year follow-up study by Adair et al.[4] and work by others demonstrate that prognosis becomes worse with increasing tumor size and axillary lymph node involvement. Just as it does in women, detection of breast cancer at an early stage in men has been shown to improve the survival rates.[315] Other analyses also support the suggestion that detection of breast cancer at these early stages is associated with reduced mortality.[29,184,201,416,576,582,601].

There has been an improved understanding of the development and growth of very small breast cancers,[561] and the ability to define relatively fast- and relatively slow-growing breast cancers and to translate those characteristics to enhanced 5-year survival rates.[281,282] Moskowitz and Gartside[419] suggest that aggressively screening younger women, and finding and treating breast lesions while they are intraductal, *in situ*, and invasive but still smaller than 5 mm in diameter, may reduce mortality. In women 50 years of age or older, the reduction in mortality due to screening has been demonstrated as compared with control groups.[511,581,582] With the improvement of breast imaging technology, the benefit is likely to extend to women under 50 as well.[75,383,419] Studies under way in Europe[205,587] and Canada[404] should resolve this issue, and available data support the hypothesis that earlier detection can lead to a reduction in mortality at all ages.[335] Detection and treatment of breast cancer at an early stage will not only result in a reduced mortality, but also offer more women the possibility of preserving their breasts. Awareness of this by women and physicians may stimulate demand for breast cancer screening.[487]

Many organizations recommend that women regularly undergo screening for breast cancer.[274,275] In particular, the American College of Radiology (ACR), the ACS, and the NCI have been historically concerned about the seriousness of the disease and the need for more effective screening programs. The NCI has adopted a more conservative position regarding mammography than the ACS has. For asymptomatic women 50 and older, both organizations recommend annual routine screening with mammography.[10,24] For younger

women, however, the NCI would restrict mammographic screening to those at high risk, i.e., women with a personal or family history of breast cancer.[292] The ACS, on the other hand, recommends a baseline mammogram for all asymptomatic women at 35 to 40 years of age, and screenings every 1 to 2 years for asymptomatic women aged 40 to 49.[11] The ACR makes similar recommendations for the various age groups.[12] These organizations also support the recommended practices of monthly BSE and regular clinical breast examinations.

The first randomized control study to assess mammography in the periodic screening of asymptomatic women was that of the Health Insurance Plan of Greater New York (HIP). There have been at least three published reports of the progress of this trial since it began.[509-511] Beginning in 1963, enrolled women were offered annual screening by physical examination and mammography for four successive years. Evaluation after 7 years showed a 30% reduction in breast cancer mortality in the group offered screening compared with the control group, and after 14 years mortality was still reduced by 24%.[511] Survival was best for those women whose cancers had been detected by mammography alone. The 1982 HIP report claims that improvement in detection of early breast cancer among women under age 50 as well as among older women through modern mammography has been demonstrated.[511] However, mortality was not reduced among the women under the age of 50. The lack of statistical significance might also arise from the small number of women younger than 50 who participated in the study.[509]

In 1973, after the publication of the 7-year HIP results, the ACS and the NCI jointly initiated the Breast Cancer Detection Demonstration Projects.[61] Five consecutive annual screening examinations were undertaken using physical examination, thermography, and mammography. Thermography was positive in 43% of the breast cancers detected in the first two screenings, but most of these positive thermographic results were negative in the initial interpretation of the mammography and physical examination findings. In other words, thermography had a high false positive rate. Further, a large proportion of minimal cancers would have been missed if mammography had been excluded and thermography alone had been used in conjunction with the physical examination (37% in the first screening and 44% in the second screening).[61] Accordingly, thermography does not appear to be suitable as a substitute for mammography for routine screening.[61] Although the BCDDP was not a controlled study and the population was self-selected, the accumulated data showed that mammography had undergone a striking technological advance since the HIP study and had become superior to physical examination in detecting breast cancer, especially minimal breast cancer. The proportion of cancers detected by mammography alone was 42% (compared with 33% in the HIP study), while the proportion detected by physical examination alone was only 9% (compared with 44% in the HIP study). One third of all detected cancers were noninfiltrating, or infiltrating but less than 1 cm in size, and the majority were detected by mammography alone. Only 20% of all detected cancers were associated with positive axillary lymph nodes, less than half that reported for all other newly diagnosed breast cancer cases in the U.S. during the same time period.[40]

A Swedish screening study initiated in 1977 was designed as a randomized, controlled prospective investigation.[579,580] Of the enrolled women aged 40 and over, one half were offered screening at 24- to 33-month intervals by single view mammography, while the other half served as controls. After 7 years, a reduction in breast cancer mortality of 31% occurred among the screened group compared with the control group. Women under the age of 50 have so far shown no mortality reduction. The study showed that among women who were screened, the proportion of stage II and more advanced cancers was 25% lower than in the control group, while the proportion of *in situ* and stage I cancers was much higher, confirming the effectiveness of mammography in detecting cancer at an early stage.[582] Recently, Tabar et al.[583] revealed further results from the Swedish trial: "Among women over 50 years of age at entry to the study, relatively few interval cancers are seen in the first two years after

a screening test; in the third year the rate rises to nearly 50% of the comparable rate in the control group. Among women aged 40 — 49 years at entry, by contrast, the rate of interval cancers even in the first post-screening year is nearly 40% of that in the control group and in the second year nearly 70%.'' These results suggest that for women aged 40 to 49 years single-view mammography every 2 years is not a sufficiently effective screening policy, because the long interval time (2 years) permits the appearance of too many interval cancers.[583] The sensitivity of screening can be increased by using two-view mammography.[19,21,94] Tabar et al.[583] recommend that annual two-view mammography screening should be performed in women 40 to 49, and that the maximum interval between two screening examinations should not exceed 18 months. ''For women over the age of 50, screening should be performed biennially and the interval should not exceed two years; little extra benefit would be gained by screening more frequently than every two years.''[583] This is less frequent than the ACS recommendation discussed earlier. Perhaps the basic biology of tumor growth, with its wide variation in doubling times, as discussed above, should be taken into account more than mortality outcomes in setting screening intervals.

Some initial results from new mammography screening studies in Canada, Sweden, the Netherlands, and Japan have been also reported.[1,39,136,176,278,581,627,631] Further results from randomized controlled trials conducted in Canada[404,430] and the U.K.[477,587,592] are expected to be published soon.[630]

Published results from mammography screening studies confirm its effectiveness in reducing mortality from breast cancer. In a Dutch study, all female residents aged 35 and over in the city of Nijmegen were invited to participate in biennial single-view mammography screening starting in 1975. All deaths from breast cancer that occurred in the invited group between 1975 and 1982 were ascertained, and a case-control study was conducted. The relative risk of dying from breast cancer among the women who had been screened compared with those not screened was 48%, implying a reduction in breast cancer mortality of 52% in the screened population.[595] A second case-control study showed that the relative risk of dying from breast cancer among women ever screened compared with those never screened increased to 51%. A 33% mortality reduction thus has been expected in the total population with an observed attendance rate of two thirds.[597] A second Dutch study was conducted in the city of Utrecht, where all women aged 50 to 64 were invited to be screened by combined mammography and physical examination. Screening was repeated at 12-, 18-, and 24-month intervals. A case-control evaluation carried out in the same manner as in the Nijmegen project revealed a reduction in breast cancer mortality of 70% among the women who were screened.[117]

By adding the results of the BCDDP and subsequent studies in Canada and the Netherlands to the results of the HIP and Swedish trials, one can conclude that the key question concerning detection of breast cancer at an early stage has been answered clearly, unambiguously, and beyond doubt. Detection at an early stage can alter the natural course of the disease. The large-scale application of this capability can result in a marked change of the breast cancer problem.[576] For example, (1) in women over the age of 50, mortality caused by breast cancer can be lowered by more than 50% in the continually screened group as compared with the never-screened one; (2) significantly better treatment can be offered to most breast cancer patients when the patient material originates from screening; and (3) screening is highly cost-effective for society.

While the theory and techniques of mammography are well established,[149,160-162,175,262,266,287,563,578] the suitability of the method for screening is still controversial regarding its benefits vs. risk of long-term carcinogenic effects to the breast due to radiation exposure.[31-34,40,134,179-182,350] This controversy, which peaked in the late 1970s, created widespread confusion and fear among women, many of whom were the very ones who would potentially benefit the greatest from mammography. Likewise, considerable uncertainty and confusion spread among many clinicians and surgeons, particularly regarding how early, how often, and on whom mammography should be performed.[84]

The carcinogenic risk from mammography screening is hypothetical, with no basis in clinical experience. Technological advances in both screen/film mammography and xeromammography have resulted in a marked reduction in radiation dose and improved image quality since the 1960s.[51,52] For example, the mean absorbed dose for a craniocaudal view, when a KODAK® MIN-R Screen combined with a Kodak® Ortho M Film is used, is only 0.05 rad,[263] compared to 5 to 8 rad in the mid-1960s.[224] For more recent details on dose reduction see Reference 52. Given the low levels of radiation exposure from state-of-the-art mammographic equipment, the theoretical risk is quite small, especially compared with the failure to detect cancers when they are early, small, and curable.[451,465] The following is from an article by Feig[178] (cf. Reference 164).

Examination with current low dose technique (mean breast dose of 0.17 rad for a two-view study) would carry a theoretical risk of about one excess cancer case/year/2 million women examined. Assuming a 50% breast cancer mortality rate, the hypothetical risk would be one excess death/4 million women examined. This level of risk, one death/4 million women/year, is extremely small and can be equated with the following: 100 miles traveled by air, 15 miles traveled by car, smoking one-fourth of one cigarette, one-third minute of mountain climbing, and 5 minutes of being a man aged 60.[458]

Another means of appreciating the very small risk from mammography is by comparison with the natural breast cancer incidence. A risk of one excess breast cancer per 2 million women examined can be compared with the much larger magnitude of the natural breast cancer incidence: 800 cases/million women/year at age 40; 1,800 cases/million women/year at age 50; and 2500 cases/million women/year at age 65.[504]

Because only a small proportion of women are presently being screened by mammography, a relatively small number of breast carcinomas are being detected at a preclinical stage. There are substantial manpower, monetary, and technological problems associated with a large-scale screening program.[252,253,381] It has been estimated that only 5% of U.S. women over the age of 50 undergo annual mammography, and probably only about one third of eligible women have had even a single mammogram.[253] The fully implemented ACS/ACR recommendations would require yearly mammograms for almost 50% of adult women. Restraints on its optimal application to the control of breast cancer are the expense of the examination and the lack of properly trained and committed radiologists.[381] High-volume practice, i.e., examining a large number of women per day, and limiting the role of radiologist to interpretation vs. performance of the examination have been suggested as means of cost reduction for mammography.[58] As indicated by Sickles,[532] however, it would be unrealistic to expect more than half of radiologists to implement reduced-price mammography screening at this time. Among the various methods suggested to reduce screening costs might be the practice of imaging each breast with one rather than two standard projections.[359,360,580] However, as discussed above, the adequacy of this approach has been questioned by several researchers, including some who are actively involved in one-view screening programs, primarily on the grounds that no single projection will identify all mammographically detectable cancers.[19,21,353,424] After conducting a comparison of the advantages of one-view vs. two-view approaches, Sickles et al.[540] recommended that baseline mammography screening be done by using two, not one, standard views per breast. Bassett et al.[57] also concluded that single-view screening should not be performed, because the small cost saved by eliminating the second view would be more than offset by the cost of the large number of "call back" examinations. In a recent study on the impact of low-cost mammography screening on existing mammography practices, Sickles[534] concluded that the introduction of low-cost screening had no significant impact on the steadily increasing mammography case loads and did not appear to be a serious economic threat to traditional screening. Indeed, this coexistence is not just possible, it is necessary if we are to have the majority of women undergo periodic mammography screening in the future.

A relatively high degree of training and experience is necessary to obtain and interpret mammograms. If high-quality and low-cost mass screening mammography is to become a

reality it might be possible to use nonphysician radiology assistants, possibly aided by computer (see discussion below), to interpret examinations.[253] Artificial intelligence techniques have been shown to help radiologists improve their diagnostic accuracy, as well as to train nonradiologist assistants.[119] The need to train radiological technicians and other nonradiologists to scan mammograms was discussed early in 1971.[8] In a recent study, Hillman et al.[284] further concluded that appropriately trained physician assistants could interpret mammograms, that interpretations by physician assistants took less time and cost less than those by radiologists, and that the dispositions recommended by physician assistants were similar to those by radiologists. As more people per unit population enter the field of medicine, salaries may decline. If this results in more radiologists with more modest incomes, unit costs of mammography may decline. On the other hand, the potential demand for mammography may work for now toward keeping salaries up and providing an attractive niche for aspiring physicians.

Screening procedures should be sensitive, reasonably specific, safe, and inexpensive.[23,41,59,123,400] As such, they would become widely available, while screening mammography is not today. The high cost may be the single greatest deterrent to the use of screening mammography today.[71,541] The issue of cost-effectiveness of screening mammography in low-risk patients has also been discussed.[323,428,488] The immediate challenge is thus to provide the highest-quality images that are accurately interpreted at a reasonable cost.[73,148,382]

Studies of lay attitudes toward mammography suggest that the recommendation of physicians is a critical intervening factor that influences the beliefs and behavior of patients.[197] In a recent study,[365] data showed that obstetricians and gynecologists referred the largest average number of patients per physician, with more than 50% of these referrals for screening mammography, and that only one third of the patients were referred for mammography by internists. The major deterrent to referral might be the perceived high cost and low yield of screening.[56] Another may be the awareness that many radiologists do not know how effective or accurate they are with the procedure.[382] For other problems associated with large-scale screening programs, see Fox et al.,[197] Hall,[252,253] Sickles et al.,[540] and Howard.[292] All these factors suggest that the cost-effectiveness or affordability of compliance with the ACR/ACS guidelines is at least doubtful, especially for women under 50.[24,55]

Mammography has been the most controversial method for breast cancer screening, compared with breast self-examination and clinical examination.[66,84,121,122,148,413] A study of compliance with the updated ACS recommendations[197] for all three types of screening shows reasonable rates of compliance for the BSE (53 to 69%) and clinical examination (70 to 78%). In contrast, only 19% of the women between the ages of 35 and 49, and 25% of the women older than 50 reported complying with the recommendation to undergo a baseline screening mammogram. It is notable that 60% of the women younger than 50, and 51% of the women older than 50, have not obtained a baseline screening mammogram. Only 25% of the older age group reported undergoing two or more mammography examinations.[197] Furthermore, these estimates are undoubtedly inflated by the use of diagnostic mammography, since most mammograms are performed for diagnostic purposes. Thus, mammography is being performed mainly for the diagnosis of symptomatic women instead of screening of asymptomatic women. It is thus clear that mammography is being underused.[84,197,292] Nevertheless, there is some evidence in the literature that most women are well disposed toward mammographic screening.[197,303] One explanation for the underuse of mammography by physicians is that the majority of referrals appear to be made for the purpose of the diagnosis of disease.[197] Further, a variety of studies suggest that physicians regard mammography as a relatively unimportant prevention strategy, even for women age 50 and older.[292] Greater efforts must be made to educate physicians and patients regarding the value of mammography and to lowering its cost.[56,198]

One way to increase screening program effectiveness and reduce total costs is to im-

plement a selective screening program, i.e., to use present knowledge about the risk factors of breast cancer to select a group of women for screening.[250,298,494] Efforts to identify high-risk women (personal or familial history of breast cancer; previous biopsy; a nipple discharge; a palpable mass, etc.) could improve this, but many women with occult carcinomas who do not fall in the risk categories would then miss screening. Another problem is the inability to respond effectively, even if clear benefits and cost-effectiveness are demonstrated, because of the lack of competent personnel and adequate facilities to provide optimum screening mammography at low cost. Thus, it is difficult to generalize about a procedure that is so emotionally charged and so dependent on the skills of the radiologist and technologist. We must evoke reproducible standards for quality assurance and determine our results and interpretative accuracy.

There has been a remarkable improvement in the examination methods of the breast, especially for mammography, during the 1970s and 1980s and assumptions were made regarding the benefits from these improvements. Mammography alone has convincingly demonstrated its ability to lower the diagnostic threshold (i.e., to detect small cancers) substantially. However, there are various, well-known biases associated with screening (lead-time bias, length bias sampling, detection bias, etc.). This is why it is vital to perform population-based, randomized, controlled trials in order to avoid decision-making on the basis of assumed benefits.[576]

However, while of low radiation risk, mammography is certainly not flawless, Moskowitz[411] stressed the important distinction between detection and diagnosis. A system, such as mammography, with the demonstrated ability to detect occult cancer may be poor at diagnosis.[332] Mammography should be used to detect lesions, but not to decide whether a lesion is benign or not unless it is a densely calcified, involuting fibroadenoma, or a lucent lipid lesion.[330] Even in a symptomatic patient, it should be used to "screen" the rest of the symptomatic breast and the contralateral breast, but not for definitive diagnosis.[334] Thus far mammographic criteria to distinguish malignant from benign carcinomas still remain ambiguous and contradictory.[111,280,414] Scientifically derived data from better-organized screening programs are clearly needed to help set up these criteria.[339]

Furthermore, although more accurate than any other modality, including physical examination, mammography may still find only 80 to 90% of breast cancers.[40] For example, a false-negative rate of about 8 to 10% can be expected in patients in whom masses are evident in physical examination but not visible in a mammogram.[40,393] Many cancers escape detection, probably because of interference by the density of the surrounding breast tissue.[446] Practical solutions to the incompleteness of image evaluation in standard mammography are addressed by Sickles[533] and Feig.[183] Several reasons for false-negative mammograms have been discussed by Martin et al.[375] and Kalisher et al.[313]

Concern remains regarding the role of screening mammography, especially in women under 50.[35,128,157,383,417-419,611] The effectiveness of screening with mammography in reducing mortality from breast cancer in women who are 50 to 74 years old has been established in studies in the Netherlands, the U.S., and Sweden.[117,401,582,595] However, mammographic screening in women under age 50 is less clearly established. This is probably because of the lack of supporting data from controlled randomized studies and hypothetical projections of radiation risk.[418,611] The generally more dense images of their breasts[446] may also contribute to a lower detectability of tumors in mammograms of younger women. Mammography is usually not recommended for women under the age of 35 when the woman is asymptomatic.[10] There has been a decrease in mortality from breast cancer in women under 50 years old, but the reduction has not been statistically significant.[254] Eddy et al.[157] also show that healthy asymptomatic women in the age group of 40 to 49 years do not have sufficient health or economic benefit from mammography to offset the costs and risks. However, a significant volume of data suggest that radiation exposure after the age of 35 has far less potential for

inducing breast cancer than it does in younger age groups.[10] The accuracy of mammography in the detection of malignancy in patients under the age of 35 years is greater than that of physical examination, and radiographic overcalls (false-positive diagnoses) in the younger patient are only 1%.[383] Mammography must be used in symptomatic young patients.[383] It has been suggested that aggressive screening of younger women (less than 50 years at entry) at yearly intervals with mammographic and clinical examinations can most likely alter the natural history of the disease as it does in older women.[397,418,419] The strongest evidence that mammography significantly reduces breast cancer deaths in women under 50 has been recently revealed by a new analysis of a long-term U.S. study.[110] They attribute the new findings in part to longer follow-up of 742 patients for at least 18 years. Comments by Tabar et al.[584] Maher,[364] Lynch et al.,[362] Greenwald and Smart,[244] Flamm,[189] Brolin,[87] Beijerinck et al.,[62] and Eddy et al.[158] also address several concerns related to screening mammography in women under 50 years old.

Although mammography has proven to be effective in detecting early breast cancers, the history of its usage provides evidence for caution in its application as a screening technique. There will, however, never be a point in time when we know everything we should like to know about the effectiveness of any particular medical approach.[399] Decisions on policy inevitably have to be made on the basis of incomplete knowledge. Prospects for change in the use of mammography will depend on the success or failure of consensus policy-making, marketing strategies, cost reductions, risk reductions, and technological improvements in sensitivity and specificity. As Howard[292] suggests: "Interventions that involve publicity in the mass media, professional education, organizational endorsements, mass mailings, and personal contact must be evaluated in terms of outcome and process measures.[118] Just as it is necessary to test the effectiveness of mammography through experimental and quasi-experimental designs, it is also necessary to test promotional strategies through systematic research." All these problems are, therefore, challenges to radiology that must be addressed.

D. BREAST SELF-EXAMINATION

Since more than 90% of breast cancer is now first detected by the women themselves, indoctrination into BSE is vital as a first step in screening.[573] Although many investigators[187,195,296] have found a positive association between BSE and detection of breast cancer at early stages, controversies still exist about this procedure.[440,593] There are also no widely accepted standards for the BSE practice.[317,318,453]

Like mammography, however, BSE (and clinical examination) have also been underused, although to different extents. Few women practice BSE on a monthly basis, as recommended, although it has long been promoted as a useful procedure in screening. Estimates of monthly practice range from 18 to 41%.[13,63,296,316,513] Of all the factors that affect women's participation in screening programs, the psychosocial characteristics of women in relation to their reactions to these programs, either mammography, clinical examination, or BSE, is a major one.[38,245] Many mass media programs have been conducted in an effort to encourage women to practice BSE, and these and the mass media themselves seem to have made women aware of BSE.[316] In a study of the efficacy of BSE in the discovery of breast cancer, it has been shown that 23% occurred in premenopausal, 72% in the postmenopausal, and 5% in perimenopausal women, and that 47% of these women never performed BSE, suggesting that educational efforts might be applied first to the postmenopausal group.[288]

Personnel involved in BSE education must deal with three challenges: (1) persuading women to perform BSE for the first time, (2) getting women to perform BSE on a regular basis, and (3) ensuring the correctness of BSE practice.[316] Dorsay et al.[154] conclude that competent BSE can be learned from a 1.5-h session class. It has been shown that the accidental discovery of a symptom leads to the detection of breast cancer tumors that are 2 cm in

diameter or more, but a systematic BSE month after month discovers symptoms of tumors that are only 0.5 to 1 cm in diameter,[215] which is an improvement in volume resolution of 8 to 64 times. Spence[559] specifically suggested that BSE should be performed every month from puberty through old age. The best time is 7 to 10 days after a menstrual period, when the breasts are least likely to be swollen or tender. After menopause or following a hysterectomy, it is a good idea to use BSE the first day of every calendar month. For more details of the BSE procedure see Spence[559] and Egan.[164]

Breast self-examination as such is only a temporary activity by women, who have somehow been motivated to inspect and palpate their breasts. The performance of BSE is not automatically integrated in any wide context, and it includes no referral system in the case of occurrence of breast cancer symptoms. To be successful, therefore, BSE must be properly taught, used, and reinforced by health professionals.[370] A comprehensive BSE-containing screening program, called the Mama Program, has been conducted in Finland (see Reference 215), which consists of (1) an initial teaching procedure, (2) a surveillance system with the use of personal calendars during the continuous program, and (3) a self-referral system to prompt mammography examination if symptoms of breast cancer are detected by the women themselves. Breast self-examination, the patient's part in the total health care, must be integrated with routine physical examination and mammography.[288] This is because studies on mortality reduction by screening show that screening by physical examination alone could reduce breast cancer mortality by 18%, that combined screening by both physical examination and mammography could reduce breast cancer mortality by 56%,[196] and that the combination of mammography and physical examination may be the most effective method of screening for breast cancer today.[352]

In screening for breast cancer where mammography examination constitutes the screening test, asymptomatic women are examined at certain intervals. Tumors down to 0.1 cm in diameter may sometimes be detected, but because of the high cost only limited groups of women in the world can be involved. In the Finnish Mama program the screening test is, however, not a single procedure at a given date, but constitutes a continuous, multicomponent program containing BSE on a monthly basis year after year. The Finnish Mama program also includes a massive referral system. Women in the program have been able to detect tumors of 1 cm in diameter, and the program can be applied in large populations in developed and developing countries without requiring a substantial increase in health care resources, provided there is a health care system with adequate diagnosis and treatment resources. The Finnish Mama program has been referred to by experts of the World Health Organization Cancer Unit in Geneva as a new sort of screening test (see Reference 215).

The competency of BSE performance is still a major issue in research on BSE efficacy. Self-reporting practice has been found not adequate as an indicator of the quality of BSE performed and it has been suggested that it not be used by itself to evaluate BSE effectiveness.[154] Reliable methods for measuring all components of BSE should continue to be developed. The development of a nonverbal method for testing two palpation skills has been one of these efforts.[294]

III. MAMMOGRAPHY

A. BRIEF HISTORICAL REVIEW

In 1913 Salomon used X-rays to image his gross mastectomy specimens.[489] But it was not until 1930 that Warren[602] reported the successful performance of mammography on patients. Contemporaries of Warren were discouraged by the unpredictable quality of mammograms. Except for a few centers, the use of mammography continued to be hindered by the lack of a reproducible method of obtaining good images.[224]

In 1960, following extensive experiments with various X-ray techniques, Egan reported

on the development of a high-milliamperage/low-kilovoltage method that resulted in dependable diagnostic quality mammographic images on industrial X-ray film.[159] By 1965, Clark, aided by a nationally funded demonstration project involving radiologists throughout the U.S., verified that the Egan technique for creating diagnostic mammographic images was sound.[112] Thus the foundations were laid for mammography becoming a routine radiographic procedure for breast evaluation.

Another breakthrough in mammography occurred in the mid-1960s when Gros[246] introduced two innovations in mammographic technology: a molybdenum target, in place of tungsten, heightened the contrast between water, fat, and calcific densities, while a built-in compression device diminished scattered radiation, motion artifacts, and separated breast structures. However, the improved image quality was accompanied by an increase in surface exposure (8 rad) compared with the Egan's technique (4 rad). In 1969, a dedicated mammographic unit became available,[217] which included a molybdenum target tube and a filter based on the emission spectrum of molybdenum.

Until 1972, mammography of acceptable quality required industrial film, and manual or slow, mechanical processing. In 1972, the DuPont Company, stimulated by the investigation of Ostrum,[441] marketed a high-definition intensifying screen combined with single-emulsion film, held in intimate contact by a vacuum, and revolutionized mammography by permitting rapid automatic processing, shorter exposures with diminished motion unsharpness, and greatly reduced surface exposure.[608] Favorable clinical results using this method were described at the Radiological Society of North America meeting in 1972.[441] Additional screen-film systems were subsequently developed by Eastman Kodak and Agfa-Gaevert.[99,548] Among those currently in wide use are the DuPont® calcium tungstate Lo-dose II film-screen system, and the Eastman Kodak® rare-earth Min-R and NMB film-screen system.[357]

The introduction of xeromammography in 1972, on the other hand, provided an alternate breast imaging method.[372,614,617] A xeromammogram is an X-ray image of the breast produced by a photoelectric process, in contrast to the photographic process used to produce a screen-film mammogram. Xeromammograms have two unique characteristics that improve the visualization of breast pathology: wide recording latitude and edge enhancement. Wolfe[616] proposed the following advantages of xeromammography over conventional mammography: easier interpretation, more information through clear recording of a whole breast on one image, and an easier and quicker developing process. The performances of xeromammography and screen-film mammography have been systematically compared with each other.[520] However, the dose of xeromammography is about five times higher than that of screen-film mammography for diagnostically equivalent images,[426] and Martin[372] notes that xeromammography has a lower spatial resolution. While clinical investigations have failed to reveal a significant difference in accuracy between screen-film mammography performed with dedicated equipment and xeromammography,[444] screen-film mammography currently requires considerably less radiation than xeromammography for the same two-view examination. For example, the mean glandular dose is 0.1 to 0.2 rad for screen-film mammography vs. 0.5 to 0.8 rad for positive-mode xeromammography and 0.3 to 0.5 rad for negative-mode xeromammography.[255,426,567] The aluminum filtration and negative mode processing that are used to reduce surface exposure to more acceptable levels in xeromammography somewhat degrade the exquisite detail characterizing the images.[521]

Since the introduction of mammography in the early 1960s, remarkable advances have led to a striking improvement in image quality and reduction in radiation dose.[129,165,224,225] While initially xeromammography yielded images with higher contrast, compared with mammograms produced on industrial X-ray film, and a clearer depiction of calcifications and margins of masses,[199,272,449,616,624] dedicated X-ray units and new film-screen combinations have been developed for standard mammography to yield better images at considerably lower radiation doses than ever before.[51,52,357,463,483] Screen-film mammograms can

be obtained today using dedicated mammographic X-ray units at radiation dose levels of at least ten times lower than the dose levels of the direct-exposure film methods that were used a few years ago.[263]

B. STATE OF THE ART

Special imaging problems arise in mammography[159] since the imaging conditions are unique. The differences in attenuation of the various soft tissue structures in the female breast are small, and it is necessary to use X-rays with low photon energy in order to get a sufficiently high contrast in the mammographic film.[435] Film-screen mammography is a well-established low-dose technique (at the cost of some blurring, especially compared with xeromammography) for detection of breast cancer.[357,577] Nevertheless, while xeromammography improves the contrast at the cost of high radiation dose, mammographic technique has been under continuous development, and extensive studies of the choice of screen-film combination, spatial resolution, and contrast exist.[265,435,531] It also has been emphasized that radiologists must search not only for the classic mammographic features of malignancy, say microcalcifications,[167] but also for more subtle and "indirect" signs in predicting the presence of developing breast cancer in order to make a better judgment/diagnosis.[414,526,528] This is simply because benign and malignant nonpalpable abnormalities at these early stages may have similar radiographic appearance.[280]

The factors that may affect the quality of any radiographic image include the composition of the target of the X-ray tube, the size and shape of the focal spot on the target, the distance of the focal spot from the object, and the distance of the object from the recording medium. Also of importance is the composition of the object being imaged, the characteristics of the recording system, as well as the darkroom and film developing technique employed.[20] Since contrast between the soft tissues of the breast is inherently low and because relatively minor changes in mammary structure can signify the presence of a malignant breast tumor, the margin for error is more critical in mammography than in most other forms of radiography. There have been a few studies on image quality attainable in mammography[85,162,268,423,426,466,566] and new photographic techniques have been tried to obtain images at low dose. Some of them are reproduction on reversal film,[156] multiple-film techniques,[405] negative mode xeromammography,[91] autoradiographic enhancement,[30] stationary focused grid,[131] moving grid,[535] and magnification mammography.[28,150,388,425,517,518,529,536,575] Radiation dose requirements by these techniques vary considerably, and the tradeoffs between dose and image quality have been discussed by many investigators.[265,387,426]

During the past few years, considerable emphasis has been placed on better understanding of the mammographic imaging process and on radiation dose reduction. More accurate methods of measuring radiation exposure in the energy range of mammography, and more relevant calculations of radiation dose to the breast tissue that is at risk, have been realized.[262,263,265,547] Studying the dependence of absorbed dose on radiographic modality, radiographic technique, and breast thickness, Skubic and Fatouros[547] revealed the following results. (1) Breast thickness and incident half-value layer (HVL) of the incident beam are sufficient to characterize the normalized breast dose (average glandular dose per incident roentgen). (2) The average breast dose depends on both beam HVL and kVp; the dependence on breast thickness is more pronounced for screen-film mammography, indicating the need for firm compression. (3) Screen-film mammography shows substantial dose savings over xeromammography for thinner breasts imaged without a grid; this dose advantage disappears for thicker breasts and is generally reversed when a grid is used. However, it should be noted that Skubic and Fatouros' work had concentrated on the dosimetric aspects of mammographic imaging. Equally important is the effect of the X-ray technique on image quality. The relationship between absorbed dose and image quality should be further investigated.[423,466] Evaluating mammography techniques using breast phantoms has been reported.[9,166,565]

Many of the technical changes that occurred in mammography during the last decade are directly related to the development of screen-film systems.[149] The new dedicated units for screen-film mammography have smaller focal spots, longer (and fixed) source-to-image distance to reduce geometric unsharpness, more effective compression devices to eliminate motion and to separate mammary structures, moving grids to reduce scattered radiation, automatic exposure control for more consistent quality, configurations that promote easy and rapid positioning by permitting the patient to stand during exposures, and an alternate even smaller focal spot for the production of magnified images.[225,226,263-265,387-389,438,531] The fact that screen-film mammography is growing rapidly[357,568,577] may be due in part to (1) public awareness of breast cancer and the importance of detection at an early stage; (2) recently revised recommendations of the ACS; (3) interest in the results of the mammography screening studies in Sweden, the U.S., Canada, and Netherlands; and (4) improved mammographic imaging at significantly lower radiation dose.

For screen-film mammography, it has been recommended that overhead tungsten target tubes, such as used for conventional screen-film radiography, not be used because the subject contrast is too low.[264] Only the dedicated X-ray units with either a molybdenum target tube and a molybdenum filter or a specially designed tungsten target tube with a beryllium window are recommended.[265] (Subject contrast is defined as the ratio of the X-ray intensity transmitted through one part of the breast to the intensity transmitted through a more absorbing adjacent part,[265] although other definitions, say Dhawan et al.'s,[142] may be more appropriate.) The shape of the focal spot has an impact on its imaging performance, and the focal spot shape is furthermore a function of the filament shape and position.[406] X-ray tubes for mammography usually use cathodes that follow the traditional design of a helical coil filament. As Gold et al.[225] indicated, "an exception is an experimental cathode containing a ribbon-shaped filament, the flat surface of which causes the distribution of its emitted electron field striking the anode to be uniform or flat rather than twin-peaked like the field from a helical coil filament. The uniform focal spot yields an improved modulation transfer function."[377]

The emission X-ray spectra for mammographic screen-film combinations have been studied by several investigators.[188,267,309] It has been found that the energy distribution of the image-forming photons transmitted through the breast also influences subject contrast.[188,269,304] Dedicated molybdenum target X-ray units are widely used and settings of less than 28 kVp are generally recommended with these units.[265] The use of low-energy photons, such as those produced by the 17.9 and 19.5 keV characteristic lines from the molybdenum target, provide high subject contrast for breasts compressed to an average thickness of about 3 to 4 cm. Because of the greater filtering effect of a thick, dense breast, absorption differences among structures become smaller in the resulting "hardened" X-ray beam. (The lower energy X-ray photons are absorbed or scattered first, leaving mostly higher energy, i.e., "harder" photons to pass through the remainder of the breast.) Therefore, subject contrast is not as high as with average-sized and fatty breasts.

Motion blurring, which is caused by movement of the patient during exposure, can be minimized by using a short exposure time and by firmly compressing the breast.[265] Geometric blurring is affected by the size, shape, and intensity distribution of the X-ray tube focal spot in combination with focal spot-to-object and object-to-image detector distances.[261,473,497] To minimize geometric blurring, the focal spot size and object-to-image detector distance should be minimized, whereas focal spot-to-object distance should be maximized.[263] During the past few years, several studies[263-265,521] have indicated that the effect of geometric blurring is a significant limiting factor in obtaining maximum resolution of the breast image. This remains a limitation in some of the early dedicated mammographic units. While the current dedicated units are better in this respect, some units could be improved to ensure that the image detector (such as film), but not geometric blurring is the limiting factor in resolution.[265] For screen-film mammography, light diffusion (spreading of the light emitted by the screen

before it is recorded by the film) also causes blurring. Factors include thickness and size of the screen phosphor, light-absorbing dyes and pigments in the screen, and screen-film contact.[482,606] Screen-film combinations for mammography utilize a single high-definition screen in contact with a single-emulsion film, instead of the double-coated film (with one emulsion on either side of the support, and sandwiched between two intensifying screens). The latter is most commonly used in general radiography. Cassettes designed for mammography with front panels that provide low X-ray absorption and intimate screen-film contact also reduce blur.[265]

Good breast compression is a very important factor in reducing scattered radiation in screen-film mammography.[43,44,621] Multiply scattered radiation significantly reduces subject contrast, especially when imaging thick, dense breasts. In addition to contributing to a reduction in scattered radiation, compression can provide several other advantages: immobilization of the breast reduces blurring caused by motion; juxtaposition of structures in the breast closer to the image detector reduces geometric blurring; production of a more uniformly thick breast, which, in turn, results in more even penetration by X-ray radiation and less difference in radiographic density in the area between the chest wall and the nipple; reduction of radiation dose; and the spreading of breast tissue enables suspicious lesions to be more easily identified.[265] Compression also provides the opportunity to optimize the X-ray photon energy for a given X-ray optical thickness,[314] which has not yet been exploited. Eklund[170] discussed three innovations that may be useful in mammographic compression. In a study on patient discomfort during screen-film mammography, Jackson et al.[301] concluded that the vast majority of women found vigorous compression comfortable or tolerably uncomfortable, and half or more of women with severe pain would return for further mammographic examination if so advised by their physician. Because of the occasional cyst rupture, radiologists should be aware that breast masses may disappear during the performance of mammography, even though they should be encouraged to continue using firm compression.[452] On the other hand, rupture of malignant cysts could disseminate many malignant cells. Research on this problem, or on improved imaging without compression, may be warranted, although the frequency of cystic carcinomas is only 0.1% of cysts.[152]

The use of specially designed grids for mammography can further reduce scattered radiation and improve contrast, which is most important when imaging thick, dense breasts.[45,97,168,535] It has been demonstrated that radiation passing through the breast to the detector contains a significant amount of scattered radiation, as much as 40 to 85% of the primary radiation,[43-45,310] and that a 40 to 80% range of scattered radiation will reduce image contrast by 30 to 45%.[43,310] Moving grids are now included with most of the new, dedicated mammographic X-ray units.[535] For use with older dedicated systems without a built-in grid, an ultrahigh-strip-density, stationary, focused grid that fits inside a standard mammographic cassette is commercially available.[131] Although the application of grid techniques to mammography improves image quality, patient exposure is also increased. Thus they are not recommended for fatty breasts, where they tend not to improve the image quality.[225] It may be possible to offset the increased radiation dose required when grids are used by using either a higher kilovoltage setting, or a recording system that provides higher speed, or a combination of several factors.[265]

Slit radiography has been known for many years to be a technique that reduces scatter,[47,302,491] but it has not come into general use. However, development work in slit radiography continues both with film and electronic systems.[46,558,600] Slit radiography can make low-contrast images more readily detectable by film, but film often cannot make these images perceptible to the unaided eye.[423] Moreover, when slit radiography removes the background, the dynamic range of the X-ray image can increase beyond the acceptance range of film;[558] however, electronic systems now have the ability to accept larger dynamic ranges than film, and are thus able to take fuller advantage of slit radiography. A new

version of slit radiography to remove such background effects as scatter, off-focal radiation and intensifier glare has been reported.[79] Yester et al.[621] revealed their initial experimental results of scatter reduction obtained in slit mammography.

For increasing the diagnostic information content of the radiogram, direct radiographic magnification has been used in different fields of radiology,[151,216] and its value has also been realized in mammography.[28,150,388,425,517,518,529,536,575] If utilized in appropriately selected patients, magnification mammography can be expected to substantially improve diagnostic accuracy and favorably affect management decisions.[575] In magnification mammography, an air gap is interposed between breast and film, so that the projected radiographic image is enlarged[388,425] and the scattered radiation reaching the film is reduced.[48,150] Scattering by the air in this gap has not been investigated, and may be of some importance. Because of the resultant increase in imaging distance, one must use higher kVp, faster film, longer exposures, or a combination of these factors to produce magnification mammograms. Magnification technique also requires the use of an X-ray tube that has a very small focal spot, to reduce the considerable unsharpness that otherwise would accompany geometric image enlargement.[519] The value of microfocal spot mammography has been repeatedly emphasized in the literature with respect to breast microcalcifications.[271,518,519] Laboratory evidence suggests that the largest acceptable focal spot size for 1.5x magnification mammography is 0.3 mm in greatest diameter.[425] Greater amounts of magnification require even smaller focal spots. A possible alternative is digital or optical deconvolution of the focal spot from the image (cf. Reference 22). Compared with standard screen-film mammography with dedicated units, microfocal spot direct radiographic magnification of the breast, using either xeroradiographic or screen-film recording systems, produces images with improved resolution and reduced effective noise.[271,536,564] In magnification mammography, an improvement in image quality can be realized by adjusting the separation distance (magnification) to the optimum range.[388] It is also important for magnification mammography equipment to permit vigorous breast compression, primarily because the relatively long exposure times used for magnification imaging provide an increased opportunity for image blurring due to motion unsharpness,[529] and any motion is also magnified. Because magnification mammography requires considerably more radiation, its major role currently is to supplement the occasionally inadequate information provided by conventional mammography.[518] Faster screen-film combinations are expected to permit a significant reduction in dose with an accompanying reduction by the magnification of the increased noise inherent in the faster image detector.[28,54]

While limiting the number of mammographic views or projections per examination lowers the radiation risk,[361] this limited number of views yields an unacceptably low rate of cancer detection.[19,21] Other investigators favor xeromammography for seeing fine details and imaging microcalcifications with better contrast.[449,550] However, xeromammography requires a higher radiation dose than film-screen methods and has lower spatial resolution.[372] It has been suggested that the information in mammograms can be enhanced by subtraction film techniques.[385] Therefore, the balance between state-of-the-art methods to provide sufficient details about minimal breast cancer at early stages, and the radiation risk from high X-ray dose has been a controversial problem in X-ray mammography.[521,526] Thus it is important to develop methods that extract as much information as possible from mammograms.[85] A combination of film-screen mammographic and xeromammographic examination may optimize the diagnostic abilities of mammographic examination.[444] This may be accomplished without additional radiation dose by producing xerography-like images from digitized film mammograms.[239,550]

Digital image processing techniques have been suggested for the feature enhancement of mammograms.[385,389] Algorithms based on computerized adaptive neighborhood image processing to enhance the contrast of selected features of a mammogram were reported by Gordon and Rangayyan.[237,239] Early versions of these methods not only enhanced the contrast

of mammographic features, but also enhanced the noise and/or digitization effects so much that desired features often cannot be seen clearly.[142] Dhawan et al.[142] made a comparison of enhanced features using different contrast functions. They found that a suitable contrast enhancement function is important to bring out desired features and is also difficult to select. A generalized polynomial-based contrast enhancement model that can be tuned or set to specific mammographic features is presented in Dhawan et al.[143] Recently, Dhawan and Le Royer[141] demonstrated a new method of defining adaptive neighborhoods and a global model to compute the best contrast enhancement function based on *a priori* knowledge of the type of mammographic features one wants to enhance. Results show that the new algorithm is very efficient and tunable in many aspects to enhance the diagnostic information better with little or no enhancement of noise and other noise-like background variations.[141] New techniques have been developed, based on region growing techniques, to determine the adaptive neighborhoods.[471,472] The method has now been generalized to include adaptive neighborhood versions of different standard digital image processing techniques.[471,472] We are working on a further generalization in which pictures are segmented into a picture-dependent set of "feature pixels" or "fixels", which are local regions defined by an adaptive neighborhood function. Most classical image processing algorithms can be generalized from ordinary square pixels to fixels. These new image processing techniques may succeed in bringing out the desired, but unseen or barely seen features of a mammogram for better human visibility, without the requirement of additional X-ray dose. They may also permit a reduction in dose. However, full utilization of image enhancement will require either electronic imaging or use of new microdensitometers, as discussed below.

As mentioned earlier, a major problem expected with any mammographic screening program would involve the interpretation of the large volume of images produced. In addition to a shortage of trained radiologists, it is difficult to maintain interest and concentration when interpreting large numbers of images that show only a small number of occasional abnormalities.[615] Some automated prescreening methods have been suggested, utilizing recent advances in image processing and pattern recognition techniques. Following the original work of Winsberg et al.,[612] Ackerman and Gose[2] developed computer techniques for pattern classification of features in xeromammograms and showed that a computer can categorize a hand-designated suspicious area of the breast image with the accuracy of a radiologist. A series of algorithms to localize abnormal breast areas has been developed by Kimme et al.[325] Wee et al.[607] quantified the shapes of calcifications using piecewise linear discriminant functions. Smith et al.[552] have developed an efficient algorithm for distinguishing between benign and malignant lesions based on intensity distributions. Hand et al.[256] presented techniques to isolate suspicious areas from the total image. Spiesberger[560] detected microcalcifications using gray level statistics and measures of brightness and compactness. Semmlow et al.[508] described a specific implementation to screen xeromammograms for breast cancer and illustrated the necessity for realistic testing procedures when evaluating systems employing pattern recognition techniques. Recently, Gale et al.[206] investigated the feasibility of identifying specific mammographic features (by eye, rather than by computer processing), and carrying out a computer-assisted diagnosis, using discriminant function analysis. Computerization procedures have also been proposed for the management of screening mammography centers.[260,541]

The potential use of computers to analyze mammograms or xeromammograms has been convincingly demonstrated. In addition to relieving humans of the more tedious aspects of a screening program, and improving the cost-benefit ratio of such a program, a computer evaluation would produce quantitative, objective data (geographical and time-invariant), which are further useful for standardization and quality control. Therefore, the development of automated systems for screening radiographic images of the breast would contribute significantly to a mass screening program, if they could be shown to have lower false-

negative rates than trained radiologists. There is a clear need for further research in this area.

C. EXPECTED TRENDS

The primary goal of the future development of mammography is further improvement in image quality, leading to increased diagnostic accuracy. Dose reduction should continue to be sought, but not at the expense of diagnostic sensitivity and specificity.[226] Because a further breakthrough in mammographic rare-earth screen technology is not anticipated, most X-ray film manufacturers are now focusing their research efforts on increasing the sensitivity of film emulsions in order to further decrease dose without diminishing diagnostic information, for instance, by creating emulsions with oriented, flat silver halide crystals.[225] Films of greater sensitivity will be useful to offset the loss of image quality resulting from increased noise, being combined with microfocal spot magnification. (The sources of noise include X-ray photon fluctuations, scatter, film grain size, film development artifacts, background noise, etc.)

At present, radiographic film serves three functions: as a detector (along with intensifying screens), as a display, and as a storage medium. While film is an excellent medium for recording X-ray information with wide dynamic range (about 12 bits), fewer than 8 bits of this range may be perceived by display on a conventional viewbox, even with the use of spot lighting for dark areas.[556] The human eye often limits the use of available gray scale and spatial resolution.[70] Accurate film digitization via laser scanning permits recording and display of the entire 12-bit dynamic range of film while retaining high spatial resolution.[86] High-quality film digitizers have recently become available for use in clinical testing.[549] A system for digital processing of film radiographs, therefore can combine the excellent characteristics of film as a detector (in terms of dynamic range and spatial resolution) with the flexible image processing and display capabilities of a digital system.

The microdensitometer has been widely used to digitize information from photographic film. In this instrument, microscope optics and mechanical scanning ensure an adequate spatial resolution, while the measurement of light-intensity transmittance (or density) itself is ambiguous because of the influence of the film-grain noise. The measured value of light-intensity transmittance contains an important output noise term that also depends on the optics of the microdensitometer (the Callier effect).[391] Because of the Callier effect, the effective light-intensity transmittance can differ from its calibrated value.[514] Chavel and Lowenthal[107,108] analyzed the influence of the film-grain noise on microdensitometer measurement by using partial-coherence theory. Swing,[574] Kinzly,[328] and Reynolds and Smith[475] introduced the conditions for microdensitometer linearity. When these conditions are met by special optics, a microdensitometer may operate as a linear system, and an unambiguous optical transfer function can be defined. Recently, Sheng and Duvernoy[514] gave a more complete analysis for microdensitometers, in which both the coherence in the illumination and the film-grain noise are considered.

The ultimate form of film microdensitometry would be a method that measures the coordinates of each silver grain. Such systems have been built for autoradiography over areas limited to the width of a cell, a few microns.[355] A high degree of parallelism in data acquisition would have to be attained to make grain counting practical for whole mammograms. Such a technique might make it possible to measure single X-ray photons using film. If accomplished, this could be a route to further dose reduction (though the spatial and density trade-offs in detection efficiency of film vs. screen-film would have to be taken into account).

Most commercial microdensitometers only digitize film at 8-bit resolution or a dynamic range of 256:1. An attempt to overcome this limitation by scanning an image twice at two light levels has been made by Rangayyan and Gordon[470] for videodensitometry. However,

a better approach nowadays is to use a densitometer capable of up to 12-bit density resolution (dynamic range of 4096:1) using charge coupled device (CCD) sensors (Eikonix, Bedford, MA) or 10-bit laser scanning.[227]

While high spatial resolution of the order of 4096 × 4096 pixels, and 12-bit gray scale quantization, can be achieved now, no electronic display devices are currently available to display such an image. The largest image that can be displayed is limited to 2560 × 2048 pixels on the latest electronic devices (MegaScan, Gibsonia, PA). Display controllers with the capability of displaying such a portion of a large image and real-time zooming over the full image are also commercially available (MegaScan, Gibsonia, PA; Pixar, San Rafael, CA). Gray scale resolution is, however, limited by the ability of the human eye to distinguish gray levels. Thus it is necessary to use density slicing or other histogram manipulations[480] over the 12-bit range (as is done in computed tomography displays). Laser film writers/ recorders are available[18] to record such displayed high-resolution images back on film (after digital image processing).

One potentially fruitful area for research is electronic digital mammography, bypassing film altogether.[106,203,225,226,330,332,336,337,436,437,491] The occasionally soaring cost of silver-based film and the expense of storing and retrieving it has created a long-term need for a more cost-effective alternative to film-based radiographic procedures. Digital mammographic systems may use specially designed photoelectronic imaging devices to eliminate the use of film as the primary recording medium (cf. References 204, 308, 455, and 572). Aside from the obvious advantages of accuracy and performance, since the images are digital, many digital processing techniques are available without further instrumentation to significantly enhance the diagnostic quality of the final images. Advantages of such digital systems over traditional film-based ones also include the capability for electronic archival and matching with computerized patient records, flexibility of display, and so on. Digital imaging systems incorporating linear array X-ray sensors have been developed for a range of applications in diagnostic radiology.[72,312,464,555,585] Conventional mammography does not efficiently use all the X-ray photons passing through the breast. High-efficiency detector systems are being developed that will be more effective than film/screen and xeromammography in detecting X-ray photons.[337] This will permit a marked reduction in the dose required. The addition of microfocal spot magnification to grids[575] or scanning slits to reduce scattered radiation[491,586,621] could also lead to future digital mammography systems that are both practical and effective. A digital image can also take advantage of the potential avidity of breast cancer for iodinated contrast material,[105] and the precontrast image can be subtracted from the postcontrast image, revealing areas of increased uptake of iodine.[332,336] The potential for dual-energy image subtraction[305-307] may produce significant improvements in radiographic detection of breast cancer.

Chang et al.[106] reported that a low-dose digital mammography system with a resolution of up to 2 lp/mm (250 μm) was under development (lp = line pairs). Fritz et al.[203] have developed a prototype system to evaluate the use of CT-type linear array sensors for digital mammography. While the resolution is now 400 μm, the targeted resolution of this system is 100 μm. Some available digital radiography units even have up to 15 lp/mm (about 33 μm) resolution with magnification and microfocal spot X-ray tubes, but only a few installations use such equipment for mammography.[203] Furthermore, the number of photons at the image detectors for a resolution of 30 μm or higher are insufficient for the contrast by which the breast tissue structure is clearly defined for the dose now in general use.[203] A digital mammography system using CCD technology with a target resolution of 5 lp/mm (100 μm) is also reportedly undergoing investigation.[203]

Gold et al.[225,226] have proposed that a detector array coupled with an intensifying screen below the breast could transmit the X-ray signals emanating from above the breast to a television monitor where contrast could be enhanced by digital manipulation. The advances

in X-ray television systems[273,279] are believed to stimulate this investigation. Alternatively, digital imaging could be coupled to a reusable selenium plate detector. Used with a dedicated mammography X-ray unit, the pattern of charges on the plate could be converted into digital form from which the image might be stored and manipulated on a computer.[225,226] Digital imaging could also be coupled to a phosphor-coated plate; after X-ray exposure of the breast with dedicated mammographic equipment, a scanning laser could "read out" the information on the plate, converting it to a digital form suitable for digital image processing.[226,557] It has been reported that lasers have been used to produce line-scan images of extremely high resolution, up to 10,000 times as many pixels as a standard TV picture.[18] The imaging of microcalcifications may thus be practical by this technique. Even if the definition of the microcalcifications were to be obscured because of a volume effect, they might still increase the density of the digitized pixel sufficiently to become detectable when contrast is increased on the display monitor.[556] Seeley et al.[501] pointed out that contrast resolution has the greatest effect on general diagnostic accuracy. However, spatial resolution has the greatest impact on design costs, transmission-speed requirements, and storage needs. For example, for a 1024×1024 image with a 10-bit resolution, doubling the spatial resolution will increase the amount of information to be manipulated in each image by 300%, whereas doubling the contrast resolution will increase the amount of information to be manipulated by only 10%. As Kopans[332] indicated, "ten-line pair per millimeter resolution can be achieved, but this generates 200 megabytes of information per image. Low-cost image display devices are not capable of displaying such a large amount of information, and initial studies will require preliminary viewing of the entire breast at low information density." Since higher resolution systems are becoming available,[7,190,203,502,503] digital mammography should soon attain clinical utility.

Mammography is now the chief tool in detecting early breast cancer, yet it is far from perfect because of its two-dimensional (2D) character. Gordon[232] recently proposed a new method for detection of early breast cancer by using three-dimensional (3D) digital subtraction techniques via a geometric unwarping procedure. This cannot be done directly because breast tissue is soft, flexible, and changes shape over time. Each time the breast is compressed for mammography, it is placed in a somewhat different orientation, and, of course, normal menstrual cycle changes and aging would have altered its size and shape as well. Therefore, it is necessary to first find the 3D transformation or "geometric unwarping" (cf. Reference 6) that relates a current 3D image of a breast to an earlier 3D image. The proposed method[232] is a combination of 3D image enhancement using optimal adaptive neighborhoods (cf. References 141-143,471, and 472), 3D registration for matching corresponding enhanced voxels (cf. References 240 and 241), and global or piecewise best fit[625] or octree fitting[300] methods for defining the parameters of the transformation, followed by 3D recursive filtration[90] to improve the signal-to-noise ratio of the 3D digital subtraction radiograph. The solution to this problem would open the way for a 3D approach to diagnosis of early breast cancer.[232]

Production of the 3D images needed for 3D digital subtraction itself requires new approaches to computed tomography. First of all, there is a known advantage to taking projections at viewing angles in three-dimensional space that are not coplanar.[234,594] This has yet to be tried. Thus, in the following discussion, we assume that 3D images are obtained by stacking a set of serial 2D (CT) sections. Attention must be paid to keeping the total dose compatible with that of two-view screen-film mammography, especially if screening of asymptomatic women is the goal. In commercial X-ray CT machines, 180 or more views are taken. Thus we are faced with two prospects: (1) use very few photons per view, or (2) use very few views.[229] The former has yet to be tried, because of a lack of mathematics capable of reconstructing an image from very noisy, if numerous, projections. The latter approach was tackled in the context of CT via teleradiology of radiographs[235-238,467-469,553] and finally solved in the context of detection of early melanoma via *in situ* 3D computer

light microscopy of transilluminated nevi.[139] Usable images from only three views, showing detail unobtainable by any standard CT algorithm with the same number of views, were calculable.[140] However, the sensitivity of these new "geometric deconvolution" algorithms to noise has yet to be determined. (See Frieden and Zoltani[202] and Heffernan and Robb[276] for other methods for CT using only three to four views.) One way of reducing the dose while collecting data for 3D imagery is to use a steerable X-ray microbeam[231] aimed at the ends of the mammary ducts, where most breast carcinomas are presumed to begin.[628] CT algorithms that can reconstruct just local regions,[551] or emphasize them[230] are available. The duct system for each breast could possibly be defined in a single "baseline 3D mammogram". This would lead to a new, quantitative understanding of the internal anatomy of the individual breast and its variations.

It has been suggested that mammograms, as normally viewed, display only about 3% of the total information detected.[85] It may be possible to enhance mammograms to bring out the diagnostic information. We can apply the criterion of "negentropy" as a measure of information.[80,138,237] From information theory, we know that the bound information, i.e., information connected with certain specific physical problems, appears as a negative term in the total entropy of the physical system.[80] This implies that the bound information is equal to the decrease in entropy or increase in negentropy, where negentropy is defined as the negative of entropy.[80] In the case of images, where there are several possible gray levels, one may measure the entropy or average information per level of an element by the expected value of the information contained in each possible level.[251] Histogram analysis shows that enhancement techniques can improve the gray level distribution of the original image over the entire dynamic range.[138,142] Thus enhancement techniques that lead to higher entropy may be extracting the more relevant information.

IV. CT, MRI, AND OTHER MODALITIES FOR BREAST IMAGING

Because of accumulating evidence that detection at an early stage improves prognosis, because of its demonstrated ability to detect cancer at nonpalpable stages, and because of its high spatial resolution, mammography has been in the forefront of methods of breast imaging. Its widespread use has been tempered by the issue of possible risk from low doses of ionizing radiation, as well as by the fact that, although more accurate than any other modality, including physical examination, it may still find only 80 to 90% of breast cancers.[40] These factors have served to stimulate some medical investigators and manufacturers of medical equipment to conduct and support studies of alternative breast imaging procedures:[163,330,522,530] computed tomography (CT) scanning utilizes X-rays to produce high-contrast images (especially with the injection of a contrast medium) in a cross-sectional display; diagnostic ultrasonography stresses the differentiation of benign cysts from diagnostically indeterminate solid masses that require biopsy; evolving experimental procedures, such as magnetic resonance imaging (MRI), transillumination light scanning (diaphanography), and digital subtraction angiography of the breast (DSAB) currently are undergoing preliminary evaluation; and an older procedure, thermography, seems to operate at a high level of effectiveness only for advanced cancer. All these alternatives already have or may eventually have the ability to provide clinically useful information that complements the information currently available from X-ray mammography. However, none of these procedures is, for now, expected to replace mammography as the first-line imaging technique for the detection and diagnosis of benign and malignant breast lesions.[331,374]

A new imaging modality may have an important role in diagnosis even though it is inadequate for detection. New technologies, such as CT, MRI, transillumination light scanning, DSAB, and ultrasound offer a wide selection for patient examination. Each newly

proposed modality has caused a flurry of interest and optimism.[461] For several reasons, these modalities have not always had the rigorous evaluation they deserve.[331,421,422] Evaluation of new imaging modalities has been relatively inefficient in the past. If a new method is not proven to detect very small, highly curable breast tumors, its wide use may delay diagnosis significantly and lead to an otherwise avoidable loss of life. It has been suggested, therefore, that minimum guidelines for the clinical evaluation of any new breast imaging modality should be adopted.[421,422]

A. COMPUTED TOMOGRAPHIC MAMMOGRAPHY

Computed tomography scanning has gained acceptance as a diagnostic imaging procedure primarily by virtue of its ability to portray density differences much smaller than those demonstrable by conventional plain film X-ray techniques. Unfortunately, these density differences cannot be used directly in examining the breast because there is considerable overlap in the CT numbers of many breast cancers, several types of benign breast lesions, and dense collections of normal fibroglandular breast tissue.[100,522] Only by imaging the breast twice, both before and after intravenous iodide administration, can CT scanning produce levels of diagnostic accuracy comparable with X-ray mammography.[530] It has been shown that the great majority of breast cancers demonstrate at least a 5% increase in CT number following iodide administration, whereas most benign lesions do not.[100-104,219,220] The radiological contrast enhancement by contrast agent represents, thus, the principal CT criterion for the differentiation of benign from malignant lesions.

Two identical prototype units of a dedicated breast CT scanner (CT/M) were made available in the late 1970s. Clinical trials with one unit demonstrated slightly increased cancer detection for CT scanning over mammography,[104] whereas the other showed no difference.[220] This equipment, developed by General Electric, gave a false-positive rate with benign lesions higher than that of standard mammography.[100,220,516] The reason is probably simply the low spatial resolution of the GE CTM: an ordinary 0.1-mm microcalcification is washed out by a factor of 10,000 in the 1 mm × 1 mm × 1 cm volume element that was used. In addition to shortcomings for detection of early breast cancer, this test showed that CT scanning is inappropriate as a primary diagnostic test for breast cancer, because of the high cost of the examination, the need for intravenous iodide administration, and the relatively high radiation dose involved.[105] Paulus[450] summarized the present situation as follows: "The high cost of dedicated CT mammographic units, lengthy examination time, use of large volumes of contrast media, requirement of physician involvement, large space requirements, high overhead, lower diagnostic accuracy, and increased radiation compared to mammography precluded routine or screening use of breast CT. Clinical investigation of CT mammography was initially enthusiastic.[101,104] However, it has been virtually discontinued both here and abroad."

Despite the lack of general clinical utility for breast CT scanning, there are several specific, narrowly defined situations in which the examination can prove helpful. For example, by virtue of its cross-sectional image display, it can be used to achieve prebiopsy localization of the rare nonpalpable mammographic lesion that it so close to the chest wall as to be visible on only one mammographic projection.[144,330,333] Because it readily indicates chest wall thickness and also may demonstrate the position of the internal mammary lymph node chains, its use has been advocated in treatment planning for women who receive radiotherapy for primary breast cancer.[427] Most importantly, CT scanning has utility among patients with known breast cancer in searching for subclinical metastasis to regional lymph nodes and to deeper structures by contiguous tumor spread.[354,394] Breast CT also appears to be a useful diagnostic tool for follow-up studies of postirradiation of breast cancer, follow-up studies for postmastectomy patients, and a screening procedure for high-risk patients, especially those with dense breasts.[105]

As discussed in Section III.C, the current situation of breast CT scanning may soon turn around with the development of arrays of electronic detectors with a resolution of up to 15 μm[492,493] for low-dose digital mammography.[337] It has been shown that the addition of dual energy subtraction imaging can improve the detection of microcalcifications, though it does not help much in soft tissue discrimination.[306,307,437] Ultimately, we may nevertheless find it optimal to combine dual energy with CT and geometric unwarping.

There is another promising approach that is yet to be explored: understanding the physiological processes that cause malignant tissues to have an increased affinity for iodinated contrast material.[522] This may prove useful for breast MRI (see below) by facilitating production of successful paramagnetic contrast agents for breast cancer detection.

B. BREAST MAGNETIC RESONANCE IMAGING

In vivo MRI of the breast has been possible only for the past few years, and current experience is far too incomplete to indicate whether it will play a significant role in the diagnosis of benign and malignant breast diseases. Initial investigations were done using whole-body imaging coils,[171,228,366,367,448,481,537] with limited success. More recently, the development of high-resolution surface coils has resulted in superior breast images, capable of demonstrating smaller lesions and finer structural details.[127,172-174,386,570,571,618,619]

Although limited in scope, current clinical experience with breast MRI already indicates many of its strengths and weaknesses. MRI is superior to mammography in differentiating solid from cystic lesions, and equivalent to mammography in providing information regarding different parenchymal patterns.[127] Breast MRI also has an appreciable advantage over mammography in patients with areas of asymmetric dysplastic breast tissue.[173] Fatty and fibroglandular regions of the breast are clearly distinguished, and areas of dense fibroglandular tissue are imaged with a greater range of contrast than either mammography or CT scanning. Large (and some small) breast lesions also are readily portrayed, especially if surrounded by substantial amounts of fatty tissue.[173] Even with surface coils, the spatial resolution of MRI is, however, far inferior to mammography.[530] Moreover, the tiny clustered calcifications of intraductal carcinoma and the fine spiculations of invasive breast cancer are not imaged.[127,332] One of the reasons for this is that calcification, like bone, gives little or no MRI signal. There has also been difficulty in identifying some masses adjacent to dense areas of fibroglandular tissue. Although experimental intravenous paramagnetic agents, which highlight differences in signal intensity between regions of differing tissue perfusion, have been considered as potential adjuvants to extend the usefulness of MRI for breast cancer detection, intravenous injection and possible toxicity would prevent their use in screening programs.[485] Not only for these reasons, but especially because of the very high cost of examination, it is exceedingly unlikely that MRI will be used for breast cancer screening.[127,225,330,530,591] The cost could, however, come down substantially if the new, relatively high-temperature superconductors are developed into practical magnets.

Despite these shortcomings for screening, breast MRI offers considerable promise in breast disease diagnosis, as a complement to mammography and physical examination. Currently there is no test short of open or needle biopsy that reliably excludes the diagnosis of malignancy for solid masses. If MRI could provide this ability, even if only for several specific benign lesions, it would prove to be a valuable adjunct to the standard diagnostic evaluation. Current clinical investigations of breast MRI are beginning to address this important issue.[127,530] Attempts to distinguish benign from malignant solid masses solely on the basis of their morphological features have not met with great success,[174,283,332] since MRI has lower spatial resolution than mammography. "Parallel efforts also have failed to differentiate benign from malignant disease simply on the basis of variations in lesion intensity using different MRI radiofrequency pulse sequences."[530] Currently the breast MRI technique has no established clinical indications.[530] However, it must be remembered that compared

with the relatively mature modalities of CT scanning and transillumination light scanning, breast MRI truly is in its infancy. There are many potentially fruitful lines of investigation that have not yet begun to be explored. For example, it is possible to combine X-ray CT and MRI pixels in a way that extracts more information than available from viewing CT and MRI images side by side.[233] It will be many years before the diagnostic potential of breast MRI is fully evaluated.

C. BREAST TRANSILLUMINATION

Transillumination (diaphanography) of the breast is accomplished by passing light, either visible or infrared, through the breast and observing or recording the exiting light.[371] This technique was first used years ago by Cutler[124] and later by others, and the results were not good enough to allow it to become a meaningful technique in the evaluation of the female breast. Current techniques selectively utilize the far-red and near-infrared region of the spectrum because these longer-wavelength photons penetrate more readily through breast tissue and scatter less, thus resulting in higher photon detection efficiency and higher resolution. In addition, it is thought that there may be preferential light absorption by breast cancer in this portion of the spectrum, so that areas of malignancy absorb more (and therefore transmit less) light than do benign tissues.[522] As a consequence, emphasis has shifted away from real-time viewing by the human eye, which is totally insensitive to near-infrared rays and toward hard-copy recording of images using special infrared-sensitive photographic film.[299,439] Two major breast transillumination techniques are currently used. One records images on infrared-sensitive photographic color film.[439] The advantage of this approach is its relatively low cost, but the film must be developed by a chemical process that is provided by only a few commercial photographic laboratories, resulting in delays of up to a week before images are available for interpretation. With the other technique, images are recorded by a TV camera especially sensitive to far-red and near-infrared wavelengths.[50] This results in real-time viewing using a standard TV monitor, with recording of images on video tape or by taking Polaroid photographs off the TV screen.[603] Postacquisition signal processing has been incorporated into some equipment, providing images that indicate the relative infrared-to-red transmission in addition to total light transmission.[530]

Reports on the efficacy of transillumination light scanning to detect breast cancer have shown discrepant results. Bartrum and Crow[50] were the first to critically assess the transillumination technique. They were optimistic in their preliminary assessment. Sickles[525] reported that the sensitivity of mammography is much higher than that of transillumination. Geslien et al.[218] used the same type of equipment as Bartrum and Crow, but reported results similar to those of Sickles. Gisvold et al.[221] used equipment that was essentially the same as that used by Bartrum and Crow, and Geslien et al., and showed that mammography is superior for detecting malignancy. Of 67 pathologically proven breast cancers, 64 (95.5%) were detected by mammography and 45 (67.2%) were detected by transillumination. One of the reasons why there is such a discrepancy is that they used both different number of examination views and different scanning directions. Other reports have noted varied findings, and further studies are being conducted.[69,155,371,439] The primary theoretical limitation to transillumination techniques is that only a very small portion of the incident light, if any, is transmitted in a straight path through the breast. Thus, the great majority of photons are scattered extensively, thereby producing low-resolution images.[330] The fact that current equipment uses large-area light sources and short imaging distances further degrades the transillumination image.[332] The major weaknesses of diaphanography appear to be a relative inability to image deep lesions, and a questionable ability to detect the small cancers (1 cm) now routinely detected by mammography.[522] Drexeler et al.[155] showed that even under ideal conditions, a lesion could not be detected at a depth greater than twice its diameter by transillumination. Monsees et al.[409] also concluded that transillumination light scanning is

not competitive with mammography as a screening method for breast cancer detection. Several authors have suggested clinical utility for transillumination in specific circumstances when mammography results in questionable or equivocal findings.[218] However, there has been no conclusive demonstration that transillumination can serve even as an adjunct to mammography and physical examination in the evaluation of either symptomatic or asymptomatic patients. At the present time, transillumination has no established clinical indications and therefore remains an investigational tool.

Because of the light scatter problem it is not likely that current transillumination devices will gain widespread clinical acceptance.[530] Scatter reduction methods, say the use of low-energy lasers, or by raster scanning with a fiber optic point source touching the breast and by carrying out an inverse radiative transfer (3D deconvolution) computation,[98,462] should be investigated further. The basic physical properties of light absorption in the breast should also be investigated. The possibility exists for defining wavelengths for breast transillumination that clearly discriminate breast carcinomas from surrounding benign tissues.

D. BREAST SONOGRAPHY

The search for a breast cancer screening technique that avoids the potential hazards of ionizing radiation led to the production and evaluation of dedicated mammographic, sonographic scanners. Kobayashi[329] presented a good review on early developments in breast sonography. For more recent developments in breast sonography see Cole-Beuglet,[113] and Egan.[164] Efforts to establish the ultrasonic characteristics of breast structures and breast carcinomas have also been reported.[341,496]

Although no controlled clinical protocols on comparative studies of sonographical and mammographic examinations of the breast had been proposed, Egan et al.[169] designed a protocol to evaluate the efficacy of breast sonography in a clinical setting. The potential usefulness of automated breast sonography as a screening device has been suggested by reports of sonographic cancer detection rates approaching those of X-ray mammography.[114,132] However, later reports have shown that a large number of nonpalpable tumors detected by mammography were missed by sonography.[115,169,338,378,379,484,538,539] Sonography, while capable of imaging and categorizing most palpable breast masses, often failed to detect small, nonpalpable cancers. Differentiation of benign from malignant solid masses cannot be reliably accomplished by sonography. It also could not detect cancers smaller than 1 cm in size, and almost never images cancers that present only as clustered calcifications on mammograms.[527] Although large, benign calcifications produced shadowing, microcalcifications, often the sole indicators of breast cancer, remained largely undetectable.[538]

For palpable masses, any hand-held, real-time unit having a transducer frequency no less than 5 MHz is adequate to identify simple cysts, thereby averting unnecessary biopsies. Hand-held, real-time sonography may be a useful adjunct to mammography for patients with palpable and nonpalpable masses considered indeterminate on mammograms.[484] Automated water-path instruments designed specifically for whole-breast examination make it possible to systematically examine the breast in its entirety, an essential feature when breast sonography is used to search for nonpalpable lesions.[384] Relative to that of mammography, the accuracy of automated whole breast ultrasound has probably been overestimated.

Sonography, in spite of its failure as a screening method, has emerged as the single most helpful adjunct to mammography in the evaluation of the clinically or mammographically abnormal breast.[169,257,285,338,454] Cysts, fibroadenomas, and carcinomas are the most common masses in the female breast,[259,335] and accurate separation of cysts from other breast lesions is of great clinical importance. The most important clinical role for breast sonography currently is the differentiation of cysts from solid masses. In this endeavor, accuracy rates of 96 to 100% have been reported,[191,539] far exceeding those of mammography and physical examination.

Other proposed, but not yet established, applications of sonography include imaging dense breasts,[258,527] the application of Doppler techniques to make benign-malignant differentiations of sonographically detectable masses,[42,340] and, perhaps, the initial evaluation of asymptomatic women under 35 years of age.[169,258] Another proposed application is the evaluation of tissue surrounding augmentation prostheses, where the effectiveness of X-ray mammography and physical examination is limited.[116] Ultrasound-guided aspiration biopsy of nonpalpable lesions is beginning to be explored.[335] The detection of axillary lymph node metastases in breast cancer by ultrasound has also been reported.[89] Continuing refinements in transducer design and signal processing techniques can be expected to produce better images. The development of acoustic transmission computed tomography for *in vivo* determination of sonic attenuation and velocity[243,499] should permit much more successful imaging of fatty tissues, currently a major weakness limiting the utility of breast sonography.[226]

E. BREAST THERMOGRAPHY

Thermography was first utilized for breast disease when Lawson[347] made the observation that breast cancers were associated with an elevation of the temperature of the overlying skin. Various types of thermography are currently in use, such as telethermography (using an electronic infrared detector),[523] liquid crystal thermography,[222,420] computer-assisted thermography,[588,613,626] and microwave thermography.[49,429] A totally different method of infrared thermography was developed using one- and two-dimensional arrays of Schottky barrier imaging devices with charge coupled device (CCD) readouts.[145] This system, operating in the region of high-contrast infrared output from the human body (3.4 to 4.2 μm), offers the promise of providing higher resolution than existing thermographic systems. However, throughout its 30-and-more-year history, the use of thermography for breast cancer detection has been controversial.

The mechanism of tumor thermogenesis and heat transfer is still poorly understood. It is usually assumed that an abnormal thermal gradient associated with a cancer is a product of its accelerated metabolism. The work of Lawson and Chughtai[348] has provided support for this hypothesis. Until recently, conduction of heat was considered to play the primary role in the recording of superficially located abnormalities, resulting in a so-called overlying "hot spot" on the thermogram. Conversely, venous convection was thought to be the primary mode of heat transfer for deeper-seated abnormalities. The deeper cancers were believed to increase the temperature of adjacent blood, which then coursed from deep veins to superficial veins on its way to a plexus of rich venous anastomoses beneath the areola. Love,[358] however, has recently disputed these theories and has shown that the metabolic rate of most cancers is too low to account for the measured temperature increase. According to Love, blood perfusion, and not the local heat from the tumor, is the main factor controlling the variation in local skin temperature, which becomes a direct indicator of subsurface blood flow. According to this theory, the increased blood perfusion is part of a generalized response to the tumor. Indirect support for the tissue perfusion hypothesis may be obtained from the mammograms of patients with carcinoma of the breast. It has been noted that approximately 75% of all cancers will be associated with a local increased caliber of the veins in the affected breast.[147]

Because most of the reported investigations on breast thermography have been anecdotal and/or lacked definitive comparisons with other modalities, the value of thermography cannot be accurately assessed. There is little evidence to indicate that thermography lowers the stage at detection, and neither does a positive thermogram in screening seem to have a strong predictive value.[415] Yet, because thermography is rapid, noninvasive, and safe, it was once included as a screening modality in the Breast Cancer Detection Demonstration Projects. However, the cancer detection rate of thermography was only 42%, a clinically unacceptable level, especially compared with rates of 57% for physical examination and 91% for mam-

mography, so it was abandoned.[61] Presently, thermography has severe limitations in the detection of breast cancer. It is least reliable in the detection of the small cancers that are most amenable to successful therapy. It is felt that thermography may still be an investigational tool, to be used in breast cancer screening only when a specific protocol is available that allows subsequent objective evaluation of results. Initial overconfidence in thermography led to the development of computer image processing techniques for the analysis of thermograms.[223] The role of thermography in determining prognosis and treatment of breast cancer patients should continue to be scientifically investigated. It is especially important that additional research be undertaken to determine the nature of tumor thermogenesis.

F. DIGITAL SUBTRACTION ANGIOGRAPHY OF THE BREAST

The most common, difficult problem encountered in screening is the differentiation of benign lesions from malignant cancers. Typically, malignant breast tumors constitute only 10 to 30% of all breast lesions submitted for biopsy.[196,290,395,419] As reported by Moskowitz,[414] a sharply defined 1-cm nodular density, a common nonpalpable mammographic finding usually representing a fibroadenoma, has an approximately 2% chance of being malignant. Even with the addition of other noninvasive diagnostic modalities, say ultrasound, transillumination light scanning, or MRI, mammography cannot, with certainty and accuracy, differentiate malignant from benign breast lesions without some form of invasive surgical intervention: either needle or open biopsy. Although biopsy plus pathologic examination represents the most accurate method for differentiating between benign and malignant breast lesions, surgical biopsy is disfiguring, risks infection, and may enhance metastasis. Further, the costs associated with surgeon and pathologist involvement, operating facilities, and patient hospitalization increase the cost of cancer diagnosis. Needle biopsy represents a less expensive alternative to this procedure, but it is reliable only if findings are positive, since a negative result may be due to missing the lesion.

Preliminary clinical results demonstrate the potential of the new, noninvasive diagnostic procedure, digital subtraction angiography of the breast (DSAB), for differentiation of benign and malignant lesions, and justify further investigations of its use as an alternative to surgical biopsy. Flynn et al.,[192] Ackerman et al.,[3] and Watt et al.[604,605] reported their initial experience with DSAB for the diagnosis of breast lesions detected by mammography. They investigated whether intravenous DSAB can provide accurate differentiation based on the vascularity of a lesion and the kinetics of iodinated contrast material. It is believed[192] that the metabolically altered blood flow characteristics of malignant tumors, as reflected by the kinetics of iodinated contrast material, may be valuable in distinguishing malignant and benign breast lesions, and that the subtle uptake of iodine in malignant tumors consequent to an intravenous contrast injection may be observed with DSAB by utilizing specialized techniques (immobilization for the following of late phases, magnification techniques using low kVp, and removal of the grid). Watt et al.[606] found that DSAB consistently demonstrated retention of contrast material and abnormal vasculature in malignant lesions, but not in benign lesions. In the 22 breast lesions for which there was histopathologic correlation, DSAB correctly categorized 8 of 9 malignant and 11 of 13 benign lesions. Criteria for malignancy include the presence of abnormal vessels feeding the lesion and a "blush" (localized, prolonged retention of contrast material) in the area of the lesion.[605] They claimed that although the number of examinations in this series is too low for statistical significance, the preliminary results suggested that DSAB may provide a noninvasive, accurate, cost-effective tool in the diagnosis of breast cancer. There are also reports on technical factors in DSAB technique published recently. For example, Block et al.[76] have invented a device that facilitates patient positioning and provides good compression of the breast during digital subtraction angiography. It is believed that with further development of digital subtraction angiography techniques[351] this modality may be a useful adjunct to mammography in the diagnosis of breast cancer.

V. SUMMARY

Breast cancer is the most common malignant neoplasm and the leading cause of cancer deaths in women. The means to prevent breast cancer has not yet been found. Despite the lack of preventive measures, benefits from early detection, diagnosis, and treatment include a high operative cure rate, less morbidity, a need for less extensive tissue removal, and a better opportunity for rehabilitation than is seen with more advanced lesions.

Mammography is at present the only reliable means of detecting nonpalpable cancers, and can detect many small breast cancers in early stages, when they may be curable. It should be applied more widely, especially in screening asymptomatic women aged 50 or over. Clinical breast examination and breast self-examination are also recommended for asymptomatic women for the detection of early breast cancer.

In recent years, there has been great interest in developing alternative techniques for breast imaging. Such new technologies as computed tomography, magnetic resonance imaging, transillumination diaphanography, ultrasound, thermography, and digital subtraction angiography may eventually offer a wide selection for options. Potentially fruitful areas for research are digital mammography, applications of digital image processing and pattern recognition techniques in digital mammography, and computer-aided diagnosis.

ACKNOWLEDGMENTS

REFERENCES

1. **Abe, R., Kimura, M., Sato, T., Yoshida, K., Hariu, T., Kanno, H., Takayashi, K., Matoba, N., and Kumagai, N.,** Trial of early detection of breast cancer by mass screening, *Cancer*, 56, 1479, 1985.
2. **Ackerman, L. V. and Gose, E.,** Breast lesion classification by computer and xeroradiography, *Cancer*, 30, 1025, 1972.
3. **Ackerman, L. V., Watt, A. C., Shetty, P., Flynn, M. J., Burke, M., Kambouris, A., Fine, G., and Wilderman, S.,** Breast lesions examined by digital angiography, *Radiology*, 155, 65, 1985.
4. **Adair, F., Berg, J., Joubert, L., and Robbins, G. F.,** Long-term follow-up of breast cancer patients: the 30-year report, *Cancer*, 33, 1145, 1974.
5. **Adami, H.-O., Hansen, J., Jung, B., and Rimsten, A. J.,** Age at first birth, parity and risk of breast cancer in a Swedish population, *Br. J. Cancer*, 42, 651, 1980.
6. **Adams, J., Patton, C., Reader, C., and Zamora, D.,** Hardware for geometric warping, Offprint from *Electronic Imaging*, April issue, 1984.
7. **Alcorn, G. E. and Burgess, A. S.,** Fabrication of an X-ray imaging detector, *Appl. Opt.*, 25, 4500, 1986.
8. **Alcorn, F. S., O'Donnel, E., and Ackerman, L. V.,** The protocol and results of training nonradiologists to scan mammograms, *Radiology*, 99, 523, 1971.
9. **Alcorn, F. S., Gold, R. H., and Paulus, D. D., Jr.,** Mammographic phantoms and image quality control, in *Breast Carcinoma: Current Diagnosis and Treatment*, Feig, S. A. and McLelland, R., Eds., ACR and Masson, New York, 1983, 609.
10. **American Cancer Society,** Mammography 1982: a statement of the American Cancer Society, *CA*, 32, 226, 1982.

11. **American Cancer Society,** Mammography guidelines 1983: background statement and update of cancer-related checkup guidelines for breast cancer detection in asymptomatic women aged 40 — 49, *CA,* 33, 255, 1983.

12. **American College of Radiology,** Policy statement: guidelines for mammography, American College of Radiology, Reston, VA, 1982.

13. **Amsel, Z., Grover, P. L., and Balshem, A. M.,** The impact of physician reinforcement on breast self-examination practice, *J. Fam. Pract.,* 19, 236, 1984.

14. **Anderson, D. E.,** Some characteristics of familial breast cancer, *Cancer,* 28, 1500, 1971.

15. **Anderson, D. E.,** Genetic study of breast cancer: identification of a high risk group, *Cancer,* 34, 1090, 1974.

16. **Anderson, D. E.,** Breast cancer in families, *Cancer,* 40, 1855, 1977.

17. **Anderson, D.,** Are pre- and postmenopausal breast cancer separate diseases?, in *Current Controversies in Breast Cancer,* Ames, F. C., Blumenschein, G. R., and Montague, E. D., Eds., University of Texas Press, Austin, 1984, 37.

18. **Anderson, J. M.,** High-resolution laser line-scan imaging, *Laser Focus,* 23(10), 160, 1987.

19. **Andersson, I.,** Mammographic screening for breast carcinoma. III. Appearance of carcinoma and number of projections to be used at screening, *Acta Radiol. Diagn.,* 22, 407, 1981.

20. **Andersson, I.,** Mammography in clinical practice, *Med. Radiogr. Photogr.,* 62(2), 1, 1986.

21. **Andersson, I., Hildell, J., Muhlow, A., and Petterson, H.,** Number of projections in mammography: influence on detection of breast disease, *Am. J. Roentgenol.,* 130, 349, 1978.

22. **Andrews, H. C. and Hunt, B. R.,** *Digital Image Restoration,* Prentice-Hall, Englewood Cliffs, NJ, 1977.

23. **Anon.,** Screening for breast cancer, *Lancet,* 1, 851, 1985.

24. **Anon.,** Survey of physicians' attitudes and practices in early cancer detection, *CA,* 35, 197, 1985.

25. **Anon.,** Another look at the pill and breast cancer, *Lancet,* 2, 985, 1985.

26. **Apter, D. and Vihko, R.,** Early menarche, a risk factor for breast cancer, indicates early onset of ovulatory cycles, *J. Clin. Endocrinol. Metab.,* 57, 82, 1983.

27. **Armstrong, B.,** Recent trends in breast-cancer incidence and mortality in relation to changes in possible risk factors, *Int. J. Cancer,* 17, 204, 1976.

28. **Arnold, B. A., Eisenberg, H., and Bjarngard, B. E.,** Magnification mammography: a low dose technique, *Radiology,* 131, 743, 1979.

29. **Ashikari, R., Huvos, A. G., and Snyder, R. E.,** Prospective study of non-infiltrating carcinoma of the breast, *Cancer,* 39, 435, 1977.

30. **Askins, B. S., Brill, A. B., Rao, G. U. V., and Novak, G. R.,** Autoradiographic enhancement of mammograms: investigation of a new dose reduction technique, *Radiology,* 130, 103, 1979.

31. **Bailar, J. C., III,** Mammography: a contrary view, *Ann. Intern. Med.,* 84, 77, 1976.

32. **Bailar, J. C., III,** Screening for early breast cancer: pros and cons, *Cancer,* 39, 2783, 1977.

33. **Bailar, J. C., III,** Mammographic screening: a reappraisal of benefits and risks, *Clin. Obstet. Gynecol.,* 21, 1, 1978.

34. **Bailar, J. C., III,** Radiation harzards of X-ray mammography, in *Late Biological Effects of Ionizing Radiation,* Vol. 1, International Atomic Energy Agency, Vienna, 1978, 251.

35. **Bailar, J. C., III,** Mammography before age 50 years?, *JAMA,* 259, 1548, 1988.

36. **Bain, C., Speizer, F. E., Rosner, B., Belanger, C., and Hennekens, C. H.,** Family history of breast cancer as a risk indicator for the disease, *Am. J. Epidemiol.,* 111, 301, 1980.

37. **Bain, C., Willett, W., Rosner, B., Speizer, F. E., Belanger, C., and Hennekens, C. H.,** Early age at first birth and decreased risk of breast cancer, *Am. J. Epidemiol.,* 114, 705, 1981.

38. **Baines, C. J.,** Some thoughts on why women do not do breast self-examination, *Can. Med. Assoc. J.,* 128, 255, 1983.

39. **Baines, C. J., Miller, A. B., Wall, C., McFarlane, D. V., Simor, I. S., Jong, R., Shapiro, B. J., Audet, L., Petitclerc, M., Ouimet-Oliva, D.,** Sensitivity and specificity of first screen mammography in the Canadian National Breast Screening Study: preliminary report from five centers, *Radiology,* 160, 295, 1986.

40. **Baker, L. H.,** Breast cancer detection demonstration projects: five-year summary report, *CA,* 32, 194, 1982.

41. **Baker, S. R.,** Comments on "screening mammography—potential problems on the horizon," *Invest. Radiol.,* 21, 891, 1986.

42. **Bamber, J. C., Sambrrok, M., Minasian, H., and Hill, C. R.,** Doppler study of blood flow in breast cancer, in *Ultrasonic Examination of the Breast,* Jellins, J. and Kobayashi, T., Eds., John Wiley & Sons, Chichester, 1983, 371.

43. **Barnes, G.T.,** Characteristics of scatter, in *Reduced Dose Mammography,* Logan, W. W. and Muntz, E. P., Eds., Masson, New York, 1979, 223.

44. **Barnes, G. T. and Brezovich, I. A.,** Contrast: effect of scattered radiation, in *Breast Carcinoma — the Radiologist's Expanded Role,* John Wiley & Sons, New York, 1977, 73.

45. **Barnes, G. T. and Brezovich, I. A.,** The intensity of scattered radiation in mammography, *Radiology,* 126, 243, 1978.
46. **Barnes, G. T. and Brezovich, I. A.,** The design and performance of a scanning multiple slit assembly, *Med. Phys.,* 6, 197, 1979.
47. **Barnes, G. T., Cleare, H. M., and Brezovich, I. A.,** Reduction of scatter in diagnostic radiology by means of a scanning multiple slit assembly, *Radiology,* 120, 691, 1976.
48. **Barrett, H. H. and Swindell, W.,** *Radiological Imaging: the Theory of Imaging Formation, Detection, and Processing,* Academic Press, New York, 1981.
49. **Barrett, A. H., Myers. P. C., and Sadowsky, N. L.,** Microwave thermography in the detection of breast cancer, *Am. J. Roentgenol.,* 134, 365, 1980.
50. **Bartrum, R. J., Jr. and Crow, H. C.,** Transillumination light scanning to diagnose breast cancer: a feasibility study, *Am. J. Roentgenol.,* 142, 409, 1984.
51. **Bassett, L. W. and Gold, R. H., Eds.,** *Mammography, Thermography, and Ultrasound in Breast Cancer Detection,* Grune & Stratton, New York, 1982.
52. **Bassett, L. W. and Gold, R. H., Eds.,** *Breast Cancer Detection: Mammography and Other Methods in Breast Imaging,* 2nd ed., Grune & Stratton, Orlando, 1987.
53. **Bassett, M. T. and Kreiger, N.,** Social class and black-white differences in breast cancer survival, *Am. J. Public Health,* 76, 1400, 1986.
54. **Bassett, L. W., Arnold, B. A., Borger, D., Eisenberg, H. C., Gold, R. H., Mahn, G. R., and Holland, W. P.,** Reduced dose magnification mammography, *Radiology,* 141, 665, 1981.
55. **Bassett, L. W., Bunnell, D. H., Cerny, J. A., and Gold, R. H.,** Screening mammography: a survey of 4200 referring physicians, *Radiology,* 157(P), 53, 1985.
56. **Bassett, L. W., Bunnell, D. H., Cerny, J. A., and Gold, R. H.,** Screening mammography: referral practices of Los Angeles physicians, *Am. J. Roentgenol.,* 147, 689, 1986.
57. **Bassett, L. W., Bunnell, D. H., Jahanshani, R., Gold, R. H., Arndt, R. D., and Linsman, J.,** Breast cancer detection: one versus two views, *Radiology,* 165, 95, 1987.
58. **Bassett, L. W., Diamond, J. J., Gold, R. H., and McLelland, R.,** Survey of mammography practices, *Am. J. Roentgenol.,* 149, 1149, 1987.
59. **Battista, R. N.,** Adult cancer prevention in primary care: patterns of practice in Quebec, *Am. J. Public Health,* 73, 1036, 1983.
60. **Baum, M.,** *Breast Cancer: the Facts,* Oxford University Press, Oxford, 1981.
61. **Beahrs, O. H., Shapiro, S., and Smart, C.,** Report of the working group to review the National Cancer Institute American Cancer Society Breast Cancer Detection Demonstration Projects, *J. Natl. Cancer Inst.,* 62, 639, 1979.
62. **Beijerinck, D., Rombach, J. J., Collette, H. J. A., and de Waard, F.,** Mammography screening in women under age 50 years, *JAMA,* 260, 475, 1988.
63. **Bennett, S. E., Lawrence, R. S., Fleisch-Mann, K. H., Gifford, C. S., and Slack, W. V.,** Profile of women practicing breast self-examination, *JAMA,* 249, 488, 1983.
64. **Berg, J. W.,** Clinical implications of risk factors for breast cancer, *Cancer,* 53, 589, 1984.
65. **Berkowitz, G. S.,** Risk factors, in *Breast Disease,* Marchant, D. J., Ed., Churchill Livingstone, New York, 1986, 13.
66. **Berlin, N. I.,** Breast cancer screening: the case for screening women younger than 50 years, *JAMA,* 245, 1060, 1981.
67. **Bernstein, L., Ross, R. K., Lobo, R. A., Hanisch, R., Krailo, M. D., and Henderson, B. E.,** The effects of moderate physical activity on menstrual cycle patterns in adolescence: implications for breast cancer prevention, *Br. J. Cancer,* 55, 681, 1987.
68. **Betsill, W. L., Rosen, P. P., Leiberman, P. H., and Robbins, G. F.,** Intraductal carcinoma: long-term follow-up after treatment by biopsy alone, *JAMA,* 239, 1863, 1978.
69. **Bews, J.,** The Optical Properties of Biological Tissue, Ph.D. dissertation, Department of Physics, The University of Manitoba, 1988.
70. **Biberman, L. M., Ed.,** *Perception of Displayed Information,* Plenum Press, New York, 1973.
71. **Bird, R. E. and McLelland, R.,** How to initiate and operate a low-cost screening mammography center, *Radiology,* 161, 43, 1986.
72. **Bjorkholm, P. J., Annis, M., and Frederick, E. E.,** Digital radiography, in *Application of Optical Instrumentation in Medicine,* Vol. 8, Gray, J., Haus, A. G., Hendee, W. R., and Properzio, W. S., Eds., SPIE, Bellingham, WA, 1980, 137.
73. **Bjornsson, S., Brekkan, A., and Tulinius, H.,** Mass screening for breast cancer, *Scand. J. Soc. Med.,* 14, 3, 1987.
74. **Bjurstam, N.,** The value of mammography in estimating the prognosis for patients with breast cancer, *Recent Results Cancer Res.,* 90, 173, 1984.
75. **Bland, K. I., Buchana, J. B., Mills, D. L., Kuhns, J. G., Moore, C., Spratt, J. S., and Polk, H. C.,** Analysis of breast cancer screening in women younger than 50 years, *JAMA,* 245, 1037, 1981.

76. **Block, R. W., Flynn, M. J., Ackerman, L. V., Watt, A. C., Erich, D. A., and Ressler, C. J.**, New device for positioning the breast during angiography, *Radiology*, 155, 824, 1985.

77. **Blot, W. J., Fraumeni, J. F., Jr., and Stone, B. J.**, Geographic patterns of breast cancer in the United States, *J. Natl. Cancer Inst.*, 59, 1407, 1977.

78. **Boice, J. D., Jr. and Monson, R. R.**, Breast cancer in women after repeated fluoroscopic examinations of the chest, *J. Natl. Cancer Inst.*, 59, 823, 1977.

79. **Bonar, D. C.**, Dose efficiency improvement by rotating adjustable apertures in an image intensifer X-ray diagnostic system, in *Digital Radiography*, Brody, W. R., Ed., SPIE, Bellingham, Washington, 1981, 81.

80. **Brillouin, L.**, *Science and Information Theory*, 2nd ed., New York, Academic Press, 1962.

81. **Brinkley, D. and Haybrittle, J. L.**, The curability of breast cancer, *Lancet*, 2, 95, 1975.

82. **Brinton, L. A., Williams, R. R., Hoover, R. N., Stegens, N. L., Feinleib, M., and Fraumeni, J. F., Jr.**, Breast cancer risk factors among screening program participants, *J. Natl. Cancer Inst.*, 62, 37, 1979.

83. **Brinton, L. A., Hoover, R., and Fraumeni, J. F., Jr.**, Reproductive factors in the aetiology of breast cancer, *Br. J. Cancer*, 47, 757, 1983.

84. **Broadbent, R. V. and Reid, M. H.**, Mammography — misunderstood and underutilized, *Postgrad. Med.*, 7, 93, 1981.

85. **Brodie, I. and Gutcheck, R. A.**, Radiographic information theory and application to mammography, *Med. Phys.*, 9, 79, 1982.

86. **Brody, W. R.**, *Digital Radiography*, Raven Press, New York, 1983.

87. **Brolin, R. E.**, Mammography screening in women under age 50 years, *JAMA*, 260, 475, 1989.

88. **Brooks, P. G.**, The current status of stress telethermometry in the detection and monitoring of breast disease, in *Current Controversies in Breast Cancer*, Ames, F. C., Blumenschein, G. R., and Montague, E. D., Eds., University of Texas Press, Austin, 1984, 573.

89. **Bruneton, J. N., Caramella, E., Hery, M., Aubanel, D., Manzino, J. J., and Picard, J. L.**, Axillary lymph node metastases in breast cancer: preoperative detection with US, *Radiology*, 158, 325, 1986.

90. **Bruton, L. T. and Bartley, N. R.**, Highly selective three dimensional recursive beam filters using intersecting resonant planes, *IEEE Trans. Circuits Sys.*, CAS-30, 190, 1983.

91. **Buchanan, J. B. and Jager, R. M.**, Single view negative mode xeromammography: an approach to reduce radiation exposure in breast cancer screening, *Radiology*, 123, 63, 1977.

92. **Buchanan, J. B., Spratt, J. S., and Heuser, L. S.**, Tumor growth, doubling time, and the inability of the radiologist to diagnose certain cancers, *Radiol. Clin. North. Am.*, 21, 115, 1983.

93. **Buell, P.**, Changing incidence of breast cancer in Japanese-American women, *J. Natl. Cancer Inst.*, 51, 1479, 1973.

94. **Bunnell, D. H., Bassett, L. W., Jahnshani, R., Gold, R. H., Arndt, R., and Linsman, J.**, Breast radiology: single- versus two-view mammography, *Radiology*, 161(P), 178, 1986.

95. **Burns, P. E., Lees, A. W., Hurlburt, M. E., May, C. L., and Grace, M.**, Reproductive events and family history as risk factors for breast cancer in northern Alberta, *Can. Med. Assoc. J.*, 124, 1451, 1981.

96. **Canadian Cancer Society**, *Facts on Breast Cancer*, Canadian Cancer Society Press, Waterloo, Ontario, 1982.

97. **Chan, H. P., Sepahdari, S., and Doi, K.**, Physical and clinical evaluation of ultra-high strip-density grids in mammography, *Radiology*, 149(P), 277, 1983.

98. **Chandrasekhar, S.**, *Radiative Transfer*, Dover Publications, New York, 1960.

99. **Chang, C. H. J., Sibala, J. L., Martin, N. L., and Riley, R. C.**, Film mammography: new low radiation technology, *Radiology*, 121, 215, 1976.

100. **Chang, C.H. J., Sibala, J. L., Gallagher, J. H., Riley, R. C., Templeton, A. W., Beasley, P. V., and Porte, R. A.**, Computed tomography of the breast: a preliminary report, *Radiology*, 124, 827, 1977.

101. **Chang, C. H. J., Sibala, J. L., Fritz, S. L., Gallagher, J. H., Dwyer, S. J., III, and Templeton, A. W.**, Computed tomographic evaluation of the breast, *Am. J. Roentgenol.*, 131, 459, 1978.

102. **Chang, C. H. J., Sibala, J. L., Lin, F., Jewell, W. R., and Templeton, A. W.**, Preoperative diagnosis of potentially precancerous breast lesions by computed tomography breast scanner: preliminary study, *Radiology*, 129, 209, 1978.

103. **Chang, C. H. J., Sibala, J. L., Fritz, S. L., Dwyer, S. J., III, and Templeton, A. W.**, Specific value of computed tomographic breast scanner (CT/M) in diagnosis of breast diseases, *Radiology*, 132, 647, 1979.

104. **Chang, C. H. J., Sibala, J. L., Fritz, S. L., Dwyer, S. J., III, Templeton, A. W., Lin, F., and Jewell, W. R.**, Computed tomography in detection and diagnosis of breast cancer, *Cancer*, 46, 939, 1980.

105. **Chang, C. H. J., Nesbit, D. E., Fisher, D. R., Fritz, S. L., Dwyer, S. L., III, Templeton, A. W., Lin, F., and Jewell, W. R.**, Computed tomographic mammography using a conventional body scanner, *Am. J. Roentgenol.*, 138, 553, 1982.

106. **Chang, C. H. J., Fritz, S. L., Dwyer, S. J., III, Templeton, A. W., Gupta, N. K., Kirchmer, N. A., and Martin, N. L.**, Digital mammography: a new application of technology in breast imaging, *Radiology*, 149(P), 277, 1983.

107. Chavel, P. and Lowenthal, S., Noise and coherence in optical image processing. I. The Callier effect and its influence on image contrast, *J. Opt. Soc. Am.*, 68, 559, 1978.

108. Chavel, P. and Lowenthal, S., Film grain noise in partially coherent imaging, *Opt. Eng.*, 19, 404, 1980.

109. Choi, N. W., Howe, G. R., Miller, A. B., Mathews, V., Morgan, R. W., Munan, L., Burch, J. D., Feather, J., Jain, M., and Kelly, A., An epidemiologic study of breast cancer, *Am. J. Epidemiol.*, 107, 510, 1978.

110. Chu, K. C., Smart, C. R., and Tarone, R. E., Analysis of breast cancer mortality and stage distribution by age for the Health Insurance Plan clinical trial, *J. Natl. Cancer Inst.*, 80, 1125, 1988.

111. Ciatto, S., Cataliotti, L., and Distante, V., Nonpalpable lesions detected with mammography: review of 512 consecutive cases, *Radiology*, 165, 99, 1987.

112. Clark, R. C., Copeland, M. M., Egan, R. L., Gallager, H. S., Geller, H., Lindsay, J. P., Robins, L. C., and White, E. C., Reproducibility of the technique of mammography (Egan) for cancer of the breast, *Am. J. Surg.*, 109, 127, 1965.

113. Cole-Beuglet, C., Ultrasound, in *Breast Cancer Detection: Mammography and Other Methods in Breast Imaging*, 2nd ed., Bassett, L. W. and Gold, R. H., Eds., Grune & Straton, Orlando, 1987, 153.

114. Cole-Beuglet, C., Goldberg, B. B., Kurtz, A. B., Patchefsky, A. S., and Shaber, G. S., Ultrasound mammography: a comparison with radiographic mammography, *Radiology*, 139, 693, 1981.

115. Cole-Beuglet, C., Goldberg, B. B., Kurtz, A. B., Patchefsky, A. S., Shaber, G. S., and Rubin, C. S., Clinical experience with a prototype real-time dedicated breast scanner, *Am. J. Roentgenol.*, 139, 905, 1982.

116. Cole-Beuglet, C., Schwartz, G., Kurtz, A. B., Patchefsky, A. S., and Goldberg, B. B., Ultrasound mammography for the augmented breast, *Radiology*, 146, 737, 1983.

117. Collette, H. J. A., Rombach, J. J., Day, N. E., and de Waard, F., Evaluation of screening for breast cancer in a non-randomized study (the DOM Project) by means of a case-control study, *Lancet*, 1, 1224, 1984.

118. Coleman, J., Menzel, H., and Katz, E., Social processes in physicians' adoption of a new drug, *J. Chronic Dis.*, 9, 1, 1959.

119. Cook, H. M. and Fox, M. D., Artificial intelligence applied to mammographic image analysis, presented at the Electronic Imaging '87 Conference, November 2 to 5, 1987, Boston, MA.

120. Council on Scientific Affairs of American Medical Association, Early detection of breast cancer, *JAMA*, 252, 3008, 1984.

121. Culliton, B. J., Mammography controversy: NIH's entree into evaluating technology, *Science*, 198, 171, 1977.

122. Culliton, B. J., Cancer Institute unilaterally issues new restrictions on mammography, *Science*, 196, 853, 1977.

123. Cummings, K. M., Funch, D. P., Mettlin, C., and Jennings, E., Family physicians' beliefs about breast cancer screening by mammography, *J. Fam. Pract.*, 17, 1029, 1983.

124. Cutler, M., Transillumination as an aid in the diagnosis of breast lesions, with special reference to its value in cases of bleeding nipple, *Surg. Gynecol. Obstet.*, 48, 721, 1929.

125. Cutler, S. J., Devesa, S. S., and Barclay, T. H. C., The magnitude of the breast cancer problem, *Recent Results Cancer Res.*, 57, 1, 1976.

126. Cuzick, J., Wang, D. Y., and Bulbrook, R. D., The prevention of breast cancer, *Lancet*, 1, 83, 1986.

127. Dash, N., Lupetin, A. R., Daffner, R. H., Deeb, Z. L., Sefczek, R. J., and Schapiro, R. L., Magnetic resonance imaging in the diagnosis of breast diseases, *Am. J. Roentgenol.*, 146, 119, 1986.

128. Day, N. E., Baines, C. J., Chamberlain, J., Hakama, M., Miller, A. B., and Prorok, P., UICC Project on Screening for Cancer: report of the workshop on screening for breast cancer, *Int. J. Cancer*, 38, 303, 1986.

129. de Paredes, S. E., Frazier, A. B., Hartwell, G. D., Strash, A. M., Scheer, C., Smith, D. C., Barnette, P. A., Noel, W., and Kenneweg, D., Development and implementation of a quality assurance program for mammography, *Radiology*, 163, 83, 1987.

130. Dershaw, D. D., Male mammography, *Am. J. Roentgenol.*, 146, 127, 1986.

131. Dershaw, D. D., Masterson, M. E., Malik, S., and Cruz, N. M., Mammography using an ultrahigh-strip-density, stationary, focused grid, *Radiology*, 156, 541, 1985.

132. Devere, C., Current status of ultrasonic breast scanning, *Appl. Radiol.*, 9, 145, 1980.

133. Devesa, S. S. and Diamond, E. L., Association of breast cancer and cervical cancer incidences with income and education among whites and blacks, *J. Natl. Cancer Inst.*, 65, 515, 1980.

134. Devitt, J. E. and Miller, A. B., Dialogue: mammography, a surgeon's experience, an epidemiologist's critique, the surgeon's reply, *Can. Med. Assoc. J.*, 120, 1370, 1979

135. de Waard, F., Premenopausal and postmenopausal breast cancer: one disease or two?, *J. Natl. Cancer Inst.*, 63, 549, 1979.

136. de Waard, F., Collette, H. J., Rombach, J. J., Baanders-van Halewijn, E. A., and Honig, C., The DOM Project for the early detection of breast cancer, Utrecht, The Netherlands, *J. Chronic Dis.*, 37, 1, 1984.

137. **de Waard, F., Cornelis, J. P., Aoki, K., and Yoshida, M.,** Breast cancer incidence according to weight and height in two cities in the Netherlands and in Aichi Prefecture, Japan, *Cancer*, 40, 1269, 1977.

138. **Dhawan, A. P. and Gordon, R.,** Reply to comments on "Enhancement of mammographic features by optimal adaptive neighborhood image processing," *IEEE Trans. Med. Imaging*, MI-6, 82, 1987.

139. **Dhawan, A. P., Gordon, R., and Rangayyan, R. M.,** Nevoscopy: three dimensional computed tomography for nevi and melanomas in situ by transillumination, *IEEE Trans. Med. Imaging*, MI-3, 54, 1984.

140. **Dhawan, A. P., Rangayyan, R. M., and Gordon, R.,** Image restoration by Wiener deconvolution in imited-view computed tomography, *Appl. Opt.*, 24, 4013, 1985.

141. **Dhawan, A. P. and Le Royer, E.,** Mammographic feature enhancement by computerized image processing, *Comput. Methods Programs Biomed.*, 27, 23, 1988.

142. **Dhawan, A. P., Buelloni, G., and Gordon, R.,** Enhancement of mammographic features by optimal adaptive neighborhood image processing, *IEEE Trans. Med. Imaging*, MI-5, 8, 1986 (Errata: MI-5, 120, 1986).

143. **Dhawan, A. P., Le Royer, E., and Gordon, R.,** Adaptive neighborhood image processing for feature enhancement of film-mammograms, *Proc IEEE 8th Annu. Conf. Eng. Med. Biol. Soc.*, 1096, 1986.

144. **Dixon, G. D.,** Preoperative computed-tomographic localization of breast calcifications, *Radiology*, 146, 836, 1983.

145. **Dobin, R., Skolnik, L., and Taylor, R.,** New detector system for high-resolution dynamic medical thermographic diagnosis, in *Application of Optical Instrumentation in Medicine*, Vol. 7, Gray, J., Ed., SPIE, Bellingham, WA, 1979, 148.

146. **Dodd, G. D.,** Radiation detection and diagnosis of breast cancer, *Cancer*, 47, 1766, 1981.

147. **Dodd, G. D.,** Heat-sensing devices and breast cancer detection, in *Breast Carcinoma: Current Diagnosis and Treatment*, Feig, S. A. and McLelland, R., Eds., ACR and Masson, New York, 1983, 207.

148. **Dodd, G. D.,** The continuing challenge of mammography, *CA*, 34, 57, 1984.

149. **Dodd, G. D.,** Mammography: state of the art, *Cancer*, 53, 652, 1984.

150. **Doi, K.,** Advantages of magnification radiography, in *Breast Carcinoma: the Radiologist's Expanded Role*, Logan, W. W., Ed., John Wiley & Sons, New York, 1977, 83.

151. **Doi, K., Genant, H. K., and Rossmann, K.,** Comparison of image quality obtained with optical and radiographic magnification techniques in fine-detail skeletal radiography: effect of object thickness, *Radiology*, 118, 189, 1976.

152. **Donegan, W. L.,** Diagnosis, in *Cancer of the Breast*, 3rd ed., W. B. Saunders, Philadelphia, 1988, 125.

153. **Donegan, W. L. and Spratt, J. S., Eds.,** *Cancer of the Breast*, 3rd ed., W. B. Saunders, Philadelphia, 1988.

154. **Dorsay, R. H., Cuneo, W. D., Somkin, C. P., and Tekawa, I. S.,** Breast self-examination: improving competence and frequency in a classroom setting, *Am. J. Public Health*, 78, 520, 1988.

155. **Drexler, B., Davis, J. L. and Schofield, G.,** Diaphanography in the diagnosis of breast cancer, *Radiology*, 157, 41, 1985.

156. **Dronkers, D. J. and van der Zwaag, H.,** Photographic contrast enhancement in mammography, *Radiol. Clin. Biol.*, 43, 521, 1974.

157. **Eddy, D. M., Hasselblad, V., McGivney, W., and Hendee, W.,** The value of mammography screening in women under age 50 years, *JAMA*, 259, 1512, 1988.

158. **Eddy, D. M., Hasselblad, V., McGivney, W., and Hendee, W.,** Mammography screening in women under age 50 years, *JAMA*, 260, 475, 1988.

159. **Egan, R. L.,** Experience with mammography in a tumor institute: evaluation of 1000 studies, *Radiology*, 75, 894, 1960.

160. **Egan, R. L.,** Mammography and breast diseases, in *Golden's Diagnostic Radiology*, Robbins, L. L., Ed., Williams & Wilkins, Baltimore, MD, 1970, Sect. 19.

161. **Egan, R. L.,** *Mammography*, 2nd ed. Charles C Thomas, Springfield, IL, 1972.

162. **Egan, R. L.,** Mammographic image quality and exposure levels using conventional generators and type M film, *Appl. Opt. Instrum. Med.*, 7, 393, 1975.

163. **Egan, R. L.,** *Breast Imaging*, 3rd ed., University Park Press, Baltimore, 1984.

164. **Egan, R. L.,** *Breast Imaging: Diagnosis and Morphology of Breast Diseases*, W. B. Saunders, Philadelphia, 1988.

165. **Egan, R. L. and Egan, K. L.,** Detection of breast carcinoma: comparison of automated water path whole breast sonography, mammography, and physical examination, *Am. J. Roentgenol.*, 143, 493, 1984.

166. **Egan, R. L. and Fenn, J. O.,** Phantoms for evaluating mammography techniques and roentgenographic detail, *Am. J. Roentgenol.*, 102, 936, 1968.

167. **Egan, R. L., McSweeney, M. B., and Sewell, C. W.,** Intramammary calcifications without an associated mass in benign and malignant diseases, *Radiology*, 137, 1, 1980.

168. **Egan, R. L., McSweeney, M. B., and Sprawls, P.,** Grids in mammography, *Radiology*, 146, 359, 1983.

169. **Egan, R. L., McSweeney, M. B., and Murphy, F. B.,** Breast sonography and the detection of cancer, *Recent Results Cancer Res.*, 90, 90, 1984.

170. **Eklund, G. W.,** Innovations in mammographic compression, *Am. J. Roentgenol.,* 150, 791, 1988.

171. **El Yousef, S. J., Alfidi, R. J., Duchesneau, R. H., Hubay, C. A., Haaga, J. R., Bryan, P. J., LiPuma, J. P., and Ament, A. E.,** Initial experience with nuclear magnetic resonance (NMR) imaging of the human breast, *J. Comput. Assist. Tomogr.,* 7, 215, 1983.

172. **El Yousef, S. J. and Duchesneau, R. H.,** Magnetic resonance imaging of the human breast: a phase I trial, *Radiol. Clin. North Am.,* 22, 859, 1984.

173. **El Yousef, S. J., Duchesneau, R. H., Alfidi, R. J., Haaga, J. R., Bryan, P. J., and LiPuma, J. P.,** Magnetic resonance imaging of the breast, *Radiology,* 150, 761, 1984.

174. **El Yousef, S. J., O'Connell, D. M., Duchesneau, R. H., Smith, M. J., Hubay, C. A., and Guyton, S. P.,** Benign and malignant breast disease: magnetic resonance and radiofrequency pulse sequences, *Am. J. Roentgenol.,* 145, 1, 1985.

175. **Evans, K. T. and Gravelle, I. H.,** Mammography, thermography and ultrasonography in breast disease, in *Radiology in Clinical Diagnosis,* Trapnell, D. H., Ed., Butterworths, London, 1973.

176. **Fagerberg, G., Baldetorp, L., Grontoft, O., Lundstrom, B., Manson, J. C., and Nordenskjold, B.,** Effects of repeated mammographic screening on breast cancer stage distribution. Results from a randomized study of 92,934 women in a Swedish county, *Acta Radiol.* [Oncol.], 24, 465, 1985.

177. **Feig, S. A.,** Low-dose mammography: application to medical practice, *JAMA,* 242, 2107, 1979.

178. **Feig, S. A.,** Low-dose mammography: assessment of theoretical risk, in *Breast Carcinoma: Current Diagnosis and Treatment,* Feig, S.A. and McLelland, R., Eds., ACR and Masson, New York, 1983, 69.

179. **Feig, S. A.,** Assessment of the hypothetical risk from mammography and evaluation of the potential benefit, *Radiol. Clin. North Am.,* 21, 173, 1983.

180. **Feig, S. A.,** Radiation risk from mammography: is it clinically significant?, *Am. J. Roentgenol.,* 143, 469, 1984.

181. **Feig, S. A.,** Benefits and risks of mammography, *Recent Results Cancer Res.,* 90, 11, 1984.

182. **Feig, S. A.,** Projected benefits and risks from mammographic screening, *Recent Results Cancer Res.,* 105, 85, 1987.

183. **Feig, S. A.,** The importance of supplementary mammographic views to diagnostic accuracy, *Am. J. Roentgenol.,* 151, 40, 1988.

184. **Feig, S. A.,** Decreased breast cancer mortality through mammographic screening: results of clinical trials, *Radiology,* 167, 659, 1988.

185. **Feig, S. A., and Schwartz, G. F.,** Radiologic technique for biopsy of nonpalpable breast lesions, in *Breast Carcinoma: Current Diagnosis and Treatment,* Feig, S. A. and McLelland, R., Eds., ACR and Masson, New York, 1983, 265.

186. **Feig, S. A., Schwartz, F., Nerlinger, R., and Edeiken, J.,** Prognostic factors of breast neoplasms detected on screening by mammography and physical examination, *Radiology,* 133, 577, 1979.

187. **Feldman, J. G. Carter, A. C., Nicastri, A.D., and Hosat, S. T.,** Breast self-examination, relationship to stage of breast cancer at diagnosis, *Cancer,* 47, 2740, 1981.

188. **Fewell, T. R. and Shuping, R. E.,** A comparison of mammographic X-ray spectra, *Radiology,* 128, 211, 1978.

189. **Flamm, M. B.,** Mammography screening in women under age 50 years, *JAMA,* 260, 474, 1988.

190. **Flannery, B. P., Deckman, H. W., Roberge, W. G., and D'Amico, K. L.,** Three-dimensional X-ray microtomography, *Science,* 237, 1439, 1987.

191. **Fleischner, A. C., Muhletaler, C. A., Reynolds, V. H., Machin, J. E., Thieme, G. A., Bundy, A. L., Winfield, A. C., and James, A. E.,** Palpable breast masses: evaluation by high frequency, hand-held real-time sonography and xeromammography, *Radiology,* 148, 813, 1983.

192. **Flynn, M. J., Ackerman, L., Wilderman, S., Block, R., Watt, C., Rurke, M., and Shetty, P. C.,** Digital subtraction angiography (DSA) techniques for the evaluation of breast lesions, in *Medical Imaging and Instrumentation '84,* Mulvaney, J. A., Ed., SPIE, Bellingham, WA, 1984, 129.

193. **Foss, O. P., Brennhovd, I. O., Messelt, O. T., Efskind, J., and Liverud, K.,** Invasion of tumor cells into the blood-stream caused by palpation or biopsy of tumor, *Surgery,* 59, 691, 1966.

194. **Foster, H. D.,** *Reducing Cancer Mortality; A Geographical Perspective,* University of Victoria Press, Victoria, Canada, 1986.

195. **Foster, R. S., Jr. and Costanza, M. C.,** Breast self-examination practices and breast cancer survival, *Cancer,* 53, 999, 1984.

196. **Fox, S., Moskowitz, M., Saenger, E. L., Kereiakes, J. G., Milbrath, J., and Goodman, M. W.,** Benefit-risk analysis of aggressive mammographic screening, *Radiology,* 128, 359, 1978.

197. **Fox, S., Baum, J. K., Klos, D. S., and Tsou, C. V.,** Breast cancer screening: the underuse of mammography, *Radiology,* 156, 607, 1985.

198. **Fox, S., Klos, D. S., and Tsou, C. V.,** Underuse of screening mammography by family physicians, *Radiology,* 166, 431, 1988.

199. **Frankl, G.,** Xeromammography: the perils and the promise, *Radiology,* 153(P), 129, 1984.

200. **Fraumeni, J. F., Jr., Lloyd, J. W., Smith, E. M., and Wagoner, J. K.,** Cancer mortality among nuns: role of marital status in etiology of neoplastic disease in women, *J. Natl. Cancer Inst.,* 42, 455, 1969.

201. **Frazier, T. G., Copeland, E. M., Gallager, H. S., Paulus, D. D., Jr., and White, E. C.,** Prognosis and treatment in minimal breast cancer, *Am. J. Surg.,* 133, 697, 1977.

202. **Frieden, B. R. and Zoltani, C. K.,** Maximum bounded entropy: application to tomographic reconstruction, *Appl. Opt.,* 24, 3993, 1985.

203. **Fritz, S. L., Chang, C. H. J., Gupta, N. K., Martin, N. L., Laws, R. L., Anderson, W. H., Dwyer, S. J., III, Templeton, A. W., Bernardi, R., and Fox, T.,** A digital radiographic imaging system for mammography, *Invest. Radiol.,* 21, 581, 1986.

204. **Frost, M. M., Nudelman, S., Ovitt, T. W., Roehrig, H., Capp, M. P., Fisher, H., and Ouimette, D.,** Digital acquisition system for photo-electronic radiology — a performance overview, in *Application of Optical Instrumentation in Medicine,* Vol. 8, Gray, J., Haus, A. G., Hendee, W. R., and Properzio, W. S., Eds., SPIE, Bellingham, WA, 1980, 54.

205. **Gad, A., Thomas, B. A., and Moskowitz, M.,** Screening for breast cancer in Europe: achievements, problems and future, *Recent Results Cancer Res.,* 90, 179, 1984.

206. **Gale, A. G., Roebuck, E. J., Riley, P., and Worthington, B. S.,** Computer aids to mammographic diagnosis, *Br. J. Radiol.,* 60, 887, 1987.

207. **Gallager, H. S.,** Minimal breast cancer: origin of concept and definition, in *Breast Carcinoma: Current Diagnosis and Treatment,* Feig, S. A. and McLelland, R., Eds., ACR and Masson, New York, 1983, 251.

208. **Gallager, H. S.,** Minimal breast cancer: results of treatment and long-term follow-up, in *Breast Carcinoma: Current Diagnosis and Treatment,* Feig, S. A. and McLelland, R., Eds., ACR and Masson, New York, 1983, 291.

209. **Gallager, H. S.,** Problems in the classification of breast cancer, *Radiol. Clin. North Am.,* 21, 13, 1983.

210. **Gallager, H. S.,** Pathology of breast cancer, in *The 1984 Categorical Course in Breast Cancer,* Levitt, S. H., Ed., Radiology Society of North America, Minneapolis, 1984, 118.

211. **Gallager, H. S.,** Minimal breast cancer: definition and prognosis, in *Current Controversies in Breast Cancer,* Ames, F. C., Blumenschein, G. R., and Montague, E. D., Eds., University of Texas Press, Austin, 1984, 79.

212. **Gallager, H. S. and Martin, J. E.,** Early phases in the development of breast cancer, *Cancer,* 24, 1170, 1969.

213. **Gallager, H. S. and Martin, J. E.,** An orientation to the concept of minimal breast cancer, *Cancer,* 28, 1519, 1971.

214. **Gaskill, S. P., McGuire, W. L., Osborne, C. K., and Stern, M. P.,** Breast cancer mortality and diet in the United States, *Cancer Res.,* 39, 3628, 1979.

215. **Gastrin, G.,** Self-examination in early detection of breast cancer: is it effective?, *Recent Results Cancer Res.,* 105, 106, 1987.

216. **Genant, H. K., Doi, K., and Mall, J. C.,** Optical versus radiographic magnification for fine-detail skeletal radiography, *Invest. Radiol.,* 10, 160, 1975.

217. **Gershon-Cohen, J., Hermel, M. B., and Birsner, J. W.,** Advances in mammographic techniques, *Am. J. Roentgenol.,* 108, 424, 1970.

218. **Geslien, G. E., Fisher, J. R., and DeLaney, C.,** Transillumination in breast cancer detection: screening failures and potential, *Am. J. Roentgenol.,* 144, 619, 1985.

219. **Gisvold, J. J., Karsell, P. R., and Reese, D. F.,** Computerized tomographic mammography, in *Breast Carcinoma: the Radiologist's Expanded Role,* Logan, W. W., Ed., John Wiley & Sons, New York, 1977, 219.

220. **Gisvold, J. J., Reese, D. F., and Karsell, P. R.,** Computed tomographic mammography (CTM), *Am. J. Roentgenol.,* 133, 1143, 1979.

221. **Gisvold, J. J., Brown, L.R., Swee, R. G., Raygor, D. J., Dickerson, N., and Ranfranz, M. K.,** Comparison of mammography and transillumination light scanning in the detection of breast lesions, *Am. J. Roentgenol.,* 147, 191, 1986.

222. **Gohagan, J. K., Rodes, N. D., Blackwell, C. W., Darby, W. P., Farrell, C., Herder, T., Pearson, D. K., Spitznagel, E. L., and Wallace, M. D.,** Individual and combined effectiveness of palpation, thermography, and mammography in breast cancer screening, *Prev. Med.,* 9, 713, 1980.

223. **Goin, J. E. and Haberman, J. D.,** Automated breast cancer detection by thermography: performance goal and diagnostic feature identification, *Pattern Recog.,* 16, 125, 1983.

224. **Gold, R. H. and Bassett, L. W.,** Mammography: history and state of the art, in *Breast Carcinoma: Current Diagnosis and Treatment,* Feig, S. A. and McLelland, R., Eds., ACR and Masson, New York, 1983, 95.

225. **Gold, R. H., Bassett, L. W., and Kimme-Smith, C.,** Breast imaging: state-of-the-art, *Invest. Radiol.,* 21, 298, 1986.

226. **Gold, R. H., Sickles, E. A., Bassett, L. W., McSweeney, M., Feig, S. A., and Milbrath, J. R.,** Diagnostic imaging of the breast, *Invest. Radiol.,* 19(Suppl.), S43, 1984.

227. **Goldberg, M., Robertson, J., and Belanger, G.,** Evaluating digital radiology imaging requirements by diagnostic reporting, *Proc. SPIE,* 914, 1225, 1988.

228. **Goldsmith, M., Koutcher, J. A., and Damadian, R.,** NMR in cancer. XIII. Application of the NMR malignancy index to human mammary tumors, *Br. J. Cancer,* 38, 547, 1978.

229. **Gordon, R.,** Dose reduction in computerized tomography (guest editorial), *Invest. Radiol.,* 11, 508, 1976.

230. **Gordon, R.,** High speed reconstruction of the finest details available in X-ray projections, in *Reconstruction Tomography in Diagnostic Radiology and Nuclear Medicine,* Ter-Pogossian, M. M., Phelps, M. E., and Brownell, G. L., Eds., University Park Press, Baltimore, 1977, 77.

231. **Gordon, R.,** Feedback control of exposure geometry in dental radiography workshop, *Appl. Opt.,* 18, 1769, 1979.

232. **Gordon, R.,** Toward robotic X-ray vision: new directions for computed tomography, *Appl. Opt.,* 24, 4124, 1985.

233. **Gordon, R. and Coumans, J.,** Combining multiple imaging techniques for *in vivo* pathology; a quantitative method for coupling new imaging modalities, *Med. Phys.,* 11, 79, 1984.

234. **Gordon, R. and Herman, G. T.,** Three-dimensional reconstruction from projections: a review of algorithms, *Int. Rev. Cytol.,* 38, 111, 1974.

235. **Gordon, R. and Rangayyan, R. M.,** Computed tomography from a few ordinary radiographs, *IEEE Trans. Biomed. Eng.,* BME-29, 626, 1982.

236. **Gordon, R. and Rangayyan, R. M.,** Computed tomography from a few ordinary radiographs, *Proc. IEEE COMPMED-82,* 54, 1982.

237. **Gordon, R. and Rangayyan, R. M.,** Radiographic feature enhancement, information content, and dose reduction in mammography and cardiac angiography, *Proc. 5th IEEE-EMBS Frontiers Eng. and Comput. Health Care Conf.,* 1983, 161.

238. **Gordon, R. and Rangayyan, R. M.,** Geometric deconvolution: a meta-algorithm for limited view computed tomography, *IEEE Trans. Biomed. Eng.,* BME-30, 806, 1983.

239. **Gordon, R. and Rangayyan, R. M.,** Feature enhancement of film mammograms using fixed and adaptive neighborhoods, *Appl. Opt.,* 23, 560, 1984 (Errata: 23, 2055, 1984).

240. **Goshtasby, A.,** Piecewise linear mapping functions for image registration, *Pattern Recog.,* 19, 459, 1986.

241. **Goshtasby, A.,** Piecewise cubic mapping functions for image registration, *Pattern Recog.,* 20, 525, 1987.

242. **Gray, G. E., Pike, M. C., and Henderson, B. E.,** Breast cancer incidence and mortality rates in different countries in relation to known risk factors and dietary practices, *Br. J. Cancer,* 39, 1, 1979.

243. **Greenleaf, J. F. and Bahn, R. C.,** Clinical imaging with transmissive ultrasonic computerized tomography, *IEEE Trans. Biomed. Eng.,* BME-28, 177, 1981.

244. **Greenwald, P. and Smart, C. R.,** Mammography screening in women under age 50 years, *JAMA,* 260, 474, 1988.

245. **Greer, S., Morris, T., and Pettingale, K. W.,** Psychological responses to breast cancer: effect on outcome, *Lancet,* 2, 785, 1979.

246. **Gros, C. M.,** Methodologie. Symposium sur le sein, *J. Radiol. Electrol,* 48, 638, 1967.

247. **Gullino, P. M.,** Natural history of breast cancer: progression from hyperplasia to neoplasia as predicted by angiogenesis, *Cancer,* 39, 2697, 1977.

248. **Haggensen, C. D.,** *Diseases of the Breast,* 3rd ed., W. B. Saunders, Philadelphia, 1986.

249. **Haggensen, C. D., Bodian, C., and Haggensen, D. E., Jr., Eds.,** *Breast Carcinoma: Risk and Detection,* W. B. Saunders, Philadelphia, 1981.

250. **Hakama, M.,** Selective screening by risk groups, in *Screening for Cancer. I. General Principles on Evaluation of Screening for Cancer and Screening for Lung, Bladder and Oral Cancer,* Prorok, P. C. and Miller, A. B., Eds., International Union Against Cancer, Geneva, 1984, 71.

251. **Hall, E. L.,** *Computer Image Processing and Reconstruction,* Academic Press, New York, 1979.

252. **Hall, F. M.,** Screening mammography, *Am. J. Roentgenol.,* 147, 195, 1986.

253. **Hall, F. M.,** Screening mammography — potential problems on the horizon, *N. Engl. J. Med.,* 314, 53, 1986.

254. **Hall, F. M.,** Screening mammography, *Am. J. Roentgenol.,* 147, 1092, 1986.

255. **Hammerstein, G. R., Miller, D. W., White, D. R., Masterson, M. E., Woodard, H. Q., and Laughlin, J. S.,** Absorbed radiation dose in mammography, *Radiology,* 130, 485, 1979.

256. **Hand, W., Semmlow, J. L., Ackerman, L. V., and Alcorn, F. S.,** Computer screening of xeromammograms: a technique for defining suspicious areas of the breast, *Comput. Biomed. Res.,* 12, 445, 1979.

257. **Harper, P. and Kelly-Fry, E.,** Ultrasound visualization of the breast in symptomatic patients, *Radiology,* 137, 465, 1980.

258. **Harper, A. P., Kelly-Fry, E., and Noe, J. S.,** Ultrasound breast imaging — the method of choice for examining the young patient, *Ultrasound Med. Biol.,* 7, 231, 1981.

259. **Harper, P.,** *Ultrasound Mammography,* University Park Press, Baltimore, 1985.

260. **Haug, P. J., Tocino, I. M., Clayton, P. D., and Bair, T. L.,** Automated management of screening and diagnostic mammography, *Radiology,* 164, 747, 1987.

261. **Haus, A. G.,** Effect of geometric unsharpness in mammography and breast xeroradiography, in *Breast Carcinoma: the Radiologist's Expanded Role,* Logan, W. W., Ed., John Wiley & Sons, New York, 1977, 93.

262. **Haus, A. G.,** Physical principles and radiation dose in mammography, in *Breast Carcinoma: Current Diagnosis and Treatment,* Feig, S. A. and McLelland, R., Eds., ACR and Masson, New York, 1983, 99.

263. **Haus, A. G.,** Screen-film mammography update: X-ray units, breast compression, grids, screen-film characteristics, and radiation dose, in *Medical Imaging and Instrumentation '84,* Mulvaney, J. A., Ed., SPIE, Bellingham, WA, 1984, 152.

264. **Haus, A. G.,** Trends in Screen-Film Mammography: Grids, Small Focal Spots, High-Speed Screen-Film Combination, Controlled Film Processing, Reduced Radiation Dose, Eastman Kodak Company, Rochester, NY, 1986.

265. **Haus, A. G.,** Recent trends in screen-film mammography: technical factors and radiaton dose, *Recent Results Cancer Res.,* 105, 37, 1987.

266. **Haus, A. G. and Erickson, L.,** Image quality factors and radiation dose in mammography, *J. Imaging Tech.,* 10, 29, 1984.

267. **Haus, A. G., Metz, C. E., Chiles, J. T., and Rossmann, K.,** The effect of X-ray spectra from molybdenum and tungsten target tubes on image quality in mammography, *Radiology,* 118, 705, 1976.

268. **Haus, A. G., Doi, K., Metz, C. E., and Bernstein, J.,** Image quality in mammography, *Radiology,* 125, 77, 1977.

269. **Haus, A. G., Metz, C. E., and Doi, K.,** Determination of X-ray spectra incident on and transmitted through breast tissue, *Radiology,* 124, 511, 1977.

270. **Haus, A. G., Paulus, D. D., Dodd, G. D., and Bencomo, J.,** Evaluation of magnification mammography, in *Recent and Future Developments in Medical Imaging,* Baily, N., Ed., SPIE, Bellingham, WA, 1978, 85.

271. **Haus, A. G., Paulus, D.D., Dodd, G. D., Cowart, R. W., and Bencomo, J.,** Magnification mammography: evaluation of screen-film and xeroradiographic techniques, *Radiology,* 133, 223, 1979.

272. **Haus, A. G., Dodd, G. D., and Paulus, D. D.,** Historical review of mammographic imaging techniques in terms of image quality and reduced radiation dose, in *Application of Optical Instrumentation in Medicine,* Vol. 7, Gray, J., Ed., SPIE, Bellingham, WA, 1979, 120.

273. **Hay, G. A.,** Traditional X-ray imaging, in *Scientific Basis of Medical Imaging,* Wells; P. N. T., Ed., Churchill Livingstone, Edinburgh, 1982, 1.

274. **Health and Public Policy Committee of American College of Physicians,** The use of diagnostic tests for screening and evaluating breast cancer, *Ann. Int. Med.,* 103, 143, 1985.

275. **Hebert, G., Carrier, R., McFarlane, D. V., and Charlebois, S.,** Guidelines for detection of breast cancer: an update on investigative methods. A report of the Ad Hoc Committee on Mammography of the Canadian Association of Radiologists, *J. Can. Assoc. Radiol.,* 35, 6, 1984.

276. **Heffernan, P. B. and Robb, R. A.,** Difference image reconstruction from a few projections for nondestructive materials inspection, *Appl. Opt.,* 24, 4105, 1985.

277. **Helmrich, S. P., Shapiro, S., Rosenberg, L., Kaufman, D. W., Slone, D., Bain, C., Miettinen, O. S., Stolley, P. D., Rosenshein, N. B., Knapp, R. C., Leavitt, T., Jr., Schottenfeld, D., Engle, R. L., Jr., and Levy, M.,** Risk factors for breast cancer, *Am. J. Epidemiol.,* 117, 35, 1983.

278. **Hendriks, J. H. and Verbeek, A. L.,** Population screening for breast cancer by mammography in The Netherlands. Expectations, early results, negative effects and conditions for large-scale screening, *Diagn. Imag. Clin. Med.,* 54, 186, 1985.

279. **Henshaw, E. T.,** X-ray image intensifier television systems, in *Physical Aspects of Medical Imaging,* Moores, B. M., Parker, R. P., and Pullan, B. R., John Wiley & Sons, Chichester, 1981, 267.

280. **Hermann, G., Janus, C., Schwartz, I. S., Krivisky, B., Bier, S., and Rabinowitz, J. G.,** Nonpalpable breast lesions: accuracy of prebiopsy mammographic diagnosis, *Radiology,* 165, 323, 1987.

281. **Heuser, L. S., Spratt, J. S., Jr., Polk, H. C., Jr., and Buchanan, J. B.,** Relation between mammary cancer growth kinetics and intervals between screenings, *Cancer,* 43, 857, 1979.

282. **Heuser, L. S., Spratt, J. S., Jr., and Polk, H. C., Jr.,** Growth rates of primary breast cancers, *Cancer,* 43, 1888, 1979.

283. **Heywang, S. H., Fenzl, G., Hahn, D., Eiermann, W., and Beck, R.,** MR imaging of the breast: histopathologic correlation, *Radiology,* 157(P), 323, 1985.

284. **Hillman, B. J., Fajardo, L. L., Hunter, T. B., Mockbee, B., Cook, C. E., Hagaman, R. M., Bjelland, J. C., Frey, C. S., and Harris, C. J.,** Mammogram interpretation by physician assistants, *Am. J. Roentgenol.,* 149, 907, 1987.

285. **Hilton, S. V., Leopold, G. R., Olson, L. K., and Willson, S. A.,** Real-time breast sonography: application in 300 consecutive patients, *Am. J. Roentgenol.,* 147, 479, 1986.

286. **Hirayama, R.,** Epidemiology of breast cancer with special reference to the role of diet, *Prev. Med.,* 7, 173, 1978.

287. **Hoeffken, W. and Lanyi, M.,** *Mammography,* W. B. Saunders, Philadelphia, 1977.

288. **Hoehn, J. L., Pierce, W., and Olsen, T. G.,** Efficacy of breast self-examination in the discovery of breast cancer, in *Current Controversies in Breast Cancer*, Ames, F. C., Blumenschein, G. R., and Montague, E. D., Eds., University of Texas Press, Austin, 1984, 581.

289. **Holleb, A. I.,** Guidelines for the cancer-related checkup: five years later, *CA*, 35, 194, 1985.

290. **Homer, M. J.,** Breast imaging: controversies, pitfalls, and some practical thoughts, *Radiol. Clin. North Am.*, 23, 459, 1985.

291. **Horne, J. M.,** Searching for shortage: a population-based analysis of medical care utilization in "under-doctored" and "undoctored" communities in rural Manitoba, in *Proc. 3rd Canadian Conf. Health Economics 1986*, Horne, J. M., Ed., Dept. of Social and Preventive Med., University of Manitoba, Winnipeg, Canada, 1987, 173.

292. **Howard, J.,** Using mammography for cancer control: an unrealized potential, *CA*, 37, 33, 1987.

293. **Howard, D. R. and Taylor, C. R.,** A method for distinguishing benign from malignant breast lesions utilizing antibody present in normal human sera, *Cancer*, 43, 2279, 1979.

294. **Howe, H. L.,** Breast self-examination palpation skill: a methodological note, *J. Chron. Dis.*, 38, 995, 1985.

295. **Howe, G. R., Sherman, G. J., Semenciw, R. M., and Miller, A. B.,** Estimated benefits and risks of screening for breast cancer, *Can. Med. Assoc. J.*, 124, 399, 1981.

296. **Huguley, C. M., Jr. and Brown, R. L.,** The value of breast self-examination, *Cancer*, 47, 989, 1981.

297. **Hunt, S. C., Williams, R. R., Skolnick, M. H., Lyon, J. L., and Smart, C. R.,** Breast cancer and reproductive history from genealogical data, *J. Natl. Cancer Inst.*, 64, 1047, 1980.

298. **Imrey, H. H., Williams, B. T., Schmale, J. D., Imrey, P. B., and Moll, J. D.,** Risk factors and breast cancer screening recommendations: a case-control validity study of the HHA approach, in *Health Risk Estimation, Risk Reduction and Health Promotion*, Landry, F., Ed., Canadian Public Health Association, Ottawa, 1983, 405.

299. **Isard, H. J.,** Diaphanography: transillumination of the breast revisited, in *Breast Disease: Diagnosis and Treatment*, Schwartz, G. F. and Marchant, D., Eds., Elsevier/North-Holland, Amsterdam, 1981, 67.

300. **Jackins, C. L. and Tanimoto, S. L.,** Oct-trees and their use in representing three-dimensional objects, *Comput. Graphics Image Process.*, 14, 249, 1980.

301. **Jackson, V. P., Lex, A. M., and Smith, D. J.,** Patient discomfort during screen-film mammography, *Radiology*, 168, 421, 1988.

302. **Jaffe, C. and Webster, E. W.,** Radiographic contrast improvement by means of slit radiography, *Radiology*, 116, 631, 1975.

303. **Jakobsen, S., Beckmann, J., Beckmann, M., and Brunner, S.,** Mammography: attitudes and reactions, *Recent Results Cancer Res.*, 105, 73, 1987.

304. **Jennings, R. J., Eastgate, R. J., and Siedband, M. P.,** Optimal X-ray spectra for screen-film mammography, *Med. Phys.*, 8, 629, 1981.

305. **Johns, P. C., Drost, D. J., Yaffe, M. J., and Fenster, A.,** Dual energy mammographic imaging, *Proc. SPIE*, 419, 201, 1983.

306. **Johns, P. C., Drost, D. J., Yaffe, M. J., and Fenster, A.,** Dual-energy mammography, *J. Can. Assoc. Radiol.*, 35, 98, 1984.

307. **Johns, P. C., Drost, D. J., Yaffe, M. J., and Fenster, A.,** Investigation of dual-energy radiography for breast cancer detection, *Med. Phys.*, 11, 391, 1984.

308. **Johnson, C. B.,** A review of electro-optical imaging devices for medical applications, in *Application of Optical Instrumentation in Medicine*, Zarnstorff, W. C., Hendee, W. R., and Carson, P. L., Eds., SPIE, Redondo Beach, 1973, 3.

309. **Johnson, G. A. and O'Fughludha, F.,** Simulation of mammographic X-ray spectra, *Med. Phys.*, 7, 189, 1980.

310. **Jost, G.,** Evaluation of grid technique in mammography, in *Reduced Dose Mammography*, Logan, W. W. and Muntz, E. P., Eds., Masson, New York, 1979, 253.

311. **Kalache, A., Vessey, M. P., and McPherson, K.,** Lactation and breast cancer, *Br. Med. J.*, 280, 223, 1980.

312. **Kalender, W. A., Hubener, K.-H., and Jass, W.,** Digital scanned projection radiography: optimization of image characteristics, *Radiology*, 149, 299, 1983.

313. **Kalisher, L.,** Factors influencing false negative rates in xeromammography, *Radiology*, 133, 297, 1979.

314. **Kalos, M. H., Davis, S. A., Mittelman, P. S., and Mastras, P.,** Conceptual design of a vapor volume fraction instrument (Technical Report), Nuclear Development Corporation of America, White Plains, NY, 1961.

315. **Kapdi, C.C. and Parekh, N. J.,** The male breast, *Radiol. Clin. North Am.*, 21, 137, 1983.

316. **Kegeles, S. S.,** Breast self-exam: current status and concerns, *Patient Educ. Newsletter*, 7(2), 1, 1984.

317. **Kegeles, S. S.,** Education for breast self-examination: why, who, what, and how?, *Prev. Med.*, 14, 702, 1985.

318. **Keller, K., George, E., and Podell, R. N.,** Clinical breast examination and breast self-examination experience in a family practice population, *J. Fam. Pract.*, 11, 887, 1980.

319. **Kelsey, J. L.,** A review of the epidemiology of human breast cancer, *Epidemiol. Rev.*, 1, 74, 1979.

320. **Kelsey, J. L. and Hildreth, N. G.,** Causative factors in breast cancer, in *Contemporary Issues in Oncology; Breast Cancer*, Margolese, G., Ed., Churchill Livingstone, New York, 1983, 23.

321. **Kelsey, J. L., Fischer, D. B., Holford, T. R., LiVolsi, V. A., Mostow, E. D., Goldenberg, I. S., and White, C.,** Exogenous estrogens and other factors in the epidemiology of breast cancer, *J. Natl. Cancer Inst.*, 67, 327, 1981.

322. **Kelsey, J. L., Hildreth, N. G., and Thompson, W. D.,** Epidemiologic aspects of breast cancer, *Radiol. Clin. North Am.*, 21, 3, 1983.

323. **Kennedy, B. J.,** Cost-effectiveness of screening mammography in low-risk patients, *JAMA*, 256, 406, 1986.

324. **Khaw, B. A., Strauss, H. W., Cahill, S. L., Soule, H. R., Edginton, T., and Cooney, J.,** Sequential imaging of ¹¹¹Indium labeled monoclonal antibody in human mammary tumors hosted in nude mice, *J. Nucl. Med.*, 25, 592, 1984.

325. **Kimme, C., O'Loughlin, B. J., and Sklansky, J.,** Automatic detection of suspicious abnormalities in breast radiographs, in *Data Structures, Computer Graphics, and Pattern Recognition*, Klinger, A., Fu, K. S., and Kunii, T. L., Eds., Academic Press, New York, 1977, 427.

326. **Kimme-Smith, C., Bassett, L.W., Gold, R. H., Roe, D., and Orr, J.,** Mammographic dual-screen-dual-emulsion-film combination: visibility of simulated microcalcifications and effect on image contrast, *Radiology*, 165, 313, 1987.

327. **King, H. and Locke, F. B.,** Cancer mortality among Chinese in the United States, *J. Natl. Cancer Inst.*, 65, 1141, 1980.

328. **Kinzly, R. E.,** Partially coherent imaging in a microdensitometer, *J. Opt. Soc. Am.*, 62, 386, 1972.

329. **Kobayashi, T.,** Review: ultrasonic diagnosis of breast cancer, *Ultrasound Med. Biol.*, 1, 383, 1975.

330. **Kopans, D. B.,** "Early" breast cancer detection using techniques other than mammography, *Am. J. Roentgenol.*, 143, 465, 1984.

331. **Kopans, D. B.,** What is a useful adjunct to mammography?, *Radiology*, 161, 560, 1986.

332. **Kopans, D. B.,** Nonmammographic breast imaging techniques: current status and future developments, *Obstet. Gynecol. Clin. North Am.*, 14, 651, 1987.

333. **Kopans, D. B. and Meyer, J. E.,** Computed tomography guided localization of clinically occult breast carcinoma — the "N" skin guide, *Radiology*, 145, 211, 1982.

334. **Kopans, D. B., Meyer, J. E., Cohen, A. M., and Wood, W. C.,** Palpable breast masses: the importance of preoperative mammography, *JAMA*, 246, 2819, 1981.

335. **Kopans, D. B., Meyer, J. E., Lindfors, K. K., and Bucchianeri, S. S.,** Breast sonography to guide cyst aspiration and wire localization of occult solid lesions, *Am. J. Roentgenol.*, 143, 489, 1984.

336. **Kopans, D. B., Meyer, J. E., and Sadowsky, N.,** Breast imaging, *N. Engl. J. Med.*, 310, 960, 1984.

337. **Kopans, D. B., Bjorkholm, P., and Webster, E.,** Minimal dose digital breast radiography, *Radiology*, 153(P), 162, 1984.

338. **Kopans, D. B., Meyer, J. E., and Lindfors, K. K.,** Whole-breast US imaging: four-year follow-up, *Radiology*, 157, 505, 1985.

339. **Kopans, D. B. and Swann, C. A.,** Observations on mammographic screening and false-positive mammograms, *Am. J. Roentgenol.*, 150, 785, 1988.

340. **Kossoff, G., Jellins, J., and Reeve, T. S.,** Potential solutions to the limitations of the sonographic examination of the breast, in *Ultrasonic Examination of the Breast*, Jellins, J. and Kobayashi, T., Eds., John Wiley & Sons, Chichester, 1983, 229.

341. **Kroll, J., Kotwich, J., and Tabrett, M.,** The diagnosis of benign disease and the exclusion of malignancy in patients with breast symptoms, *Semin. Ultrasound*, 3, 38, 1982.

342. **Kusama, S., Spratt, J. S., Jr., Donegan, W. L., Watson, F. R., and Cunningham, C.,** The gross rates of growth of human mammary carcinoma, *Cancer*, 30, 594, 1972.

343. **Kushner, R.,** *Alternatives: New Developments in the War on Breast Cancer*, 2nd ed., Kensington Press, Cambridge, MA, 1984.

344. **Land, C. E.,** Estimating cancer risks from low doses of ionizing radiation, *Science*, 209, 1197, 1980.

345. **Land, C. E., Boice, J. D., Shore, R. E., Norman, J. E., and Tokunaga, M.,** Breast cancer risk from low dose exposure to ionizing radiation: results of parallel analysis of three exposed populations of women, *J. Natl. Cancer Inst.*, 65, 353, 1980.

346. **Land, C. E. and McGregor, D.H.,** Breast cancer incidence among atomic bomb survivors: implications for radiobiologic risk at low doses, *J. Natl. Cancer Inst.*, 62, 17, 1979.

347. **Lawson, R. N.,** Implications of surface temperatures in the diagnosis of breast cancer, *Can. Med. Assoc. J.*, 75, 309, 1956.

348. **Lawson, R. N. and Chughtai, M. S.,** Breast cancer and body temperature, *Can. Med. Assoc. J.*, 88, 68, 1963.

349. **Lee, Y.-T. N. and Spratt, J. S., Jr.,** Rate of growth of soft tissue metastases of breast cancer, *Cancer*, 29, 344, 1972.

350. **Lester, R. G.,** Risk versus benefit in mammography, *Radiology*, 124, 1, 1977.

351. **Levin, D. C., Schapiro, R. M., Boxt, L. M., Dunham, L., Harrington, D. P., and Ergun, D. L.,** Digital subtraction angiography: principles and pitfalls of image improvement techniques, *Am. J. Roentgenol.*, 143, 447, 1984.

352. **Libshitz, H. I.,** Breast cancer screening techniques, in *Current Controversies in Breast Cancer*, Ames, F. C., Blumenschein, G. R., and Montague, E. D., Eds., University of Texas Press, Austin, 1984, 63.

353. **Libshitz, H. I., Fetouh, S., Isley, J., and Lester, R. G.,** One-view mammographic screening, *Radiology*, 120, 719, 1976.

354. **Lindfors, K. K., Meyer, J. E., Busse, P. M., Kopans, D. B., Munzenrider, J. E., and Sawicka, J. M.,** CT evaluation of local and regional breast cancer recurrence, *Am. J. Roentgenol.*, 145, 833, 1985.

355. **Lipkin, L. E., Lemkin, P., and Carman, G.,** Automated autoradiographic grain counting in human determined context, *J. Histochem. Cytochem.*, 22, 755, 1974.

356. **Locke, F. B. and King, H.,** Cancer mortality risk among Japanese in the United States, *J. Natl. Cancer Inst.*, 65, 1149, 1980.

357. **Logan, W. W.,** Screen/film mammography: technique, in *Breast Carcinoma: Current Diagnosis and Treatment*, Feig, S. A. and McLelland, R., Eds., ACR and Masson, New York, 1983, 141.

358. **Love, T. J.,** Thermography as an indicator of blood perfusion, *Ann. NY Acad. Sci.*, 335, 429, 1980.

359. **Lundgren, B. and Helleberg, A.,** Single oblique-view mammography for periodic screening for breast cancer in women, *J. Natl. Cancer Inst.*, 68, 351, 1982.

360. **Lundgren, B. and Jakobsson, S.,** Single view mammography; a simple and efficient approach to breast cancer screening, *Cancer*, 38, 1124, 1976.

361. **Lundgren, B. and Jakobsson, S.,** Single-view mammographic screening: three-year follow-up of interval cancer cases, *Radiology*, 130, 109, 1979.

362. **Lynch, H. T., Watson, P., Schreiman, J., Fitzsimmons, M. L., Conway, T., and Lynch, J.,** Mammography screening in women under age 50 years, *JAMA*, 260, 473, 1988.

363. **MacDonald, I.,** The natural history of mammary carcinoma, *Am. J. Surg.*, 111, 435, 1966.

364. **Maher, J. C.,** Mammography screening in women under age 50 years, *JAMA*, 260, 473, 1988.

365. **Mann, L. C., Hawes, D. R., Ghods, M., Bednar, E. J., and Potchen, E. J.,** Utilization of screening mammography: comparison of different physician specialities, *Radiology*, 164, 121,1987.

366. **Mansfield, P., Morris, P. G., Ordidge, R. J., Coupland, R. E., Bishop, H. M., and Blamey, R. W.,** Carcinoma of the breast images by nuclear magnetic resonance (NMR), *Br. J. Radiol.*, 52, 242, 1979.

367. **Mansfield, P., Morris, P. G., Ordidge, R. J., Pykett, I. L., Bansert, V., and Coupland, R. E.,** Human whole body imaging and detection of breast tumors by NMR, *Philos. Trans. R. Soc. London Ser. B.*, 289, 503,1980.

368. **Manton, K. G. and Stanllard, E.,** A two-disease model of female breast cancer: mortality in 1969 among white females in the United States, *J. Natl. Cancer Inst.*, 64, 9, 1980.

369. **Manton, K. G. and Stanllard, E.,** Multistage models for carcinogenesis, *J. Natl. Cancer Inst.*, 65, 215, 1980.

370. **Marchant, D. J.,** Physical examination and breast self-examination, in *Breast Carcinoma: Current Diagnosis and Treatment*, Feig, S. A. and McLelland, R., Eds., ACR and Masson, New York, 1983, 371.

371. **Marshall, V., Williams, D. C., and Smith, K. D.,** Diaphanography as a means of detecting breast cancer, *Radiology*, 150, 339, 1984.

372. **Martin, J. E.,** Xeromammography — an improved diagnostic method: review of 250 biopsied cases, *Am. J. Roentgenol.*, 117, 90, 1973.

373. **Martin, J. E.,** Mammographic diagnosis of minimal breast cancer, in *Breast Carcinoma: Current Diagnosis and Treatment*, Feig, S. A. and McLelland, R., Eds., ACR and Masson, New York, 1983, 257.

374. **Martin, J. E.,** Breast imaging techniques: mammography, ultrasonography, computed tomography, thermography, and transillumination, *Radiol. Clin. North Am.*, 21, 149, 1983.

375. **Martin, J. E., Moskowitz, M., and Milbrath, J. R.,** Breast cancer missed by mammography, *Am. J. Roentgenol.*, 132, 737, 1979.

376. **Marx, J. L.,** Monoclonal antibodies in cancer, *Science*, 216, 761, 1982.

377. **Matsui, H. and Katsuhiro, O.,** A uniform focal spot X-ray tube with improved MTF and KW rating, *Radiology*, 156, 227, 1985.

378. **Maturo, V. G., Zusmer, N. R., Gilson, A. J., and Bear, B.,** Ultrasonic appearance of mammary carcinoma with a dedicated whole-breast scanner, *Radiology*, 142, 713, 1982.

379. **Maturo, V. G., Zusmer, N. R., Gilson, A. J., Smoak, W. M., Janowitz, W. R., Bear, B.E., Goddard, J., and Dick, D. E.,** Ultrasound of the whole breast utilizing a dedicated automated breast scanner, *Radiology*, 137, 457, 1980.

380. **McGregor, D. H., Land, C. E., Choi, K., Tokuoka, S., Liu, P. I., Wakabayashi, T., and Beebe, G. W.,** Breast cancer incidence among atomic bomb survivors, Hiroshima and Nagasaki, 1950 — 1969, *J. Natl. Cancer Inst.*, 59, 799, 1977.

381. **McLelland, R.,** Mammography 1984: challenge to radiology, *Am. J. Roentgenol.,* 142, 1, 1984.
382. **McLelland, R.,** Screening mammography, *Am. J. Roentgenol.,* 147, 1091, 1986.
383. **McSweeney, M. B. and Egan, R. L.,** Breast cancer in the younger patient: a preliminary report, *Recent Results Cancer Res.,* 90, 36, 1984.
384. **McSweeney, M. B. and Murphy, C. H.,** Whole-breast sonography, *Radiol. Clin. North Am.,* 23, 157, 1985.
385. **McSweeney, M. B., Sprawls, P., and Egan, R. L.,** Enhanced image mammography, *Am. J. Roentgenol.,* 140, 9, 1983.
386. **McSweeney, M. B., Small, W. C., Cerny, V., Sewell, W., Powell, R. W., and Goldstein, J. H.,** Magnetic resonance imaging in the diagnosis of breast disease: use of transverse relaxation times, *Radiology,* 153, 741, 1984.
387. **McSweeney, M. B., Sprawls, P., and Egan, R. L.,** Special techniques in mammography, *Recent Results Cancer Res.,* 90, 69, 1984.
388. **McSweeney, M. B., Sprawls, P., and Egan, R. L.,** Magnification mammography, *Recent Results Cancer Res.,* 90, 75, 1984.
389. **McSweeney, M. B., Sprawls, P., and Egan, R. L.,** Enhanced-image mammography, *Recent Results Cancer Res.,* 90, 79, 1984.
390. **McWhorter, W. P. and Mayer, W. J.,** Black/white differences in type of initial breast cancer treatment and implications for survival, *Am. J. Public Health,* 77, 1515, 1987.
391. **Mees, C. E.K. and James, T. H., Eds.,** *The Theory of the Photographic Process,* 3rd ed., Chap. 9, Macmillan, New York, 1966.
392. **Melton, L. J., III, Brian, D. D., and Williams, R. L.,** Urban-rural differential in breast cancer incidence and mortality in Olmsted County, Minnesota, 1935 — 1974, *Int. J. Epidemiol.,* 9, 155, 1980.
393. **Meyer, J. E. and Kopans, D. B.,** Breast physical examination by the mammographer, *Appl. Radiol.,* 12, 103, 1983.
394. **Meyer, J. E. and Munzenrider, J. E.,** Computed tomographic demonstration of internal mammary lymph-node metastasis in patients with locally recurrent breast carcinoma, *Radiology,* 139, 661, 1981.
395. **Meyer, J. E., Kopans, D. B., Stomper, P. C., and Lindfors, K. K.,** Occult breast abnormalities: percutaneous preoperative needle localization, *Radiology,* 150, 335, 1984.
396. **Miller, A. B.,** Role of nutrition in the etiology of breast cancer, *Cancer,* 39, 2704. 1977.
397. **Miller, A. B.,** Controversies in screening for breast cancer, in *Contemporary Issues in Clinical Oncology: Breast Cancer,* Margolese, R. G., Ed., Churchill Livingstone, New York, 1983, 1.
398. **Miller, A. B.,** The epidemiology of breast cancer, in *Current Controversies in Breast Cancer,* Ames, F. C., Blumenschein, G. R., and Montague, E. D., Eds., University of Texas Press, Austin, 25, 1984.
399. **Miller, A. B.,** Screening for breast cancer: a review, *Eur. J. Cancer Clin. Oncol.,* 24, 49, 1988.
400. **Miller, A. B. and Bulbrook, R. D.,** Screening, detection, and diagnosis of minimal breast cancer, *Lancet,* 1, 1109, 1982.
401. **Miller, A. B., and Tsechkovski, M.,** Imaging technologies in breast cancer control: summary of a report of a World Health Organization meeting, *Am. J. Roentgenol.,* 148, 1093, 1987.
402. **Miller, A. B., Kelly, A., Choi, N. W., Mathews, V., Morgan, R. W., Munan, L., Burch, J. D., Feather, J., Howe, G. R., and Jain, M.,** A study of diet and breast cancer, *Am. J. Epidemiol.,* 107, 499, 1978.
403. **Miller, A. B., Barclay, T. H. C., Choi, N. W., Grace, M. G., Wall, C., Plante, M., Howe, G. R., Cinader, B., and Davis, F. G.,** A study of cancer, parity and age at first pregnancy, *J. Chronic Dis.,* 33, 595, 1980.
404. **Miller, A. B., Howe, G. R., and Wall, C.,** The National Study of Breast Cancer Screening. Protocol for a Canadian randomized controlled trial of screening for breast cancer in women, *Clin. Invest. Med.,* 4, 227, 1981.
405. **Miller, E. R.,** A multiple-film technique for contrast enhancement and/or reduction of patient exposure, *Radiology,* 110, 361, 1974.
406. **Milne, E. N. C. and Roeck, W. W.,** Determinants and indices of focal spot performance — the concept of three-dimensionality, in *Medical X-ray Photo-Optical Systems Evaluation,* Weaver, K. E., Wagner, R. F., and Goodenough, D. J., Eds., SPIE, Palos Verdes Estates, CA, 1975, 124.
407. **Minton, J. P., Abou-Issa, H., Foecking, M. K., and Sriram, M. G.,** Caffeine and unsaturated fat diet significantly promotes DMBA-induced breast cancer in rats, *Cancer,* 51, 1249, 1983.
408. **Mole, R. H.,** The sensitivity of the human breast to cancer induction by ionizing radiation, *Br. J. Radiol.,* 51, 401, 1978.
409. **Monsees, B., Destouet, J. M., and Totty, W. G.,** Light scanning versus mammography in breast cancer detection, *Radiology,* 163, 463, 1987.
410. **Moolgavkar, S. H.,** Multistage models for carcinogenesis, *J. Natl. Cancer Inst.,* 65, 215, 1980.
411. **Moskowitz, M.,** Screening is not diagnosis, *Radiology,* 133, 265, 1979.
412. **Moskowitz, M.,** Mammographic screening: significance of minimal breast cancer, *Am. J. Roentgenol.,* 136, 735, 1981.

413. **Moskowitz, M.,** Minimal breast cancer redux, *Radiol. Clin. North Am.,* 21, 93, 1983.

414. **Moskowitz, M.,** The predictive value of certain mammographic signs in screening for breast cancer, *Cancer,* 51, 1007, 1983.

415. **Moskowitz, M.,** Screening for breast cancer: how effective are our tests? A critical review, *CA,* 33, 26, 1983.

416. **Moskowitz, M.,** Mammography to screen asymptomatic women for breast cancer, *Am. J. Roentgenol.,* 143, 457, 1984.

417. **Moskowitz, M.,** Benefit-versus-risk ratio of mammographic screening techniques, in *Current Controversies in Breast Cancer,* Ames, F.C., Blumenschein, G. R., and Montague, E. D., Eds., University of Texas Press, Austin, 1984, 67.

418. **Moskowitz, M.,** Breast cancer: age-specific growth rates and screening strategies, *Radiology,* 161, 37, 1986.

419. **Moskowitz, M., and Gartside, P. S.,** Evidence of breast cancer mortality reduction: agressive screening in women under age 50, *Am. J. Roentgenol.,* 138, 911, 1982.

420. **Moskowitz, M., Fox, S. H., del Re, R. B., Milbrath, J. R., Bassett, L. W., Gold, R. H., and Shaffer, K. A.,** The potential value of liquid-crystal thermography in detecting significant mastopathy, *Radiology,* 140, 659, 1981.

421. **Moskowitz, M., Feig, S. A., Cole-Beuglet, C., Fox, S. H., Haberman, J. D., Libshitz, H. I., and Zermeno, A.,** Evaluation of new imaging procedures for breast cancer: proper process, *Am. J. Roentgenol.,* 140, 591, 1983.

422. **Moskowitz, M., Feig, S. A., Cole-Beuglet, C., Fox, S. H., Haberman, J. D., Libshitz, H. I., and Zermeno, A.,** Evaluation of new imaging procedures for breast cancer, *Recent Results Cancer Res.,* 90, 55, 1984.

423. **Motz, J. W. and Danos, M.,** Image information content and patient exposure, *Med. Phys.,* 5, 8, 1978.

424. **Muir, B. B., Kirkpatrick, A. E., Roberts, M. M., and Duffy, S.W.,** Oblique-view mammography: adequacy for screening, *Radiology,* 151, 39, 1984.

425. **Muntz, E. P. and Logan, W. W.,** Focal spot size and scatter suppression in magnification mammography, *Am. J. Roentgenol.,* 133, 453, 1979.

426. **Muntz, E. P., Wilkinson, E., and George, F. W.,** Mammography at reduced doses: present performance and future possibilities, *Am. J. Roentgenol.,* 134, 741, 1980.

427. **Munzenrider, J. E., Tchakarova, I., Castro, M., and Carter, B.,** Computerized body tomography in breast cancer. I. Internal mammary nodes and radiation treatment planning, *Cancer,* 43, 137, 1979.

428. **Mushlin, A. I.,** Cost-effectiveness of screening mammography in low-risk patients, *JAMA,* 256, 407, 1986.

429. **Myers, P. C., Barrett, A. H., and Sadowsky, N. L.,** Microwave thermography of normal and cancerous breast tissue, *Ann. NY Acad. Sci.,* 335, 443, 1980.

430. **National Cancer Institute of Canada,** National breast-cancer screening study gets underway, *Can. Med. Assoc. J.,* 122, 243, 1980.

431. *Annual Report of the National Cancer Institute of Canada,* National Cancer Institute of Canada, Toronto, 1987.

432. Mammography — A User's Guide, NCRP Report No. 85, National Council on Radiation Protection and Measurements, Bethesda, MD, 1986.

433. **Nemoto, T., Vana, J., Bedwani, R. N., Baker, H. W., McGregor, F. H., and Murphy, G. P.,** Management and survival of female breast cancer: results of a national survey by the American College of Surgeons, *Cancer,* 45, 2917, 1980.

434. **Newsome, J. F. and McLelland, R.,** A word of caution concerning mammography, *JAMA,* 255, 528, 1986.

435. **Nielsen, B.,** Image quality in mammography: physical and technical limitations, *Recent Results Cancer Res.,* 105, 1, 1987.

436. **Nishikawa, R. M. and Yaffe, M. J.,** An investigation of digital mammographic imaging, *Proc. SPIE,* 419, 192, 1983.

437. **Nishikawa, R. M. and Yaffe, M. J.,** Scanned-projection digital mammographic imaging, *Med. Phys.,* 11, 390, 1984.

438. **Nishikawa, R. M. and Yaffe, M. J.,** Signal-to-noise properties of mammographic film-screen systems, *Med. Phys.,* 12, 32, 1985.

439. **Ohlsson, B., Gundersen, J., and Nilsson, D. M.,** Diaphanography: a method for evaluation of the female breast, *World J. Surg.,* 4, 701, 1980.

440. **O'Malley, M. S. and Fletcher, S. W.,** Screening for breast cancer with breast self-examination: a critical review, *JAMA,* 257, 2197, 1987.

441. **Ostrum, B. J., Becker, W., and Isard, H. J.,** Low-dose mammography, *Radiology,* 109, 323, 1973.

442. **Ottman, R., Pike, M. C., King, M.-C., and Henderson, B. E.,** Practical guide for estimating risk for familial breast cancer, *Lancet,* 2, 556, 1983.

443. **Paffenbarger, R. S., Jr., Kampert, J. B., and Chang, H. G.,** Characteristics that predict risk of breast cancer before and after the menopause, *Am. J. Epidemiol.,* 112, 258, 1980.

444. **Pagani, J. J., Bassett, L. W., Gold, R. H., Benedetti, J., Arndt, R. D., Linsman, J., and Scanlan, R. L.,** Efficacy of combined film-screen/xeromammography: preliminary report, *Am. J. Roentgenol.,* 135, 141, 1980.

445. **Page, D. L., DuPont, W. D., Rogers, L. W., and Landenberger, M.,** Intraductal carcinoma of the breast: follow-up after biopsy alone, *Cancer,* 49, 751, 1982.

446. **Page, D. and Winfield, A. C.,** The dense mammogram, *Am. J. Roentgenol.,* 147, 487, 1986.

447. **Parsons, C. A., Ed.,** *Diagnosis of Breast Disease: Imaging, Clinical Features and Pathology,* University Park Press, Baltimore, 1983.

448. **Pastakia, B.,** Detection of breast tumors by nuclear magnetic resonance imaging, *J. Natl. Cancer Inst.,* 63, 273, 1979.

449. **Paulus, D. D.,** Xeromammography, in *Breast Carcinoma: Current Diagnosis and Treatment,* Feig, S. A. and McLelland, R., Eds., ACR and Masson, New York, 1983, 115.

450. **Paulus, D. D.,** Imaging in breast cancer, in *The 1984 Categorical Course in Breast Cancer,* Levitt, S. H., Ed., The Radiology Society of North America, Minneapolis, 1984, 218.

451. **Paulus, D.,** Detection of minimal breast cancer, in *Current Controversies in Breast Cancer,* Ames, F. C., Blumenschein, G. R., and Montague, E. D., Eds., University of Texas Press, Austin, 1984, 85.

452. **Pennes, D.R. and Homer, M. J.,** Disappearing breast masses caused by compression during mammography, *Radiology,* 165, 327, 1987.

453. **Pennypacker, H. S., Bloom, H. S., Criswell, E. L., Neelakantan, P., Goldstein, M. K., and Stein, G. H.,** Toward an effective technology of instruction in breast self-examination, *Int. J. Mental Health,* 11, 98, 1982.

454. **Pera, A. and Freimanis, A. K.,** The choice of radiologic procedures in the diagnosis of breast disease, *Obstet. Gynecol. Clin. North Am.,* 14, 635, 1987.

455. **Peschmann, K. R., Couch, J. L., and Parker, D. L.,** New developments in digital X-ray detection, in *Digital Radiography,* Brody, W.R., Ed., SPIE, Bellingham, WA, 1981, 50.

456. **Pike, M. C., Henderson, B. E., Casagrande, J. T., Rosario, I., and Gray, G. E.,** Oral contraceptive use and early abortion as risk factors for breast cancer in young women, *Br. J. Cancer,* 43, 72, 1981.

457. **Pike, M. C., Siiteri, P. K., and Welsch, C. W., Eds.,** *Banbury Report 8: Hormones and Breast Cancer,* Cold Spring Harbor Laboratory, 1981.

458. **Pochin, E. E.,** *Why be Quantitative About Radiation Risk Estimates?,* Lecture No. 2, the Lauriston S. Taylor Lecture Series in Radiation Protection and Measurements, National Council on Radiation Protection and Measurements, 1978.

459. **Polk, H. C., Jr.,** Improved understanding of mammary cancer, *Cancer,* 57, 411, 1986.

460. **Pollack, E. S. and Horm, J. W.,** Trends in cancer incidence and mortality in the United States, 1969 — 76, *J. Natl. Cancer Inst.,* 64, 1091, 1980.

461. **Potchen, E. J. and Sierra, A. E.,** The detection and cure of breast cancer, *Obstet. Gynecol. Clin. North Am.,* 14, 667, 1987.

462. **Preisendorfer, R. W.,** *Radiative Transfer on Discrete Spaces,* Pergamon Press, Oxford, 1965.

463. **Price, J. L. and Butler, P. D.,** Reduction of radiation and exposure times in mammography, *Br. J. Radiol.,* 43, 251, 1970.

464. **Pullan, B. R.,** Digital radiology, in *Physical Aspects of Medical Imaging,* Moores, B. M., Parker, R. P., and Pullan, B. R., Eds., John Wiley & Sons, Chichester, 1981, 275.

465. **Rabinowitz, J. G. and Hermann, G.,** Mammography, in *Breast Disease,* Marchant, D. J., Ed., Churchill Livingstone, New York, 1986, 107.

466. **Ram, G.,** Optimization of ionizing radiation usage in medical imaging by means of image enhancement techniques, *Med. Phys.,* 9, 733, 1982.

467. **Rangaraj, M. R. and Gordon, R.,** Computed tomography for remote areas via teleradiology, in *Picture Archiving and Communication Systems (PACS) for Medical Applications,* Duerinckx, A. J., Ed., SPIE, Bellingham, WA, 1982, 182.

468. **Rangayyan, R. M. and Gordon, R.,** Streak preventive image reconstruction with ART and adaptive filtering, *IEEE Trans. Med. Imag.,* MI-1, 173, 1982.

469. **Rangayyan, R. M. and Gordon, R.,** Computed tomography from ordinary radiographs for teleradiology, *Med. Phyics,* 10, 687, 1983.

470. **Rangayyan, R. M. and Gordon, R.,** Expanding the dynamic range of X-ray videodensitometry using ordinary image digitizing devices, *Appl. Opt.,* 23, 3117, 1984.

471. **Rangayyan, R. M. and Nguyen, H. N.,** Pixel-independent image processing techniques for enhancement of features in mammograms, *Proc. 8th IEEE Eng. Med. Biol. Conf.,* 1986, 1113.

472. **Rangayyan, R. M. and Nguyen, H. N.,** Pixel-independent image processing techniques for noise removal and feature enhancement, *IEEE Pacific Rim Conf. Communications, Computers, Signal Processing,* Vancouver, 1987, 81.

473. **Rao, G. U. V.,** Evaluation of the focal spot characteristics of diagnostic X-ray tubes, in *Medical X-ray Photo-Optical Systems Evaluation,* Weaver, K. E., Wagner, R. F., and Goodenough, D. J., Eds., SPIE, Palos Verdes Estates, CA, 1975, 139.

474. **Ray, C. and Baum, M.,** *Psychological Aspects of Early Breast Cancer,* Springer-Verlag, New York, 1985.

475. **Reynolds, G. O. and Smith, A. E.,** Experimental demonstration of coherence effects and linearity in microdensitometry, *Appl. Opt.,* 12, 1259, 1973.

476. **Ries, L. G., Pollock, E. S., and Young J. L.,** Cancer patient survival: surveillance, epidemiology, and end results program, 1973 — 79, *J. Natl. Cancer Inst.,* 70, 693, 1983.

477. **Roberts, M. M., Alexander, F. E., Anderson, T. J., Forrest, A. P. M., Hepburn, W., Huggins, A., Kirkpatrick, A. E., Lamb, J., Lutz, W., and Muir, B. B.,** The Edinburgh randomised trial of screening for breast cancer: description of method, *Br. J. Cancer,* 50, 1, 1984.

478. **Romsdahl, M. M., McGrath, R. G., Hoppe, E., and McGrew, E. A.,** Experimental model for the study of tumor cells in the blood, *Acta Cytol.,* 9, 141, 1965.

479. **Rosen, P. P., Lieberman, P. H., Braun, D. W., Jr., Kosloff, C., and Adair, F.,** Lobular carcinoma *in situ* of the breast: detailed analysis of 99 patients with average follow-up of 24 years, *Am. J. Surg. Pathol.,* 2, 225, 1978.

480. **Rosenfeld, A. and Kak, A. C.,** *Digital Picture Processing,* 2nd ed., Vol. 2, Academic Press, New York, 1982.

481. **Ross, R. J., Thompson, J. S., Kim, K., and Bailey, R. A.,** Nuclear magnetic resonance imaging and evaluation of human breast tissue: preliminary clinical trials, *Radiology,* 143, 195, 1982.

482. **Roth, B., Hamilton, J. F., Jr., and Bunch, C. P.,** Fundamental aspects of mammographic photoreceptors: screens, in *Reduced Dose Mammography,* Logan, W. W. and Muntz, E. P., Eds., Masson, New York, 1979, 529.

483. **Rothenburg, L. N., Kirth, R. L. A., and Snyder, R. E.,** Patient exposures from film and xeroradiographic mammography techniques, *Radiology,* 117, 701, 1975.

484. **Rubin, E., Miller, V. E., Berland, L. L., Han, S. Y., Koehler, R. E., and Stanley, R. J.,** Hand-held real-time breast sonography, *Am. J. Roentgenol.,* 144, 623, 1985.

485. **Runge, V. M., Clanton, J. A., Lukehart, C. M., Partain, C. L., and James, A. E., Jr.,** Paramagnetic agents for contrast-enhanced NMR imaging: a review, *Am. J. Roentgenol.,* 141, 1209, 1983.

486. **Ryan, K. P., Dillman, R. O., DeNardo, S. J., DeNardo, G. L., Beauregard, J., Hagan, P. L., Amox, D. G., Clutter, M. L., Burnett, K. G., Rulot, C. M., Sobol, R. E., Abramson, I., Bartholomew, R. K., Frincke, J. M., Birdwell, C. R., Carlo, D. J., O'Grady, L. F., and Halpern, S. E.,** Breast cancer imaging with In-111 human IgM monoclonal antibodies: preliminary studies, *Radiology,* 167, 71, 1988.

487. **Sadowsky, N. and Kopans, D. B.,** Breast cancer, *Radiol. Clin. North Am.,* 21, 51, 1983.

488. **Saenger, E. L. and Moskowitz, M.,** Cost-effectiveness of screening mammography in low-risk patients, *JAMA,* 256, 406, 1986.

489. **Salomon, A.,** Beitrage zur Pathologie und Klinik des Mammakarzinoms, *Arch. Klin. Chir.,* 101, 573, 1913.

490. **Sartwell, P. E., Arthes, F. G., and Tonascia, J. A.,** Exogenous hormones, reproductive history, and breast cancer, *J. Natl. Cancer Inst.,* 59, 1589, 1977.

491. **Sashin, D., Morris, C., and Ricci, J. L.,** An evaluation of low light level television for breast cancer detection, *Proc. SPIE,* 70, 384, 1975.

492. **Sato, T., Ikeda, O., Yamakoshi, Y., and Tsubouchi, T.,** X-ray tomography for microstructural object, *Appl. Opt.,* 20, 3880, 1981.

493. **Sato, T., Takanashi, N., and Yamakoshi, Y.,** Two-dimensional X-ray imaging system for very small objects using scanning slit detection, *Appl. Opt.,* 23, 2857, 1984.

494. **Schechter, M. T., Miller, A. B., Baines, C. J., and Howe, G. R.,** Selection of women at high risk of breast cancer for initial screening, *J. Chron. Dis.,* 39, 253, 1986.

495. **Schlom, J., Colcher, D., Hand, P. H., Wunderlich, D., Nuti, M., Teramoto, Y. A., and Kufe, D.,** Potential of monoclonal antibody technology in the management of human mammary carcinoma, in *Current Controversies in Breast Cancer,* Ames, F. C., Blumenschein, G. R., and Montague, E. D., Eds., University of Texas Press, Austin, 1984, 219.

496. **Schneck, C. D. and Lehman, D. A.,** Sonographic anatomy of the breast, *Semin. Ultrasound,* 3, 13, 1982.

497. **Schnitger, H., Dietz, H., and Geldner, E.,** Focal spot intensity distribution and its influence on loadability and geometrical image blurring, in *Medical X-ray Photo-Optical Systems Evaluation,* Weaver, K. E., Wagner, R. F., and Goodenough, D. J., Eds., SPIE, Palos Verdes Estates, CA, 1975, 181.

498. **Schottenfeld, D. and Fraumeni, J. F., Jr., Eds.,** *Cancer Epdemiology and Prevention,* W. B. Saunders, Philadelphia, 1982.

499. **Schreiman, J. S., Gisvold, J. J., Greenleaf, J. F., and Bahn, R. C.,** Ultrasound transmission computed tomography of the breast, *Radiology,* 150, 523, 1984.

500. Schwartz, G. F., Clinical implications of breast cancer risk factors, in *Breast Carcinoma: Current Diagnosis and Treatment*, Feig, S. A. and McLelland, R., Eds., ACR and Masson, New York, 1983, 89.

501. Seeley, G. W., Fisher, H. D., Stempski, M. O., Borgstrom, M., Bjelland, J., and Capp, M. P., Total digital radiology department: spatial resolution requirements, *Am. J. Roentgenol.*, 148, 421, 1987.

502. Seguin, F. H., Burstein, P., Bjorkholm, P. J., Homburger, F., and Adams, R. A., High-resolution tomography of small laboratory animals, in *Technical Digest, Topical Meeting on Industrial Applications of Computed Tomography and NMR Imaging*, Gordon, R., Ed., Washington, D.C., Optical Society of America 1984, MC5-1.

503. Seguin, F. H., Burstein, P., Bjorkholm, P. J., Homburger, F., and Adams, R. A., X-ray computed tomography with 50-μm resolution, *Appl. Opt.*, 24, 4117, 1985.

504. Seidman, H., *Statistical and Epidemiological Data on Cancer of the Breast*, American Cancer Society, New York, 1980.

505. Seidman, H. and Mushinski, M. H., Breast cancer: incidence, mortality, survival, and prognosis, in *Breast Carcinoma: Current Diagnosis and Treatment*, Feig, S. A. and McLelland, R., Eds., ACR and Masson, New York, 1983, 9.

506. Seidman, H., Stellman, S. D., and Mushinski, M. H., A different perspective on breast cancer risk factors: some implications of the nonattributable risk, *CA*, 32, 301, 1982.

507. Seidman, H., Mushinski, M. H., Gelb, S. K., and Silverberg, E., Probabilities of eventually developing or dying of cancer — United States, 1985, *CA*, 35, 36, 1985.

508. Semmlow, J. L., Shadagopappan, A., Ackerman, L. V., Hand, W., and Alcorn, F. S., A fully automated system for screening xeromammograms, *Comput. Biomed. Res.*, 13, 350, 1980.

509. Shapiro, S., Evidence on screening for breast cancer from a randomized trial, *Cancer*, 39, 2772, 1977.

510. Shapiro, S., Strax, P., and Venet, L., Periodic breast cancer screening in reducing mortality from breast cancer, *JAMA*, 215, 1777, 1971.

511. Shapiro, S., Venet, W., Strax, P., Venet, L., and Roeser, R., Ten- to fourteen-year effect of screening on breast cancer mortality, *J. Natl. Cancer Inst.*, 69, 349, 1982.

512. Sheikh, K. M. A., Quismorio, F. A., Friou, G. J., and Lee, Y., Ductular carcinoma of the breast: serum antibodies to tumor-associated antigens, *Cancer*, 44, 2083, 1979.

513. Sheley, J. F., Inadequate transfer of breast cancer self-detection technology, *Am. J. Public Health*, 73, 1318, 1983.

514. Sheng, Y. and Duvernoy, J., Bilinear system analysis for microdensitometers, *J. Opt. Soc. Am.*, 3, 1320, 1986.

515. Shore, R. E., Hempelmann, L. H., Kowaluk, E., Mansur, P. S., Pasternack, B. S., Albert, R. E., and Haughie, G. E., Breast neoplasms in women treated with X-rays for acute postpartum mastitis, *J. Natl. Cancer Inst.*, 59, 813, 1977.

516. Sibala, J. L., Chang, C. H. J., Lin, F., and Jewell, W. R., Computed tomographic mammography: diagnosis of mammographically and clinically occult carcinoma of the breast, *Arch. Surg.*, 116, 114, 1981.

517. Sickles, E. A., Magnification mammography, in *Breast Carcinoma: The Radiologist's Expanded Role*, Logan, W. W., Ed., John Wiley & Sons, New York, 1977, 177.

518. Sickles, E.A., Microfocal spot magnification using xeroradiographic and screen-film recording systems, *Radiology*, 131, 599, 1979.

519. Sickles, E. A., Further experience with microfocal spot magnification mammography in the assessment of clustered breast microcalcifications, *Radiology*, 137, 9, 1980.

520. Sickles, E. A., Xeromammography versus screen-film mammography: pros and cons of the two techniques, *West. J. Med.*, 134, 273, 1981.

521. Sickles, E. A., Mammographic detectability of breast microcalcifications, *Am. J. Roentgenol.*, 139, 913, 1982.

522. Sickles, E. A., Breast CT scanning, heavy-ion mammography, NMR imaging, and diaphanography, in *Breast Carcinoma: Current Diagnosis and Treatment*, Feig, S. A. and McLelland, R., Eds., Masson, New York, 1983, 233.

523. Sickles, E. A., Breast thermography, in *Breast Carcinoma: Current Diagnosis and Treatment*, Feig, S. A. and McLelland, R., Eds., Masson, New York, 1983, 227.

524. Sickles, E. A., Early detection of breast cancer: a symposium, *Am. J. Roentgenol.*, 143, 455, 1984.

525. Sickles, E. A., Breast cancer detection with transillumination and mammography, *Am. J. Roentgenol.*, 142, 841, 1984.

526. Sickles, E. A., Mammographic features of "early" breast cancer, *Am. J. Roentgenol.*, 143, 461, 1984.

527. Sickles, E. A., Breast imaging: a view from the present to the future, *Diagn. Imag. Clin. Med.*, 54, 118, 1985.

528. Sickles, E. A., Mammographic features of 300 consecutive nonpalpable breast cancers, *Am. J. Roentgenol.*, 146, 661, 1986.

529. Sickles, E. A., The role of magnification technique in modern mammography, *Recent Results Cancer Res.*, 105, 19, 1987.

530. **Sickles, E. A.,** Computed tomography scanning, transillumination, and magnetic resonance imaging of the breast, *Recent Results Cancer Res.*, 105, 31, 1987.

531. **Sickles, E. A.,** Comparison of mammographic screen-film systems, *Recent Results Cancer Res.*, 105, 52, 1987.

532. **Sickles, E. A.,** Reduced-price mammography screening, *Am. J. Roentgenol.*, 149, 1153, 1987.

533. **Sickles, E. A.,** Practical solutions to common mammographic problems: tailoring the examination, *Am. J. Roentgenol.*, 151, 31, 1988.

534. **Sickles, E. A.,** Impact of low-cost mammography screening on nearby mammography practices, *Radiology*, 168, 59, 1988.

535. **Sickles, E. A. and Weber, W. N.,** High-contrast mammography with a moving grid: assessment of clinical utility, *Am. J. Roentgenol.*, 146, 1137, 1986.

536. **Sickles, E. A., Doi, K., and Genant, H. K.,** Magnification film mammography: image quality and clinical studies, *Radiology*, 125, 69, 1977.

537. **Sickles, E. A., Davis, P. L., and Crooks, L. E.,** NMR characteristics of benign and malignant breast tissues: preliminary report, *Radiology*, 149, 92, 1983.

538. **Sickles, E. A., Filly, R. A., and Callen, P. W.,** Breast cancer detection with sonography and mammography: comparison using state-of-the-art equipment, *Am. J. Roentgenol.*, 140, 843, 1983.

539. **Sickles, E. A., Filly, R. A., and Callen, P. W.,** Benign breast lesions: ultrasound detection and diagnosis, *Radiology*, 151, 467, 1984.

540. **Sickles, E. A., Weber, W. N., Galvin, H. B., Ominsky, S. H., and Sollito, R. A.,** Baseline screening mammography: one vs. two views per breast, *Am. J. Roentgenol.*, 147, 1149, 1986.

541. **Sickles, E. A., Weber, W. N., Galvin, H. B., Ominsky, S. H., and Sollitto, R. A.,** Mammographic screening: how to operate successfully at low cost, *Radiology*, 160, 95, 1986.

542. **Silverberg, E.,** Cancer statistics, 1984, *CA*, 34, 7, 1984.

543. **Silverberg, E.,** Cancer statistics, 1985, *CA*, 35, 19, 1985.

544. **Silverberg, E. and Lubera, J.,** Cancer statistics, 1986, *CA*, 36, 9, 1986.

545. **Silverberg, E. and Lubera, J.,** Cancer statistics, 1987, *CA*, 37, 3, 1987.

546. **Silvestrini, R., Sanfilippo, O., and Tedesco, G.,** Kinetics of human mammary carcinomas and their correlation with the cancer and the host characteristics, *Cancer*, 34, 1252, 1974.

547. **Skubic, S. E. and Fatouros, P. P.,** Absorbed breast dose: dependence on radiographic modality and technique, and breast thickness, *Radiology*, 161, 263, 1986.

548. **Skucas, J., Logan, W. W., Gorski, J., and Cullinan, A.,** Improved mammography system, *NY State J. Med.*, 76, 1992, 1976.

549. **Smathers, R. L. and Brody, W. R.,** Digital radiography: current and future trends, *Br. J. Radiol.*, 58, 285, 1985.

550. **Smathers, R. L., Bush, E., Drace, J., Stevens, M., Sommer, F. G., Brown, B. W., Jr., and Karras, B.,** Mammographic microcalcifications: detection with xerography, screen-film, and digitized film display, *Radiology*, 159, 673, 1986.

551. **Smith, K. T. and Keinert, F.,** Mathematical foundations of computed tomography, *Appl. Opt.*, 24, 3950, 1985.

552. **Smith, K. T., Wagner, S. L., Guenther, R. B., and Solmon, D. C.,** The diagnosis of breast cancer in mammograms by the evaluation of density patterns, *Radiology*, 125, 383, 1977.

553. **Soble, P. J., Rangayyan, R. M., and Gordon, R.,** Quantitative and qualitative evaluation of geometric deconvolution of distortion in limited-view computed tomography, *IEEE Trans. Biomed. Eng.*, BME-32, 330, 1985.

554. **Sohrabi, A., Sandoz, J., Spratt, J. S., and Polk, H. C., Jr.,** Recurrence of breast cancer: obesity, tumor size, and axillary lymph node metastases, *JAMA*, 244, 264, 1980.

555. **Sommer, F. G. and Brody, W. R.,** Contrast resolution of line-scanned digital radiography, *J. Comput. Assist. Tomogr.*, 6, 373, 1982.

556. **Sommer, F. G., Smathers, R. L., Wheat, R. L., Alvarez, R. E., Brody, W. R., and Cassel, D. M.,** Digital processing of film radiographs, *Am. J. Roentgenol.*, 144, 191, 1985.

557. **Sonoda, M., Takano, M., Miyahara, J., and Kato, H.,** Computed radiography utilizing scanning laser stimulated luminescence, *Radiology*, 148, 833, 1983.

558. **Sorenson, J. A. and Nelson, J. A.,** Slit radiography: problems and potential, in *Application of Optical Instrumentation in Medicine*, Vol. 8, Gray, J., Haus, A. G., Hendee, W. R., and Properzio, W. S., Eds., SPIE, Bellingham, WA, 1980, 240.

559. **Spence, W. R.,** *The Good News About Breast Care*, Health Edco, Waco, TX 1986.

560. **Spiesberger, W.,** Mammogram inspection by computer, *IEEE Trans. Biomed. Eng.*, BME-26, 213, 1979.

561. **Spratt, J. S.,** The relationship between the rates of growth of cancers and the intervals between screening examinations necessary for effective discovery, *Cancer Detect. Prev.*, 4, 301, 1981.

562. **Spratt, J. S. and Spratt, J. A.,** Growth rates, in *Cancer of the Breast*, 3rd ed., Donegan, W. L. and Spratt, J. S., Eds., W. B. Saunders, Philadelphia, 1988, 270.

563. **Stanton, L.,** Mammography imaging techniques, in *The Physics of Medical Imaging: Recording System Measurements and Techniques,* Haus, A. G., Ed., American Institute of Physics, New York, 1979, 492.

564. **Stanton, L. and Logan, W. W.,** Mammography with magnification and grids: detail visibility and dose measurements, in *Reduced Dose Mammography,* Logan, W. W. and Muntz, E. P., Eds., Masson, New York, 1979, 259.

565. **Stanton, L., Villafana, T., Day, J. L., and Lightfoot, D. A.,** A breast phantom method for evaluating mammography technique, *Invest. Radiol.,* 13, 291, 1978.

566. **Stanton, L., Villafana, T., Day, J. L., Lightfoot, D. A., and Stanton, R. E.,** A study of mammographic exposure and detail visibilty using three systems: Xerox-125, Min-R, and Xonics-XERG, *Radiology,* 132, 455, 1979.

567. **Stanton, L., Villafana, T., Day, J. L., and Lightfoot, D. A.,** Dosage evaluation in mammography, *Radiology,* 150, 577, 1984.

568. **Stanton, L., Day, J. L., Villafana, T., Miller, C. H., and Lightfoot, D. A.,** Screen-film mammographic technique for breast cancer screening, *Radiology,* 163, 471, 1987.

569. **Staszewski, J.,** Age at menarche and breast cancer, *J. Natl. Cancer Inst.,* 47, 935, 1971.

570. **Stelling, C. B., Wang, P. C., Lieber, A., Mattingly, S. S., Griffen, W. O., and Powell, D. E.,** MR imaging of the female breast using a prototype breast coil, *Radiology,* 153(P), 163, 1984.

571. **Stelling, C. B., Wang, P. C., Lieber, A., Mattingly, S. S., Griffen, W. O., and Powell, D. E.,** Prototype coil for magnetic resonance imaging of the female breast, *Radiology,* 154, 457, 1985.

572. **Stone, R. T., Macovski, A., and Brody, W. R.,** High purity germanium detector array, in *Digital Radiography,* Brody, W. R., Ed., SPIE, Bellingham, WA, 1981, 55.

573. **Strax, P.,** Utilization of diagnostic techniques for cancer of the breast — early diagnosis, *Recent Results Cancer Res.,* 57, 26, 1976.

574. **Swing, R. E.,** Conditions for microdensitometer linearity, *J. Opt. Soc. Am.,* 62, 386, 1972.

575. **Tabar, L.,** Microfocal spot magnification mammography, *Recent Results Cancer Res.,* 90, 62, 1984.

576. **Tabar, L.,** Screening for breast cancer: an overview, *Recent Results Cancer Res.,* 105, 58, 1987.

577. **Tabar, L. and Dean, P. B.,** Screen/film mammography: quality control, in *Breast Carcinoma: Current Diagnosis and Treatment,* Feig, S. A. and McLelland R., Eds., ACR and Masson, New York, 1983, 161.

578. **Tabar, L. and Dean, P. B.,** Basic principles of mammographic diagnosis, *Diagn. Imag. Clin. Med.,* 54, 146, 1985.

579. **Tabar, L. and Gad, A.,** Screening for breast cancer: the Swedish trial, *Radiology,* 138, 219, 1981.

580. **Tabar, L., Gad, A., Akerlund, E., and Holmberg, L.,** Screening for breast cancer in Sweden, in *Breast Carcinoma: Current Diagnosis and Treatment,* Feig, S. A. and McLelland, R., Eds., ACR and Masson, New York, 1983, 315.

581. **Tabar, L., Gad, A., Holmberg, L., and Ljungquist, U.,** Significant reduction in advanced breast cancer: results of the first seven years of mammography screening in Kopparberg, Sweden, *Diagn. Imag. Clin. Med.,* 54, 158, 1985.

582. **Tabar, L., Fagerberg, C. J. G., Gad, A., Baldetorp, L., Holmberg, L. H., Grontoft, O., Ljungquist, U., Lundstrom, B., Manson, J. C., Eklund, G., and Day, N. E.,** Reduction in mortality from breast cancer after mass screening with mammography. Randomised trial from the Breast Cancer Screening Working Group of the Swedish National Board of Health and Welfare, *Lancet,* 1, 829, 1985.

583. **Tabar, L., Faberberg, G., Day, N. E., and Holmberg, L.,** What is the optimum interval between mammographic screening examinations? An analysis based on the latest results of the Swedish two-county breast cancer screening trial, *Br. J. Cancer,* 55, 547, 1987.

584. **Tabar, L., Day, N. E., and Dean, P. B.,** Mammography screening in women under age 50 years, *JAMA,* 260, 473, 1988.

585. **Tesic, M. M., Mattson, R. A., Barnes, G. T., Sones, R. A., and Stickney, J. B.,** Digital radiography of the chest: design features and considerations for a prototype unit, *Radiology,* 148, 259, 1983.

586. **Tesic, M. M., Sones, R. A., and Morgan, D. R.,** Single-slit digital radiography: some practical considerations, *Am. J. Roentgenol.,* 142, 697, 1984.

587. **Thomas, B. A., and Price, J. L.,** The Guildford breast screening project: 6-year assessment, *Recent Results Cancer Res.,* 105, 67, 1987.

588. **Threatt, B., Norbeck, J. M., Ullman, N. S., Kummer, R., and Roselle, P. F.,** Thermography and breast cancer: an analysis of a blind reading, *Ann. NY Acad. Sci.,* 335, 501, 1980.

589. **Tibblin, G.,** Breast cancer and the condom, *Clin. Invest. Med.,* 4, 153, 1981.

590. **Tokunaga, M., Norman, J. E., Jr., Asano, M., Tokuoka, S., Ezaki, H., Nishimori, I., and Tsuji, Y.,** Malignant breast tumors among atomic bomb survivors, Hiroshima and Nagasaki, 1950 — 74, *J. Natl. Cancer Inst.,* 62, 1347, 1979.

591. **Turner, D. A., Alcorn, F. S., Shorey, W. D., Stelling, C. B., Mategrano, V. C., Merten, C. W., Silver, B., Economou, S. G., Straus, A. K., Witt, T. R., and Norusis, M. J.,** Carcinoma of the breast: detection with MR imaging versus xeromammography, *Radiology,* 168, 49, 1988.

592. **U.K. Trial of Early Detection of Breast Cancer Group,** Trial of early detection of breast cancer: description of method, *Br. J. Cancer,* 44, 618, 1981.

593. **U.S. Preventive Services Task Force,** Recommendations for breast cancer screening, *JAMA,* 257, 2196, 1987.

594. **Vainshtein, B. K.,** Synthesis of projecting functions, *Sov. Phys. Dokl.,* 16, 69, 1971.

595. **Verbeek, A. L. M., Hendriks, J. H., Holland, R., Mravunac, M., Sturmans, F., and Day, N. E.,** Reduction of breast cancer mortality through mass screening with modern mammography: first results of the Nijmegen project, 1975 — 1981, *Lancet,* 1, 1222, 1984.

596. **Verbeek, A. L. M., Hendriks, J. H., Peeters, P. H., and Sturmans, F.,** Mammographic breast pattern and the risk of breast cancer, *Lancet,* 1, 591, 1984.

597. **Verbeek, A. L., Hendriks, J. H., Holland, R., Mravunac, M., and Sturmans, F.,** Mammographic screening and breast cancer mortality: age-specific effects in Nijmegen Project, 1975 — 82 (Letter), *Lancet,* 1, 865, 1985.

598. **Vessey, M. P., McPherson, K., Yeates, D., and Doll, R.,** Oral contraceptive use and abortion before first term pregnancy in relation to breast cancer risk, *Br. J. Cancer,* 45, 327, 1982.

599. **Vessey, M. P., McPherson, K., Roberts, M. M., Neil, A., and Jones, L.,** Fertility in relation to the risk of breast cancer, *Br. J. Cancer,* 52, 625, 1985.

600. **Wagner, R. F., Barnes, G. T., and Askins, B. S.,** Effect of reduced scatter on radiographic information content and patient exposure: a quantitative demonstration, *Med. Phys.,* 7, 13, 1980.

601. **Wanebo, H. J., Huvos, A. G., and Urban, J. A.,** Treatment of minimal breast cancer, *Cancer,* 33, 349, 1974.

602. **Warren, S. L.,** A roentgenologic study of the breast, *Am. J. Roentgenol.,* 24, 113, 1930.

603. **Watmouth, D. J.,** A light torch for the transillumination of female breast tissues, *Br. J. Radiol.,* 55, 142, 1982.

604. **Watt, A. C., Ackerman, L.V., Shetty, P. C., Burke, M., Flynn, M., Grodsinsky, C., Fine, G., and Wilderman, S.,** Differentiation between benign and malignant disease of the breast using digital subtraction angiography of the breast, *Cancer,* 56, 1287, 1985.

605. **Watt, A. C., Ackerman, L. V., Windham, J. P., Shetty, P. C., Burke, M. W., Flynn, M. J., Grodsinsky, C., Fine, G., and Wilderman, S. J.,** Breast lesions: differential diagnosis using digital subtraction angiography, *Radiology,* 159, 39, 1986.

606. **Wayrynen, R. E.,** Fundamental aspects of mammographic receptors: Film process, in *Reduced Dose Mammography,* Logan, W. W. and Muntz, E. P., Eds., Masson, New York, 1979, 521.

607. **Wee, W. G., Moskowitz, M., Chang, N. C., Ting, V. C., and Pemmeraju, S.,** Evaluation of mammographic calcification using a computer program, *Radiology,* 116, 717, 1975.

608. **Weiss, J. P. and Wayrynen, R. E.,** Imaging system for low-dose mammography, *J. Appl. Photogr. Eng.,* 2, 7, 1976.

609. **Wigle, D. T.,** Breast cancer and fertility trends in Canada, *Am. J. Epidemiol.,* 105, 428, 1977.

610. **Williams, W. R., Badzioch, M. D., and Anderson, D. E.,** Epidemiology of male breast cancer, in *Current Controversies in Breast Cancer,* Ames, F. C., Blumenschein, G. R., and Montague, E. D., Eds., University of Texas Press, Austin, 1984, 589.

611. **Williams, S. M., Kaplan, P. A., Petersen, J. C., and Lieberman, R. P.,** Mammography in women under age 30: is there clinical benefit?, *Radiology,* 161, 49, 1986.

612. **Winsberg, F., Elkin, M., Macy, J., Jr., Bordaz, V., and Weymouth, W.,** Detection of radiographic abnormalities in mammograms by means of optical scanning and computer analysis, *Radiology,* 89, 211, 1967.

613. **Winter, J. and Stein, M. A.,** Computer image processing techniques for automated breast thermogram interpretation, *Comput. Biomed. Res.,* 6, 522, 1973.

614. **Wolfe, J. N.,** Xerography of the breast, *Radiology,* 91, 231, 1968.

615. **Wolfe, J. N.,** Mammography, *Radiol. Clin. North Am.,* 12, 189, 1974.

616. **Wolfe, J. N.,** *Xeroradiography of the Breast,* 2nd ed., Charles C Thomas, Springfield, IL, 1983.

617. **Wolfe, J. N., Dooley, R. P., and Harkins, L. E.,** Xeroradiography of the breast: a comparative study with conventional film mammography, *Cancer,* 28, 1569, 1971.

618. **Wolfman, N. T., Moran, P. R., and Moran, R.,** Dedicated MR receiver coil allowing simultaneous breast imaging, *Radiology,* 153(P), 163, 1984.

619. **Wolfman, N. T., Moran, R., Moran, P. R., and Karstaedt, N.,** Simultaneous MR imaging of both breasts using a dedicated receiver coil, *Radiology,* 155, 241, 1985.

620. **Wynder, E. L. and Rose, D. P.,** Diet and breast cancer, *Hosp. Pract.,* 19(4), 73, 1984.

621. **Yester, M. V., Barnes, G. T., and King, M. A.,** Experimental measurements of the scatter reduction obtained in mammography with a scanning multiple slit assembly, *Med. Phys.,* 8, 158, 1981.

622. **Young, J. L., Ries, L. G., and Pollock, E. S.,** Cancer patient survival among ethnic groups in the United States, *J. Natl. Cancer Inst.,* 73, 341, 1984.

623. **Yu, G. S. M., Kadish, A. S., Johnson, A. B., and Marcus, D. M.,** Breast carcinoma associated antigen: an immunocytochemical study. A brief scientific report, *Am. J. Clin. Pathol.,* 74, 453, 1980.

624. **Zeman, G. H., Rao, G. U. V., and Osterman, F. A.,** Evaluation of xeromammographic image quality, *Radiology,* 119, 689, 1976.

625. **Zhou, X. and Gordon, R.,** Geometric unwarping for digital subtraction mammography, in Vision Interface '88, Davis, W. A., Kasvand, T., and Krzyzak, A., Eds., Canadian Information Society, Toronto, 1988, 25.

626. **Ziskin, M. C., Negin, M., Piner, C., and Lapayowker, M. S.,** Computer diagnosis of breast thermograms, *Radiology,* 115, 341, 1975.

627. **Zuur, C. and Broerse, J. J.,** Risk- and cost-benefit analysis of breast screening programs derived from absorbed dose measurements in The Netherlands, *Diagn. Imag. Clin. Med.,* 54, 211, 1985.

628. **Hartman, W. H.,** personal communication.

629. **Trichopoulos, D., MacMahon, B., and Cole, P.,** Menopause and breast cancer risk, *J. Natl. Cancer Inst.,* 48, 605, 1972.

630. **Chamberlain, J.,** First results on mortality reduction in the UK Trial of early detection of breast cancer, *Lancet,* 2, 411, 1988.

631. **Andersson, I., Aspegren, K., Janzon, L., Landberg, T., Lindholm, K., Linell, K., Ljungberg, O., Ranstam, J., and Sigfusson, B.,** Mammographic screening and mortality from breast cancer: the Malmö mammographic screening trial, *Br. Med. J.,* 297, 943, 1988.

APPENDIX 4

GENERATION OF NOISE IN BINARY IMAGES

This appendix has been reprinted from *CVGIP: Graphical Models and Image Processing*, vol. 53, no. 5, 1991.

NOTE

Generation of Noise in Binary Images*

Xiaohua Zhou and Richard Gordon

Department of Electrical and Computer Engineering, University of Manitoba, Winnipeg, Canada R3T 2N2

We present an algorithm for binary noise generation, with which noisy images with specific noise levels can be generated for any given binary image. It should facilitate the experimental evaluation of different image processing and classification algorithms on binary images. © 1991 Academic Press, Inc.

I. INTRODUCTION

There are a variety of operations [1], such as coding, contour following, and skeletonization, performed on binary images (also referred to as binary patterns, or bilevel images/patterns). Medical image processing [2], engineering drawing/processing [3], and other machine manipulations of imagery data often incorporate binary image processing at some stage in their application. Classification of binary patterns [4, 5] is also an important topic in pattern recognition. In evaluating various image processing and classification algorithms on binary images, it is often necessary to analyze their tolerance and sensitivity to noise. It is apparent that a simple and practical algorithm for generating controlled amounts of binary noise would find many applications.

II. METHOD

A. Definitions and Terminologies

Let *binary* image f be represented by

$$f_i = \begin{cases} 1, & \text{object}, \\ 0, & \text{background}, \end{cases} \tag{1}$$

where $i = 1, 2, \ldots, N$, and N is the total number of pixels in the region **R** of an image **I** under consideration. **R** could be any subset of **I**, but it would generally be convex and connected, such as a rectangle or circle. By definition we have the *mean* and *variance* of f

$$\bar{f} = \frac{1}{N} \sum_{i=1}^{N} f_i, \tag{2}$$

and

$$\sigma^2 = \frac{1}{N} \sum_{i=1}^{N} (f_i - \bar{f})^2. \tag{3}$$

By letting N_o be the number of pixels for the object within the region **R**, we have the variance of the signal

$$\begin{aligned}
\sigma_s^2 &= \frac{1}{N} \left[\sum_{i=1}^{N_o} (1 - \bar{f})^2 + \sum_{i=1}^{N-N_o} \bar{f}^2 \right] \\
&= \frac{1}{N} [N_o(1 - \bar{f}^2) + (N - N_o)\bar{f}^2] \\
&= \frac{1}{N} \left[N_o \left(1 - \frac{N_o}{N} \right)^2 + (N - N_o) \left(\frac{N_o}{N} \right)^2 \right] \\
&= \frac{N_o}{N} \left(1 - \frac{N_o}{N} \right).
\end{aligned} \tag{4}$$

Similarly, if N_n denotes the number of pixels for the noise, i.e., the number of pixels that are to be altered, within the same region **R**, we have the variance of the noise

$$\sigma_n^2 = \frac{N_n}{N} \left(1 - \frac{N_n}{N} \right). \tag{5}$$

The *signal-to-noise ratio* (SNR), a measure of noise level in decibels [6], may be determined by

$$\text{SNR} = 10 \log_{10} \left(\frac{\sigma_s^2}{\sigma_n^2} \right). \tag{6}$$

ZHOU AND GORDON

FIG. 1. Graph of N_n/N vs SNR.

FIG. 2. Test image (a) in a square: $N = 4225$, $N_o = 1030$, $N_o/N = 0.24$. Noisy images with SNRs of 15 dB (b), 10 dB (c), 5 dB (d), 0 dB (e), and -1.3 dB (f).

where σ_s^2 and σ_n^2 are the variance of the signal and noise, respectively.

B. *Noise Generation*

The generation of binary noise for a binary image may be carried out by randomly selecting some N_n of the total pixels N of the image and reversing their values from 0 to 1 or vice versa. The random pixel selection is performed according to a uniform distribution between 1 and N.

Now consider the specific problem of calculating N_n from the given N, N_o, and the desired SNR. In other words, how many pixels in the image are altered to achieve the desired noise level? By substituting the expressions for σ_s and σ_n into Eq. (6), and making simple rearrangements, we have

$$\left(\frac{N_n}{N}\right)^2 - \frac{N_n}{N} + A = 0, \tag{7}$$

where the constant A is given by

$$A = 10^{-\text{SNR}/10} \frac{N_o}{N} \left(1 - \frac{N_o}{N}\right). \tag{8}$$

The solution of the above equation (7) is, therefore,

$$N_n = \frac{N}{2} (1 \pm B), \tag{9}$$

where

$$B = \left[1 - 4 \cdot 10^{-\text{SNR}/10} \frac{N_o}{N} \left(1 - \frac{N_o}{N}\right)\right]^{1/2}. \tag{10}$$

Some observations can be made from Eq. (9). Because of the characteristics of binary images, the curve of σ_s^2 versus N_o/N is parabolic with a maximum at $N_o/N = 1/2$ in [0, 1] (see Eq. (4)). In other words, when $N_o/N < 1/2$, the smaller the number of object pixels, the less the variance of signal. When $N_o/N > 1/2$, the larger the number of object pixels, the less the variance. The former statement is obvious. The understanding of the latter is, however, based upon the fact that the higher the number of object pixels, the less room for the variation of the pattern. This is simply because binary images take only two possible pixel values. These observations are also true in the case of noise. Keeping these remarks in mind, we select the number of noise pixels from Eq. (9) as follows. When $N_o/N < 1/2$, we choose the negative sign for the second term of Eq. (9), even though the positive sign will give the same SNR value. We choose the negative sign arbitrarily when $N_o/N = 1/2$. The positive sign is chosen for $N_o/N > 1/2$. Explicitly, we have

$$N_n = \begin{cases} \dfrac{N}{2} (1 - B), & \text{for } \dfrac{N_o}{N} \leq \dfrac{1}{2}, \\[2mm] \dfrac{N}{2} (1 + B), & \text{otherwise}, \end{cases} \tag{11}$$

where B is calculated from Eq. (10). A graph of N_n/N versus SNR is shown in Fig. 1.

Note that only a limited number of negative SNRs could possibly be generated for a given binary image, i.e., a fixed N_o/N. For instance, for $N_o/N = 1/2$, the least SNR that could be created is 0.

III. EXAMPLES AND CONCLUSIONS

Four experiments were carried out to demonstrate the proposed method. For all examples noisy images with
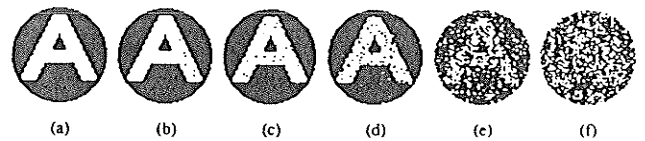
FIG. 3. Test image (a) in a square: $N = 3313$, $N_o = 1030$, $N_o/N = 0.31$. Noisy images with SNRs of 15 dB (b), 10 dB (c), 5 dB (d), 0 dB (e), and -0.6 dB (f).
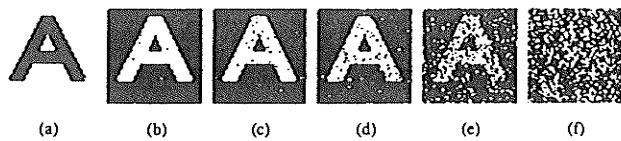
FIG. 4. Inverse of Fig. 2a as a test image (a): $N = 4225$, $N_o = 3195$. $N_o/N = 0.76$. Noisy images with SNRs of 15 dB (b), 10 dB (c), 5 dB (d), 0 dB (e), and −1.3 dB (f).
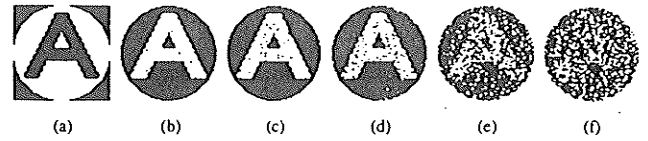
FIG. 5. Inverse of Fig. 4a as a test image (a): $N = 3313$, $N_o = 2283$. $N_o/N = 0.69$. Noisy images with SNRs of 15 dB (b), 10 dB (c), 5 dB (d), 0 dB (e), and −0.6 dB (f).

SNRs of 15, 10, 5, and 0 dB were generated. Images with the least possible SNRs (−0.6 dB for a square region and −1.3 dB for a circle region) were also created. We deliberately select test patterns (Figs. 2a and 3a) with $N_o/N < 1/2$ for the first and second experiments. In the first experiment, the generated noisy images, of which noise pixels are created for the test image in a square region, are shown in Figs. 2b–2f. For the second example, noise pixels are constrained to be inside a circle only (Figs. 3b–3f).

In the third and fourth experiments (Figs. 4 and 5), test patterns are simply the inverted counterpart of the patterns in the first two examples. That is, for these patterns $N_o/N > 1/2$. The created noisy images are shown in Figs. 4b–4f and 5b–5f. Note that it is because $N_o/N > 1/2$ that these noisy images appear as the negatives of those with the same SNRs generated from the first two test patterns.

In summary, a method of binary noise generation has been developed in this note. With this method noisy im-

ages with different noise levels can be generated for any given binary image in any specific region. This method should facilitate the experimental evaluation of different image processing and classification algorithms on binary images.

REFERENCES

1. J. C. Stoffel (Ed.), *Graphical and Binary Image Processing and Applications*, Artech House, Dedham, MA, 1982.
2. H. J. Trussell, Processing of X-ray images, *Proc. IEEE* 69, 1981, 615–627.
3. W. Pferd and G. Stocker, Optical fibers for scanning digitizers, *Bell Syst. Tech. J.* 60, 1981, 523–534.
4. J. R. Ullman, Binarization using associate addressing, *Pattern Recognit.* 6, 1974, 127–135.
5. L. G. Shapiro, Inexact matching of line drawings in a syntactic pattern recognition system, *Pattern Recognit.* 10, 1978, 313–321.
6. K. R. Castleman, *Digital Image Processing*, Prentice–Hall, Englewood Cliffs, NJ, 1979.

APPENDIX 5

SOURCE CODE OF ZERNIKE MOMENTS FUNCTIONS

This appendix contains C source code of functions for computing Zernike moments (Chapter 5), as well as recognizing orientation and detecting symmetric axes in planar objects using the phase information in Zernike moments (Chapter 6).

```
/************************************************************************

  zernikemoment.h

  This header file contains constants, types, and function prototypes.

  (C) Copyright The Laboratory of Dr. Richard Gordon. 1991.
  All rights reserved.

 ************************************************************************/


#include    <math.h>


#ifndef NULL
#define NULL            0L          /* null pointer value */
#endif

#define PI                  3.141593    /* π */
#define TWO_PI              6.283185    /* 2π */
#define RADIAN_TO_DEGREE    57.29578    /* radian to degree fator */
#define DEGREE_TO_RADIAN    0.017453    /* degree to radian fator */

#define MAX_X           65              /* max picture size in horiz., and */
#define MAX_Y           MAX_X           /* in vert. direction */
#define MAX_N           17              /* max order in computing Zerike moments */

#define SMALL_REAL      1.0e-16         /* small float/double value */
#define TOLERANCE       1.0e-4          /* fractional precision for optimization */

#define ZM_ABS_NORM     0               /* absolute norm */
#define ZM_EUCL_NORM    1               /* Euclidean norm */
#define ZM_MAX_NORM     2               /* maximum norm */


/* some useful macros */
#define MAX(a,b) ((a) > (b) ? (a) : (b))
#define VECTORMAG(a,b) sqrt((a)*(a)+(b)*(b))


/* function prototypes */
double golden(double ax, double bx, double cx, double (*f)(double x),
    double tol, double *xmin);

double get_rnl_val(int n, int l, double r);
int cal_zernike_moment_val(int nx, int ny, int **f, int n, int l,
    double *cnl, double *snl);
int cal_zernike_moments(int nx, int ny, int **f, int nmin, int nmax,
```

```
        double **cnl, double **snl, double **anl);
int test_zm_moment(void);

int **imatrix(int nrl, int nrh, int ncl, int nch);
void free_imatrix(int **m, int nrl, int nrh, int ncl, int nch);
double **dmatrix(int nrl, int nrh, int ncl, int nch);
void free_dmatrix(double **m, int nrl, int nrh, int ncl, int nch);
int get_pict(char *fname, int *nx, int *ny, int **f);
int put_pict(char *fname, int nx, int ny, int **f);
double factorial(int n);
int cal_rnl_coeffs(int nmax, char *zm);
int get_zm_index(int n, int m);
int get_polar_coords(double x0, double y0, int x, int y, double *theta,
        double *rho);
int get_zernike_moments(int nmin, int nmax, char *zm, double **cnl,
        double **snl);

double zm_orien_abs_norm(double theta);
double zm_orien_eucl_norm(double theta);
double zm_orien_max_norm(double theta);
int get_zm_orien(int nmin, int nmax, char *zm1, char *zm2, int norm,
        double *orien, double *err);
int test_zm_orien(void);

double zm_symmaxis_abs_norm(double theta);
double zm_symmaxis_eucl_norm(double theta);
double zm_symmaxis_max_norm(double theta);
int get_zm_symmaxis(int nmin, int nmax, char *zm, int norm,
        double *axis, double *err);
int test_zm_symmaxis(void);

int zm_contrib(int n, double **cnl, double **snl, int nx, int nx,
        double **f);
int zm_recons(int nmin, int nmin, double **cnl, double **snl, int nx,
        int ny, char *fname);
int test_zm_recons(void);
```

```
/************************************************************************

  zm_general.c

  This file contains general functions about Zernike moments.
```

```
*************************************************************************/


#include <stdio.h>
#include <stdlib.h>
#include "zernikemoment.h"



/************************************************************************


    name:           imatrix

    description:    Allocates an int matrix with range [nrl..nrh][ncl..nch].
                    The returned value is the matrix's address, if successful;
                    otherwise, a NULL pointer is returned instead.

    syntax:         int **imatrix(int nrl, int nrh, int ncl, int nch)

    written by:     X. Zhou
    date:           September 16, 1991

*************************************************************************/
int **imatrix(
    int nrl,      /* the lower bound, and */
    int nrh,      /* the upper bound of the rows index */
    int ncl,      /* the lower bound, and */
    int nch       /* the upper bound of the columns index */
) {
    int i, **m;

    /* allocate pointers to rows */
    m = (int **)malloc((unsigned) (nrh-nrl+1)*sizeof(int*));
    if (!m) return NULL;
    m -= nrl;

    /* allocate rows and set pointers to them */
    for (i = nrl; i <= nrh; i++) {
        m[i]=(int *)malloc((unsigned) (nch-ncl+1)*sizeof(int));
        if (!m[i]) return NULL;
        m[i] -= ncl;
```

```
    }
    /* return pointer to array of pointers to rows */
    return m;
}



/*********************************************************************


    name:           free_imatrix

    description:    Frees an int matrix allocated with imatrix().

    syntax:         void free_imatrix(int **m, int nrl, int nrh, int ncl,
                    int nch)

    written by:     X. Zhou
    date:           September 16, 1991

*********************************************************************/
void free_imatrix(
    int **m,      /* the int matrix */
    int nrl,      /* the lower bound, and */
    int nrh,      /* the upper bound of the rows index */
    int ncl,      /* the lower bound, and */
    int nch       /* the upper bound of the columns index */
) {
    int i;

    for (i = nrh; i >= nrl; i--) free((char*) (m[i]+ncl));
    free((char*) (m+nrl));
}



/*********************************************************************


    name:           dmatrix

    description:    Allocates a double matrix with range [nrl..nrh][ncl..nch].
                    The returned value is the matrix's address, if successful;
                    otherwise, a NULL pointer is returned instead.

    syntax:         double **dmatrix(int nrl, int nrh, int ncl, int nch)

    written by:     X. Zhou
    date:           September 16, 1991

*********************************************************************/
double **dmatrix(
    int nrl,     /* the lower bound, and */
```

```c
    int nrh,    /* the upper bound of the rows index */
    int ncl,    /* the lower bound, and */
    int nch     /* the upper bound of the columns index */
) {
    int     i;
    double  **m;

    /* allocate pointers to rows */
    m = (double **)malloc((unsigned) (nrh-nrl+1)*sizeof(double*));
    if (!m) return NULL;
    m -= nrl;

    /* allocate rows and set pointers to them */
    for (i = nrl; i <= nrh; i++) {
        m[i] = (double *)malloc((unsigned) (nch-ncl+1)*sizeof(double));
        if (!m[i]) return NULL;
        m[i] -= ncl;
    }
    /* return pointer to array of pointers to rows */
    return m;
}



/*******************************************************************

    name:           free_dmatrix

    description:    Frees a double matrix allocated with dmatrix().

    syntax:         void free_dmatrix(double **m, int nrl, int nrh, int ncl,
                    int nch)

    written by:     X. Zhou
    date:           September 16, 1991

*******************************************************************/
void free_dmatrix(
    double **m, /* the double matrix */
    int nrl,    /* the lower bound, and */
    int nrh,    /* the upper bound of the rows index */
    int ncl,    /* the lower bound, and */
    int nch     /* the upper bound of the columns index */
) {
    int i;

    for (i = nrh; i >= nrl; i--) free((char*) (m[i]+ncl));
    free((char*) (m+nrl));
}
```

```
/*****************************************************************


    name:           get_pict

    description:    Get the picture F from the file FNAME. The size is
                    returned in NX and NY.

    syntax:         int get_pict(char *fname, int *nx, int *ny, int **f)

    errors:          0 - no error
                    -1 - cannot open the file FNAME
                    -2 - picture size (NX, NY) too large

    written by:     X. Zhou
    date:           September 16, 1991

*****************************************************************/
int get_pict(
    char    *fname,     /* file name contains the desired picture */
    int     *nx,        /* returned picture size in horiz., and */
    int     *ny,        /* the vert. directions */
    int     **f         /* the returned picture data */
) {
    int     i, j;
    FILE    *in, *fopen();

    if ((in = fopen(fname, "r")) == NULL) return -1;
    clearerr(in);
    fscanf(in, "%d\t%d\n", nx, ny);
    if ((*nx) > MAX_X || (*ny) > MAX_Y)        /* picture size too large */
        return -2;
    for (j = 0; j < (*ny); j++)
        for (i = 0; i < (*nx); i++)
            fscanf(in, "%d\t", &f[j][i]);
    return 0;
}



/*****************************************************************


    name:           put_pict

    description:    Save the picture F of size NX and NY to the file FNAME.

    syntax:         int put_pict(char *fname, int nx, int ny, int **f)

    errors:          0 - no error
                    -1 - cannot open the file FNAME
```

```
                        -2 - picture size (NX, NY) too large

    written by:     X. Zhou
    date:           September 16, 1991


**********************************************************************/
int put_pict(
    char    *fname,     /* the desired file name */
    int     nx,         /* the picture size in horiz., and */
    int     ny,         /* the vert. directions */
    int     **f         /* the picture data to be saved */
) {
    int     i, j, value;
    FILE    *out, *fopen();

    if ((out = fopen(fname, "w")) == NULL) return -1;
    clearerr(out);
    fprintf(out, "%d\t%d\n", nx, ny);
    for (j = 0; j < ny; j++)
    {
        for (i = 0; i < nx; i++)
            fprintf(out, "%d\t", f[j][i]);
        fprintf(out, "\n");
    }
    fclose(out);
    return 0;
}




/********************************************************************


    name:           factorial

    description:    Compute the factorial N! as the returned, in double
                    precision.

    syntax:         double factorial(int n)

    written by:     X. Zhou
    date:           September 16, 1991


**********************************************************************/
double factorial(
    int n
) {
    int     n0 = n;
    double  p = n;

    if (n0 <= 0) return 1.0;
```

```c
    while (n0 >= 2) p *= --n0;
    return p;
}



/********************************************************************

    name:             cal_rnl_coeffs

    description:      Compute the Zernike polynomial coefficients up to order
                      NMAX, and save them in the given file ZM.

    syntax:           int cal_rnl_coeffs(int nmax, char *zm)

    errors:            0 - no error
                      -1 - cannot save the Zernike polynomial coefficients

    written by:       X. Zhou
    date:             September 16, 1991

********************************************************************/
int cal_rnl_coeffs(
    int nmax,          /* max order for computing Zernike polynomial coeffs */
    char *zm           /* */
) {
    int     l, s, n, nml, npl2, nml2;
    double  p;
    FILE    *out, *fopen();

    if ((out = fopen(zm, "w")) == NULL) return -1;
    clearerr(out);

    fprintf(out, "Radial Poltnomial Coefficients for Zernike Moment Calculation\n\n",
    for (n = 0; n <= nmax; n++)
    {
        fprintf(out, "***** order n = %d\n", n);
        for (l = 0; l <= n; l++)
        {
            nml = n-l;
            if ((nml & 1) == 0)      /* n-l is an even number */
            {
                fprintf(out, "   ** angular dependence l = %d\n", l);
                nml2 = nml / 2;
                npl2 = (n+l) / 2;
                for (s = 0; s <= nml2; s++)
                {
                    p = factorial(n-s)/factorial(s)/factorial(npl2-s)/factorial(nml2-s
                    if (s & 1) p = -p;
                    fprintf(out, "s = %d;\tp = %20.1f\n", s, p);
```

```c
                    }
                    fprintf(out, "    **\n");
                }
            }
            fprintf(out, "*****\n\n");
        }
        fclose(out);
        return 0;
    }



/**********************************************************************


        name:           get_zm_index

        description:    Get, as the returned value, the Zernike moment index of
                        the order N and angular dependence M.

        syntax:         int get_zm_index(int n, int m)

        written by:     X. Zhou
        date:           September 16, 1991

**********************************************************************/
int get_zm_index(
    int n,   /* the order */
    int m    /* the angular dependence */
) {
    int i, n21, s0, s = 0;

    if (n == 0) return 1;    /* zero order */

    if ((n & 1) == 0)        /* n is an even number */
    {
        n21 = floor((n-1)/2) + 1;
        s0 = 0;
    }
    else
    {
        n21 = floor(n/2);
        s0 = n21 + 1;
    }
    for (i = 1; i <= n21; i++) s += i;
    s += s + s0 + (floor(m/2) + 1);
    return s;
}



/**********************************************************************
```

```
        name:               get_polar_coords

        description:        Convert the Cartesian coords (x,y) to polar coords
                            (theta, rho). Theta is from the X-AXIS and positive
                            counterclockwise.

        syntax:             int get_polar_coords(double x0, double y0,
                            int x, int y, double *theta, double *rho)

        errors:              0 - no error
                            -1 - picture size too small

        written by:     X. Zhou
        date:           September 16, 1991

*********************************************************************************/
int get_polar_coords(
    double x0,          /* the picture's centre */
    double y0,
    int     x,          /* the Cartesian coords */
    int     y,
    double *theta,      /* the returned polar coords */
    double *rho
) {
    double r, dx, dy;

    r = (x0 > y0) ? x0 : y0;      /* take the long side as diameter */
    if (fabs(r) < SMALL_REAL) return -1;
    dx = (x+0.5) - x0;
    dy = (y+0.5) - y0;
    *theta = atan2(-dy, dx);
    if ((*theta) < SMALL_REAL)   /* always return positive angle value */
        *theta += TWO_PI;
    *rho = sqrt(dx*dx + dy*dy) / r;
    return 0;
}



/******************************************************************************

        name:               get_zernike_moments

        description:        Get the Zernike moments CNL and SNL of orders NMIN to
                            NMAX from the files ZM.

        syntax:             int get_zernike_moments(int nmin, int nmax,
                            char *zm, double **cnl, double **snl)
```

```
        errors:             0 - no error
                           -1 - cannot open the file zm
                           -2 - the number of items per line not matched
                           -3 - the order or angular dependence does not match
                                that in the moment file

        written by:    X. Zhou
        date:          September 16, 1991

**********************************************************************/
int get_zernike_moments(
    int     nmin,          /* the min and */
    int     nmax,          /* min orders of Zernike moment */
    char    *zm,           /* the object file name */
    double  **cnl,         /* the real part, and */
    double  **snl          /* the imaginary part of the Zernike moments */
) {
    int     j, k;          /* tmp vars */
    int     n, l;          /* order and angular dependence */
    double  c, s, a;       /* intermediate moment vars */
    FILE    *in, *fopen();

    if ((in = fopen(zm, "r")) == NULL) return -1;

    clearerr(in);
    for (n = 0; n < nmin; n++)  /* skip the unwanted ones in ZM */
        for (l = 0; l <= n; l++) {
            if ((n-l & 1) == 0) {    /* n-l is an even number */
                if (fscanf(in, "%d,%d:\t%lf\t%lf\t%lf\n",
                    &j, &k, &c, &s, &a) != 5) return -2;
            }
        }
    for (n = nmin; n <= nmax; n++)
        for (l = 0; l <= n; l++) {
            if ((n-l & 1) == 0) {    /* n-l is an even number */
                if (fscanf(in, "%d,%d:\t%lf\t%lf\t%lf\n",
                    &j, &k, &c, &s, &a) != 5) return -2;
                if (j!=n || k!=l) return -3;
                cnl[n][l] = c;
                snl[n][l] = s;
            }
        }
    fclose(in);
    return 0;
}
```

```
/**********************************************************************

  zm_moment.c

  This file contains functions for computing Zernike moments.

  (C) Copyright The Laboratory of Dr. Richard Gordon. 1991.
  All rights reserved.

 **********************************************************************/


#include <stdio.h>
#include <string.h>
#include "zernikemoment.h"



/**********************************************************************

      name:              get_rnl_val

      description:       Compute, as the returned value, the radial Zernike
                         polynomial value of order N, angular dependence L at
                         distance R.

      syntax:            double get_rnl_val(int n, int l, double r)

      written by:        X. Zhou
      date:              September 16, 1991

 **********************************************************************/
double get_rnl_val(
    int n,          /* Zernike moment order */
    int l,          /* angular dependence */
    double r        /* radial distance */
) {
    double  r2, R0 = 0.0;

    if (n < 0 || l > n) return R0;
    r2 = r * r;
    switch (n)
    {
    case 0:
        if (l == n) R0 = 1.0;
        break;
    case 1:
        if (l == n) R0 = r;
        break;
    case 2:
```

```
        if (l == 0) R0 = 2.0*r2-1.0;
        else if (l == n) R0 = r2;
        break;
    case 3:
        if (l == 1) R0 = r*(3.0*r2-2.0);
        else if (l == n) R0 = r*r2;
        break;
    case 4:
        if (l == 0) R0 = 6.0*(r2-1.0)*r2+1.0;
        else if (l == 2) R0 = r2*(4.0*r2-3.0);
        else if (l == n) R0 = r2*r2;
        break;
    case 5:
        if (l == 1) R0 = r*((10.0*r2-12.0)*r2+3.0);
        else if (l == 3) R0 = r*r2*(5.0*r2-4.0);
        else if (l == n) R0 = r*r2*r2;
        break;
    case 6:
        if (l == 0) R0 = ((20.0*r2-30.0)*r2+12.0)*r2-1.0;
        else if (l == 2) R0 = r2*((15.0*r2-20.0)*r2+6.0);
        else if (l == 4) R0 = r2*r2*(6.0*r2-5.0);
        else if (l == n) R0 = r2*r2*r2;
        break;
    case 7:
        if (l == 1) R0 = r*(((35.0*r2-60.0)*r2+30.0)*r2-4.0);
        else if (l == 3) R0 = r*r2*((21.0*r2-30.0)*r2+10.0);
        else if (l == 5) R0 = r*r2*r2*(7.0*r2-6.0);
        else if (l == n) R0 = r*r2*r2*r2;
        break;
    case 8:
        if (l == 0) R0 = (((70.0*r2-140.0)*r2+90.0)*r2-20.0)*r2+1.0;
        else if (l == 2) R0 = r2*(((56.0*r2-105.0)*r2+60.0)*r2-10.0);
        else if (l == 4) R0 = r2*r2*((28.0*r2-42.0)*r2+15.0);
        else if (l == 6) R0 = r2*r2*r2*(8.0*r2-7.0);
        else if (l == n) R0 = r2*r2*r2*r2;
        break;
    case 9:
        if (l == 1) R0 = r*((((126.0*r2-280.0)*r2+210.0)*r2-60.0)*r2+5.0);
        else if (l == 3) R0 = r*r2*(((84.0*r2-168.0)*r2+105.0)*r2-20.0);
        else if (l == 5) R0 = r*r2*r2*((36.0*r2-56.0)*r2+21.0);
        else if (l == 7) R0 = r*r2*r2*r2*(9.0*r2-8.0);
        else if (l == n) R0 = r*r2*r2*r2*r2;
        break;
    case 10:
        if (l == 0) R0 = ((((252.0*r2-630.0)*r2+560.0)*r2-210.0)*r2+30.0)*r2-1.0;
        else if (l == 2) R0 = r2*((((210.0*r2-504.0)*r2+420.0)*r2-140.0)*r2+15.0);
        else if (l == 4) R0 = r2*r2*(((120.0*r2-252.0)*r2+168.0)*r2-35.0);
        else if (l == 6) R0 = r2*r2*r2*((45.0*r2-72.0)*r2+28.0);
        else if (l == 8) R0 = r2*r2*r2*r2*(10.0*r2-9.0);
```

```c
        else if (l == n) R0 = r2*r2*r2*r2*r2;
        break;
    case 11:
        if (l == 1) R0 = r*(((((462.0*r2-1260.0)*r2+1260.0)*r2-560.0)*r2+105.0)*r2-6.0
        else if (l == 3) R0 = r*r2*((((330.0*r2-840.0)*r2+756.0)*r2-280.0)*r2+35.0);
        else if (l == 5) R0 = r*r2*r2*(((165.0*r2-360.0)*r2+252.0)*r2-56.0);
        else if (l == 7) R0 = r*r2*r2*r2*((55.0*r2-90.0)*r2+36.0);
        else if (l == 9) R0 = r*r2*r2*r2*r2*(11.0*r2-10.0);
        else if (l == n) R0 = r*r2*r2*r2*r2*r2;
        break;
    case 12:
        if (l == 0) R0 = ((((((924.0*r2-2772.0)*r2+3150.0)*r2-1680.0)*r2+420.0)*r2-42.0
        else if (l == 2) R0 = r2*((((((792.0*r2-2310.0)*r2+2520.0)*r2-1260.0)*r2+280.0)
        else if (l == 4) R0 = r2*r2*((((495.0*r2-1320.0)*r2+1260.0)*r2-504.0)*r2+70.0)
        else if (l == 6) R0 = r2*r2*r2*(((220.0*r2-495.0)*r2+360.0)*r2-84.0);
        else if (l == 8) R0 = r2*r2*r2*r2*((66.0*r2-110.0)*r2+45.0);
        else if (l == 10) R0 = r2*r2*r2*r2*r2*(12.0*r2-11.0);
        else if (l == n) R0 = r2*r2*r2*r2*r2*r2;
        break;
    case 13:
        if (l == 1) R0 = r*(((((((1716.0*r2-5544.0)*r2+6930.0)*r2-4200.0)*r2+1260.0)*r2
        else if (l == 3) R0 = r*r2*((((((1287.0*r2-3960.0)*r2+4620.0)*r2-2520.0)*r2+630
        else if (l == 5) R0 = r*r2*r2*(((((715.0*r2-1980.0)*r2+1980.0)*r2-840.0)*r2+126
        else if (l == 7) R0 = r*r2*r2*r2*(((286.0*r2-660.0)*r2+495.0)*r2-120.0);
        else if (l == 9) R0 = r*r2*r2*r2*r2*((78.0*r2-132.0)*r2+55.0);
        else if (l == 11) R0 = r*r2*r2*r2*r2*r2*(13.0*r2-12.0);
        else if (l == n) R0 = r*r2*r2*r2*r2*r2*r2;
        break;
    case 14:
        if (l == 0) R0 = (((((((3432.0*r2-12012.0)*r2+16632.0)*r2-11550.0)*r2+4200.0)*r
        else if (l == 2) R0 = r2*((((((3003.0*r2-10296.0)*r2+13860.0)*r2-9240.0)*r2+31
        else if (l == 4) R0 = r2*r2*((((((2002.0*r2-6435.0)*r2+7920.0)*r2-4620.0)*r2+12
        else if (l == 6) R0 = r2*r2*r2*(((((1001.0*r2-2860.0)*r2+2970.0)*r2-1320.0)*r2+
        else if (l == 8) R0 = r2*r2*r2*r2*(((364.0*r2-858.0)*r2+660.0)*r2-165.0);
        else if (l == 10) R0 = r2*r2*r2*r2*r2*((91.0*r2-156.0)*r2+66.0);
        else if (l == 12) R0 = r2*r2*r2*r2*r2*r2*(14.0*r2-13.0);
        else if (l == n) R0 = r2*r2*r2*r2*r2*r2*r2;
        break;
    case 15:
        if (l == 1) R0 = r*(((((((6435.0*r2-24024.0)*r2+36036.0)*r2-27720.0)*r2+11550.
        else if (l == 3) R0 = r*r2*((((((5005.0*r2-18018.0)*r2+25740.0)*r2-18480.0)*r2
        else if (l == 5) R0 = r*r2*r2*((((((3003.0*r2-10010.0)*r2+12870.0)*r2-7920.0)*r
        else if (l == 7) R0 = r*r2*r2*r2*((((1365.0*r2-4004.0)*r2+4290.0)*r2-1980.0)*r
        else if (l == 9) R0 = r*r2*r2*r2*r2*(((455.0*r2-1092.0)*r2+858.0)*r2-220.0);
        else if (l == 11) R0 = r*r2*r2*r2*r2*r2*((105.0*r2-182.0)*r2+78.0);
        else if (l == 13) R0 = r*r2*r2*r2*r2*r2*r2*(15.0*r2-14.0);
        else if (l == n) R0 = r*r2*r2*r2*r2*r2*r2*r2;
        break;
    case 16:
```

```c
            if (l == 0) R0 = (((((((12870.0*r2-51480.0)*r2+84084.0)*r2-72072.0)*r2+34650.0
            else if (l == 2) R0 = r2*((((((((11440.0*r2-45045.0)*r2+72072.0)*r2-60060.0)*r2
            else if (l == 4) R0 = r2*r2*((((((8008.0*r2-30030.0)*r2+45045.0)*r2-34320.0)*r
            else if (l == 6) R0 = r2*r2*r2*((((((4368.0*r2-15015.0)*r2+20020.0)*r2-12870.0)
            else if (l == 8) R0 = r2*r2*r2*r2*(((((1820.0*r2-5460.0)*r2+6006.0)*r2-2860.0)*
            else if (l == 10) R0 = r2*r2*r2*r2*r2*(((560.0*r2-1365.0)*r2+1092.0)*r2-286.0)
            else if (l == 12) R0 = r2*r2*r2*r2*r2*r2*((120.0*r2-210.0)*r2+91.0);
            else if (l == 14) R0 = r2*r2*r2*r2*r2*r2*r2*(16.0*r2-15.0);
            else if (l == n) R0 = r2*r2*r2*r2*r2*r2*r2*r2;
            break;
        case 17:
            if (l == 1) R0 = r*(((((((((24310.0*r2-102960.0)*r2+180180.0)*r2-168168.0)*r2+9
            else if (l == 3) R0 = r*r2*(((((((19448.0*r2-80080.0)*r2+135135.0)*r2-120120.0
            else if (l == 5) R0 = r*r2*r2*((((((12376.0*r2-48048.0)*r2+75075.0)*r2-60060.0
            else if (l == 7) R0 = r*r2*r2*r2*((((((6188.0*r2-21840.0)*r2+30030.0)*r2-20020.
            else if (l == 9) R0 = r*r2*r2*r2*r2*((((2380.0*r2-7280.0)*r2+8190.0)*r2-4004.0
            else if (l == 11) R0 = r*r2*r2*r2*r2*r2*(((680.0*r2-1680.0)*r2+1365.0)*r2-364.
            else if (l == 13) R0 = r*r2*r2*r2*r2*r2*r2*((136.0*r2-240.0)*r2+105.0);
            else if (l == 15) R0 = r*r2*r2*r2*r2*r2*r2*r2*(17.0*r2-16.0);
            else if (l == n) R0 = r*r2*r2*r2*r2*r2*r2*r2*r2;
            break;
        case 18:
            if (l == 0) R0 = ((((((((48620.0*r2-218790.0)*r2+411840.0)*r2-420420.0)*r2+252
            else if (l == 2) R0 = r2*(((((((((43758.0*r2-194480.0)*r2+360360.0)*r2-360360.0
            else if (l == 4) R0 = r2*r2*(((((((31824.0*r2-136136.0)*r2+240240.0)*r2-225225
            else if (l == 6) R0 = r2*r2*r2*((((((18564.0*r2-74256.0)*r2+120120.0)*r2-10010
            else if (l == 8) R0 = r2*r2*r2*r2*((((((8568.0*r2-30940.0)*r2+43680.0)*r2-30030
            else if (l == 10) R0 = r2*r2*r2*r2*r2*((((3060.0*r2-9520.0)*r2+10920.0)*r2-546
            else if (l == 12) R0 = r2*r2*r2*r2*r2*r2*(((816.0*r2-2040.0)*r2+1680.0)*r2-455
            else if (l == 14) R0 = r2*r2*r2*r2*r2*r2*r2*((153.0*r2-272.0)*r2+120.0);
            else if (l == 16) R0 = r2*r2*r2*r2*r2*r2*r2*r2*(18.0*r2-17.0);
            else if (l == n) R0 = r2*r2*r2*r2*r2*r2*r2*r2*r2;
            break;
        default:;
        }
        return R0;
}


/*******************************************************************************


        name:           cal_zernike_moment_val

        description:    Compute Zernike moment (CNL, SNL) of order N and
                        angular dependence L for picture F of size NX x NY
                        by direct numerical integration.

        syntax:         int cal_zernike_moment_val(int nx, int ny, int **f,
                        int n, int l,
```

```
                    double *cnl, double *snl)

     errors:         0 - no error
                    -1 - picture size <= 0

     written by:     X. Zhou
     date:           September 16, 1991

*************************************************************************/
cal_zernike_moment_val(
     int     nx,       /* the horiz. size, and */
     int     ny,       /* the vert. size of the picture */
     int     **f,      /* the picture */
     int     n,        /* the order, and */
     int     l,        /* the angular dependence of Zernike moment */
     double  *cnl,     /* the real part, and */
     double  *snl      /* the imaginary part of Zernike moments computed */
) {
     int     col, row;       /* coords */
     double  Rnl;            /* */
     double  x0, y0;         /* the pict's centre */
     double  dx, dy, x, y, theta, rho, ltheta;
     double  scale, tempVal, sumC, sumS;

     if (x0 <= 0 || y0 <= 0) return -1;
     x0 = 0.5 * nx;       /* get the pict's centre */
     y0 = 0.5 * ny;
     dx = 1.0 / x0;       /* get the sampling interval in each dimension */
     dy = 1.0 / y0;
     sumC = sumS = 0.0;
     for (row = 0; row < ny; row++)
         for (col = 0; col < nx; col++)
         {
             tempVal = f[row][col];
             if (fabs(tempVal) > SMALL_REAL) /* take non-zero point only */
             {
                 if (get_polar_coords(x0, y0, col, row, &theta, &rho) == 0)
                     if (rho - 1.0 <= SMALL_REAL)
                     {
                         tempVal *= get_rnl_val(n, l, rho);
                         if (l == 0 || fabs(theta) < SMALL_REAL)
                             sumC += tempVal;
                         else
                         {
                             ltheta = l * theta;
                             sumC += tempVal * cos(ltheta);
                             sumS += tempVal * sin(ltheta);
                         }
                     }
             }
```

```
            }
        }
    scale = dx*dy * (n+1.0) / PI;
    *cnl = scale * sumC;
    *snl = -scale * sumS;
    return 0;
}



/******************************************************************


    name:           cal_zernike_moments

    description:    Compute a set of Zernike moments CNL, SNL (ANL) from
                    order NMIN to NMAX for picture F of size NX x NY.

    syntax:         int cal_zernike_moments(int nx, int ny, int **f,
                    int nmin, int nmax, double **cnl, double **snl,
                    double **anl)

    errors:          0 - no error
                    -1 - min order nmin > max order nmax
                    -2 - nmax > max possible order MAX_N
                    -3 - error from function cal_zernike_moment_val

    written by:     X. Zhou
    date:           September 16, 1991

******************************************************************/
int cal_zernike_moments(
    int     nx,     /* the horiz. size, and */
    int     ny,     /* the vert. size of the picture */
    int     **f,    /* the picture */
    int     nmin,   /* the min order, and */
    int     nmax,   /* the max order of Zernike moments to be computed */
    double  **cnl,  /* the real part, */
    double  **snl,  /* the imaginary part, and */
    double  **anl   /* the magnitude of Zernike moments computed */
) {
    int     n, l;
    double  c, s;

    if (nmin > nmax) return -1;     /* parameter check */
    if (nmax > MAX_N) return -2;
    for (n = nmin; n <= nmax; n++)
        for (l = 0; l <= n; l++)
            if ((n-l & 1) == 0)     /* n-l is an even number */
            {
                if (cal_zernike_moment_val(nx, ny, f, n, l, &c, &s) != 0)
```

```
                              return -3;
                    cnl[n][l] = c;
                    snl[n][l] = s;
                    anl[n][l] = sqrt(c*c+s*s);
                }
        return 0;
}



/**********************************************************************


    name:               test_zm_moment

    description:        Test the Zernike moment computation function
                        cal_zernike_moments, where the picture data is stored
                        in the file "char_a", and the desired Zernike moments
                        orders are from 0 to 16.

    syntax:             int test_zm_moment(void)

    errors:              0 - no error
                        -1 - cannot allocate dynamic storage
                        -2 - cannot open the picture data file
                        -3 - error occurred in computing Zernike moments
                        -4 - cannot save the computed moments

    written by:         X. Zhou
    date:               September 16, 1991

**********************************************************************/
int test_zm_moment(
    void
) {
    #define nmin        0               /* min & max moment orders */
    #define nmax        16
    #define pict_name   "char_a"    /* picture file name */

    int     n, l, nx, ny;
    char    fname[256];
    FILE    *out, *fopen();
    int     **f;
    double  **cnl, **snl, **anl;

    /* allocate dynamic storage for the picture */
    if ((f = imatrix(0, MAX_X, 0, MAX_Y)) == NULL) return -1;
    if (get_pict((char*)pict_name, &nx, &ny, f) != 0)
    {
        free_imatrix(f, 0, MAX_X, 0, MAX_Y);
        return -2;
```

```c
    }

    /* allocate dynamic storage for the moments */
    cnl = dmatrix(0, MAX_N, 0, MAX_N);
    snl = dmatrix(0, MAX_N, 0, MAX_N);
    if ((anl = dmatrix(0, MAX_N, 0, MAX_N)) == NULL)
    {   /* if anl is OK, cnl & snl must be all right */
        free_dmatrix(snl, 0, MAX_N, 0, MAX_N);
        free_dmatrix(cnl, 0, MAX_N, 0, MAX_N);
        free_imatrix(f, 0, MAX_X, 0, MAX_Y);
        return -1;
    }
    if (cal_zernike_moments(nx, ny, f, nmin, nmax, cnl, snl, anl) != 0)
        return -3;

    strcpy(fname, pict_name);
    strcat(fname, ".zm");
    if ((out = fopen(fname, "w")) == NULL) return -4;
    clearerr(out);
    for (n = nmin; n <= nmax; n++)
        for (l = 0; l <= n; l++)
        {
            if ((n-l & 1) == 0)        /* n-l is an even number */
                fprintf(out, "%d,%d:\t%12.6f\t%12.6f\t%12.6f\n",
                n, l, cnl[n][l], snl[n][l], anl[n][l]);
        }
    fclose(out);

    free_dmatrix(anl, 0, MAX_N, 0, MAX_N);  /* clean up */
    free_dmatrix(snl, 0, MAX_N, 0, MAX_N);
    free_dmatrix(cnl, 0, MAX_N, 0, MAX_N);
    free_imatrix(f, 0, MAX_X, 0, MAX_Y);
    return 0;
}
```

```
/*********************************************************************

  zm_optim.c

  This file contains functions for optimization.

  (C) Copyright The Laboratory of Dr. Richard Gordon. 1991.
  All rights reserved.

*********************************************************************/


#include <stdio.h>
#include <math.h>

#define R 0.61803399      /* Golden ratios */
#define C (1.0-R)
#define SHFT(a,b,c,d) (a)=(b);(b)=(c);(c)=(d);
#define ITERMAX 100       /* Max allowed #iterations to revent infinite loop */

double golden(double ax, double bx, double cx, double (*f)(double x),
    double tol, double *xmin);
double func1(double x);
int test_golden(void);

/* The function golden is from the book "Numerical Recipes in C: The Art of */
/* Scientific Computing" by W.H. Press, B.P. Flannery, S.A. Teukolsky, and */
/* W.T. Vetterling, Cambridge University Press, Cambridge, 1988. */

/* Given a function f, and given a bracketing triplet of abscissas ax, */
/* bx, cx (such that bx is between ax and cx, and f(bx) is less than both */
/* f(ax) and f(cx)), this routine performs a golden section search for the */
/* minimum, isolating it to a fractional precision of about tol. The */
/* abscissa of the minimum is returned as xmin, and the minimum function */
/* value is returned as golden, the returned function value. */
double golden(
    double ax,         /* abscissas ax, bx, cx such that ax < bx < cx, and */
    double bx,         /* f(bx) < f(ax) and f(bx) < f(cx) */
    double cx,
    double (*f)(double x),   /* the function where the minimum is to be found */
    double tol,        /* fractional precision */
    double *xmin       /* the abscissa of the minimum */
) {
    int     iter=0;
    double  f0, f1, f2, f3, x0, x1, x2, x3;

    x0=ax;   /* At any given time we will keep track of four points, */
    x3=cx;   /* x0,x1,x2,x3. */
    if (fabs(cx-bx) > fabs(bx-ax)) {    /* Make x0 to x1 the smaller segment, */
```

```c
        x1=bx;
        x2=bx+C*(cx-bx);                        /* and fill in the new point to be tried. */
    }
    else {
        x2=bx;
        x1=bx-C*(bx-ax);
    }
    f1=(*f)(x1);     /* The initial function evaluations. Note that we never */
    f2=(*f)(x2);     /* need to evaluate the function at the original endpoints. */
    while (fabs(x3-x0) > tol*(fabs(x1)+fabs(x2)) && iter<ITERMAX) {
        if (f2 < f1) {                          /* One possible outcome, */
            SHFT(x0,x1,x2,R*x1+C*x3)    /* its housekeeping, */
            SHFT(f0,f1,f2,(*f)(x2))     /* and a new function evaluation. */
        }
        else {                                  /* The other outcome, */
            SHFT(x3,x2,x1,R*x2+C*x0)
            SHFT(f3,f2,f1,(*f)(x1))     /* and its new function evaluation. */
        }
        iter++;
    }                       /* Back to see if we are done. */
    if (f1 < f2) {  /* We are done. Output the best of the two */
        *xmin=x1;   /* current values. */
        return f1;
    }
    else {
        *xmin=x2;
        return f2;
    }
}


/* generate a function with xmin = 0.351841; fmin = 0.827184 in [0,1] */
double func1(
    double x     /* the abscissa */
) {
    return exp(-x)+x*x;
}


/* test for the golden function */
int test_golden(void) {
    int     i, j, k;
    double  a = 0.0, b = 1.0, c, fa, fb, fc, xmin, fmin, func1(), golden();

    fmin = golden(a, b, c, func1, 0.0001, &xmin);
    printf("xmin = %12.6lf;\tfmin = %12.6lf\n", xmin, fmin);
    return 0;
}
```

```
/*********************************************************************

  zm_orien.c

  This file contains functions for recognition of orientation by using the
  phase information in Zernike moments.

  (C) Copyright The Laboratory of Dr. Richard Gordon. 1991.
  All rights reserved.

 *********************************************************************/


#include <stdio.h>
#include "zernikemoment.h"

extern int Nmin, Nmax;
extern double **C1nl, **S1nl, **C2nl, **S2nl;


/*********************************************************************

     name:           zm_orien_abs_norm

     description:    Compute the specially defined angular error function
                     for orientation recognition using the absolute norm.

     syntax:         double zm_orien_abs_norm(double theta)

     written by:     X. Zhou
     date:           September 16, 1991

 *********************************************************************/
double zm_orien_abs_norm(
    double theta     /* the abscissa */
) {
    int     n, l;
    double  err=0.0, mt, cosine, sine, dc, ds, anl=0.0;

    for (n = Nmin; n <= Nmax; n++)
        for (l = 0; l <= n; l++)
            if ((n-l & 1) == 0) {
                mt = l*theta;
                cosine = cos(mt);
                sine = sin(mt);
                dc = C2nl[n][l] - (C1nl[n][l]*cosine+S1nl[n][l]*sine);
                ds = S2nl[n][l] - (S1nl[n][l]*cosine-C1nl[n][l]*sine);
                err += VECTORMAG(dc, ds);
                anl += VECTORMAG(C1nl[n][l], S1nl[n][l]);
```

```
            }
    return err/anl;
}



/*********************************************************************

    name:          zm_orien_eucl_norm

    description:   Compute the specially defined angular error function
                   for orientation recognition using the Euclidean norm.

    syntax:        double zm_orien_eucl_norm(double theta)

    written by:    X. Zhou
    date:          September 16, 1991

*********************************************************************/
double zm_orien_eucl_norm(
    double theta     /* the abscissa */
) {
    int     n, l;
    double  err=0.0, mt, cosine, sine, dc, ds, anl2=0.0;

    for (n = Nmin; n <= Nmax; n++)
        for (l = 0; l <= n; l++)
            if ((n-l & 1) == 0) {
                mt = l*theta;
                cosine = cos(mt);
                sine = sin(mt);
                dc = C2nl[n][l] - (C1nl[n][l]*cosine+S1nl[n][l]*sine);
                ds = S2nl[n][l] - (S1nl[n][l]*cosine-C1nl[n][l]*sine);
                err += dc*dc + ds*ds;
                anl2 += C1nl[n][l]*C1nl[n][l] + S1nl[n][l]*S1nl[n][l];
            }
    return err/anl2;
}



/*********************************************************************

    name:          zm_orien_max_norm

    description:   Compute the specially defined angular error function
                   for orientation recognition using the maximum norm.

    syntax:        double zm_orien_max_norm(double theta)

    written by:    X. Zhou
```

        date: September 16, 1991

```
***********************************************************************/
double zm_orien_max_norm(
    double theta     /* the abscissa */
) {

    int      n, l;
    double   err=0.0, mt, cosine, sine, dc, ds, tmp, anl=0.0;

    for (n = Nmin; n <= Nmax; n++)
        for (l = 0; l <= n; l++)
            if ((n-l & 1) == 0) {
                mt = l*theta;
                cosine = cos(mt);
                sine = sin(mt);
                dc = C2nl[n][l] - (C1nl[n][l]*cosine+S1nl[n][l]*sine);
                ds = S2nl[n][l] - (S1nl[n][l]*cosine-C1nl[n][l]*sine);
                tmp = VECTORMAG(dc, ds);
                err = MAX(err, tmp);
                tmp = VECTORMAG(C1nl[n][l], S1nl[n][l]);
                anl = MAX(anl, tmp);
            }
    return err/anl;
}



/********************************************************************

    name:             get_zm_orien

    description:      Compute the orientation ORIEN and minimum error ERR of
                      an object ZM2 with respect to the reference object ZM1
                      with the optimization norm NORM. Zernike moments from
                      order NMIN to NMAX are used in the computation.

    syntax:           int get_zm_orien(int nmin, int nmax, char *zm1,
                      char *zm2, int norm, double *orien, double *err)

    errors:            0 - no error
                      -1 - improper orders NMIN and NMAX
                      -2 - cannot allocate dynamic storage
                      -3 - cannot get the Zernike moments
                      -4 - unknown optimization norm

    written by:       X. Zhou
    date:             September 16, 1991


********************************************************************/
```

```c
int get_zm_orien(
    int      nmin,         /* the min and */
    int      nmax,         /* min orders of Zernike moment */
    char     *zm1,         /* Zernike moments of the reference object */
    char     *zm2,         /* Zernike moments of the object */
    int      norm,         /* the minimization norm used */
    double   *orien,       /* the orientation, and */
    double   *err          /* the min err */
) {
    int      k;            /* loop index */
    double   dt=0.5*PI;    /* [0, 2π] is divided into 4 sub-intervals */
    double   ta, tb, tc, tmin, ea, eb, ec, emin;
    double   (*func)(double x);

    /* check for improper parameters */
    if (nmin < 0 || nmin > nmax || nmax >= MAX_N) return -1;

    /* allocate dynamic storage */
    C1nl = dmatrix(0, MAX_N, 0, MAX_N);
    S1nl = dmatrix(0, MAX_N, 0, MAX_N);
    C2nl = dmatrix(0, MAX_N, 0, MAX_N);
    if ((S2nl = dmatrix(0, MAX_N, 0, MAX_N)) == NULL)
    {
        free_dmatrix(C2nl, 0, MAX_N, 0, MAX_N);
        free_dmatrix(S1nl, 0, MAX_N, 0, MAX_N);
        free_dmatrix(C1nl, 0, MAX_N, 0, MAX_N);
        return -2;
    }


    /* get the Zernike moments in zm1 and zm2 */
    if (get_zernike_moments(nmin, nmax, zm1, C1nl, S1nl) != 0)
    {
        free_dmatrix(S2nl, 0, MAX_N, 0, MAX_N);
        free_dmatrix(C2nl, 0, MAX_N, 0, MAX_N);
        free_dmatrix(S1nl, 0, MAX_N, 0, MAX_N);
        free_dmatrix(C1nl, 0, MAX_N, 0, MAX_N);
        return -3;
    }
    if (get_zernike_moments(nmin, nmax, zm2, C2nl, S2nl) != 0)
    {
        free_dmatrix(S2nl, 0, MAX_N, 0, MAX_N);
        free_dmatrix(C2nl, 0, MAX_N, 0, MAX_N);
        free_dmatrix(S1nl, 0, MAX_N, 0, MAX_N);
        free_dmatrix(C1nl, 0, MAX_N, 0, MAX_N);
        return -3;
    }

    Nmin = nmin;      /* for computing the error function */
    Nmax = nmax;
```

```c
    *orien = *err = 1.0e+20;     /* initialization */

    switch (norm) {
    case ZM_ABS_NORM:    /* absolute norm */
        func = zm_orien_abs_norm;
        break;
    case ZM_EUCL_NORM:   /* Euclidean norm */
        func = zm_orien_eucl_norm;
        break;
    case ZM_MAX_NORM:    /* maximum norm */
        func = zm_orien_max_norm;
        break;
    default:
        free_dmatrix(S2nl, 0, MAX_N, 0, MAX_N);
        free_dmatrix(C2nl, 0, MAX_N, 0, MAX_N);
        free_dmatrix(S1nl, 0, MAX_N, 0, MAX_N);
        free_dmatrix(C1nl, 0, MAX_N, 0, MAX_N);
        return -4;       /* unknown norm */
    }

    /* We know that there's a minimum in [0, 2π]. */
    ta = 0.0;
    tc = dt;
    for (k = 0; k < 4; k++) {
        tb = ta + 0.38196601*(tc-ta);
        emin = golden(ta, tb, tc, func, TOLERANCE, &tmin);
        ta = tc;
        tc += dt;
        if (*err > emin) {  /* find a minimum in the interval [0, 2π] */
            *err = emin;
            *orien = tmin;
        }
    }
    *orien *= RADIAN_TO_DEGREE;     /* convert to angle in degrees */

    free_dmatrix(S2nl, 0, MAX_N, 0, MAX_N);     /* clean up */
    free_dmatrix(C2nl, 0, MAX_N, 0, MAX_N);
    free_dmatrix(S1nl, 0, MAX_N, 0, MAX_N);
    free_dmatrix(C1nl, 0, MAX_N, 0, MAX_N);
    return 0;
}



/********************************************************************

    name:          test_zm_orien

    description:   Test the orientation recognition function get_zm_orien.
```

```
    syntax:            int test_zm_orien(void)

    errors:             0 - no error
                       -1 - error occurred in function get_zm_orien

    written by:        X. Zhou
    date:              September 16, 1991

**********************************************************************/
int test_zm_orien(
    void
) {
    #define nmin    0                   /* min & max moment orders */
    #define nmax    16
    #define zm1     "char_a.zm"     /* file name for moments set #1 */
    #define zm2     "char_a60.zm"   /* file name for moments set #2 */
    #define norm    ZM_EUCL_NORM    /* the Euclidean norm */

    double  orien;  /* the desired orientation (in degrees) */
    double  err;    /* the minimum error */

    /* reconstrucing the picture */
    if (get_zm_orien(nmin, nmax, zm1, zm2, norm, &orien, &err) != 0)
        return -1;
    /* orien = 59.8601; err = 0.0093; */

    return 0;
}
```

```
/**************************************************************************

  zm_recons.c

  This file contains functions for image reconstruction from Zernike moments.

  (C) Copyright The Laboratory of Dr. Richard Gordon. 1991.
  All rights reserved.

**************************************************************************/



#include <stdio.h>
#include <string.h>
#include "zernikemoment.h"




/**************************************************************************

      name:            zm_contrib

      description:     Accumulate the Nth order contribution from the Zernike
                       moments CNL and SNL to the image F of size NX and NY.

      syntax:          int zm_contrib(int n, double **cnl, double **snl,
                       int nx, int nx, double **f)

      errors:           0 - no error
                       -1 - cannot get the polar coords

      written by:      X. Zhou
      date:            September 16, 1991

**************************************************************************/
int zm_contrib(
    int     n,      /* add contribution from the nth order Zernike moment */
    double  **cnl,  /* the real part, and */
    double  **snl,  /* the imaginary part of the moments */
    int     nx,     /* the picture size in horiz., and */
    int     ny,     /* the vert. directions */
    double  **f     /* the reconstructed image */
) {
    int     l, k, col, row;
    double  x0, y0, theta, rho, lt, sum;

    x0 = 0.5 * nx;
    y0 = 0.5 * ny;
    for (row = 0; row < ny; row++)
```

```c
        for (col = 0; col < nx; col++)
        {
            if (get_polar_coords(x0, y0, col, row, &theta, &rho) != 0)
                return -1;        /* cannot get the polar coords */
            sum = f[row][col];
            if (rho-1.0 <= SMALL_REAL)        /* inside the unit circle */
            {
                if (n&1 == 0)    /* n is an even number */
                    sum += cnl[n][0] * get_rnl_val(n, 0, rho);
                for (l = 1; l <= n; l++)
                    if ((n-l & 1) == 0)        /* n-l is an even number */
                    {
                        lt = l * theta;
                        sum += 2.0 * get_rnl_val(n, l, rho)
                                * (cnl[n][l]*cos(lt) - snl[n][l]*sin(lt));
                    }
            }
            else    /* outside the unit circle */
                sum = HUGE_VAL;
            f[row][col] = sum;
        }
    return 0;
}



/*******************************************************************

    name:           zm_recons

    description:    Reconstruct an image of size NX and NY from its Zernike
                    moments of order NMIN to NMAX {CNL and SNL}. The
                    reconstructed images are separately saved as FNAME.nn,
                    where nn indicates that the image is reconstructed from
                    zero order up to nnth order of Zernike moments.

    syntax:         int zm_recons(int nmin, int nmin, double **cnl,
                    double **snl, int nx, int ny, char *fname)

    errors:          0 - no error
                    -1 - cannot save the Zernike polynomial coefficients
                    -2 - cannot allocate dynamic memory

    written by:     X. Zhou
    date:           September 16, 1991

*******************************************************************/
int zm_recons(
    int     nmin,   /* the min order, and */
    int     nmax,   /* the max order of Zernike moments */
```

```c
    double   **cnl,   /* the real part, and */
    double   **snl,   /* the imaginary part of the moments */
    int      nx,      /* the picture size in horiz., and */
    int      ny,      /* the vert. directions */
    char     *fname   /* the desired picture file name */
) {
    int      n, l, i, j, value;
    char     theName[256], theStr[256];
    int      **f;      /* the reconstructed picture */
    double   **fd;     /* the picture in double precision */

    /* check for improper parameters */
    if (nmin < 0 || nmin > nmax || nmax >= MAX_N) return -1;

    /* allocate dynamic memory */
    if ((f = imatrix(0, nx, 0, ny)) == NULL) return -2;
    if ((fd = dmatrix(0, nx, 0, ny)) == NULL)
    {
        free_imatrix(f, 0, nx, 0, ny);
        return -2;
    }

    n = nmin;    /* initializations */
    for (j = 0; j < ny; j++)
        for (i = 0; i < nx; i++)
            fd[j][i] = 0.0;

    do {
        if (zm_contrib(n, cnl, snl, nx, ny, fd) == 0)
        {
            strcpy(theName, fname);
            sprintf(theStr, "%02d", n);        /* typically, 00 <= n <= 99 */
            strcat(theName, theStr);
            for (j = 0; j < ny; j++)            /* truncated to integer */
                for (i = 0; i < nx; i++)
                    f[j][i] = (fd[j][i]==HUGE_VAL) ? 0 : fd[j][i];
            put_pict(theName, nx, ny, f);   /* save the picture from up to */
        }                                   /* nth order of moments */
    } while (++n <= nmax);

    free_dmatrix(fd, 0, nx, 0, ny);      /* clean up */
    free_imatrix(f, 0, nx, 0, ny);
    return 0;
}


/*****************************************************************************

    name:           test_zm_recons
```

```
        description:     Test the image reconstruction function zm_recons.

        syntax:          int test_zm_recons(void)

        errors:           0 - no error
                         -1 - cannot allocate dynamic memory
                         -2 - cannot get the Zernike moments
                         -3 - error occurred in function zm_recons

        written by:      X. Zhou
        date:            September 16, 1991

************************************************************************/
int test_zm_recons(
    void
) {
    #define nmin    0               /* min & max moment orders */
    #define nmax    16
    #define zm      "char_a.zm" /* file name for Zernike moments */
    #define nx      33              /* picture size */
    #define ny      33

    double  **cnl, **snl;

    /* allocate dynamic memory for the moments */
    cnl = dmatrix(0, MAX_N, 0, MAX_N);
    if ((snl = dmatrix(0, MAX_N, 0, MAX_N)) == NULL)
    {
        free_dmatrix(cnl, 0, MAX_N, 0, MAX_N);
        return -1;
    }

    /* get the Zernike moments in ZM */
    if (get_zernike_moments(nmin, nmax, zm, cnl, snl) != 0) return -2;

    /* reconstrucing the picture */
    if (zm_recons(nmin, nmax, cnl, snl, nx, ny, zm) != 0) return -3;

    free_dmatrix(snl, 0, MAX_N, 0, MAX_N);  /* clean up */
    free_dmatrix(cnl, 0, MAX_N, 0, MAX_N);
    return 0;
}
```

```
/*******************************************************************

  zm_symmaxis.c

  This file contains functions for detection of symmetric axis by using the
  phase information in Zernike moments.

  (C) Copyright The Laboratory of Dr. Richard Gordon. 1991.
  All rights reserved.

********************************************************************/


#include <stdio.h>
#include "zernikemoment.h"


extern int Nmin, Nmax;
extern double **C1nl, **S1nl;


/*******************************************************************

     name:              zm_symmaxis_abs_norm

     description:       Compute the specially defined angular error function
                        for symmetric axis detection using the absolute norm.

     syntax:            double zm_symmaxis_abs_norm(double theta)

     written by:        X. Zhou
     date:              September 16, 1991

********************************************************************/
double zm_symmaxis_abs_norm(
     double theta      /* the abscissa */
) {
     int      n, l;
     double   err=0.0, mt, anl=0.0;

     for (n = Nmin; n <= Nmax; n++)
         for (l = 0; l <= n; l++)
             if ((n-l & 1) == 0) {
                 mt = l*theta;
                 err += fabs(S1nl[n][l]*cos(mt)+C1nl[n][l]*sin(mt));
                 anl += VECTORMAG(C1nl[n][l], S1nl[n][l]);
             }
     return err/anl;
}
```

```
/***********************************************************************

     name:               zm_symmaxis_eucl_norm

     description:        Compute the specially defined angular error function
                         for symmetric axis detection using the Euclidean norm.

     syntax:             double zm_symmaxis_eucl_norm(double theta)

     written by:         X. Zhou
     date:               September 16, 1991

*************************************************************************/
double zm_symmaxis_eucl_norm(
     double theta      /* the abscissa */
) {
     int      n, l;
     double   err=0.0, mt, tmp, anl2=0.0;

     for (n = Nmin; n <= Nmax; n++)
          for (l = 0; l <= n; l++)
               if ((n-l & 1) == 0) {
                    mt = l*theta;
                    tmp = Slnl[n][l]*cos(mt)+Clnl[n][l]*sin(mt);
                    err += tmp*tmp;
                    anl2 += Clnl[n][l]*Clnl[n][l]+Slnl[n][l]*Slnl[n][l];
               }
     return err/anl2;
}



/***********************************************************************

     name:               zm_symmaxis_max_norm

     description:        Compute the specially defined angular error function
                         for symmetric axis detection using the maximum norm.

     syntax:             double zm_symmaxis_max_norm(double theta)

     written by:         X. Zhou
     date:               September 16, 1991

*************************************************************************/
double zm_symmaxis_max_norm(
     double theta      /* the abscissa */
) {
```

```
    int     n, l;
    double  err=0.0, mt, tmp, anl=0.0;

    for (n = Nmin; n <= Nmax; n++)
        for (l = 0; l <= n; l++)
            if ((n-l & 1) == 0) {
                mt = l*theta;
                tmp = fabs(Slnl[n][l]*cos(mt)+Clnl[n][l]*sin(mt));
                err = MAX(err, tmp);
                tmp = VECTORMAG(Clnl[n][l], Slnl[n][l]);
                anl = MAX(anl, tmp);
            }
    return err/anl;
}



/*********************************************************************


    name:           get_zm_symmaxis

    description:    Compute the symmetric axis AXIS and minimum error ERR
                    of an object ZM with the optimization norm NORM.
                    Zernike moments from order NMIN to NMAX are used in
                    the computation.

    syntax:         int get_zm_symmaxis(int nmin, int nmax, char *zm,
                    int norm, double *axis, double *err)

    errors:          0 - no error
                    -1 - orders nmin and nmax improper
                    -2 - cannot allocate dynamic storage
                    -3 - cannot get the Zernike moments
                    -4 - unknown optimization norm

    written by:     X. Zhou
    date:           September 16, 1991

*********************************************************************/
int get_zm_symmaxis(
    int     nmin,       /* the min and */
    int     nmax,       /* min orders of Zernike moment */
    char    *zm,        /* Zernike moments of the object */
    int     norm,       /* the minimization norm used */
    double  *axis,      /* the symmetric axis, and */
    double  *err        /* the min err */
) {
    int     j, k;       /* loop index */
    double  dt=0.25*PI; /* [0, π] is divided into 4 segments */
    double  ta, tb, tc, tmin, ea, eb, ec, emin;
```

```
    double  (*func)(double x);

    /* check for improper parameters */
    if (nmin < 0 || nmin > nmax || nmax >= MAX_N) return -1;

    /* allocate dynamic storage */
    Clnl = dmatrix(0, MAX_N, 0, MAX_N);
    if ((Slnl = dmatrix(0, MAX_N, 0, MAX_N)) == NULL)
    {
        free_dmatrix(Clnl, 0, MAX_N, 0, MAX_N);
        return -2;
    }

    /* get the Zernike moments in ZM */
    if (get_zernike_moments(nmin, nmax, zm, Clnl, Slnl) != 0)
    {
        free_dmatrix(Slnl, 0, MAX_N, 0, MAX_N);
        free_dmatrix(Clnl, 0, MAX_N, 0, MAX_N);
        return -3;
    }

    Nmin = nmin;     /* for computing the error function */
    Nmax = nmax;
    *axis = *err = 1.0e+20;     /* initialization */

    switch (norm) {
    case ZM_ABS_NORM:   /* absolute norm */
        func = zm_symmaxis_abs_norm;
        break;
    case ZM_EUCL_NORM:  /* Euclidean norm */
        func = zm_symmaxis_eucl_norm;
        break;
    case ZM_MAX_NORM:   /* maximum norm */
        func = zm_symmaxis_max_norm;
        break;
    default:
        free_dmatrix(Slnl, 0, MAX_N, 0, MAX_N);
        free_dmatrix(Clnl, 0, MAX_N, 0, MAX_N);
        return -4;      /* unknown norm */
    }

    /* We know that there's a minimum in [0, π]. */
    ta = 0.0;
    tc = dt;
    for (k = 0; k < 4; k++) {
        tb = ta + 0.38196601*(tc-ta);
        emin = golden(ta, tb, tc, func, TOLERANCE, &tmin);
        ta = tc;
        tc += dt;
```

```c
        if (*err > emin) {  /* find a minimum in the interval [0, 2π] */
            *err = emin;
            *axis = tmin;
        }
    }
    *axis *= RADIAN_TO_DEGREE;          /* convert to angle in degrees */

    free_dmatrix(S1nl, 0, MAX_N, 0, MAX_N);      /* clean up */
    free_dmatrix(C1nl, 0, MAX_N, 0, MAX_N);
    return 0;
}


/*********************************************************************

    name:           test_zm_symmaxis

    description:    Test the symmetric axis detection function
                    get_zm_symmaxis.

    syntax:         int test_zm_symmaxis(void)

    errors:          0 - no error
                    -1 - error occurred in function get_zm_symmaxis

    written by:     X. Zhou
    date:           September 16, 1991

*********************************************************************/
int test_zm_symmaxis(
    void
) {
    #define nmin    0                   /* min & max moment orders */
    #define nmax    16
    #define zm      "char_a.zm"     /* file name for Zernike moments */
    #define norm    ZM_EUCL_NORM    /* the Euclidean norm */

    double  axis;   /* the desired symmetric axis (in degrees) */
    double  err;    /* the minimum error */

    /* recognizing the symmetric axis */
    if (get_zm_symmaxis(nmin, nmax, zm, norm, &axis, &err) != 0) return -1;
    /* axis = 90.0048; err = 1.0098e-7; */

    return 0;
}
```

```
33   33
0    0    0    0    0    0    0    0    0    0    0    0    0    0    0    0    0    0    0    0    0    0
0    0    0    0    0    0    0    0    0    0    0    0    0    0    0    0    0    0    0    0    0    0
0    0    0    0    0    0    0    0    0    0    0    0    0    0    0    0    0    0    0    0    0    0
0    0    0    0    0    0    0    0    0    0    0    0    0    0    0    0    0    0    0    0    0    0
0    0    0    0    0    0    0    0    0    0    0    0    0    0    1    1    1    1    1    0    0    0
0    0    0    0    0    0    0    0    0    0    0    0    0    0    1    1    1    1    1    0    0    0
0    0    0    0    0    0    0    0    0    0    0    0    0    1    1    1    1    1    1    1    0    0
0    0    0    0    0    0    0    0    0    0    0    0    0    1    1    1    1    1    1    1    0    0
0    0    0    0    0    0    0    0    0    0    0    0    1    1    1    1    1    1    1    1    1    0
0    0    0    0    0    0    0    0    0    0    0    0    1    1    1    1    1    1    1    1    1    0
0    0    0    0    0    0    0    0    0    0    0    1    1    1    1    1    0    1    1    1    1    1
0    0    0    0    0    0    0    0    0    0    0    1    1    1    1    1    0    1    1    1    1    1
0    0    0    0    0    0    0    0    0    0    1    1    1    1    1    0    0    0    1    1    1    1
0    0    0    0    0    0    0    0    0    0    1    1    1    1    1    0    0    0    1    1    1    1
0    0    0    0    0    0    0    0    0    1    1    1    1    1    0    0    0    0    0    1    1    1
0    0    0    0    0    0    0    0    0    1    1    1    1    1    0    0    0    0    0    1    1    1
0    0    0    0    0    0    0    0    1    1    1    1    1    1    1    1    1    1    1    1    1    1
0    0    0    0    0    0    0    0    1    1    1    1    1    1    1    1    1    1    1    1    1    1
0    0    0    0    0    0    0    1    1    1    1    1    1    1    1    1    1    1    1    1    1    1
0    0    0    0    0    0    0    1    1    1    1    1    1    1    1    1    1    1    1    1    1    1
0    0    0    0    0    0    1    1    1    1    1    0    0    0    0    0    0    0    0    0    0    0
0    0    0    0    0    0    1    1    1    1    1    0    0    0    0    0    0    0    0    0    0    0
0    0    0    0    0    1    1    1    1    1    0    0    0    0    0    0    0    0    0    0    0    0
0    0    0    0    0    1    1    1    1    1    0    0    0    0    0    0    0    0    0    0    0    0
0    0    0    0    1    1    1    1    1    0    0    0    0    0    0    0    0    0    0    0    0    0
0    0    0    0    1    1    1    1    1    0    0    0    0    0    0    0    0    0    0    0    0    0
0    0    0    0    0    0    0    0    0    0    0    0    0    0    0    0    0    0    0    0    0    0
0    0    0    0    0    0    0    0    0    0    0    0    0    0    0    0    0    0    0    0    0    0
0    0    0    0    0    0    0    0    0    0    0    0    0    0    0    0    0    0    0    0    0    0
0    0    0    0    0    0    0    0    0    0    0    0    0    0    0    0    0    0    0    0    0    0
0    0    0    0    0    0    0    0    0    0    0    0    0    0    0    0    0    0    0    0    0    0
0    0    0    0    0    0    0    0    0    0    0    0    0    0    0    0    0    0    0    0    0    0
0    0    0    0    0    0    0    0    0    0    0    0    0    0    0    0    0    0    0    0    0    0
```